In Silico Design and Synthesis of Small-Molecule Intrinsic Organic Semiconductors for Organic Electronics

Leighton Owen Jones

Supervised by Prof. Long Lin

Submitted in accordance with the requirements for the degree of

Doctor of Philosophy

The University of Leeds

School of Chemistry

May 2017

Intellectual Property and Publication Statement

The candidate confirms that the work submitted is his own, except where work which has formed part of jointly-authored publications has been included. The contribution of the candidate and the other authors to this work has been explicitly indicated below. The candidate confirms that appropriate credit has been given within the thesis where reference has been made to the work of others.

Details of jointly-authored publications:

L. Jones, C. Pask, M. Gulcur, A. Kazlauciunas and L. Lin*, "Synthesis and characterisation of fused-heterocyclic molecular rods: a combined experimental and theoretical study on diethynyl-dithienothiophenyl derivatives", *Chemistry Select*, manuscript accepted.

L. Jones, X. Luo, A. Kazlauciunas and L. Lin*, "A bifunctional smart material: the synthesis of a metal-free black pigment for optoelectronic applications from an organic semiconducting molecular rod", *Pigments and Resin Technology*, **2017**, *47*, manuscript accepted.

L. Jones and L. Lin*, "A theoretical study on the isomers of the B5TB heteroacene for improved properties in organic electronics", *Comp. Theor. Chem.,* **2017**, *1115*, 22-29, DOI: 10.1016/j.comptc.2017.05.039.

L. Jones and L. Lin*, "An *in silico* study on the isomers of pentacene: the case for air-stable and alternative $C_{22}H_{14}$ acenes for organic electronics", *J. Phys. Chem. A*, **2017**, *121*, 2804-2813, DOI:10.1021/acs.jpca.6b11770.

L. Jones and B. Whitaker*, "Modeling a halogen dance reaction mechanism, a density functional theory study", *J. Comp. Chem.*, **2016**, *37*, 1697-1703, DOI: 10.1002/jcc.24385.

Acknowledgements

Abstract

On a global scale, the mass production of organic semiconductors for electronic applications in flexible display technology, among others, is linked to both research and consumer demand. To overcome challenges, the fabrication of the organic electronic devices has moved from high-cost small-molecule vapour-phase deposition type techniques, to relatively low-cost solution processing of the organic thin film transistors (OTFTs).

Initial studies in this work focused on the modelling, prediction and synthesis of two-dimensional planar structures. These studies probed the isomeric structures of pentacene. Quantum mechanics/density functional theory calculations found that at least five out of a total of 12 isomers (inclusive) are both air-stable and have the same order of magnitude for the hole and electron rates of charge transfer as that of pentacene; suggesting that isomeric candidates of the initial target structure are worthy of thorough investigation.

A second study on planar structures focused on novel and rationally designed molecules, six isomers inclusive, in an attempt to develop a challenging but high-performing seven fused-ring heteroacene. The study gave the interesting result that one structure is suitable for not just OTFTs, but also non-linear optics, inferring that highly functional optoelectronic switches are possible from a single OTFT.

A small library of rod-like structures were probed to contrast with the nature of the structures investigated so far. These contain linear components that separate the planar aromatic components in the molecules. It was discovered that these structures are highly flexible and soluble in common organic solvents, showing promise for applications as solution processed OTFTs.

In summary, key discoveries of the study include (i) world-class candidates could be out-competed by their own isomers; (ii) new heteroacenes conceived could have bifunctional outputs for two separate fields in organic electronics; (iii) novel molecular rods were synthesised and found to have excellent solubility in common organic solvents, thereby enabling large-scale fabrication of flexible display technologies.

Table of Contents

List of Figures

List of Tables

List of Schemes

- 14 -

List of Equations

Abbreviations

Chemical (Common name)

B5TB	Dibenzopentathiophene	HMDS	Hexamethyldisilazane
BTBT	Benzothienobenzothiophenes	LB154	Leeds Black 154
DATT	Dianthracenethienothiophene	LDA	Lithium diisopropylamine
DBDTT	Dibenzodithienothiophene	NBS	N-bromosuccinimide
DBTT	Dibenzothienothiophene	OSC	Organic semiconductor
DCM	Dichloromethane	OTS	Octyltrichlorosilane
DMAc	Dimethylacetamide	PEN	Pentacene
DMF	Dimethylformamide	PPh$_3$	Tetrakistriphenylphosphine
DMSO	Dimethylsulfoxide	TBAF	Tetrabutylammonium fluoride
DNTT	Dinaphthothienothiophene	TCNQ	7,7,8,8-Tetracyanoquinodimethane
DTBDT	Dithienobenzodithiophene	THF	Tetrahydrofuran
DTBT	Dithienobenzothiophene	TIPS	Triisropylsilyl
DTT	Dithienothiophene	TMSA	Trimethylsilylacetylene

General

AMBER	Assisted Model Building Energy Refinement	FET	Field effect transistor
B3LYP	Becke three-parameter Lee Yang Par	FGI	Functional group interconversion
BJ	Becke-Johnson damping	FMO	Frontier molecular orbital
BLYP	Becke Lee Yang Par	FT-IR	Fourier-transformed infrared
CAM	Coulomb-attenuating method	HD	Halogen dance
CCSD	Coupled-cluster singles and doubles	HF	Hartree-Fock
COSY	Correlated spectroscopy	HMQC	Heteronuclear multiple quantum coherence
D1-3	Grimme's Dispersion (first to third order)	HOMO	Highest occupied molecular orbital
DEPT	Distortionless enhancement by polarisation transfer	HPLC	High-performance liquid chromatography
DFT	Density functional theory	HRMS	High-resolution mass spectrometry
DSC	Dynamic scanning calorimetry	IE	Ionisation energy
EA	Electron affinity	INDO	Intermediate neglect of differential overlap

EPT	Electron propagator theory	OVGF	Outer valence Green's Function
KT	Koopmans' Theorem	IRC	Intrinsic reaction coordinates
LC	Long-range corrected	P3	Third order pole
LCMS	Liquid chromatography-mass spectrometry	PCM	Polarisable continuum models
LUMO	Lowest unoccupied molecular orbital	PES	Potential energy surface
MM	Molecular mechanics	ppm	Parts per million
MMFF	Merck molecular force field	QCISD	Quadratic configuration interaction singles and doubles
MNDO	Modified neglect of diatomic overlap	QM	Quantum mechanics
MP	Møller-Plesset	SHG	Single harmonic generation
MTR	Multi-trapping and release	STQN	Synchronous transit-guided quasi-Newton
NLO	Nonlinear optic	TD-DFT	Time-dependent DFT
NMR	Nuclear magnetic resonance	TFT	Thin film transistor
OFET	Organic field effect transistor	TGA	Thermal gravimetric analysis
OSC	Organic semiconductor	UFF	Universal force field
OTFT	Organic thin film transistor	VH	Vilsmeier-Haack

Chapter 1

Introduction

Organic electronics constitutes a broad spectrum of interdisciplinary fields spanning those of chemistry, physics and engineering, which utilise molecular materials to impart optoelectronic phenomena for applications in technology, from solar cells for energy conversion to flexible display screens in smart technology[1–3] (Figure 1). Conventionally, electronics were based on inorganic materials that suffered from brittleness, synthetic limitations and high processing temperatures[4,5]. These drawbacks were overcome with organic materials that enable flexibility and charge transfer. Moreover, the organic structures opened up a vast number of opportunities for physical property tuning and enhancement of the devices *via* synthetic and structural manipulation of the active optoelectronic component. These components, although diverse and tailored to their applications, all have one common requirement: the ability to conduct charge. Charge transfer is achieved with electronic devices called transistors[6,7] (Figure 2) that are made of semiconducting materials. Small-molecule organic semiconductors (OSCs), are discrete and atomically precise materials that are routinely developed for the next generation of smart technology. It is clear that organic semiconductors are integral to numerous material-related technologies and improvements in the specific field of organic semiconductors also develops those of all other charge-transfer related fields[8].

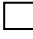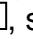Organic electronics has been under intense investigations since the

Figure 1. A selection of technology applications[8] which include (top left to bottom right) smart paper e-readers, mobile phones, tablets and wearable devices.
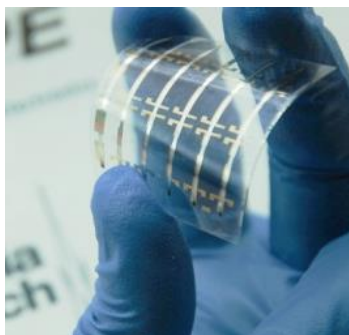
Figure 2. A flexible transistor substrate showing multiple electrodes ready for organic semiconductor deposition.

first organic transistor was reported during the mid-1980s, and many molecular materials have been both experimentally and theoretically developed[9]. This level of scientific study has yielded a multitude of chemical structures, not all of which are high performing[10]. The ability to vary the molecular size, shape and solubility gave significant early improvements, but the greatest leap occurred when the structures were derivatised with the addition of heterocyclic units that were mixed with the conventional benzene-based aromatics[8]. These derivatives included the variation of the heteroatoms other than sulfur or nitrogen in the heterocycles, such as oxygen, selenium, and silicon; their functionalisation with solubilising alkyl chains for large-scale manufacture; halogen substitution such as fluorine for electron stability and enhanced single-crystal packing in the solid state; and the nature of the bonding array, such as oligomeric or fused-ring aromatics[11].

These vast developments have proved beneficial in the development of organic electronics to meet the growing demand, yet there are still limitations in 'design rules' to date. For example, structure-property relationships based on molecular dimensions do no always correlate, evidenced famously with the planar 7,7,8,8-tetracyanoquinodimethane (TCNQ) and buckminsterfullerene C_{60} for electron charge transfer; both are high performing but the former has nitrile units while the latter has no heteroatoms and is spherical. Couple this apparent dichotomy with the numerous structures synthesised to date, the fundamental physical characteristics of high-performing organic semiconducting candidates are becoming increasingly difficult to rationalise, especially when there are different interpretations of the charge transfer mechanisms. An integrated approach is needed to overcome the challenges and this turns the

investigations to the field of theoretical computational chemistry and the process of virtual screening.

Computational investigations overcome the relatively slow rate of iterative experimental synthesis and testing, as libraries of chemical structures can be *in silico* designed and screened for both their stability and charge transfer properties. Developments in quantum mechanics has led to easier handling and deployment of the theories, such as density functional theory (DFT). Combining DFT virtual screening with synthetic investigations cuts resources and provides a powerful approach to the advancement of the next generation of high-performing organic semiconducting candidates for organic electronic technology.

Interestingly, out of all the fields of organic electronics, organic semiconductors are investigated the least (Figure 3), even though it is the most common component. Solar cells and photovoltaics originated in the literature during the 1970s, owing in part to the research on conventional inorganic materials. From the 1980's, nonlinear optics, organic electronics and organic semiconducting phenomena were investigated, but at a much lesser volume. By the mid-1990's, organic light emitting diodes emerged and later in
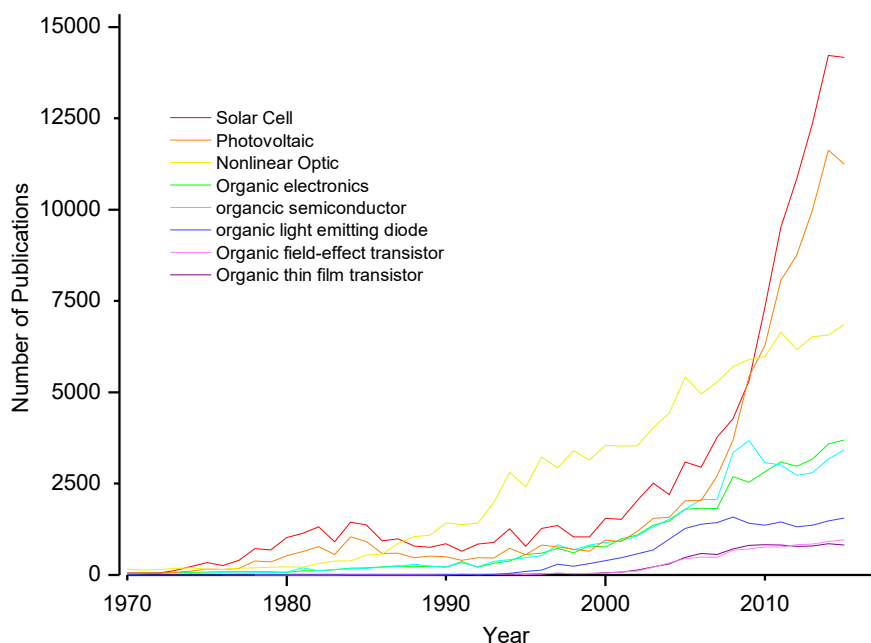
Figure 3. The number of publications per year on Scopus (papers, reviews, conference proceedings, and book chapters) containing the given search term, in the title, abstract or key words.

the 2000's, research increased with the organic thin film transistors and the addition of an applied field gave rise to the organic field effect transistor. Up until 2016, solar cell research is the highest published and fastest growing field in electronic devices, being inorganic or organic-based, followed by photovoltaic and non-linear optics. The least published fields in organic electronics are organic field-effect transistors and organic thin-film transistors, suggesting that this area, primarily focusing on charge transport (hole or electron), is still emerging and expected to grow with the advent of thinner and more flexible consumer technology.

Chapter 2

Literature Review

2.1 Organic Semiconductor Discoveries

The earliest work that can be contributed to semiconductor properties begins with inorganic semiconductors and dates back to Faraday[12] in 1833 when he noted that silver sulfide exhibited a negative temperature coefficient. Since then, there has been successive breakthroughs with photovoltaics but the first amplifier was invented by de Forest as a thermionic triode valve in 1906 and was called the Audion[13]. The Professor of physics at Leipzig, Lilienfeld, was the first to file a patent for conceptual devices described as a field effect transistor. The first was filed in 1926[14] but not granted until 1930, however, there was scepticism if they would have functioned as a practical device. The first published experimental evidence was reported by Hilsch and Pohl in 1938, which inspired Brattain at AT&T Bell Laboratories to "put a grid in the semiconductor diode and eureka the result would be an active triode with amplifying possibilities"[15], developing the first transistor in 1947[16]. The device was a point contact type due to the physical contact of the components and consisted of a germanium semiconductor, as illustrated in Figure 4.
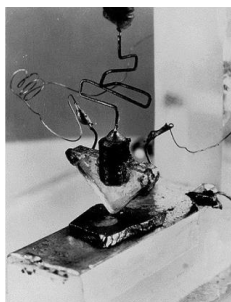
Figure 4. The First transistor from AT & T Bell Laboratories[16].

The word transistor is derived from the words transfer and resistor; whereby a transistor is a device which amplifies the current or switches the electrical potential applied between the source and drain electrodes acting as an on/off switch. The device is considered to be bipolar because its conduction is thought to consist of the recombination of electrons and holes in the electronic states of a material. Field effect transistors are unipolar as they consist of only one type of charge carrier and control the flow of current between the source and drain electrodes by an electric field which is created by a gate electrode. The connection between the source and drain electrodes is called the channel and if consisting of organic semiconducting material, then

the device is called an organic field effect transistor (OFET). Throughout the 1950's, devices became known collectively as *discrete* which are electronic units such as resistors, capacitors, diodes or transistors and are fabricated on a single electronic circuit to make multi-composite devices such as radios and computers. In 1956, Bardeen, Brattain and Shockley shared the Nobel Prize in physics[17] for "their researches on semiconductors and their discovery of the transistor effect".

Since the discovery of OFET device[18] in the 1980s, they have attracted much attention. OFETs consist of an organic semiconducting layer, a gate insulator layer, and three terminals (drain, source, and gate electrodes). OFETs are not only essential components for the next generation of cheap and flexible organic circuits in display technology, but they also provide an important insight into the charge transport of π-conjugated systems. They act as tools for the exploration of the structure-property relationships of π-conjugated systems, such as the charge transfer field-effect mobility (μ, the drift velocity of carriers under unit electric field)[4,19–23].

2.2 Organic Semiconducting Devices

2.2.1 Organic Field Effect Transistors (OFETs)

The purpose of a field effect transistor (FET) is to modulate or control the flow of electric current. This is achieved with a device consisting of several layers, stacked in a sandwich-like array and includes source/drain electrodes, a semiconducting layer, an insulating layer and a gate electrode as illustrated in Figure 5, showing four common FET architectures[10]. In a p-type semiconductor, the holes (positive charge) are the majority of charge carriers in the electronic band structure and are of low density with respect to any given plane in the bulk in the absence of any applied fields; n-type semiconductors have an excess of electrons (negative charge). Once a negative voltage is applied to the gate generating an electric field, the holes are polarised or attracted towards the semiconductor/insulator interface and here their density becomes significant enough to promote the electrical conduction from the source to the drain electrodes. Conversely, when a positive voltage is applied to the gate electrode the holes or charge carriers are reduced and the effect may be possible to be extended throughout the thickness of the semiconductor layer. Therefore, the gate electrode modulates the carrier density in the semiconductor, and can also be monitored with the source and drain electrodes, yielding a triple-electrode device for the control and measurement of current.
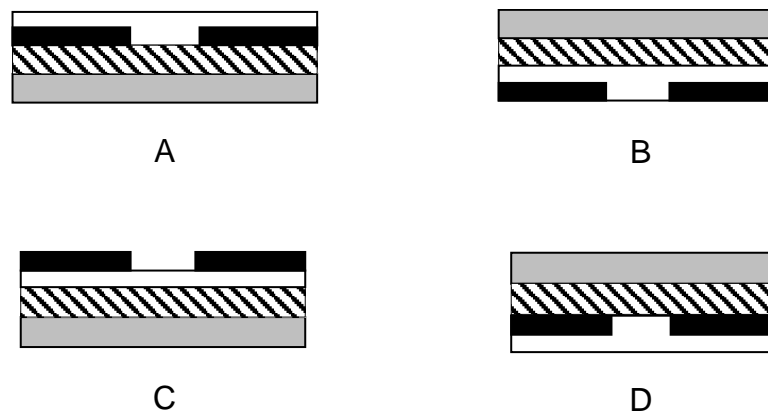
Figure 5. Four common FET device architectures, A bottom gate bottom contact, B top gate bottom contact, C bottom gate top contact and D top gate top contact; the components are semiconductor ▢, source/drain ■, insulator ▨, gate ▢, reference point = semiconductor.

Metals are conductors as they have partially filled conduction bands and electrons can be easily promoted from the highest occupied level (Fermi level) into the next available unoccupied level. Semiconductors on the other hand, exist as two types, intrinsic and extrinsic. Intrinsic inorganic semiconductors are electrical insulators at $T = 0$ K, but may conduct if the band gap is small enough for the electrons to be thermally promoted from the valence band into the conduction band. Extrinsic inorganic semiconductors generally require the addition of a dopant which provides localised energy levels that are closest to either the valence (p-type) or conduction (n-type) bands as illustrated in Figure 6.
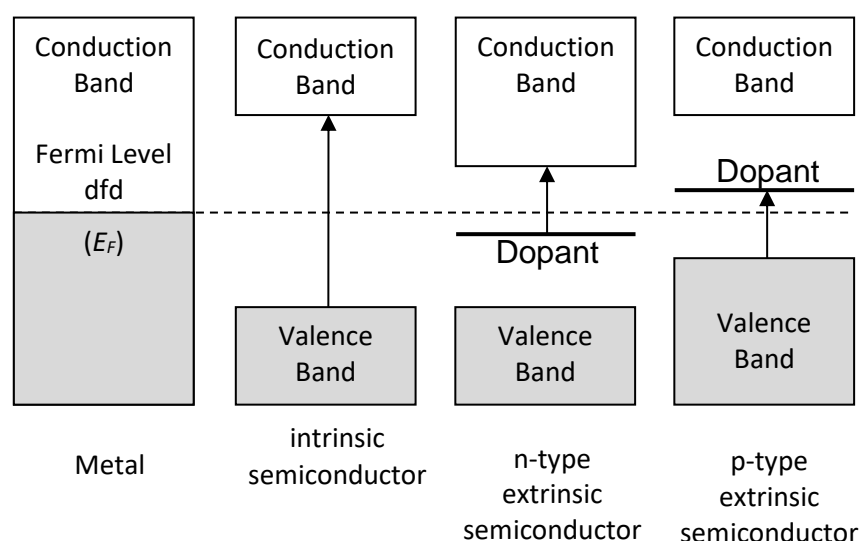
Figure 6. Energy bands of a metal and two inorganic semiconductor types (p- and n-type).

Figure 6 can be modified for small-molecule OSCs if the highest occupied molecular orbital (HOMO) level of the valence and the lowest unoccupied molecular orbital (LUMO) level of the conduction bands are considered. For example, under the conditions that a HOMO level of a semiconductor is close to the Fermi level of a metal, which provides a low energy difference or barrier, and with a negative gate voltage applied, then holes are easily injected and the semiconductor is p-type. The device operates as a conducting channel forms at the semiconductor-metal interface and charge-carriers can be driven from source to drain by applying a second bias potential. If electron injection is easier than hole injection, where the LUMO

level is closer to the Fermi level than the HOMO level, then the semiconductor is n-type.

Figure 7 shows the broadening of the HOMO and LUMO levels in the solid state, representing a more realistic picture of an OTFT. In the solid state, there are many molecules and thus many contributions to the FMOs, each one being of slightly different energy due to the different molecular arrangement sin the solid state, minor lattice defects and impurities. One consequence, is that the LUMO has one node less than the HOMO, and gives rise to fewer LUMO levels in the solid state. One assumption is that due to the greater number of HOMO states, organic molecules will be more biased towards p-type behaviour, but this is not strictly true for all OSCs[24].
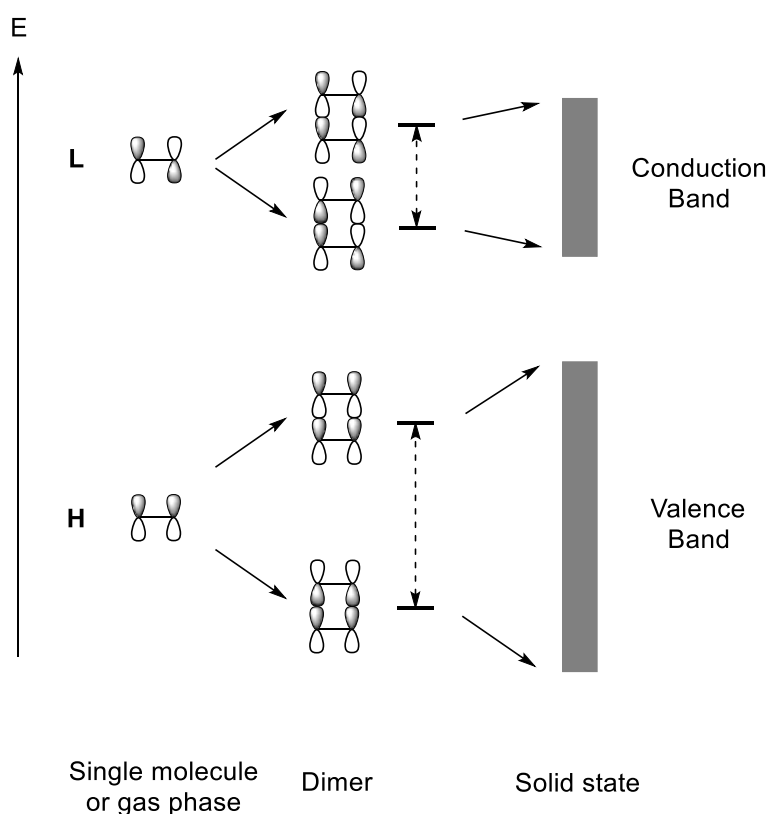
Figure 7. FMO bonding and antibonding arrangements of a single organic molecule (or gas phase), the HOMO and LUMO level splittings of two organic molecules and the valence and conduction bands of many organic molecules in the solid state.

2.3 Charge Transfer Mechanisms

The study of hole and electron charge transport dates back more than 60 years[25–27] when the nature of photo and electronic behaviour in organic semiconductors were first studied[28–30]. Purity was recognised early on as an important factor, which led to studies on high-purity organic crystals[31–36] particularly by industry such as Xerox, Kodak and IBM among others[37–40]. The theoretical work by Kenkre and co-workers[41–43] described electron-phonon interactions (phonons are lattice vibrations of the solid-state material) in highly ordered systems, while Scher, Lax and Montroll focused on disordered materials[44,45]. To date, there is no definitive or exact model that yet exists for a wide temperature range and satisfies all device architectures and molecular structures[46]. Hence, a general overview of the two most important types of charge transfer mechanisms are briefly discussed.

2.3.1 Multiple Trapping and Release (MTR)

This model assumes the charge transport is dependent on the gate voltage bias, such that in the presence of a small bias, traps are localised and the mobility is small. With a large bias, these traps are filled to the point of saturation, until they are released by a thermally-activated process[21,47]. In practice, the bias is constant, but the effect takes time to permeate through the dielectric and thus the effect of the bias on the charges in the semiconducting layer is increased with time until the saturation regime is occurred; upon which the charge transfer mobility is measured.

2.3.2 Polaron Hopping

A number of early theories were successfully applied such as band theory[48] and the polaron effective mass approach[49], but these were restricted to specific cases. Generalised approaches were developed on the electronic coupling over a range of parameters such as temperature and included the density matrix approach[50] or more recently the dynamical mean-field theory[51]. The consensus now is that the overall charge transfer mobility is a combination of two components, the tunnelling (coherent transfer) which dominates at low temperatures and hopping (incoherent transfer) contributions, which dominates at high temperatures; high temperature as

described in charge transfer models is generally any temperature above cryogenic conditions, *i.e.* room temperature.

In this model, charge being either an electron or a hole, is transported through a material by polaron hopping between localised states[21]; where a polaron is the deformation of the solid-state molecular lattice around the electron or hole. These localised charge states are on the molecules, and thus the charge hops from one molecule to another, sometimes being trapped in between molecules on crystallographic defects or impurities that are left over from synthesis. The activation energy required to propagate the charge beyond the trap gives rise to the thermal-activated nature of the polaron hopping model at elevated temperatures.

The small polaron theory[52] combines the above concepts and includes the contribution of the binding energy between the polaron and phonon interactions. Considering the polaron energy is half of the reorganisation energy, this theory is simplified into the exact equation of an older classical charge transfer model called Marcus Theory[53]. Its simplicity enables the three key charge transfer properties, namely the internal reorganisation energy, the transfer integral and the rate of charge transfer, to be routinely calculated[54] for both the hole and electron charges and aid experimental investigations[55,56] for the *in silico* design of high-performing organic semiconductors.

2.3.3 Summary

The observation of low-performing OSCs with high transfer integrals (100-200 meV) is found to only be due to its purity, which is now considered to be the most significant factor in charge transfer. The origin of the charge carrier trap states is more useful for practical OSC devices. It is commonly thought that impurities arising from the synthesis have a band gap which is too large to reside within that of the OSC and have lower HOMO levels or higher LUMO levels which cannot therefore act as trap sites. Thus, the presence of impurities will only act as a scattering centre for the delocalised carriers, rather than be charge traps; the net charge-transfer mobility will inevitably decrease but the underlying mechanistic factors is of importance to improve the field of OSCs.

Oxygen doping is found to be one of the greatest contributors to defects in the solid state, due to the presence of epoxides and ethers formed with the exposure of the OSCs to air. The oxygenated defects tend to impart a negative charge and act as traps for the hole, but in other cases as p-dopants thus improving some OSCs such as picene. The presence of oxygen is one of the most important factors for both understanding the mechanism of charge transport and measuring the charge mobility.

Recent models such as the extended polaronic band theory[57] based on localised dynamic disorder are still being debated in the literature[46], it is therefore acceptable to use the classical Marcus Theory for comparison between similar molecular systems, particularly with regards to properties such as reorganisation energies and transfer integrals. The charge transport phenomena in OFETs was also found to be a combination of the MTR and polaron hopping with oligothiophenes[55], and thus it is clear that more work needs to be done on charge transfer mechanisms. It is still worth noting the progress of developing theories in the literature, but for immediate practical purposes, classical theories are suitable for studies such as virtual screenings *a priori* to experimental investigations.

2.4 Molecular Classes of Small Organic Semiconductors

Small molecules have been widely studied for semiconductors because they are easy to purify and readily form crystalline films for electronic devices[10]. The small molecules are aromatic hydrocarbons in nature and consist of multiple fused rings called acenes or with heteroatom derivatives called heteroacenes. Their conjugation is typically linear, such that the rings are bonded together giving ladder-like molecules. They commonly consist of, but not limited to, a central core with several aromatic fused rings both sides and capped with aromatic or alkyl groups. The purpose of both the molecular structure and the terminal groups are to facilitate close packing in the solid state, leading to crystallinity and thus better semiconductor properties.

A rich diversity of molecular structures are currently available and new ones are routinely synthesised from rational design to improve the physical properties such as charge transport. This leads to numerous derivatives in the literature and eventually to wide structural classes of semiconducting molecules, some of which have been briefly highlighted in this section. The acenes, for example, consist of two to seven fused phenyl units and selected structures are illustrated in Figure 8. Charge-carrier mobility usually increases with the number of fused aromatic rings on the molecule, due to greater π-π interactions obtainable in the crystalline state. One significant disadvantage of the acenes is their poor solubility in common organic solvents resulting in both purification and fabrication difficulties, due to their hydrophobic, fused rings. Therefore, derivatisation with alkyl or hetero substituents are advantageous for improvement of both chemical and physical properties. These substituents can be joined to the centre or *peri* positions such as the symmetric acenes or acenequinones (**1**), or towards the end of the molecules like the halogenoacenes (**2**) and asymmetric quinones (**3**). Both halogen and carbonyl substitution can alter the electronic and electrostatic interactions between the molecules, thus affording different packing arrays. Alternatives to linear, rod-like structures include fused-ring clusters such as pyrenes (**4**), or propeller-like molecules which have naphthyl cores with alkyl side groups (**5**). Other combinations exist with perylenes (**6**), where halogen substituents and derivatised terminal groups structures such as succinates and succinamides.
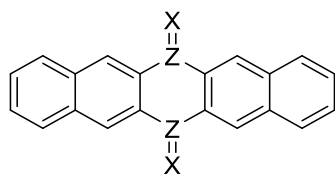
X = H,O; Z = C,N

Symmetric Acenes and acenequinones (**1**)
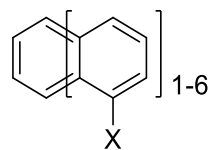
X = Cl, Br

Halogenoacenes (**2**)
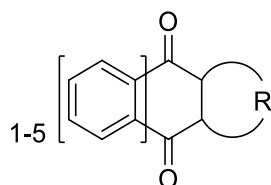
R = alkyl, aryl

Asymmetric acenequinones (**3**)
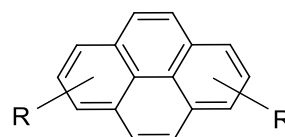
R = aryl, thio

Pyrenes (**4**)
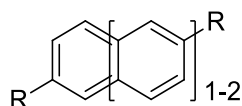
R = anthryl, thio, thienothio, alkyl

Naphthyls (**5**)
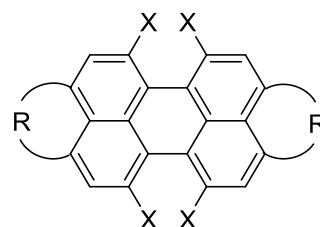
R = H, succinate, succinimide X = H, F, Cl, Br

Perylenes (**6**)

Figure 8. Class types for fused-ring acene-based small molecules.

If heteroatoms are substituted in place of carbon atoms in the fused rings, the result are a series of molecules generally called heteroacenes. They are a mixture of both phenyl rings and five membered heterocycles, such as indoles, furans and thiophenes. These can be arranged in a number of ways, where two common configurations include the heterocycle either at the centre (benzodi[hetero]phenes, **7**) or on the edges (dibenzo[hetero]phenes[58], **8**); a third variant is to combine these to give the heterocycle both at the centre and at the edges which are separated by phenyl rings (di(benzothieno)thiophenes, **9**), as illustrated in Figure 9.

Z = S, Se;

R = aryl, alkyl

Benzodithiophenes

(**7**)

Z = S, Si, CR$_2$;

R = alkyl, alkyne

Dibenzothiophenes

(**8**)

Z = S, Si, CR$_2$;

R = alkyl

Di(benzothieno)thiophenes

(**9**)
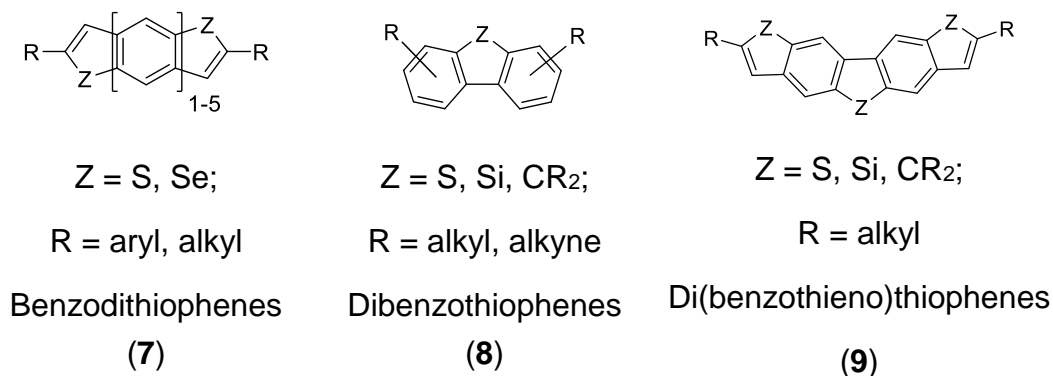
Figure 9. Heteroacenes containing phenyl and thiophene units.

Another type of heteroacene consists only of five-membered units, such as thienothiophenes (**10**) and dithioenothiophenes (**11**), but could also include other element such as silicone, carbon and nitrogen-based derivatives[59] (Figure 10). The solubility of these compounds is determined by the length and nature of the R group.

Z = CR$_2$, S, Se, Te, Si;

R = alkyl, thio, styryl

Thioenothiophenes (**10**)

Z = S, Se; Y = CR$_2$, Si, NR$_2$;

R = alkyl, thio, styryl, ketophenyl

Dithioenethiophenes (**11**)
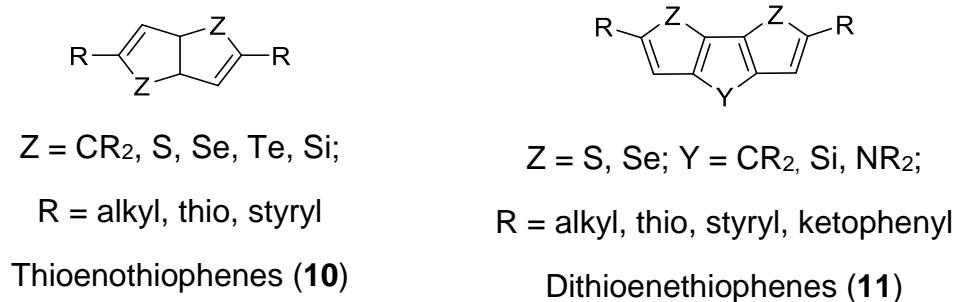
Figure 10. Five-membered heteroacenes.

A specific type of derivatives at the *peri* positions include alkyne functional groups and terminally capped with trialkylsilyl, alkyl or aryl groups which stabilises the alkyne and improves solubility (**12**, Figure 11). The change of positioning form peripheral to *peri* may alter the close packing motifs of the molecules in the crystalline state from herringbone to brick-weave or slipped-stack; this change in lamellar packing was reported with the exchange of ethyl[60] for propyl[61,62] groups. In addition to improvement to molecular packing and thus mobility, the silyl groups also impart solubility giving good solution processing possibilities.
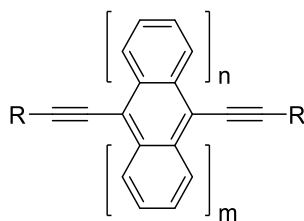
R = H, SiMe$_3$, alkyl, aryl

Figure 11. *Peri-*alkyne acenes (**12**).

While some heteroacenes can display intrinsic n-type characteristics such as indoles and thiazoles, from the nitrogen substitution in the rings, p-types can be tuned to perform as n-types, from substituting the peripheral C-H units for specific halogens such as fluorine. In general, heteroatoms tend to stabilise the structure towards electron charge transfer due to their tendency to retain excess electron charge from their electronegative strength. Hence, any conventional p-type organic semiconducting structure can be turned into an n-type *via* substitution with either nitrogen or fluorine, either directly into the rings or around the peripheral C-H positions, including the alkyl chains. It is therefore reasonable to consider the investigations of p-types primarily with the knowledge that n-type behaviour can be tuned at a later date. Specific examples of p- and n-types are given in section 2.5.

2.4.1 Leading Examples of Organic Semiconductors

Picene (**14**) was investigated by Okamoto *et al.*[63] due to the parent isomer, pentacene[64,65] (**13**), having high charge transfer physical properties but low air-stability. Low HOMO-LUMO gaps (E_g) may lead to oxidation and decompose in the presence of light. For example, **13** has an E_g gap of 1.8 eV in comparison to **14** with 3.3 eV. Under an atmosphere of oxygen, an OFET device of the bottom-gate top-contact type with **13** was observed to have a mobility in the single crystal and thin-film states of 40.0 and 5.0 cm^2 V^{-1} s^{-1} respectively; the thin film mobility of **14** is 1.1 cm^2 V^{-1} s^{-1}.
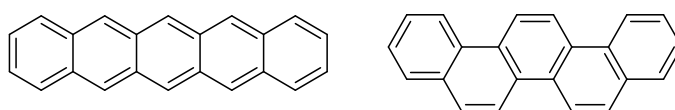
Figure 12. Pentacene (**13**) and Picene (**14**).

A tetraphenyl-substituted acene (rubrene, **15**)[66,67] was found to have the second highest mobility (24.5 cm^2 V^{-1} s^{-1}) after pentacene. Rubrene was the first high-performance OSC that broke the accepted design rule of planarity, as the peripheral phenyl rings have significant steric repulsion and hence stick out perpendicular both to the core surface and molecular axis. The reason for the high mobility, turns out to be due to the molecules stacking not just in a cofacial array between the core unit, but also in a lateral array with π-π interactions between the paddle-like phenyl rings, forming three-dimensional charge transfer capability. The issue is that rubrene is highly insoluble, and requires vacuum processing multiple times to remove impurities prior to OTFT fabrication.
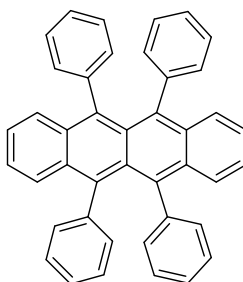
Figure 13. Structure of rubrene (**15**).

Mullen *et al.*[68] reported the synthesis of the hexyl derivative of dithienobenzodithiophene (DTBDT-Hexyl, **16**, Figure 14) in a two-step route giving product in a total yield of 86 %. The shifted co-facial crystal structure from π-π and S-S interactions promotes 2D charge mobility. It was initially fabricated into a semiconducting thin film as part of a bottom-gate, top-contact OFET device from spin coating in chloroform; the observed mobility reached 1.2 cm^2 V^{-1} s^{-1}. Using the same type of OFET architecture, new devices were fabricated *via* dip-coating in toluene reaching a charge mobility of 1.7 cm^2 V^{-1} s^{-1}.

Uemura *et al.*[69,70] reported the structures for derivatised benzothienobenzothiophenes (BTBTs, **17**); these molecules consist of a thienothiophene core fused either side with phenyl units and capped with alkyl derivatives. Two synthetic routes were reported, either starting with the core BTBT and derivatised *via* Friedel-Crafts acylation and Wolff-Kishner reduction, or Sonogashira coupling of diiodo-BTBT and catalytic hydrogenation, with an average total yield of 70 % for each pair of steps. Out of those reported, the mobilities of the alkyl derivatives C$_{11}$H$_{23}$, C$_{12}$H$_{25}$ and C$_{13}$H$_{27}$ range between 0.73-1.76, 0.44-1.71 and 1.20-2.75 cm^2 V^{-1} s^{-1} respectively. Similarly, Takimiya *et al.*[71] also synthesised phenyl derivatives using a substituted stillbene starting material. The final step between the diiodo-BTBT and phenyl derivative was accomplished with a Suzuki-Miyaura[72] coupling affording target product in a 52 % yield for that step. The DPh-BTBT obtained mobilities between 0.93-1.2 for hexamethyldisilazane (HMDS) and 1.0-2.0 cm^2 V^{-1} s^{-1} for octyltrichlorosilane (OTS) treated Si/SiO$_2$ only at 100 °C. These are exemplary molecular architecture semiconductor components for OFET devices with desired physical properties.

It is rational to continue the conjugation of a successful system such as with BTBTs, which were extended to form dinaphthothienothiophene (DNTT) molecules (**18**) by Takimiya *et al.*[73]. DNTT is synthesised in a three-step route affording target product in total yield of 39.4 %. The lowest mobility value obtained in this specific study is 0.73 cm^2 V^{-1} s^{-1} on HMDS modified Si/SiO$_2$ substrates at room temperature and highest value of 2.9 cm^2 V^{-1} S^{-1} on OTS at 60 °C; single crystals gave a mobility of 8.3 cm^2 V^{-1} S^{-1}. The DNTT molecules are air-stable and have better charge transfer properties than BTBT molecules.

Developing these types of molecular architectures further, a type of molecule called Dibenzodithienothiophene (DBDTT, **19**) was synthesised by
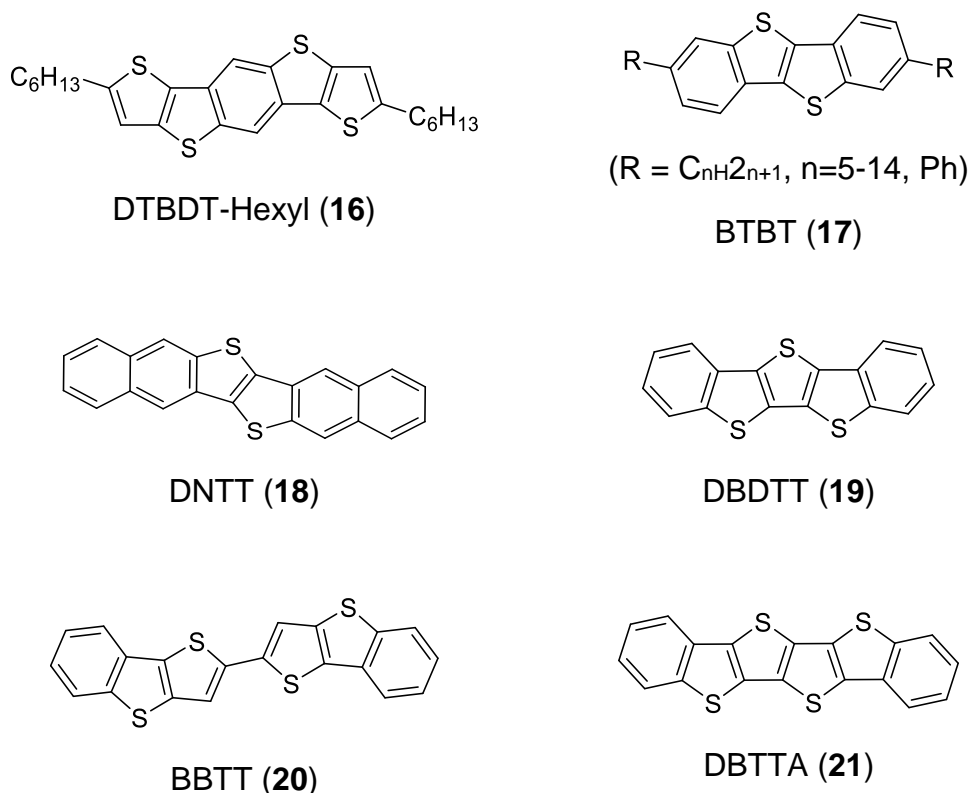
Figure 14. Molecules with thienothiophene and dithienothiophene cores.

Hu *et el.*[74], which gave single crystal mobility of 1.80 cm^2 V^{-1} S^{-1}, but no thin film due to poor solubility. BBTT (**20**) and DBTTA (**21**) have hole charge transfer mobilities of < 0.01 and 0.15 cm^2 V^{-1} s^{-1} respectively[75], showing the significant increase in mobility by an order of magnitude between the oligomeric and a fused-ring cores of these heteroacenes.

Neckers *et al.*[76] synthesised curved benzo[b]thiophene analogues of pentacene with five fused-rings each (Figure 15). The route to these two compounds involved condensation, reduction and recrystallisation steps and were column-chromatography free, which allowed for fast upscaling; the purification method in some steps involved recrystallisation. **22** and **23** are highly stable given their helicene-like nature and should have interesting optoelectronic properties in future studies.
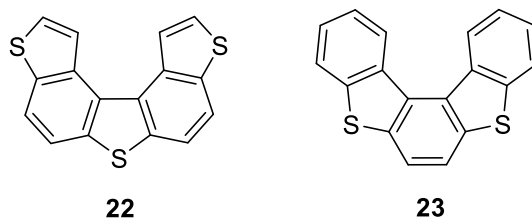
Figure 15. Benzo[*b*]thiophene analogues of pentacene.

In addition, a series of *trans*-dithienothiophene derivatives investigated by Wang, Hu *et al.*[77] has uncovered one particular species **24** (Figure 16), which consists of an oligomeric alkene bond at the centre which bridges two thiophene-based fused-ring segments and are capped with phenyl rings; this structure has a relatively high mobility range between 1.5-2.0 cm^2 V^{-1} s^{-1}. **24** is synthesised in a three-step route, starting with the Suzuki coupling of 2-dithienothiophene to phenyl boronic acid. A Vilsmeier-Haack reaction adds an aldehyde group to the available 2' position which is subsequently self-condensed in a McMurray reaction using titanium tetrachloride/zinc in tetrahydrofuran affording the product in a total yield of 50.1 %. Wang suggests that its exceptional charge mobility is due to strong intermolecular interactions arising from the phenyl units and facilitates a closer packing array in the crystalline state compared to other alkyl derivatives investigated.

24
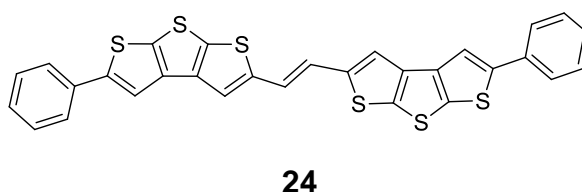
Figure 16. *Trans*-1,2-(dithienothiophene)ethene (**24**).

Figure 17 shows a derivatised all-thiophene heteroacene, septa-thiophene (**25**), although many linear variations of different number of rings have also been synthesised[78]; the long alkyl chains ensures solubility in common organic solvents. This linear structure is similar to pentacene, except the thiophene heterocycles are fused back-to-back in an alternating manner down the length of the structure. Although no mobility data is available, these are important structures with high thermal stability, in excess of 380 °C, and the single crystal packing is a π-stack arrangement, rather than herringbone
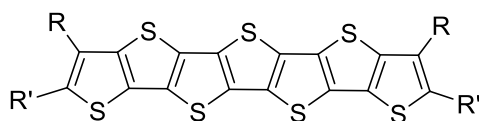
Figure 17. Derivatised septa-thiophene (**25**); R = Me, C_6H_{13}, R' = $C_{10}H_{21}$.

as observed with pentacene. The two alkyl chains ensure excellent solubility for thin-film formation and potential OFET characterisation.
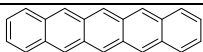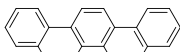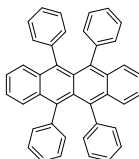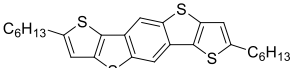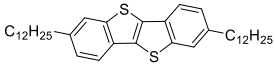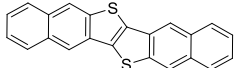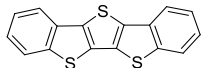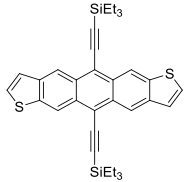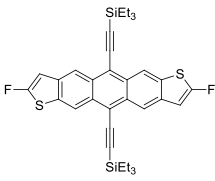
Anthony *et al.*[79] synthesised a mixed heteroacene of phenyl and thiophene rings, with silyl-derivatised *peri* alkyne substituents (**26**), as well as a fluorine derivative at the thiophene's 2-positions (**27**). The drop-cast films of **26** yielded devices with charge-mobilities up to 1.0 cm^2 V^{-1} s^{-1} (Figure 18). Unfortunately, it suffers from charge-injection barriers between electrode interfaces and photo-bleaches in several minutes upon radiation exposure. On the other hand, it is synthesised in a single step from anthradithiophenequinone in 91 % yield[80] and relatively low reaction conditions. This is due to substitution at the 5 and 5' positions of the thiophene rings and electronic changes induced due to the electron-withdrawing fluorine. Interestingly, unlike *iso*-propylsilyl derivatives, the ethylsilyl fluorinated anthradithiophene does form crystalline thin-films; with an average charge-transfer mobility of 0.7 cm^2 V^{-1} s^{-1}. Selected p-type structures and properties are collected together and presented in Table 1.

26

27
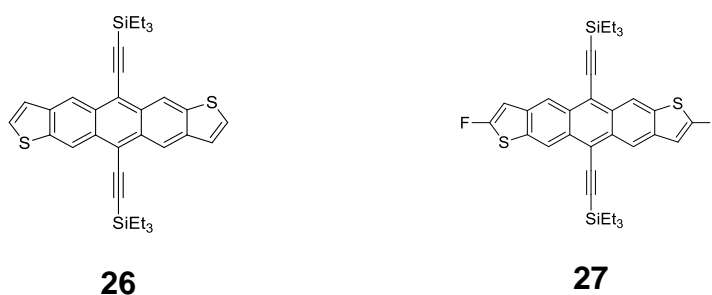
Figure 18. Alkyne-anthradithiophenes derivatives.

Table 1. FMO energies and hole mobilities of selected high-performance ($\mu > 1$ cm^2 V^{-1} s^{-1}) p-type organic semiconductor structures measured either as a single crystal (SC) or as a thin film (TF); (-) designates no value available, due to either no data or instability of the structure.

Entry	Structure	$\mathcal{E}_H$	$\mathcal{E}_L$	E_g	μ_{SC}	μ_{TF}
13		-5.00	-3.20	1.80	40.00	5.00
14		-5.50	-2.20	3.30	-	1.10
15		-5.36	-3.15	2.21	24.50	-
16		-5.56	-2.20	3.36	-	1.70
17		-5.50	-2.00	3.50	-	1.76-3.90
18		-5.44	-2.44	3.00	8.30	2.90
19		-5.60	-2.14	3.46	1.80	-
26		-	-5.31	-	-	1.00
27		-	-	-	6.00	1.50

Marks and Facchetti *et al.*[81] synthesised a particular n-type semiconductor **28** containing keto groups and fluorinated alkyl chains flanking four thiophene units bonded at the 2 and 5-positions, as shown in Figure 19, in a four-step synthesis. It has a mobility of 0.6 cm^2 V^{-1} s^{-1}, but one year later this was improved[82] to 1.7 cm^2 V^{-1} s^{-1}. Interestingly, the later report is a significant variation between a number of silica-treated substrates, showing that pre-treatment or selectively choosing the substrate is critical to achieving the best possible device performance.
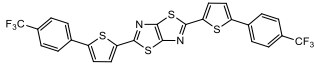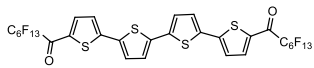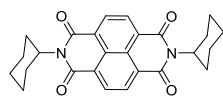
Yamashita *et al.*[83] synthesised **29**, also shown in Figure 19, which consists of a bi-fused thiazole capped with thiophene derivatives, in 18 % yield from corresponding aldehyde and dithiooximide starting reagents. Yamashita reported its mobility in 2005 to be of only 0.3 cm^2 V^{-1} s^{-1} and in 2007 a mobility of 1.2 cm^2 V^{-1} s^{-1} was observed for thin-film semiconductor OFET devices. The change is due to the silica dielectric being pre-treated with long alkyl chains which suppresses the electron trap sites. These two examples by Marks and Yamashita show that not only is the molecular structure critical for desirable properties, but the substrate's surface of the dielectric is also significant for good interaction and thus high charge mobilities. Fortunately, the substrate treatment is a type of device fabrication and is not fundamental to the molecular structures; although important, this can be removed from structural design considerations.

Cylohexyl-naphthalene diimide structures (**30**) synthesised by Shukla *et al.*[84] exhibited high n-type mobilities of 6.0 cm^2 V^{-1} s^{-1} in air, which is a significant improvement over **28** and **29**, especially as it has no fluorine substituents. Moreover, these high mobilities were reached as OTFTs before single crystal measurements, which have yet to be completed.

28

29

30
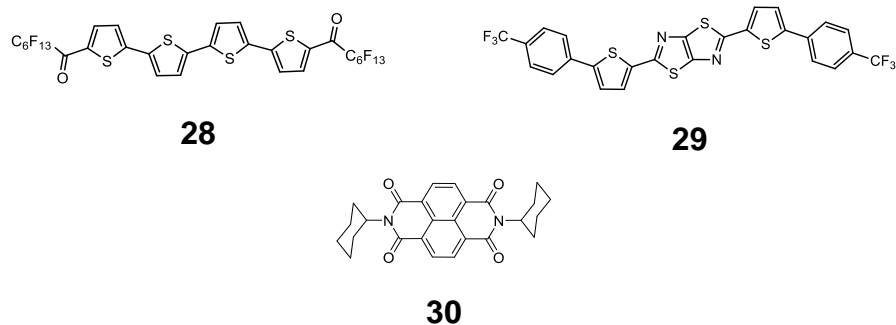
Figure 19. Some specific n-type small molecules with $\mu > 1$ cm^2 V^{-1} s^{-1}.

Table 2. FMO energies and electron mobilities of selected high-performance (μ > 1 / cm^2 V^{-1} s^{-1}) n-type organic semiconductor structures measured either as a single crystal (SC) or as a thin film (TF).

Entry	Structure	ε_H / eV	ε_L / eV	E_g / eV	μ_{SC} /	μ_{TF} /
28		-5.64	-2.68/ -2.82	2.96	-	1.20
29		-6.36	-3.96	2.40	-	1.70
30		-6.97	-3.71	3.26	-	6.0

2.5 Challenges

2.5.1 Solubility

As discussed above, organic electronics need to satisfy a number of practical requirements of devices, such as the stability and fabrication of the semiconducting thin film. This is non-trivial because the ideal molecules are inherently insoluble due to their extended π-conjugation. Techniques such as vapour deposition have been extensively used, however, it is high cost and slow production[5]. An answer to this problem is to use solution-process techniques whereby the semiconductor is rendered soluble in organic solvents through derivatisation during its synthesis, such as alkylated thiophenes[85] and acenes[86]. Another form of solution processing is the generation of the final stage of the organic semiconductor using thermal treatment or photoirradiation, and have been achieved with linear acenes[87]. However, their physical properties such as electrical conductance significantly change according to the process used, due to their close packing arrays or relative alignment towards one another in the crystalline state once processed.

Overall, there are few examples of organic semiconductors that can be solution-processed and maintain relatively high charge transfer mobilities, and include those of the benzothienobenzothiophene (BTBT) derivatives[69] (**17**) and silyl-alkyne substituted heteroacene analogues of tips-pentacene[60] (**27**); their structures are reillustrated in Figure 20. These exemplary structures highlight the nature of the bonding array for high-performing candidates with thiophene heterocycles both in the core and peripheral, with alkyl, fluorine and TES derivatives.

R = alkyl

BTBT (**17**)   (**27**)
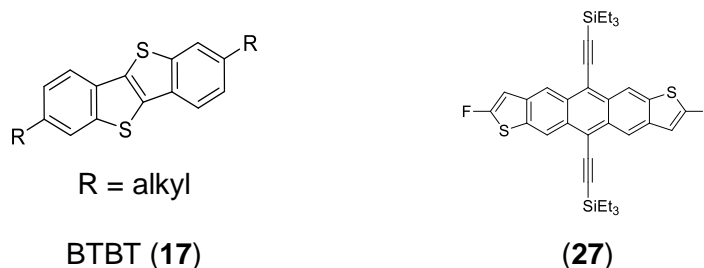
Figure 20. Exemplary structures (**17** and **27**) for solution-processed OTFTs.

2.5.2 Air-Stability

Ambient processing conditions are ideal for large scale manufacture of organic electronics but not all OSCs are suitable, such as with pentacene, and thus their air-stabilities are an important factor. While there is no specific value that governs air-stability, one measure is to compare the HOMO-LUMO gaps of identified targets against known OSCs. With an increasing number of experimental investigations[5], basic structure-property comparisons can be deduced. For example, Figure 21 shows the increasing benzothiophene homologues with two phenyl rings added each time. It is clear the HOMO-LUMO gap decreases with heteroacene length. Although the dianthracenethienothiophene (DATT)[88] (**31**) was found to be air stable with an exceptional single crystal hole mobility (12.3-16.0 cm^2 V^{-1} s^{-1}), the gap is approaching that of pentacene, and thus it can be considered that there is a limit to the length of a fused ring target and thus the charge transfer mobility obtainable with small molecule OSCs. However, it is interesting to note that the gap of DNTT is much greater than that of pentacene, even though DNTT has an extra fused ring; this is probably due to the stabilising nature of the fused TT units in the core. Thus, air-stability remains a challenging problem in organic electronics.
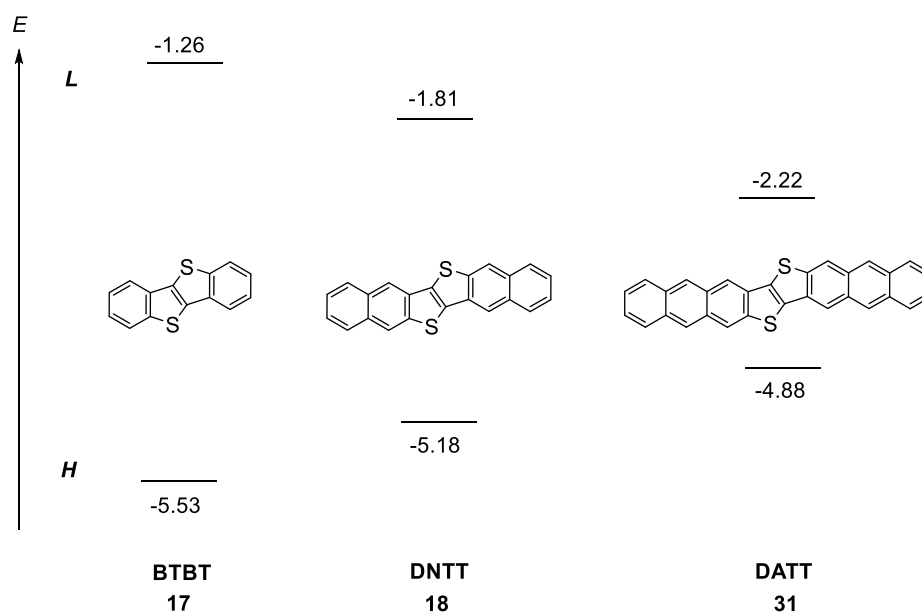
Figure 21. Decreasing HOMO-LUMO gap (in eV) with increasing heteroacene length.

2.5.3 Molecular Packing and Charge Transfer

While most types of conjugated small molecules lead to a stacked motif[10,79] from π-π interactions, it is known that aryl terminal groups facilitate edge-face (Figure 22 A) interactions from hydrogen bonding of C-H and π-surface of fused rings; together these lead to a 'herringbone' type packing. On the other hand, alkyl terminal groups block the edge-face interaction and which leads the molecules to be stacked closer together and thus giving either 'brick-weave' (Figure 22 B) or 'slipped-stacking' (Figure 22 C) motifs. In small molecules, the charge carriers move between the molecules in the direction perpendicular to the molecular face and hence parallel to the z axis of the π orbitals. Therefore, the molecules' faces which stack closer together in the crystalline state tend to facilitate greater charge-carrier mobility and are highly desirable for practical semiconducting device applications. This understanding is vital to improve the organic semiconductor charge-transfer properties and thus the overall solid-state device operations. However, morphology predictions are not exact theories and crystal engineering has to date failed to outline any principles for the design of high-performing structures other than planarity.

A   B   C
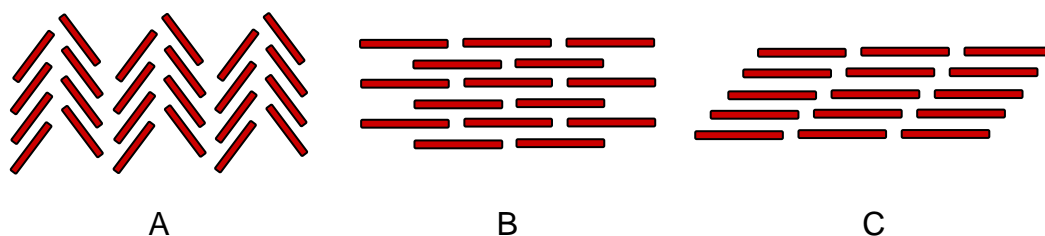
Figure 22. Organic semiconductor crystalline packing motifs of (A) edge-face, (B) brick-weave and (C) slipped-stack[8].

2.5.4 Resources

The nature of experimental investigations for the synthesis of novel structures tends to generate high quantities of chemical waste and consume large amounts of time. Once a number of structures are synthesised, they are fabricated into OFET devices and their charge transfer mobilities are

measured; for reliable data and to ascertain the greatest mobility, each structure is fabricated into five or more separate devices for each substrate conditions, potentially generating in excess of 20 devices for only four conditions, which may include variations in surface treatment, temperature, deposition flow rate, length of channel between electrodes and device architecture. The highest performing structures are identified and derivatised to generate a new library for synthesis and testing. This iterative process requires significant quantities of chemical resources for synthesis as well as the access to OFET fabrication facilities. It is clear this costly process needs development to cut resources. The potential solution arises with theoretical computational chemistry, where multiple structures have their physical properties virtually screened and compared to existing experimental observations (or use very high accuracy theories in the absence of experimental data). Computational chemistry approaches are now more easily accessible and reliable due to advances in theory and simplification of the software. The other advance is computational power, which has significantly improved over the last few decades, to the extent that virtual screening in the pharmaceutical industry is now relatively common, but is yet to be fully realised in the fields of organic electronics materials chemistry; this approach is explored further in Section 2.6.

2.6 Computational Chemistry for Materials

Although a relatively recent technology, modern computational methods, especially in chemistry, have a rich history decorated with Nobel Prize awards. In 1954, Linus Pauling was granted the prize in chemistry for his research into the nature of the chemical bond and its application to the elucidation of the structure of complex substances. Robert Mulliken won the award in 1966 for his fundamental work concerning chemical bonds and the electronics structure of molecules by the molecular orbital method; now commonly used for atomic charge analysis. The award in 1971 was given to Gerhard Herzberg for his contributions to the knowledge of electronic structure and geometry of molecules, particularly free radicals. In 1981, Kenichi Fukui and Roald Hoffmann received the award for their theories concerning the course of chemical reactions. The Fukui index, is now a commonly computed 'local descriptor' parameter regarding the reactivity of a substituent on a molecule towards electrophilic or nucleophilic attack. In 1986, Dudley Herschbach, Yuan Lee and John Polanyl received the award for their contributions concerning the dynamics of chemical elementary processes. In 1992, Rudolph Marcus received the award for his contributions to the theory of electron transfer reactions in chemical systems. Marcus theory is now the staple theory of choice for classical charge-transfer systems, due to its intuitive nature and easy applicability. With the award of 1998 Nobel Prize in chemistry being awarded to Walter Kohn for his development of density functional theory and John Pople for his development of computational methods in quantum chemistry, the foundations of computer simulation were made famous and accessible to experimentalists. In 2013, the prize was awarded to Martin Karplus, Michael Levitt and Arieh Warshel for their work on multiscale models for complex chemical systems, including electronic structure, dynamics and macromolecular structures such as DNA and enzymes.

These many awards clearly show that the fundamental investigations in physical chemistry were not single arbitrary discoveries, but a continuous and dynamic field that helped to develop and cement future computational modelling techniques. These techniques enable (1) the investigation of fundamental questions and phenomena currently unavailable to exploration by experimentalists and (2) its predictive nature enables a fast-track screening approach to help rationally-design structures based on iterative computational calculations, benchmarked against known experimental observations. These

calculations aid the development of high-performing structures, for a multitude of fields from drug-discovery to material chemistry.

The current approach to molecular modelling involves the construction of the targets in question in a molecular editing program and subsequent calculation of properties by running a certain algorithm. These algorithms are conveniently wrapped up into functionals which are specified in the calculation input as 'key words' (commands), and the raw data is received upon completion. The data is either read as given or viewed back in an editor to give direct structure-property relationships. These relationships help to formulate design rules for the creation of new targets, thus leading to libraries of candidates for investigation. These libraries can be iteratively screened through computational methods to accelerate the discovery of high-performing materials. The only drawback is that computation power is limited to (1) the number of processors, (2) the type/architecture of processors and (3) the arrangement of processors to give maximum calculation power. All three are beyond the scope of this work, but are useful to grasp the current limitations in computation, which will hopefully one day be exceeded.

2.6.1 Computational Theories

2.6.1.1 Molecular Mechanics (MM)

Molecular mechanics (MM) are methods that uses classical mechanics to model the structures and interactions of molecular systems[89]. However, these interactions are limited to dynamics, potential energy surfaces and conformational changes, and do not include properties of interest for organic electronics such as ionisation energies or charge transfer. MM methods are nevertheless hugely useful to generate a classical molecular structure before quantum mechanics calculations are performed, thereby minimising computational time for accurate methods. MM can be combined with QM giving MM/QM approaches for investigations which look at the charge transfer between a donor and acceptor system[90]; although the QM and MM calculations are still performed individually for the bulk and interfaces respectively.

The potential energy of a system is determined with MM methods from the application of a specific force field, which is a mathematical function used to determine the geometry and energy of the chemical bond strength (and therefor length) between two or more atoms. There are a number of different types of force fields, and include 'all-atom', which provides mathematical terms for every atom type; 'united' treats carbon and hydrogen atoms as one interaction centre; 'course-grained' treats whole molecules crudely and focuses on intermolecular interactions of large systems, commonly deployed in biological calculations such as for enzymes and proteins.

These types of force fields are routinely developed and are sometimes specific to certain types of molecules *i.e.* macromolecules and proteins, or generalised for a wide range of molecular structures and all atoms in the periodic table. Examples include the Assisted Model Building Energy Refinement (AMBER)[91], for proteins, the Merck Molecular Force Field (MMFF)[92] for a broad range of molecules; and the Universal Force Field (UFF)[93], a general force field with parameters for all elements in the periodic table and applicable to a broad range of small and macroscopic molecules.

2.6.1.2 Semi-Empirical Methods

Semi-empirical methods are based in quantum mechanics, namely the Hartree Fock (HF) formalism[94], and makes approximations from empirical

data. HF-based methods approximates the wave function and the energy of a 'many body system', such as atoms and molecules; HF wavefunctions are derived from the Schrodinger equation[95], but it is not necessary here to detail explicitly. Although semi-empirical type methods are not used for high accuracy calculations, they are useful for making initial calculations and determining basic properties for later more accurate calculations with other theories.

Specific methods include the intermediate neglect of differential overlap (INDO), which can be used for the calculation of electronic band structure of semiconductors[96], as well as ground and excited states using the modified neglect of diatomic overlap (MNDO) method[97,98].

2.6.1.3 *Ab Initio* Methods

'*Ab initio*' means 'from the beginning', and are invoked with computational functions that are formulated from first principles[99,100]. *Ab initio* methods are commonly described in conjunction with their theoretical levels, which is a combination of how the electrons are treated with how many electrons and orbitals are considered (*i.e.* first, second, third *etc.* row of elements in the periodic table). The number of electrons and orbitals are designated with a basis set, which dictates to the theory the specific operation to be included in the calculation. For example, low-accuracy basis sets just describe the first row of the periodic table, while higher accuracies include other rows. However, as the number of rows increase, so does the type of orbital to be considered, such as s, p, d *etc.* The basis sets can artificially increase accuracy by adding in extra orbitals and extra orbital interactions. This occurs by stretching (polarisation) and spreading (diffusion) the orbitals which has the effect of increasing the data size for each calculation; the time for the calculation increases to the power of the number of atoms. Therefore, higher accuracy calculations take longer to perform but have the advantage of reliable data.

Common basis sets known as the *split-valence* Pople basis sets, and include a number of different Gaussian functions. Small basis sets include 3-21G which include elements up to xenon, but do not account for all the electronic interactions, while 6-311G includes elements up to krypton but do include a greater proportion of interactions. Adding d-orbital polarisation (d) and diffusion (+) functions transforms a given basis set into 6-31+G(d), which is one of the most common basis sets used in *ab initio* methods. However,

even this basis set is applicable to small or planar systems and not necessarily suitable for non-planar conjugated structures and transition states. Larger basis sets that are described as 'complete' include 6-311++G(d,p). Other basis sets are available for similar accuracies but faster computation and include those of the correlation-consistent basis sets, such as valence double-zeta (VDZ) and valence triple-zeta (VTZ), although these take considerably longer to converge and thus more computational expensive in terms of time. In the theoretical level, the theory is given first, and then the basis set. Examples with post-HF and DFT methods discussed below include MP2/6-31+G(d) and B3LYP/6-31+G(d).

2.6.1.3.1 Post-HF Methods

These are a set of methods which aims to improve on the HF methods, by adding electron correlation terms into the functions which is a relatively more accurate description of the repulsion energies between electrons; whereas repulsion energies are only averaged in HF methods.

One type of post-HF method is the Møller-Plesset (MP) perturbation theory[101], which is a special case of the original Raylrigh-Schrödinger perturbation theory[102]. Briefly, the MP theory is based on one 'exact' function and an expanding series of perturbed functions, known as orders; the higher the order, the greater the accuracy. The overall function is denominated as MPn, where n=2, 3, 4, 5...*etc.* Although MPn methods are an improvement over HF methods, they suffer from poor convergence at high orders and spin-contamination errors, which relate to the mixing of degenerate energy levels, or those that are similar in energy such as the HOMO and HOMO-1 levels.

Another type is known as 'chemically accurate', where its mathematical formulation takes into account electron correlation to a greater extent than MP methods and have less than one kcal mol^{-1} of error in comparison to experimental observations. These include 'coupled cluster'[103] and 'quadratic configuration interaction'[104] and operate with both a single and a double excitation of the system, resulting in the coupled-cluster singles and doubles (CCSD) and quadratic configuration interaction singles and doubles (QCISD) methods, respectively. These are computationally expensive but are a highly accurate description of any given atomic and molecular system. In practice, only single-point calculations are performed with these methods on

pre-optimised molecular structures using other theories. An example is with calculation of the thermodynamic energy of reaction (ΔU_r), which may be of interest where experimental conditions are performed at either very low (cryogenic) or high (closed reactor) energies and thus difficult to measure.

2.6.1.3.2 Monte Carlo

Monte Carlo methods[105,106] are numerous and varied, but all focus on an iterative random sampling procedure to obtain statistical results. The accuracy depends strongly on the initial wavefunction estimate and is also extensively time consuming.

2.6.1.3.3 Density Functional Theory (DFT)

Density Functional Theory (DFT) incorporates a wide umbrella of methods, all of which use functionals[107] (functions of functions) to calculate the total electron density of a many-body system, such as molecules, which contains all the structural and physical properties. The functionals are mathematical operations that deal with the exchange correlation between a homogenous gas phase and local density approximations and now includes ground states of single molecules (gas phase), intermolecular interactions, and long-range corrections for ionic and partially-charged species. These functionals are divided between the pure (exact HF exchange) and hybrid (HF exchange with DFT-based exchange-correlation). The hybrid functionals use various percentages of HF exchange depending on the nature or property the functional is developed for. Each functional, pure or hybrid, is developed for a set of structures, bonding arrangements, intermolecular interactions or property calculations with respect to experimental observations, and in that sense, the specific functional is *customisable* depending on the requirement or system under investigation. From the perspective of applying DFT for materials discovery, the functionals can be *selected* by the user with all the added interactions for a given system and deployed within a given software. For example, while the pure functional Becke Lee Young Par (BLYP) may be useful for optimised neutral structures, ionisation energies are better modelled with (LC-BLYP). With two or more molecules, intermolecular interactions can be accounted for with Grimme's dispersion terms with either first, (D1), second (D2) and third (D3) order terms and with additional Becke-Johnson damping

(D3BJ); adding this gives LC-BLYP-D3BJ. It is clear that the customisable nature of DFT has clear advantages over other methods described previously.

In addition, a number of functionals have been written to include solution states through solvation 'polarisable continuum models' (PCMs); these put a cage like bubble around the molecule and apply the dielectric for the solvent of choice. Continuum models include the solvation quantum mechanical charge density (SMD)[108], isodensity PCM (IPCM)[109], self-consistent isodensity PCM (SCIPCM)[109] and conductor PCM (CPCM)[110,111]. The default in *ab initio* software such as Gaussian 09 is the integral equation formalism variant PCM (IEFPCM)[112,113]. These solvation models are routinely used to determine solvation-state excitations and reaction mechanisms.

Excited state functionals are also developed, known as time-dependent DFT (TD-DFT), and are used to probe both singlet and triplet excited states. Such calculations give an insight into the absorption or emission of ultra-violet, fluorescent and phosphorescent processes.

Overall, the principle disadvantage with DFT include its non-exact approximative nature; however, the ability to approximate the total density and extract all useful structure and property information is considered conversely to be its guiding advantage. Other advantages include low computational cost with regards to both power and time, extensive functional parametisation for every molecular geometry and interaction which includes excited states and long-range order, wide implementation in computational packages that are licensed to academic institutions such as Gaussian, limited spin contaminations due to the extra steps of exchange correlation, and numerous physical properties can be calculated.

2.7 Summary

A brief history of the discoveries of semiconducting behaviour and devices were reviewed, followed by common device architectures, energy conduction characteristics and charge transfer mechanisms. General molecular classes of small organic semiconductors were then illustrated, followed by more detailed discussion on specific and leading examples. It was found that although some of the highest-performing structures were acenes, these were unstable in air and requires vapour deposition under inert atmosphere, which is difficult for scaling up the production of organic electronics devices. The next leading examples were found to be the mixed class of heteroacenes, which are widely derivatised and soluble in common organic solvents, ensuring mobility measurements as a thin film and thus upscaling capability; stability was also excellent and some examples exceeded 380 °C. A selection of the most important challenges were discussed, such as stability, molecular packing for high charge transfer and overall resource issues. Due to the issues of reiterative synthetic chemistry, computational chemistry and virtual screening approaches were discussed to fast-track leading candidate discovery.

Overall, these literature insights have generated a deep level of knowledge and understanding of organic electronics and more specifically, structure-property relationships for organic semiconducting materials with applications in thin-film transistors. With these in mind, an informed project plan can be instigated to proceed with a novel and innovative research scope for the development of the next generation of OSCs across the broad spectrum of organic electronic applications.

Chapter 3

Project Plan

3.1 Aims

Rationally design, computationally model and synthesise high-performing candidates for organic optoelectronics, concerned with but not limited to, organic semiconductors for thin-film transistors, and could include optics and nonlinear optic applications. These structures will be soluble in common organic solvents for solution-processing into organic thin-film devices, such as thin-film transistors (TFTs); the molecular targets and their synthesis will be designed to be inherently soluble from their retrosynthetic strategies. Computational modelling will enable the designed structures to be virtually screened and will highlight those with superior properties out of a pool of possible candidates; such structures will be selected for synthetic investigations. This process reduces the time and chemical resources in the pursuit of high-performing organic semiconducting candidates.

3.2 Objectives

1. Explore the structural diversity of both low and high-performing candidates.
2. Identify molecular structures with appropriate functional groups that satisfy (i) solubility of the final targets in common organic solvents for solution processing; (ii) close packing of the structures in the solid phase; (iii) relatively high physical properties and identify ideal values for comparison.
3. Design two different libraries of molecular targets to investigate, focusing on structural arrangements such as their oligomeric or fused-ring nature. Where possible, diversify in terms of both heterocyclic units and heteroatomic derivatives. This ensures diversity for structure-property investigations and thus the subsequent selection of high-performing candidates.
4. Calculate fundamental physical properties that are intrinsic only to the target structures and not extrinsic to the device type or fabrication procedures. This focuses the research on the properties of the molecular structures rather than the performance of the electronic devices. Relevant physical properties for investigation include the hole mobility and stability, which can be determined form the calculation of the HOMO-LUMO energies and differences (E_g), vertical and adiabatic ionisation potentials and electron affinities, internal reorganisation energies, transfer integrals with different close-packing intermolecular distances, rates of charge

transfer, band gap (ground-1st excited state S_0-S_1) and linear polarisabilities and nonlinear hyperpolarisabilities. Compare all theoretical values with experimental observations where possible and compare to theoretical values in the literature.

5. Investigate reaction mechanisms and synthetic conditions that are relevant in the synthesis of the molecular fragments towards the target molecules. This will develop and broaden the investigations where necessary to deepen understanding and overcome any issues that may arise.

6. Conceive novel routes and synthetic conditions which may be attractive to industry, considering the highest total yield, simplicity of reaction, air and light stable intermediates, total reaction time and the commercial availability of relatively cheap materials where possible.

7. Generate and rationalise a retrosynthetically-designed forward route and synthesise the target compounds of both libraries, with full theoretical and experimental characterisation to fully elucidate their structures and their charge transfer properties. The characterisation techniques may include instruments such as NMR spectroscopy for region-positioning of the substituents through chemical shifts and coupling constants, namely with ^{1}H, ^{13}C, distortionless enhancement by polarisation transfer (DEPT), correlation spectroscopy (COSY) and heteronuclear multiple quantum coherence (HMQC); Fourier-transformed infrared (FT-IR) spectroscopy for vibrational analysis and confirmation of the synthesised functional groups and transition states; ultraviolet-visible (UV-Vis) spectroscopy for absorption with regards to optical stability, excited states and optoelectronic light-scavenging applications; mass spectrometry for compound identification pre- and post-purification (column chromatography/recrystallisation) with molecular weight, complementing the NMR data; elemental analysis for purity and X-ray single-crystal structures for absolute structure determination and solid-state analysis.

Chapter 4

Experimental

4.1 Theoretical and Computational Methods

4.1.1 General Procedures

The molecules were constructed and energy levels visualised in Avogadro (version 1.1.1)[114] and auto-optimised using UFF force field with four steps per update until δE = 0. All energies, properties and structures of any state were calculated with quantum mechanics/density functional theory (DFT) using Gaussian 09 (version D.01)[115] with various basis sets and functionals, but normally the Becke 3-parameter density functional with the Lee–Yang–Parr correlation functional (B3LYP)[116] and the complete 6-311++G(d,p) basis set[117–119] unless specified. All subsequent single-point DFT calculations for the charge transfer properties were performed in Gaussian 09 starting with the optimised structure at the same level of theory. Calculations were performed on a high-performance computer (HPC) in Leeds, the Advanced Research Computing node 2 (ARC2), which uses CentOS 5 Linux operating system and a 100 TB file system.

Marcus Theory[44] (Equation 1) was used to describe the charge transfer for organic semiconductor calculations, where the transfer is as a self-exchange between a neutral and a charged molecule. Two key parameters, the internal hole reorganisation energy (λ_h)[45], which is intrinsic only to the extent of relaxation between the neutral and cationic surfaces and upon which, the electron delocalisation of a molecular geometry plays a key part, and the hole transfer integral (t_h), which is the electronic coupling between the molecules in relation to the intermolecular separations between them. K_B is Boltzmann's constant, T is temperature (298.15 K used here) and ħ is the reduced Planck's constant. Ideally, internal reorganisation energies should be very small [46], *ca.* 0.1 eV.

A vertically ionised or reduced state is the immediate nature of a molecule which has gained or lost an electron and an adiabatic state is where the vertical state has subsequently relaxed to a minimum on its potential energy surface. The energy processes of electron-exchange, excitation and

$$k_{ct} = \left(\frac{t^2}{\hbar}\right)\left(\frac{\pi}{\lambda_{\pm}k_B T}\right)^{1/2} e^{\frac{\lambda_{\pm}}{4k_B T}}$$

Equation 1. Marcus Theory which describes charge-transfer between two adjacent molecules.
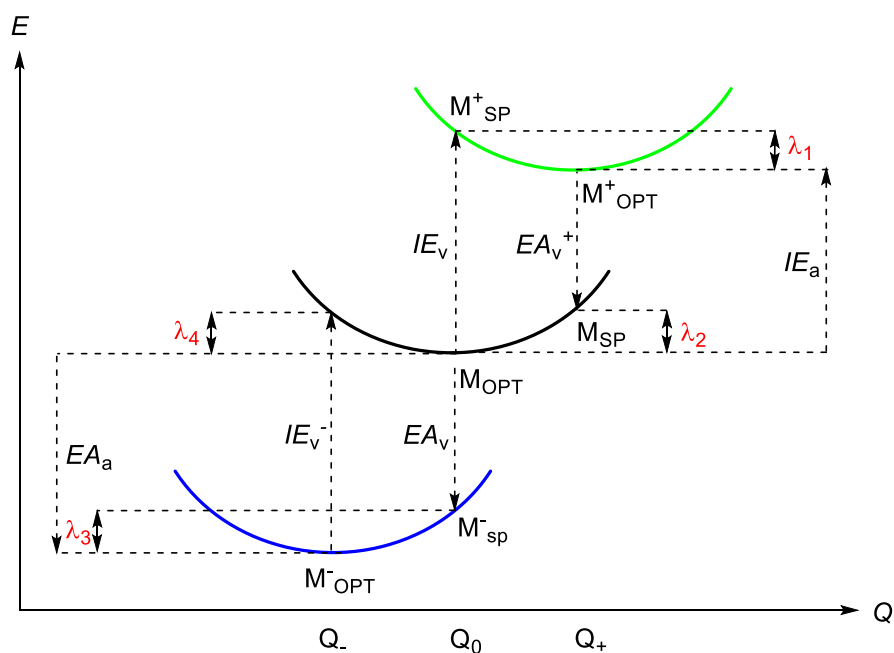
Figure 23. The ionisation energy (*IE*) and electron affinity (*EA*) pathways between the neutral (black), cation (green) and anion (blue) potential energy surfaces for the calculation of the hole (λ_h) and electron (λ_e) reorganisation energies, according to Marcus Theory.

relaxation are illustrated in Figure 23.

The internal hole reorganisation energy (λ_h) is comprised of two relaxation terms, the energy of the cationic (λ_1) and neutral (λ_2) surfaces, as defined in Equation 2.

$$\lambda_h = \lambda_1 + \lambda_2$$

Equation 2. The internal hole reorganisation energy as a sum of the reorganisation energy components of the neutral and cation states.

The cationic reorganisation energy λ_1 is determined from the difference between the vertical and adiabatic ionisation energies calculated *via* the vertical, single-point geometry of the cation (M^+_{SP}) and the optimised cation structure (M^+_{OPT}), (Equation 3).

$$\lambda_1 = E(M_{SP}^+) - E\left(M_{opt}^+\right)$$

Equation 3. The calculation of the individual reorganisation energy term for the cation state.

Addition of an electron to the minimised cationic structure returns the molecule back to its neutral potential energy surface and is performed with a vertical electron affinity of the cation, EA_v^+; the difference between this state and the minimum of the neutral molecule is λ_2 (Equation 4).

$$\lambda_2 = E(M_{SP}) - E(M_{OPT})$$

Equation 4. The calculation of the individual reorganisation energy term for the neutral state.

Similarly, the internal electron reorganisation energy λ_e, is calculated according to Equation 5, which is the difference of the relaxations between the anionic (λ_3) and the neutral (λ_4) surfaces. These terms are the differences between (i) the optimised anion (M_{OPT}) and a point on the anion surface, M SP (λ_3, Equation 6) and the optimised neutral structure and a point on its surface, $M_{SP'}$, (λ_4, Equation 7).

$$\lambda_e = \lambda_3 + \lambda_4$$

Equation 5. The electron reorganisation as the sum of the individual reorganisation energies from the anionic (λ_3) and neutral surfaces (λ_4).

$$\lambda_3 = E(M_{SP}^-) - E\left(M_{opt}^-\right)$$

Equation 6. The single point and optimised energy contributions to the anion reorganisation energy (λ_3).

$$\lambda_4 = E(M_{SP}') - E(M_{OPT})$$

Equation 7. The single point and optimised energy contributions to the neutral reorganisation energy (λ_4).

The hole transfer integral t_h is an important component in Marcus Theory and can be estimated from the 'splitting-in-dimer' method[36,42,47,48]

(Equation 5), comprising of two cofacial molecules separated by a distance d (Å) and determined from calculating half the energy difference between the HOMO and HOMO-1 levels of the dimer. The transfer integral decreases with increasing d, so a range of separations are appropriate to determine the extent of the electronic coupling interaction. Although a separation between d=3.3-3.8 Å was found to be suitable for OSCs such as pentacene[48], circum(oligo)acenes[36], and substituted acenes[43], it is reasonable to assume that not all of the other isomers in this study, some being non-planar, will have an identical packing arrangement, and thus three integrals were calculated at 3.0, 3.5 and 4.0 Å.

$$t_h = \frac{1}{2}(\Phi_H - \Phi_{H-1})$$

Equation 8. The hole transfer integral determined from half of the difference between the HOMO and HOMO-1 states.

Substituting values for λ_h and t_h into Equation 1, enables K_{CT} to be determined at any given separation d.

4.1.2 Reaction Mechanism Calculations for the Synthon Molecular Fragment

All calculations were performed with the Gaussian 09 software package as described in the general procedures, at various levels; although the basis set 6-311++G(d,p) was used for the majority of calculations. The addition of diffuse functions in the basis set was helpful to describe the long-range dipole-dipole interactions in the initial steps of the reaction. CCSD level of theory was too computationally expensive for the exploration of the global potential energy landscape (Gibbs energies).

Initial calculations found the long-range correction to DFT, Coulomb-attenuating method (CAM-B3LYP), made relatively little or no difference to the recovered activation energies or energy profiles and all subsequent calculations were performed at the B3LYP level. Dispersion functionals later applied included Grimme's D2 term, Becke-Johnson damping and wB97XD. Stationary points on the potential energy surface (PES) were obtained using the synchronous transit-guided quasi-Newton (STQN) method and the QST3 keyword; that is by specifying an intermediate molecule presumed to be close to the transition state (TS) in addition to the previously optimised structures of the reactants and products. The stationary nature of the TSs was in each case confirmed by subsequent frequency and intrinsic reaction coordinate (IRC) path following calculations. The IRC calculations were performed in vacuum.

Thermodynamic quantities (Gibbs free energies) were calculated at 1 atm and 298 K from frequency calculations and then corrected to account for the difference between the standard state in the gas phase and solution (1 atm *vs* 1 M) by adding RTln(24.46). The solution phase was investigated using a variety of methods ranging from continuum models such as the integral equation formalism polarisable continuum model (IEFPCM), a variant (SMD) and the conductor polarisable continuum model (CPCM), to the calculation of explicit solvent molecules imbedded in a continuum.

4.1.3 Organic Semiconductor Calculations

4.1.3.1 Charge Transfer for Pentacene's Isomers

For the benchmarking section, a molecule of pentacene was individually optimised with each functional, and found to be a minimum with frequency calculations, *i.e.* no imaginary frequencies were observed – see Appendix B1; the vibrational frequencies of pentacene correlate well with the literature[120,121].

Several DFT functionals were screened against the experimental values of pentacene and probed some charge-transfer interactions; these functionals include pure (BLYP, PBE) and hybrid (B3LYP, wB97XD, PBE0, B3P86, BHandH, BHandHLYP) with long-range corrections (LC and CAM) and Grimme's dispersion (D3). The properties include the HOMO, LUMO, E_g, first vertical ionisation energy (IE_V), reorganisation energy, transfer integral and rate of charge transfer. Both pure and hybrid functionals were included, along with long-range correction (LC/CAM) and Grimme's third order dispersion (D3) factor. The ionisation energy was probed with Koopmans Theorem[122–124] (KT), outer valence Green's function[125–127] (OVGF), and a variant, the third-order electron propagator[128–131] (P3).

Although the 6-31G(d) and 6-31+G(d) basis sets give satisfactory values to experimental observations[132–135], more-complete basis sets such as of 6-311G to 6-311++G(d,p) are also prevalent throughout the literature[117–119,136] for higher accuracy where needed. We also deploy the 6-311++G(d,p) basis set, owing to the unknown structures and charge transfer properties of the isomers of pentacene, particularly with regards to the dimer separations of the non-planar isomers, which do not have experimental observations for comparison.

4.1.3.2 Fused-Ring and Oligo-Fused Heteroacenes

All calculations to generate the optimised geometries and to determine the charge transfers were performed as described in the General Procedures 4.1.1 in Gaussian 09. Other than DFT, the electron propagator theories (EPT), were deployed to probe the vertical ionisation energies and include the Koopman's Theorem (KT), the Outer valence Green's Function (OVGF) and the third order pole (P3), which is a variant of OVGF; specified in the route section of the calculation script as the OVGF and OVGF=P3 keywords; KT values are automatically generated by both OVGF. For all EPT calculations, the same complete basis was used, such as the 6-311++G(d,p); the theoretical level would thus be OVGF/6-311++G(d,p), as an example. Nonlinear optic (NLO) parameters were obtained from the direct current second harmonic generation (DCSHG) option, using the POLAR keyword and specifying DCSHG as the option, such as POLAR=DCSHG; a tighter grid of data points surrounding the molecule in the calculation is necessary for the DCSHG option and fulfilled with the addition of the int=UltraFine keyword. The hyperpolarisabilities were calculated at the frequency of 1064 nm (0.0428 Har energy).

4.2 Instruments

4.2.1 Nuclear Magnetic Resonance (NMR)

^{1}H and ^{13}C NMR spectra were measured on a Bruker DPX300 or a Bruker Avance 500 spectrometer using an internal deuterium lock. Chemical shifts are reported in parts per million (ppm) downfield from and coupling constants are given in hertz (Hz). Trimethylsilane (TMS) is defined as 0 ppm for ^{1}H NMR spectra. When describing ^{1}H NMR data the following abbreviations are used; s = singlet, d = doublet, t = triplet, q = quartet, p = quintet, m = multiplet.

4.2.2 Mass Spectrometry (MS)

Positive electron impact (EI+) analysis was run on a Waters GCT Premier spectrometer. Positive and negative electrospray ionisation (ESI+/-) was performed on a Bruker Daltronics microTOF spectrometer.

4.2.3 Infrared (IR)

Spectra were recorded on a Perkin-Elmer FTIR spectrometer and the samples were analysed neat.

4.2.4 Ultra Violet - Visible Absorption Spectroscopy (UV-Vis)

The samples were run as 10 μmol solutions in chloroform or as a thin film on quartz, at 26 °C on a Shimadzu UV-3100 spectrometer, and analysed using the program UV Probe 2.3.

4.2.5 Differential Scanning Calorimetry (DSC)

Samples were run on TA Instruments DSC Q20 at a temperature gradient of 10 °C min^{-1} under nitrogen (flow = 50 mL min^{-1}); calibrated with indium and analysed using the program TA Universal Analysis 2000.

4.2.6 Thermo-Gravimetric Analysis (TGA)

Samples were run on TA Instruments TGA G50 at a temperature gradient of 10 °C min^{-1} under nitrogen (flow = 40 mL min^{-1} for balance purge and 40 mL min^{-1} for sample purge); analysed with program TA Universal Analysis 2000.

4.2.7 Single Crystal X-Ray Crystallography

For single-crystal structures, a suitable single crystal was selected and immersed in an inert oil. The crystal was then mounted on a nylon loop and attached to a goniometer head on a Rigaku SuperNova X-ray diffractometer fitted with an Atlas area detector and a kappa-geometry 4-circle goniometer, using graphite monochromated Mo-Kα (λ = 0.71073 Å) or Cu-Kα (λ = 1.54184 Å) radiation. The crystal was cooled to 120 K by an Oxford Cryostream[137] low temperature device. The full data set was recorded and the images processed using CrysAlisPro[138] software. Structure solution was achieved through the use of SHELXS[139], SHELXT[140] or Superflip[141] programs and the structural model defined by full matrix least squares on F^2 using SHELXL-97[141] or SHELXL-2014[142]. Molecular graphics were plotted using Mercury[143]; editing of CIFs and construction of tables and bond lengths and angles was achieved using Olex2. Unless otherwise stated, hydrogen atoms were placed using idealised geometric positions (with free rotation for methyl groups), allowed to move in a "riding model" along with the atoms to which they are attached, and refined isotropically.

4.3 Synthesis

4.3.1 General Synthetic Procedures

Unless stated otherwise, all reactions performed under an atmosphere of nitrogen, in flame dried glassware, having been flushed with dry nitrogen and evacuated three times prior to charging.

4.3.2 Fused-Ring Heteroacenes

4.3.2.1 Synthon Molecular Fragment

4.3.2.1.1 Target 44

2,5-Dibromo-3-thiophene Methanol (**120**)
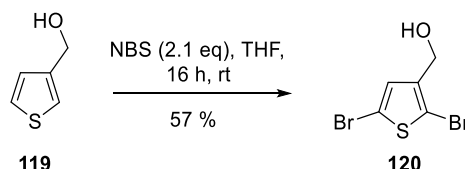
N-bromosuccinimide (13.1 g, 73.5 mmol, 2.1 eq) was added to a stirred solution of 3-thiophene methanol (4.00 g, 35 mmol) in tetrahydrofuran (40 mL) according to the general procedures. The reaction mixture was stirred at room temperature for 16 h giving a yellow liquid. The liquid was filtered over Celite (in DCM) and washed with 10 % sodium hydroxide (50 mL) solution. The organic layer was separated, dried with anhydrous sodium sulfate, gravity filtered and evaporated giving a brown liquid. The liquid was purified via flash column chromatography (1:9, ethyl acetate: petroleum ether) giving a white solid (5.40 g, 19.9 mmol, 57 %). ^{1}H (300 MHz, CDCl$_3$): 7.02 (s, 1H), 4.54 (s, 2H), 2.04 (s, OH); ^{13}C (75 MHz, CDCl$_3$): 141.4, 130.5, 111.5, 109.3, 59.3.

2-bromo-5-trimethylsilylethynylthiophene-3-methnol (**122**)
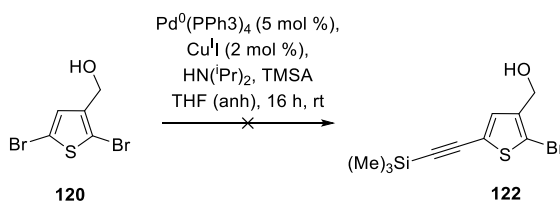
Tetrakistriphenylphosphinepalladium(0)   (0.107g,   0.0929 mmol,   5 mol %), copper(I) iodide (0.0071 g, 0.0372 mol, 2 mol %) and diisopropylamine

(1.8 mL) was added to a stirred solution of 2,5-dibromothiophene methanol (0.500 g, 1.86 mmol) in anhydrous tetrahydrofuran (12.6 mL). The reaction mixture was degassed for ten minutes then trimethylsilylacetylene (0.183 g, 1.86 mmol, 1 eq) was added dropwise. The mixture was stirred for 16 h at room temperature then filtered and concentrated *in vacuo* giving a crude yellow crystalline solid (0.645 g). The crude product was determined by ^{1}H-NMR to not be the desired molecular target and was therefore not further characterised.

2-Hexylthiophene (**70**)
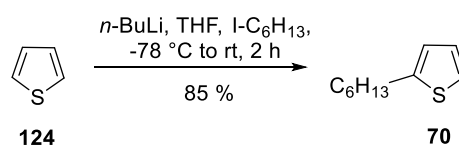
n-Butyllithium in hexane (23.4 mL, 37.5 mmol, 1.6 M, 1.05 eq) was added dropwise to a solution of thiophene (3.00g, 35.7 mmol) in anhydrous tetrahydrofuran (100 mL) and stirred at -78 °C for 45 minutes, then at 0°C for 15 minutes. 1-Iodohexane (5.53 mL, 37.5 mol, 1.05 eq) was added and the reaction stirred at -78 °C for 30 minutes, then allowed to warm to room temperature for 1 hour. The reaction was quenched with deionised water (5 mL) then poured into water (100 mL). The mixture was extracted with diethyl ether (3 × 100 mL), the organic layers collected, dried with anhydrous sodium sulfate and concentrated *in vacuo* giving a yellow oil (5.11 g, 30.4 mmol, 85 %), which was determined to be pure enough to use in the next step; [1]H (500 MHz, CDCl$_3$): 7.07 (d, *J* = 5.1 Hz, 1H), 6.89 (t, *J* = 5.1 Hz, 1H), 6.76 (d, *J* = 5.1 Hz, 1H), 2.81 (t, *J* = 8.0 Hz, 2H), 1.65 (m, 2H), 1.30 (m, 6H), 0.88 (m, 3H); [13]C (125 MHz, CDCl$_3$): 145.9, 126.6, 123.9, 122.8, 31.6, 31.5, 30.4, 29.9, 22.6, 14.1.

2-Bromo-5-hexylthiophene (**103**)
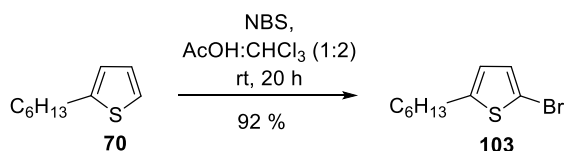
N-bromosuccinimide (1.95 g, 10.9 mmol, 1.04 eq) was added to a stirred solution of 2-hexylthiophene (1.77 g, 10.5 mmol) in chloroform:acetic acid (3:2, 50 mL) and stirred over 72 hours at room temperature. The mixture was

extracted with dichloromethane (2 × 50 mL), washed with potassium carbonate (5 %, 50 mL) and deionised water (50 mL). The organic layers were combined, dried with anhydrous sodium sulfate and concentrated *in vacuo*, giving a brown liquid. The crude product was filtered over silica (in petroleum ether) giving a pale yellow liquid (2.237 g, 9.06 mmol, 86 %); ^1H (500 MHz, CDCl$_3$): 6.82 (d, $J = 3.6$, 1H), 6.51 (d, $J = 3.6$, 1H), 2.73 (t, $J = 7.6$, 2H), 1.62 (q, $J = 7.4$ Hz, 2H), 1.30 (m, 6H), 0.88 (t, $J = 6.9$, 3H); ^{13}C (125 MHz, CDCl$_3$): 147.7, 129.2, 124.3, 108.6, 31.5, 31.4, 30.3, 28.6, 22.6, 14.08, m/z (EI+) calc. 247.1940, found 246.0078.

3-Bromo-5-hexylthiophene (**45**)
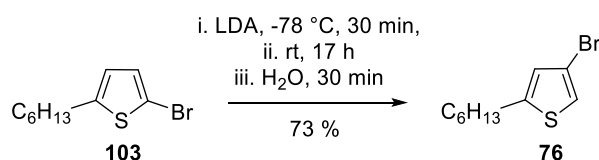
n-Butyl lithium (0.76 mL, 1.21 mmol, 1.2 eq, in hexane 1.6 M) was added to a solution of diisopropylamine (0.21 mL, 1.52 mmol, 1.5 eq) in anhydrous tetrahydrofuran (12 mL) and stirred at -78 °C for 30 minutes. 2-Bromo-5-hexylthiophene (0.250 g, 1.01 mmol) was added and the reaction was allowed to warm up to room temperature and stirred for 17 h. The reaction was quenched with deionised water (2 mL), and allowed to stir at room temperature for 30 minutes. The mixture was extracted with diethyl ether (3 × 10 mL) and washed with brine. The organic layers were collected, dried with anhydrous sodium sulfate and concentrated *in vacuo* giving the crude product as a brown liquid. The residue was filtered over silica (in hexane) affording a pure yellow oil (0.110 g, 0.444 mmol, 44 %); ^1H (500 MHz, CDCl$_3$): 7.04 (s, 1H), 6.74, (s, 1H), 2.81 (t, $J = 7.6$ Hz, 2H), 1.64 (q, $J = 7.5$ Hz,2H), 1.30 (m, 6H), 0.89 (t, $J = 6.3$ Hz, 3H); ^{13}C (125 MHz, CDCl$_3$): 147.1, 126.8, 119.9, 108.9, 31.5, 31.3, 30.0, 28.7, 22.6, 14.0.

3-Bromo-2-formyl-5-hexylthiophene (**64**)

Method 1
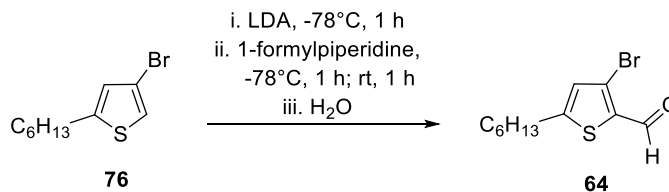
n-Butyllithium (9.11 mL, 14.6 mmol, 1.6 M in hexane) was added to a stirred solution of *N,N*-diisopropylamine (2.55 mL, 18.2 mmol) in tetrahydrofuran (60 mL) at 0 °C. The mixture was stirred for 1 h then 3-bromo-5-hexylthiophene (3.00 g, 12.15 mmol) was added. The mixture was stirred for 1 h at 0 °C then 1-formylpiperidine (1.89 mL, 17.0 mmol) was added. The mixture was stirred for 15 min and allowed to warm to room temperature for 17 h then quenched with water (10 mL). The mixture was extracted with diethyl ether, dried over sodium sulfate and the solvent removed *in vacuo* affording the crude product. The crude was purified over silica in petroleum ether (40-60 °C) and chloroform (1:1) giving an orange oil, (1.30 g, 4.72 mmol, 39 %); ^{1}H (500 MHz, CDCl$_3$): 9.91 (s, 1H), 6.88 (s, 1H), 2.86 (t, $J = 7.7$, 2H), 1.71 (q, 2H, $J = 7.35$, 7.49), 1.37 (m, 6H), 0.92 (t, $J = 6.9$, 3H); ^{13}C (125 MHz, CDCl$_3$): 182.7, 157.1, 134.5, 129.3, 120.3, 31.4, 30.9, 30.8, 26.6, 22.5, 14.0; m/z (EI+, RT) calc. 275.2040, found 274.0020; micro, calc. C 48.01, H 5.49, S 11.65, Br, 29.03, found C 46.80, H 5.40, S 11.60, Br 29.20.

Method 2
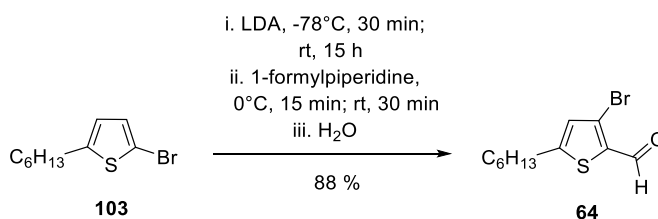
n-Butyllithium (18.3 mL, 29.2 mmol, 1.6 M in hexane) was added to a stirred solution of diisopropylamine (5.11 mL, 36.5 mmol) in tetrahydrofuran (120 mL) at -78 °C. The mixture was stirred for 15 min, then allowed to warm to 0 °C for 15 min. 2-Bromo-5-hexylthiophene (6.00 g, 24.3 mmol) was added to the reaction at -78 °C and stirred for 30 min, then allowed to warm to room temperature for 15 h. The mixture was quenched with 1-formylpiperidine (3.78 mL, 34.0 mmol) at 0 °C and stirred for 15 min, then stirred at room temperature for 30 min. The mixture was extracted with diethyl ether

(25 mL x 4), dried over sodium sulfate and the solvent removed giving a crude brown oil. The crude was purified over silica in petroleum ether (40-60 °C) and dichloromethane (1:1) affording an orange oil, (5.92 g, 21.5 mmol, 88 %); [1]H (500 MHz, CDCl$_3$): 9.91 (s, 1H), 6.88 (s, 1H), 2.86 (t, 2H, J = 7.7), 1.71 (q, 2H, J = 7.35, 7.49), 1.37 (m, 6H), 0.92 (t, 3H, J = 6.9); [13]C (125 MHz, CDCl$_3$): 182.7, 157.1, 134.5, 129.3, 120.3, 31.4, 30.9, 30.8, 26.6, 22.5, 14.0; m/z (EI+, RT) calc. 275.2040, found 274.0020.

4.3.2.1.2 Target 45

3-Hex-1-yne-5-hexylthiophene (**127**)
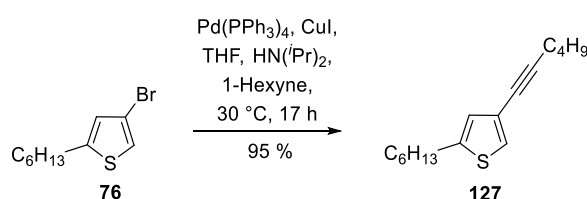
Tetrakistriphenylphosphinepalladium (0) (0.38 g, 0.329 mmol), copper iodide (0.063 g, 0.329 mmol), and diisopropylamine (4 mL) was added to a mixture of 3-bromo-5-hexylthiophene (1.63 g, 6.58 mmol) in tetrahydrofuran (40 mL). The mixture was degassed with nitrogen for 30 min, then charged with 1-hexyne (0.91 mL, 7.90 mmol) and stirred at 30 °C for 17 h. The mixture was purified *via* flash column chromatography (silica, petroleum ether 40-60 °C, dichloromethane (9:1)) affording the target product as a light orange oil (1.56 g, 6.28 mmol, 95 %); [1]H (500 MHz, CDCl$_3$): 7.11 (s, 1H), 6.73 (s, 1H), 2.5 (t, 2H, J = 7.6), 2.37 (t, 2H, J = 7.0), 1.56 (m, 4H), 1.29 (m, 8H), 0.93 (t, 3H, J = 7.3), 0.88 (t, 3H, J = 6.9); [13]C (125 MHz, CDCl$_3$): 145.4, 126.8, 125.3, 122.3, 89.1, 76.1, 31.6, 31.4, 29.9, 28.7, 22.6, 22.0, 19.1, 14.1, 13.6.

2-Tris(*n*-butyl)stannyl-3-hex-1-yne-5-hexylthiophene (**128**)
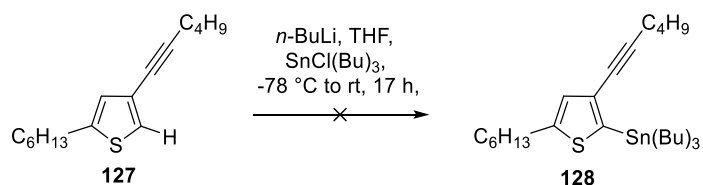
n-Butyllithium in hexane (2.5 M, 0.85 mL, 2.11 mmol) was added to a mixture of 3-Hex-1-yne-5-hexylthiophene (0.5 g, 2.01 mmol) in tetrahydrofuran (120 mL) at -78 °C; the mixture was left to stir at this temperature for 30 min.

Tributylstannyl chloride (0.75g, 2.31 mmol) was added dropwise and the mixture was stirred for 30 min, then allowed to warm to room temperature and stir for 17 h. The mixture was poured onto water (100 mL) and extracted with dichloromethane (100 mL ×3). The organic layers were collected together and washed with brine, dried with sodium sulfate and the solvent removed *in vacuo* giving a pale orange oil (1.24 g); ^{1}H (500 MHz, CDCl$_3$): 6.86 (s, 1H), 2.76 (t, 2H, J = 7.6), 2.36 (t, 2H, J = 7.1), 1.56 (m, 4H), 1.29 (m, 8H), 0.93 (t, 3H, J = 7.3), 0.88 (t, 3H, J = 6.9); ^{13}C (125 MHz, CDCl$_3$): 150.8, 138.5, 1130.3, 128.5, 87.9, 78.8, 31.6, 31.4, 29.9, 28.7, 22.6, 22.0, 19.1, 14.1, 13.6.

2-Pinicolboryl-3-hex-1-yne-5-hexylthiophene (**129**)
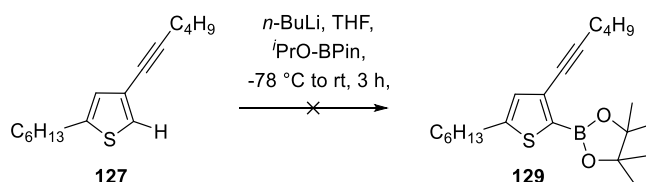
n-Butyllithium in hexane (2.5 M, 0.94 mL, 2.35mmol) was added dropwise to a solution of 3-Hex-1-yne-5-hexylthiophene (0.53 g, 2.13 mmol) in tetrahydrofuran (80 mL) at -78 °C. The mixture was stirred at this temperature for 30 min, then 2-isopropoxy-4,4,5,5-tetramethyl-1,3,2-dioxaborolane (0.48 g, 2.56 mmol) was added dropwise. The mixture was stirred at -78 °C for 30 min then allowed to warm to room temperature and stir for 3 hours. The mixture was poured onto water (20 mL), and extracted with dichloromethane (50 mL ×3). The organic layers were collected together and washed with brine, dried with sodium sulfate and evaporated *in vacuo* affording the crude product as an orange oil (0.65 g, 1.73 mmol, 81.2 %) which was confirmed with NMR and no purification was performed due to decomposition; ^{1}H (500 MHz, CDCl$_3$): 6.81 (s, 1H), 2.76 (t, 2H, J = 7.6), 2.42 (t, 2H, J = 7.6), 1.85 (m, 4H), 1.61 (m, 8H), 1.33 (s, 12H), 0.95 (t, 3H, J = 7.1), 0.87 (t, 3H, J = 7.0); ^{13}C (125 MHz, CDCl$_3$): 150.8, 138.5, 1130.3, 128.5, 87.9, 78.8, 31.6, 31.4, 29.9, 28.7, 22.6, 22.0, 19.1, 14.1, 13.6.

2-Pinicolboryl-3-bromo-5-hexylthiophene (**130**)
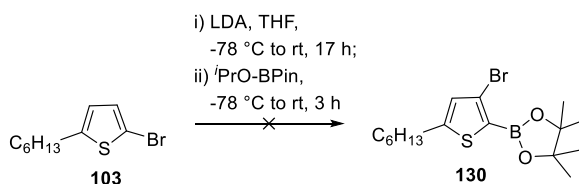
2-Bromo-5-hexylthiophene (1.0 g, 4.05 mmol) was added dropwise to a solution of *n*-butyllithium in hexane (2.5 M, 1.94 mL, 4.86 mmol), diisopropylamine (0.77 mL) and tetrahydrofuran (20 mL) at -78 °C under nitrogen over 30 min. The mixture was allowed to warm to room temperature and stir for 24 h, then quenched with 2-isopropoxy-4,4,5,5-tetramethyl-1,3,2-dioxaborolane (1.16 mL, 5.67 mmol). The mixture was poured onto water (100 mL). The layers were separated and the aqueous phase was extracted with dichloromethane (50 mL ×3). The organic layers were collected together and dried with sodium sulfate and evaporated *in vacuo* affording a brown residue. The crude product was not observed in NMR and attempts at purification with flash column chromatography were unsuccessful.

2-(4,4,5,5-tetramethyl-1,3,2-dioxaborolane)-5-hexylthiophene (**126**)
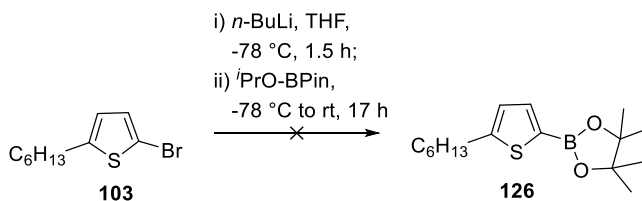
n-Butyllithium in hexane (2.5 M, 5.34 mL, 13.3 mmol) was added dropwise at -78 °C to a solution of 2-bromo-5-hexylthiophene (3.0g, 12.1 mmol) in tetrahydrofuran (40 mL). The mixture was stirred at this temperature for 1.5 h, then 2-ispropoxy-4,4,5,5-tetramethyl-1,3,2-dioxaborolane (2.93 g, 15.7 mmol) was added dropwise. The mixture was allowed to warm to room temperature, stir for 17 h, then poured onto water (10 mL). The aqueous phase was extracted with dichloromethane (100 mL ×3). The organic layers were collected together, washed with brine, dried with sodium sulfate and the solvent evaporated *in vacuo* affording a brown oil. The crude product was purified (silica, petroleum ether 40-60 °C, dichloromethane (1:1)) giving the product as a yellow oil (2.64 g, 8.99 mmol, 74 %); [1]H (500 MHz, CDCl3): 7.47 (d, 1H, *J* = 3.4), 6.86 (d, 1H, *J* = 3.4), 2.85 (t, 2H, *J* = 7.6), 1.68 (p, 2H, *J* = 7.5),

1.33 (s, 12H), 1.30 (m, 6H), 0.88 (t, 3H, $J = 6.6$); ^{13}C (125 MHz, CDCl$_3$): 153.8, 137.4, 125.8, 83.9, 31.7, 31.6, 30.2, 28.8, 24.8, 22.6, 14.1.

4.3.2.2 Core Molecular Fragment

Literature Route[144]

2,3,4,5-Tetrabromothiophene (**112**)
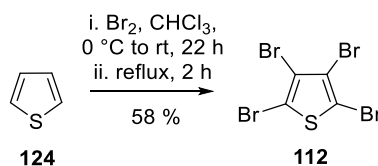
Bromine (13.6 mL, 266 mmol) was added to thiophene (5 g, 59.5 mmol) in chloroform (14 mL) at 0 °C, then allowed to warm to room temperature and continued to stir for 22 h. Chloroform (15 mL) was added and the mixture refluxed at 82 °C for 2 h, then quenched with a saturated solution of sodium thiosulfate (100 mL). The mixture was filtered giving a crude pale cream crystalline powder; the filtrate was extracted with diethyl ether (25 mL x 3) giving more crude. The total crude product was recrystallised from a chloroform/ethanol mixture giving white crystals (15.2 g, 34.6 mmol, 58.2 %); ^{13}C (125 MHz, CDCl$_3$): 117.0, 110.3.

3,4-Dibromo-2,5-diformylthiophene (**113**)
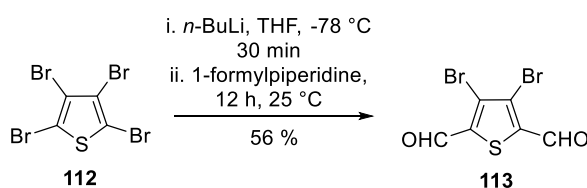
n-Butyl lithium (22 mL, 55.0 mmol, 2.5 M in hexane) was added to a stirred solution of 2,3,4,5-tetrabromothiophene (10.0 g, 25 mmol) in tetrahydrofuran (120 mL) at -78 °C and stirred for 20 min. The mixture was allowed to warm to 0 °C and stirred for 25 min, then cooled to -78 °C and quenched with 1-formylpiperidine (6.66 mL, 60.0 mmol). The mixture was stirred for 3 h then allowed to warm to room temperature and stirred overnight for 13 h. Water (20 mL) was added and the mixture was extracted with diethyl ether

(25 mL x 3), dried over sodium sulfate and the solvent removed affording a dark crude brown oil with solid residues. The crude product was purified (silica, petroleum ether 40-60 °C and dichloromethane, 5:1) giving a deep orange oil (4.16 g, 14.0 mmol, 56 %); ^{1}H (500 MHz, CDCl$_3$): 9.94 (s, 1H), ^{13}C (125 MHz, CDCl$_3$): 182.6, 151.3, 134.6, 123.7, 114.7.

Dithienothiophenyl-diethanoate (**114**)
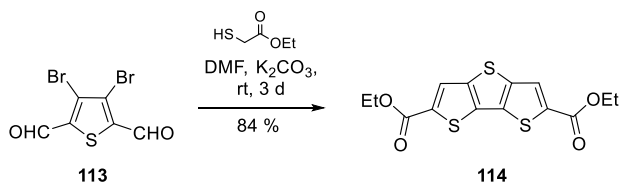
A solution of 3,4-dibromo-2,5-diformylthiophene (**12**) (4.00 g, 13.4 mmol) in dimethylformamide (50 mL) was added to a solution of ethyl-2-mercaptoacetate (2.94 mL, 26.8 mmol) and potassium carbonate (4.83 g, 34.9 mmol) in dimethylformamide (30 mL) under nitrogen at room temperature. The mixture was allowed to stir 3 days, then poured onto water (250 mL) and extracted with dichloromethane (150 mL x 3). The organic layers were collected together and washed with brine (50 mL x 3), dried with sodium sulfate then concentrated under reduced pressure giving an off-white precipitate. The precipitate was filtered and washed with cold ethanol (20 mL) affording a crude white powder (3.82 g, 84 %).

Bis(2-bromo)dithi*enothiop*hene (**54**)
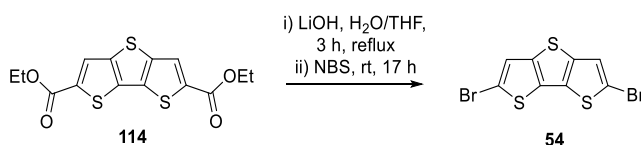
A solution of lithium hydroxide monohydrate (0.94 g, 22.3 mmol) in water (50 mL) was added to a stirred solution of the diester (**114**) (1.9 g, 5.58 mmol) in THF (30 mL) under nitrogen. The mixture was refluxed for 3 h, then cooled to 0 °C and *N*-bromosuccinimide (5.96 g, 33.5 mmol) was added and the mixture stirred for 30min, then at room temperature for 17 h. The mixture was filtered and washed with water giving a precipitate. The precipitate was filtered and recrystallised from hexane giving a white powder (1.59 g, 80 %) ^{1}H-NMR (500 MHz, CDCl$_3$): 7.28 (s, 1H); ^{13}C-NMR (125 MHz, CDCl$_3$): 123.2, 112.4;

micro, calc. C 27.13, H 0.57, S 27.17, Br 45.13, found C 27.10, H 0.60, S 26.60, Br 45.45.

4.3.2.2.2 Method Development for DTT

Double-Cyclisation Route

2,5-Di(trimethylsilylalkynyl)-3,4-dibromothiophene (**115**)
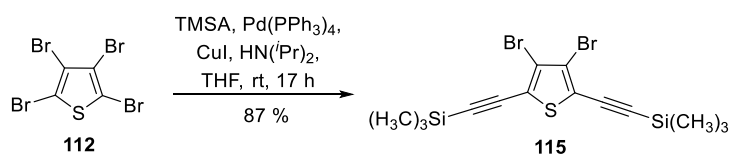
A mixture of tetrabromothiophene (2.0 g, 5.00 mmol), tetrahydrofuran (20 mL), tetrakistriphenylphosphinepalladium(0) (0.289 g, 0.250 mmol), copper (I) iodide (0.0476 g, 0.250 mmol) and diisopropylamine (4 mL) was bubbled with nitrogen for 20 min at room temperature. Trimethylsilylacetylene (1.08 g, 11.0 mmol) was added and the mixture stirred for 17 h under nitrogen at room temperature. Trimethylsilylacetylene (1 mL) was added and the mixture was stirred for 4 h at 40 °C. The mixture was filtered and evaporated to dryness. The crude product was purified with silica (flash chromatography, petroleum ether 40-60°C) affording a cream powder, (1.90 g, 4.37 mmol, 87 %); [1]H (500 MHz, CDCl$_3$): 0.08 (s, 9H); [13]C (125 MHz, CDCl$_3$): 121.5, 119.9, 106.0, 95.4.

One-Pot General Procedure (Reaction Flask Conditions)
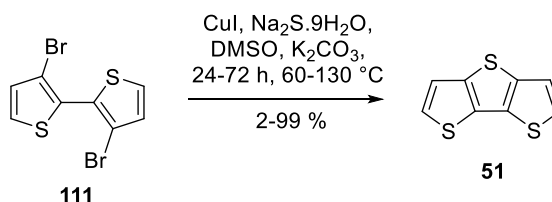
A solution of 3,3'-dibromo-2,2'-bithiophene (0.100 g, 0.309 mmol), copper (I) iodide (0.0294 g, 0.155 mmol), potassium carbonate (0.201 g, 0.617 mmol) and sodium sulfide nonahydrate (0.0282 g, 0.371 mol) in dimethylsulfoxide (2 mL) was stirred under nitrogen at 130 °C for 72 h. The mixture was poured onto water and extracted with dichloromethane (25 mL × 3). The organic layers were collected together, dried over sodium sulfate and the solvent

removed affording a crude powder. The crude was purified with flash column chromatography (silica, petroleum ether 40-60 °C: dichloromethane 9:1) and gave yellow crystals (2-99 %).

One-Pot General Procedure (Microwave Conditions)
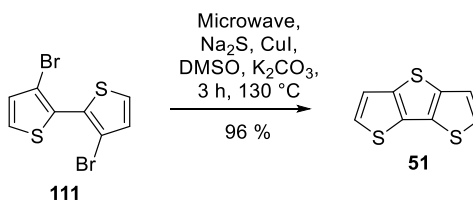
A solution of 3,3'-dibromo-2,2'-bithiophene (0.100 g, 0.309 mmol), copper (I) iodide (0.0294 g, 0.155 mmol), potassium carbonate (0.201 g, 0.617 mmol) and anhydrous sodium sulfide (0.0282 g, 0.371 mol) in dimethylsulfoxide (2 mL) was stirred in a sealed microwave reactor under nitrogen at 130 °C for 3 h. Once cool, the flask was removed and the mixture was poured onto water and extracted with dichloromethane (25 mL × 3). The organic layers were collected together, dried over sodium sulfate and the solvent removed affording a crude powder. The crude was purified with flash column chromatography (silica, petroleum ether 40-60 °C: dichloromethane 9:1) and gave yellow crystals, (96 %).

Synthesis of DTT using Copper (I) Iodide and Thiourea
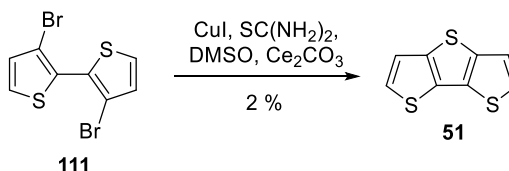
A solution of 3,3'-dibromo-2,2'-bithiophene (0.100 g, 0.309 mmol), copper (I) iodide (0.0294 g, 0.155 mmol), cesium carbonate (0.201 g, 0.617 mmol) and thiourea (0.0282 g, 0.371 mol) in anhydrous dimethylsulfoxide (2 mL) was stirred under nitrogen at 130 °C overnight for 20 h. The mixture was poured onto water and extracted with dichloromethane (25 mL × 3). The organic layers were collected together, dried over sodium sulfate and the solvent removed affording yellow crystals (2 %).

Synthesis of DTT using Copper (II) Oxide and Sodium Sulfide
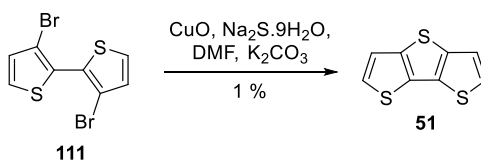
A solution of 3,3'-dibromo-2,2'-bithiophene (0.100 g, 0.309 mmol), nano copper (II) oxide (0.0123 g, 0.155 mmol), potassium carbonate (0.0854 g, 0.618 mmol) and sodium sulfide (0.288 g, 0.371 mmol) in anhydrous dimethylformamide (2 mL) was stirred under nitrogen at 130 °C over night for 20 h. The mixture was poured onto water and extracted with dichloromethane (25 mL × 3). The organic layers were collected, washed with brine and dried over sodium sulfate. The solvent was removed *in vacuo* affording yellow crystals (1 %).

Synthesis of DTT using Copper (I) Iodide and Sodium Sulfide
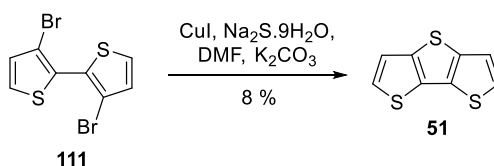
A solution of 3,3'-dibromo-2,2'-bithiophene (0.100 g, 0.309 mmol), copper (I) iodide (0.0588 g, 0.309 mmol), potassium carbonate (0.0854 g, 0.618 mmol) and sodium sulfide (0.288 g, 0.371 mmol) in anhydrous dimethyl formamide (1.5 mL) was stirred at 120 °C under nitrogen for 66 h. The mixture was poured onto water and extracted with dichloromethane (25 mL × 4). The organic layers were collected, washed with brine, dried over sodium sulfate and the solvent removed affording crude pale yellow crystals (8 %).

4.3.2.3 Condensate Intermediates

4.3.2.3.1 Target 44

Bis[3-bromo-2-hydroxymethine-5-hexylthiophene]-2,2'-dithieno[2,3-b:3',2'-d]thiophene (**116**)
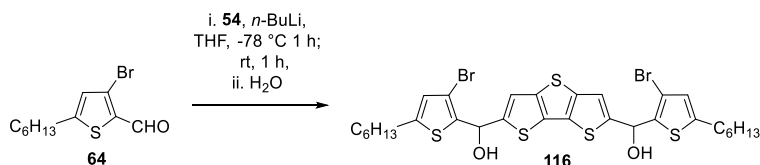
n-Butyl lithium (10.7 mL, 17.1 mmol, 1.6 M in hexane) was added dropwise to a solution of 2,2'-dibromodithienothiophene (2.75 g, 7.77 mmol) in tetrahydrofuran (150 mL) at -78 °C. After 1 h, the reaction mixture was allowed to warm to 0 °C and stirred for 30 min. The mixture was cooled to -78 °C and a solution of 3-bromo-2-formyl-5-hexylthiophene (4.81 g, 17.75 mmol) in tetrahydrofuran (10 mL) was added. After 1.5 h, the mixture was allowed to warm to room temperature for 1 h then quenched with water (20 mL). The aqueous phase was extracted with diethyl ether, dried over sodium sulfate and the solvent removed affording a crude brown oil, (7.01 g), and was used without further purification; ^1H (500 MHz, MeOD): 7.00 (s, 1H), 6.48 (s, 1H), 3.15 (s, 1H), 2.86 (t, 2H, $J = 7.7$), 1.71 (q, 2H, $J = 7.35, 7.49$), 1.37 (m, 6H), 0.92 (t, 3H, $J = 6.9$); ^{13}C (125 MHz, MeOD): 149.5, 147.2, 141.2, 140.6, 131.5, 127.5, 119.2; m/z (EI+, 250-320 °C) calc. 746.7080, found 747.9758.

Bis[3-bromo-2-methylene-5-hexylthiophene]-2,2'-dithieno[2,3-b:3',2'-d]thiophene (**117**)
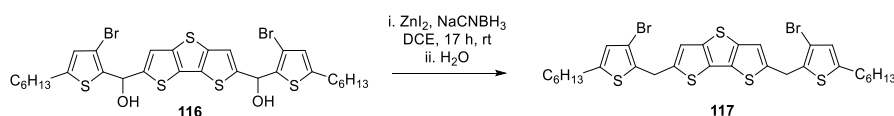
Zinc(II) iodide (9.58 g, 30.0 mmol) and sodium cyanoborohydride (8.28 g, 131.8 mmol) was added to a solution of bis[3-bromo-2-hydroxy-5-hexylthiophene]-2,2'-dithienothiophene (7.01 g, 9.37 mmol) in dichloroethane (100 mL). The reaction mixture was stirred at room temperature over night for 17 h under nitrogen, then quenched with water (20 mL). The mixture was filtered over celite, washed with brine, extracted with dichloromethane (25 mL x 2) and the solvent removed giving the crude as a viscous brown residue. The residue was purified (silica, dichloromethane) affording a deep orange residue (4.29 g, 5.98 mmol, 64 %); ^1H (500 MHz, CDCl₃): 7.08 (s, 1H), 6.65 (s, 1H), 4.32 (s, 2H), 2.73 (t, 2H), 1.6 (p, 2H, $J = 7.5$) 1.32 (m, 6H), 0.91 (t, 3H); ^{13}C (125 MHz, CDCl₃): 144.9, 142.6, 139.7, 134.0, 130.0, 126.6, 118.9, 108.4, 31.5, 31.1, 30.7, 30.2, 28.7, 22.5, 14.0; m/z (EI+, 250-320 °C) calc. 714.7100, found 711.9655; micro, calc. C 50.41, H 4.79, S 22.43, Br 22.36, found C 50.25, H 4.85, S 22.40, Br 22.50.

Bis[3-formyl-2-methylene-5-hexylthiophene]-2,2'-dithieno[2,3-b:3',2'-d]thiophene (**118**)

Method A
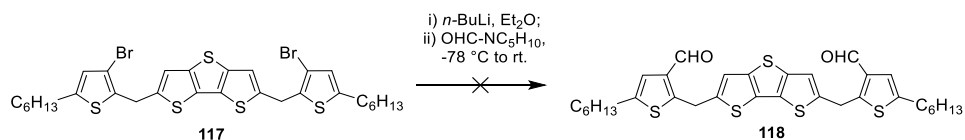
A solution of bis[3-bromo-2-methylene-5-hexylthiophene]-2,2'-dithieno[2,3-b:3',2'-d]thiophene (3.03 g, 8.44 mmol) in diethylether (40mL) and tetrahydrofuran (8 mL) was added *via* cannula to a solution of *n*-butyllithium (1.6 M in hexane, 11.6 mL, 18.6 mmol) in diethylether (20 mL) at -78 °C under nitrogen. After 1.5 h, 1-formylpiperidine (2.15 mL) was added and the mixture was allowed to stir for another 1.5 h at -78 °C before being quenched with water (10 mL). The aqueous phase was extracted with dichloromethane (50 mL ×3). The organic layers were collected together and washed with brine, dried with sodium sulfate and the solvent evaporated *in vacuo* affording a dark green residue. The crude product could not be observed in ^{1}H-NMR and purification (silica, petroleum ether 40-60 °C and dichloromethane, 9:1) did not isolate any identifiable structure.

Method B
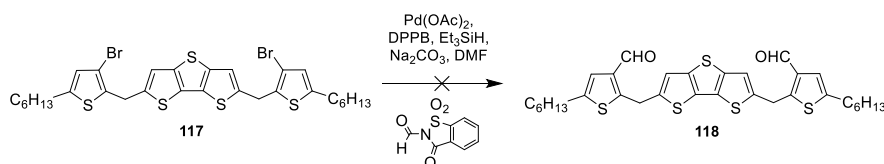
A solution of bis[3-bromo-2-methylene-5-hexylthiophene]-2,2'-dithieno[2,3-b:3',2'-d]thiophene (0.5 g, 0.70 mmol), triethylsilane (0.179 g, 1.54 mmol) and dimethylformamide (35 mL) was deoxygenated with nitrogen for 10 min, then added to a mixture of N-formylsaccharin (0.443 g, 2.10 mmol), palladium acetate (0.00942 g, 0.0420mmol), 1,4-bis(diphenylphosphino)butane (0.0224 g, 0.0525 mmol) and sodium carbonate (0.171 g, 1.609 mmol) under nitrogen. The mixture was stirred at room temperature for 10 min, then at 80 °C for 17 h. TLC revealed consumption of starting material. The mixture was poured onto water (50 mL) and the aqueous phase was extracted with dichloromethane (50mL ×3). The organic layers were collected together, dried with sodium sulfate and the

solvent removed *in vacuo* affording a brown residue. The residue was purified (silica, petroleum ether 40-60 °C and dichloromethane, 9:1) and afforded a pale yellow solid; no product was observable in ^{1}H-NMR.

4.3.2.3.2 Target 45

Bis[3-hex-2-yne-5-hexylthiophene]-2,2'-dithieno[2,3-b:3',2'-d]thiophene (**89**)

Method 1a (Suzuki)
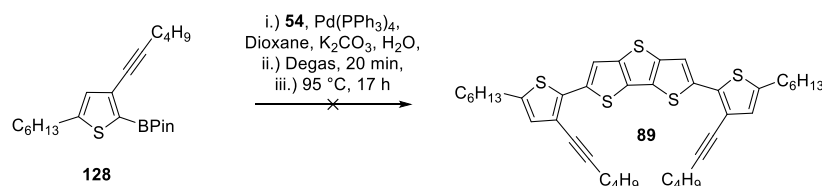
Tetrakistriphenylphosphine (0) (0.045 g, 0.039 mol), **54** (0.279 g, 0.786 mmol) and an aqueous solution of potassium carbonate (2 M, 4 mL) was added to a solution of **128** (0.65 g, 1.73 mmol) in dioxane (15 mL). The mixture was degassed with nitrogen for 20 min, then stirred at 95 °C for 17 h. TLC revealed only starting reagents. The mixture was poured onto water (100 mL) and the aqueous phase was extracted with chloroform (150 mL ×3). The organic layers were collected together and washed with brine (50 mL ×2), dried with sodium sulfate and the solvent evaporated *in vacuo* giving a brown powder. The crude product could not be identified according to ^{1}H-NMR.

Method 1b (Stille)
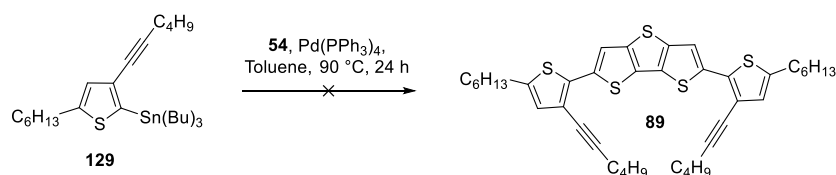
Tetrakistriphenylphosphine (0) (0.126 g, 0.109 mmol) and **54** (0.386 g, 1.09 mmol) was added to a solution of **129** (0.586 g, 1.09 mmol) in toluene (50 mL). The mixture was degassed for 10 min then stirred at 90 °C for 24 h. TLC revealed only starting reagents. The mixture was poured onto water (100 mL) and the aqueous phase was extracted with chloroform (150 mL ×3). The organic layers were collected together and washed with brine (50 mL ×2), dried with sodium sulfate and the solvent evaporated *in vacuo* giving a brown powder. The crude product could not be identified according to ^{1}H-NMR.

Method 2

Bis[5-hexylthiophene]-2,2'-dithieno[2,3-b:3',2'-d]thiophene (**93**)
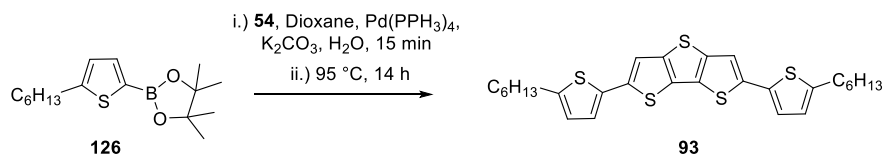
126 (0.91 g, 3.11 mmol), tetrakistriphenylphosphinepalladium (0) (0.108 g, 0.093 mmol), and an aqueous solution of potassium carbonate (2 M, 4 mL) was added to a solution of compound **54** (0.47 g, 1.30 mmol) in dioxane (25 mL). The mixture was deoxygenated with nitrogen for 15 min, then stirred at 95 °C for 22 h. The mixture was poured onto water (100 mL) and the aqueous phase was extracted with diethyl ether (150 mL ×4). The organic layers were collected together, washed with brine, dried with sodium sulfate and the solvent evaporated *in vacuo* affording a red residue. The crude was purified (silica, petroleum ether 40-60 °C and dichloromethane, 9:1) and gave an orange solid (0.25 g, 0.473 mmol, 15.2 %); ^{1}H (500 MHz, CDCl$_3$): 7.26 (s, 1H), 7.03 (d, 1H, J = 3.5), 6.71 (d, 1H, J = 3.5), 2.81 (t, 2H, J = 7.6), 1.71 (p, 2H, J = 7.5), 1.36 (m, 6H), 0.90 (t, 3H J = 6.8); ^{13}C (125 MHz, CDCl$_3$): 147.4, 145.2, 142.9, 139.9, 135.6, 127.8, 127.7, 126.2, 31.5, 31.1, 30.7, 30.2, 28.7, 22.5, 14.0.

Bis[3-bromo-5-hexylthiophene]-2,2'-dithieno[2,3-b:3',2'-d]thiophene (**91**)
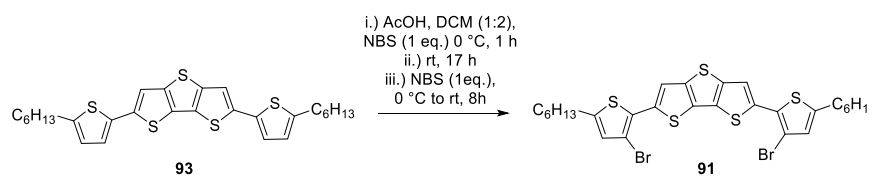
A solution of bis[5-hexylthiophene]-2,2'-dithieno[2,3-b:3',2'-d]thiophene (0.100 g, 0.189 mmol) in chloroform (50 mL) and acetic acid (25 mL) was cooled to 0 °C, then charged with 1 equivalent of N-bromosuccinimide (0.034 g, 0.191 mmol) under nitrogen. The mixture was stirred for 1 h at 0 °C then allowed to stir at room temperature for 17 h. A second equivalent of N-bromosuccinimide (0.034 g, 0.191 mmol) was added at 0 °C, then the mixture was allowed to warm back to room temperature and stir for 8 h. The mixture was poured onto water (200 mL) and extracted with chloroform (150 mL ×3) then washed with 10 % w/v potassium carbonate (50 mL ×2).

The organic layers were collected together, dried with sodium sulfate and the solvent evaporated *in vacuo* giving a brown powder. The crude product was purified (silica, petroleum ether 40-60 °C and dichloromethane, 9:1) affording the product as a yellow powder (0.061 g, 0.088 mmol, 46.5 %); ^{1}H (500 MHz, CDCl$_3$): 7.54 (s, 1H), 6.71 (s, 1H), 2.75 (t, 2H, J = 7.6), 1.67 (p, 2H, J = 7.5), 1.35 (m, 6H), 0.90 (t, 3H, J = 6.9); ^{13}C (125 MHz, CDCl$_3$): 145.5, 141.4, 135.7, 130.7, 129.5, 128.9, 119.2, 107.2, 31.5, 31.1, 30.1, 28.7 22.6, 14.1.

Sonogashira Coupling to 89
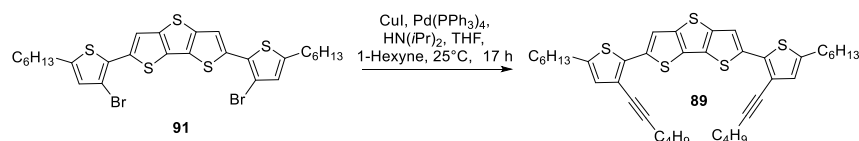
Tetrakistriphenylphosphine (0) (0.005 g, 0.0044 mmol), copper iodide (0.0005 g, 0.0027 mmol) and diisopropylamine (2 mL) was added to a solution of **91** (0.061 g, 0.089 mmol) in tetrahydrofuran. The mixture was degassed with nitrogen for 15 min and 1-hexyne (0.022 mL, 0.196 mmol) was added dropwise. The mixture was stirred at room temperature for 17 h. The mixture was immediately purified (silica, petroleum ether 40-60 °C and dichloromethane, 9:1) affording the product as a yellow powder (0.0509 g, 0.0739 mmol, 83 %); ^{1}H (500 MHz, CDCl$_3$): 7.53 (s, 1H), 6.70 (s, 1H), 2.73 (t, 2H, J = 7.7), 2.27 (t, 2H, 7.0), 1.44 (m, 10H), 0.90 (t, 6H, J = 7.2); ^{13}C (125 MHz, CDCl$_3$): 145.4, 141.4, 135.7, 130.6, 129.5, 129.9, 119.1, 107.1, 77.5, 65.3, 31.5, 31.1, 30.4, 30.1, 28.7, 22.6, 21.9, 18.9, 14.1, 13.5.

4.3.2.3.2 Target 45

Method 1
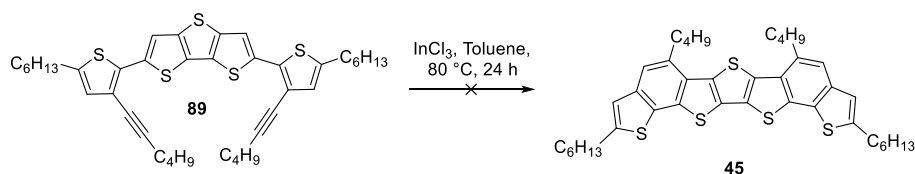
A mixture of **89** (0.086 g, 0.125 mmol), indium chloride (0.0028 g, 0.012 mmol) and toluene (12 mL) was stirred at 80 °C under nitrogen for 24 h. TLC revealed only starting reagents. The solvent was removed *in vacuo* and

the crude was purified (silica, petroleum ether 40-60 °C and dichloromethane, 9:1) and gave a yellow solid, although no product could be observed in [superscript]1H-NMR.

Method 2
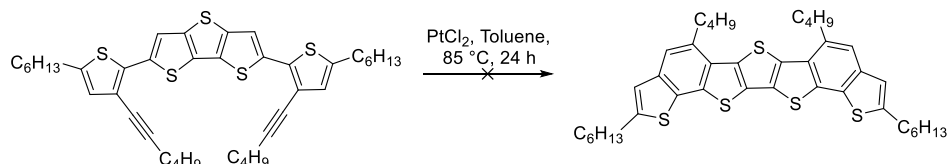
A mixture of **89** (0.0852 g, 0.124 mmol), platinum chloride (0.0033 g, 0.0124 mmol) and toluene (10 mL) was stirred at 85 °C under nitrogen for 24 h. TLC revealed only starting reagents. The solvent was removed *in vacuo* and the crude was purified (silica, petroleum ether 40-60 °C and dichloromethane, 9:1) and gave a yellow solid, although no product could be observed in [superscript]1H-NMR.

Method 3
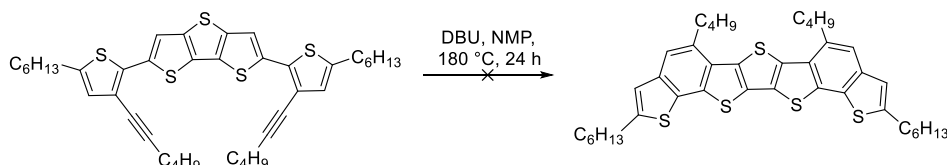
A mixture of **89** (0.0613 g, 0.089 mmol), DBU and n-methyl-2-pyrrolidone (17 mL) was stirred at 180 °C for 24 h under nitrogen. The solvent was removed *in vacuo* and the crude was purified (silica, petroleum ether 40-60 °C and dichloromethane, 9:1) and gave a yellow solid, although no product could be observed in [superscript]1H-NMR.

4.3.3 Oligo-Fused Heteroacenes

4.3.3.1 General Synthetic Procedures

i.) Pd(PPh$_3$)$_4$, CuI,
THF, amine,
ii.) N$_2$, 20 min, rt
iii.) alkyne, rt, 17 h

61-67 %

54

151-159

R= ^{c}Pr(**151**)   Ph (**155**)
TIPS (**152**)   Ph-C$_6$H$_{13}$ (**156**)
Th-C$_6$H$_{13}$ (**153**)   Ph- NMe$_2$ (**157**)
Py (**154**)   Ph-OMe (**158**)
Fl-(C$_6$H$_{13}$)$_2$ (**159**)
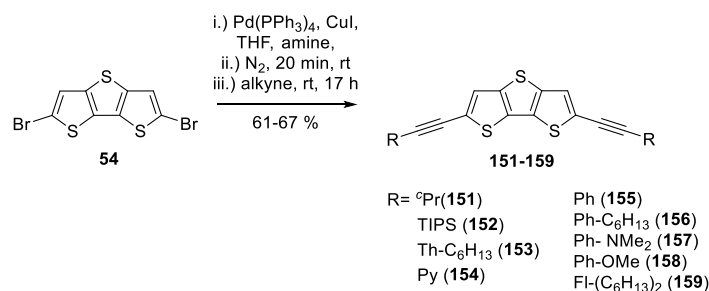
Under nitrogen a flame-dried flask was evacuated and backfilled three times, which was then charged with a solution of 2,2'-dibromodithieno[2,3-b:3',2'-d]thiophene (1 eq.), copper iodide (0.05 eq.) and tetrakistriphenylphosphine palladium (0) (0.05 eq.) in tetrahydrofuran (20 mL) and diisopropylamine (4 mL). The solution was bubbled with nitrogen for 15 min. The selected alkyne (2.1 eq.) was added dropwise and the mixture stirred for 17 h at room temperature. The mixture was filtered and the solvent evaporated giving a crude residue which was purified with flash column chromatography (40 % dichloromethane in petroleum ether 40-60 °C) then recrystallised from hexane giving yellow crystals (61-67 %).

4.3.3.2 Compounds

Bis(2-cyclopropylethynyl)dithienothiophene (**151**)

151
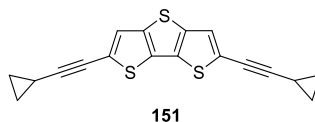
Pale cream needles (0.182 g, 68 %); ^{1}H-NMR (500 MHz, CDCl$_3$): 7.25 (s, 1H), 1.51 (q, J=3.2, 5.1, 1H), 0.892 (m, 4H); ^{13}C-NMR (125 MHz, CDCl$_3$): 140.5, 129.9, 124.3, 124.0, 99.0, 68.9, 8.4, 0.01; IR (C≡C, neat, cm^{-1}): 2212.8; m/z (ES+) calc. 324.0101, found 325.0174; micro calc. C 66.63, H 3.73, S 29.65; found: C 66.50, H 3.65, S 29.40; m.p. 142.9 °C.

Bis(2-triisopropylsilylethynyl)dithienothiophene (**152**)

152
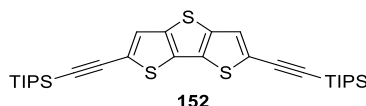
Yellow needles (0.55 g, 64 %); ^{1}H-NMR (500 MHz, CDCl$_3$): 7.39 (s, 1H), 1.15 (s, 3H), 1.13 (d, J=3.5, 18H); ^{13}C-NMR (125 MHz, CDCl$_3$): 141.6, 131.0, 125.7, 124.5, 99.5, 98.1, 18.7, 11.3; m/z (ES+) calc. 557.2216, found 559.1307; IR (C≡C, neat, cm^{-1}): 2137.6; micro calc. C 64.69, H 7.96, S 17.27; found C 64.30, H 8.00, S 17.50; m.p. 103.9 °C.

Bis(5-hexylthiophenylethynyl)dithienothiophene (**153**)

153
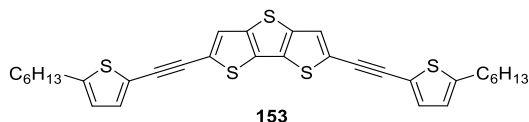
Orange fibrous powder (0.74 g, 62 %); ^{1}H-NMR (500 MHz, CDCl$_3$): 7.41 (s, 1H), 7.14 (d, J=3.6, 1H), 6.70 (d, J=3.6, 1H), 2.81 (t, J=7.5, 2H), 1.68 (p, J=7.3, 7.4, 2H), 1.34 (m, 6H), 0.89 (t, J=6.8, 3H); ^{13}C-NMR (125 MHz, CDCl$_3$): 149.5, 141.8, 132.7, 131.4, 125.0, 124.5, 124.2, 119.6, 88.84, 85.9, 31.5, 31.5, 30.3, 28.7, 22.6, 14.1; IR (C≡C, neat, cm^{-1}): 2136.9; m/z (ES+) calc. 576.1108, found: 577.1102; micro calc. C 66.62, H 5.59, S 27.79; found: C 66.40, H 5.50, S 27.60; m.p. 90 °C.

Bis(2-pyridylethynyl)dithienothiophene (**154**)

154
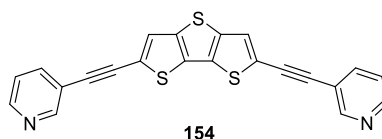
Yellow powder (0.56, 61 %); ^{1}H-NMR (500 MHz, CDCl$_3$): 8.79 (s, 1H), 8.58 (dd, J = 1.4, 4.8, 1H), 7.84 (dt, J = 3.6, 4.8, 1H), 7.51 (s, 1H), 7.32 (dd, J = 4.9, 7.8 1H); ^{13}C-NMR (125 MHz, CDCl$_3$): 152.1, 149.0, 142.1, 138.3, 131.8, 125.9, 123.6, 123.1, 119.81, 91.7, 86.2; IR (C≡C, neat, cm^{-1}): 2199.9; m/z (ES+): calc. 398.0006, found: 399.0081; micro calc. C 66.3, H 2.53, N 7.03, S 24.14; found C 66.7, H 2.60, N 7.21, S 24.5; m.p. 149.4 °C.

Bis(phenylethynyl)dithienothiophene (**155**)

155
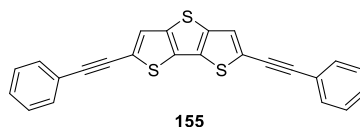
Yellow crystals (0.71 g, 65 %); ^{1}H-NMR (500 MHz, CDCl$_3$): 7.54 (m, 2H), 7.45 (s, 1H), 7.37 (m, 3H); ^{13}C-NMR (125 MHz, CDCl$_3$): 144.0, 141.6, 131.4, 128.6, 124.9, 119.7, 95.3, 82.5, 36.0, 31.7, 31.2, 28.9, 22.6, 14.1; IR (C≡C, neat, cm^{-1}): 2191.35; m/z (ES+): calc. 396.5400, found: 397.5476; micro calc. C 72.69, H 3.05, S 24.25; found C 72.81, H 3.04, S 24.51; m.p. 187.7 °C.

Bis(4-hexylphenylethynyl)dithienothiophene (**156**)

156
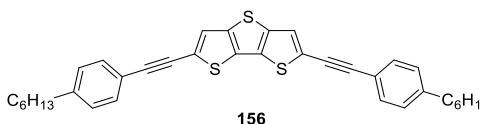
Yellow crystals (0.8 g, 67 %); ^{1}H-NMR (500 MHz, CDCl$_3$): 7.44 (d, J=8.1, 2H), 7.40 (s, 1H), 7.15 (d, J=8.1, 2H), 2.61 (t, J=7.5, 2H), 1.61 (p, J=7.2, 6.8, 2H), 1.29 (m, 6H), 0.88 (t, J=6.6, 3H); ^{13}C-NMR (125 MHz, CDCl$_3$): 144.0, 141.6, 131.4, 131.2, 128.6, 124.9, 124.5, 119.7, 95.3, 82.5, 36.0, 31.7, 31.2, 28.9, 22.6, 14.1; IR (C≡C, neat, cm^{-1}): 2197.8; m/z (ES+) calc. 564.1979, found 565.2092; micro calc. C 76.55, H 6.42, S 17.03; found C 76.3, H 6.40, S 17.3; m.p. 132.4 °C.

Bis(N,N-dimethylanylethynyl)dithienothiophene (**157**)

157
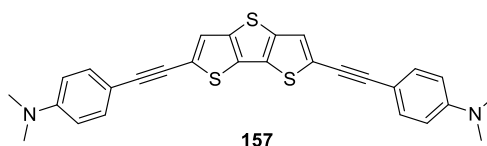
Yellow powder (0.19 g, 63 %); ^{1}H-NMR (500 MHz, CDCl$_3$): 7.41 (d, J=8.8, 2H), 7.36 (s, 1H), 6.66 (d, J=8.8, 2H), 3.01 (s, 6H); ^{13}C-NMR (125 MHz, CDCl$_3$): 150.4, 141.3, 132.7, 130.8, 125.1, 124.0, 111.8, 109.1, 96.4, 81.2, 40.2; IR (C≡C, neat, cm^{-1}): 2185.8; m/z (ES+) calc. 482.0945, found 483.0981; micro calc. C 69.67, H 4.59, N 5.80, S 19.93 ; found C 69.45, H 4.60, N 5.60, S 19.15; m.p. 260.1 °C.

Bis(Anisylethynyl)dithienothiophene (**158**)

158
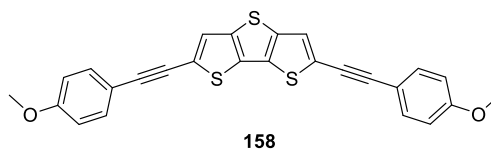
Yellow powder (0.4 g, 62 %); ^{1}H-NMR (500 MHz, CDCl$_3$): 7.48 (d, J=8.6, 2H), 7.41 (s, 1H), 6.90 (d, J=8.6, 2H), 3.84 (s, 3H); ^{13}C-NMR (125 MHz, CDCl$_3$): 160.1, 141.6, 133.1, 131.1, 124.7, 124.5, 114.6, 114.1, 95.0, 81.8, 55.4; IR (C≡C, neat, cm^{-1}): 2198.5; m/z (ES+): calc. 456.0312, found 457.0392; micro calc. C 68.39, H 3.53, S 21.07; found C 68.8, H 3.70, S 21.3; m.p. 206.0 °C.

Bis(Anisylethynyl)dithienothiophene (**159**)

159
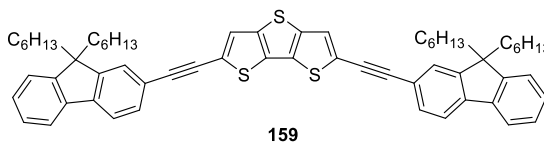
Yellow powder (0.51 g, 61 %); ^{1}H-NMR (500 MHz, CDCl$_3$): 7.70 (m, 2H), 7.52 (m, 2H), 7.48 (s, 1H), 7.34 (m, 3H), 1.98 (t, J=8.2, 4H), 1.11 (m, 4H), 1.05 (m, 8H), 0.77 (t, J=7.0, 6H), 0.63 (m, 4H); ^{13}C-NMR (125 MHz, CDCl$_3$): 151.1, 150.9, 142.0, 141.8, 140.3, 130.6, 127.7, 126.9, 125.8, 125.0, 124.5, 122.9, 120.6, 120.1, 119.8, 96.3, 83.1, 55.2, 40.4, 31.5, 29.7, 23.7, 22.6, 14.0; IR (C≡C, neat, cm^{-1}): 2195.6; m/z (ES+): calc. 909.4060, found 910.4101; micro calc. (%) C 81.89, H 7.54, S 10.58; found C 81.92, H 3.69, S 22.1; m.p. 179.7 °C.

2-Trimethylsilylethynyl-5-hexylthiophene (**163**)

163
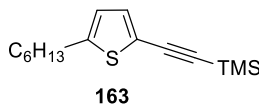
A solution of 2-bromo-5-hexylthiophene (2.00 g, 8.09 mmol), tetrakistriphenylphosphine palladium (0) (0.468 g, 0.405 mmol) and copper (I) iodide (0.0309 g, 0.162 mmol) in tetrahydrofuran (56 mL) was bubbled with nitrogen for 10 min. Diisopropylamine (8.09 mL, 57.7 mmol) was added and the solution was bubbled for 15 min. Trimethylsilylacetylene (1.72 mL, 12.1 mmol) was added and the mixture stirred for 1 h at room temperature under nitrogen overnight for 17 h. The solids were filtered off and the solvent removed affording a dark brown crystalline residue. The residue was purified

over a silica plug (100 % petroleum ether 40-60°C) giving an orange oil (1.93 g, 7.30 mol, 90 %); ^{1}H-NMR (500 MHz, CDCl$_3$): 6.86 (d, J = 3.6, 1H), 6.42 (d, J = 3.6, 1H), 2.57 (t, J = 7.5, 2H), 1.45 (t, J = 7.3, 2H), 1.10 (m, 6H), 0.69 (t, J = 6.8, 3H), 0.04 (s, 9H); ^{13}C-NMR (125 MHz, CDCl$_3$): 148.5, 132.8, 124.0, 120.5, 98.2, 97.8, 31.6, 31.6, 30.2, 28.7, 22.6, 14.1, 0.01.

4-Trimethylsilylethynylhexylbenzene (**164**)

164
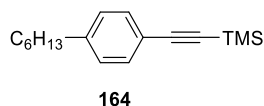
A solution of 4-bromohexylbenzene (5.00 g, 20.7 mmol), tetrakistriphenylphosphine palladium (0) (0.59 g, 0.511 mmol) and copper (I) iodide (0.0780 g, 0.410 mmol) in tetrahydrofuran (150 mL) was bubbled with nitrogen for 10 min. Diisopropylamine (20 mL) was added and the solution was bubbled for 15 min. Trimethylsilylacetylene (3.05 g, 13.0 mmol) was added and the mixture stirred for 18 h at room temperature under nitrogen overnight. The solids were filtered off and the solvent removed affording a dark brown crystalline residue. The crude was purified by flash column chromatography (petroleum ether 40-60°C) giving a clear oil (5.00 g, 94 %); ^{1}H-NMR (500 MHz, CDCl$_3$): 7.18 (d, J=8.3, 2H), 6.88 (m, 2H), 2.36 (m, 2H), 1.39 (m, 2H), 1.09 (m, 6H), 0.69 (m, 3H); ^{13}C-NMR (125 MHz, CDCl$_3$): 143.6, 141.78, 131.8, 131.2, 130.1, 128.3, 105.4, 93.2, 35.9, 35.3, 31.6, 31.3, 31.1, 28.8, 22.6, 14.0, 0.01.

2-Trimethylsilylethynyl-9,9-dihexylfluorene (**165**)

165
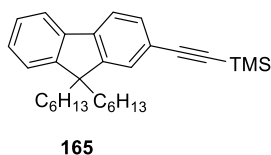
A solution of 2-bromo-9,9-dihexylfluorene (1.29 g, 3.12 mmol), tetrakistriphenyl phosphine palladium (0) (0.18 g, 0.156 mmol) and copper (I) iodide (0.0297 g, 0.156 mmol) in tetrahydrofuran (40 mL) was bubbled with nitrogen for 10 min. Diisopropylamine (5 mL) was added and the solution was bubbled for 15 min. Trimethylsilane (0.337 g, 3.43 mmol) was added and the mixture stirred for 17 h at room temperature under nitrogen overnight. The solids were filtered off and the solvent removed affording a dark brown

crystalline residue. The crude was purified by flash column chromatography (petroleum ether 40-60°C) giving a clear oil (0.99 g, 74 %);^{1}H-NMR (500 MHz, CDCl$_3$): 7.67 (m, 1H), 7.61 (d, J=7.8, 1H), 7.44 (m, 2H), 7.31 (m, 3H), 1.94 (t, J=8.9, 4H), 1.11 (m, 4H), 1.02 (m, 8H), 0.76 (t, J=7.2, 6H), 0.56 (m, 4H), 0.28 (s, 9H); ^{13}C-NMR (125 MHz, CDCl$_3$): 151.0, 150.5, 141.6, 140.3, 131.0, 127.4, 126.8, 126.2, 122.8, 121.1, 119.9, 119.4, 106.2, 93.7, 55.0, 40.3, 31.4, 29.6, 23.6, 22.5, 13.9, -0.01.

2-Ethynyl-5-hexylthiophene (**166**)
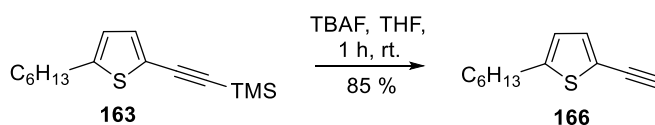
A 2 M solution of tetrabutylammonium fluoride (4.54 g, 14.4 mmol) in tetrahydrofuran (17.2 mL) was added dropwise to a solution of 2-trimethylsilylethynyl-5-hexylthiophene (**163**) (1.9 g, 7.19 mol) in tetrahydrofuran (10 mL) in air at room temperature. After 1 h, the reaction mixture was quenched with water (50 mL), then extracted with diethyl ether (25 mL × 3), washed with brine ad dried over sodium sulfate. The solvent was removed affording crude black semicrystalline residue. The crude was purified over a silica plug (100 % hexane) giving an orange oil (1.17 g, 6.08 mmol, 84.6 %); [1]H (500 MHz, CDCl$_3$): 6.86 (d, J = 3.6, 1H), 6.42 (d, J = 3.6, 1H), 3.03 (s, 1H), 2.57 (t, J = 7.5, 2H), 1.45 (p, J = 7.3, 2H), 1.10 (m, 6H), 0.69 (t, J = 6.8, 3H), 0.04 (s, 9H) ; ^{13}C-NMR (125 MHz, CDCl$_3$): 148.5, 132.8, 124.0, 120.5, 98.2, 97.8, 31.6, 31.6, 30.2, 28.7, 22.6, 14.1.

4-Ethynylhexylbenzene (**160**)
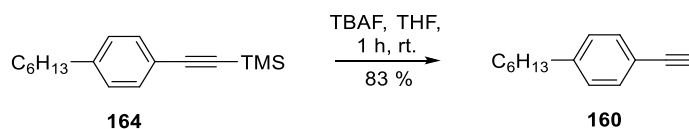
4-Trimethylsilylethynylhexylbenzene (**164**) (5.00, 19.3 mmol) was dissolved in tetrahydrofuran (50 mL) and cooled to 0 °C. Tetrabutylammonium fluoride (12.6 g, 48.3 mmol) was added in portions and the mixture was allowed to warm to room temperature and stir for 1 h. The mixture was poured onto water (250 mL) and extracted with diethyl ether (50 ml × 3). The organic layers were collected together, washed with brine (50 ml × 2) and dried over magnesium

sulfate. The solvent was removed under reduced pressure and the crude was purified with flash column chromatography (petroleum ether 40 -60 °C) affording a clear oil (3.02 g, 83 %); ^{1}H-NMR (500 MHz, CDCl$_3$): 7.31 (t, J=7.2, 2H), 7.04 (d, J=8.3, 1H), 6.96 (d, J = 8.5, 1H), 3.67 (m, 2H), 2.94 (s, 2H), 1.51 (m, 6H), 0.81 (m, 3H); ^{13}C-NMR (500 MHz, CDCl$_3$): 141.8, 132.0, 131.2, 130.2, 119.2, 98.4, 83.9, 35.3, 33.2, 31.7, 28.8, 22.6, 14.1.

2-Ethynyl-9,9-dihexylfluorene (**167**)
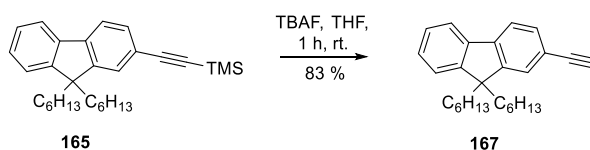
2-Trimethylsilylethynyl-9,9-dihexylfluorene (**165**) (1.00 g, 2.32 mmol) was dissolved in tetrahydrofuran (50 mL) and cooled to 0 °C. Tetrabutylamonium fluoride (4.64 mL, 1M, 4.64 mmol) was added in portions and the mixture was allowed to warm to room temperature and stir for 1 h. The mixture was poured onto water (250 mL) and extracted with diethyl ether (50 mL × 3). The organic layers were collected together, washed with brine (50 ml × 2) and dried over sodium sulfate. The solvent was removed under reduced pressure and the crude was purified with flash column chromatography (petroleum ether 40-60 °C) affording a clear oil (0.69 g, 83 %); ^{1}H-NMR (500 MHz, CDCl$_3$): 7.68 (m, 1H), 7.63 (d, J=7.7, 1H), 7.47 (m, 2H), 7.32 (m, 3H), 3.13 (s, 1H), 1.96 (t, J=8.4, 4H), 1.10 (m, 4H), 1.03 (m, 8H), 0.76 (t, J=7.2, 6H), 0.59 (m, 4H); ^{13}C-NMR (500 MHz, CDCl$_3$): 151.1, 150.7, 141.9, 140.3, 131.1, 127.6, 126.9, 126.5, 122.9, 120.1, 120.1, 119.6, 84.8, 76.9, 55.1, 40.3, 31.5, 29.7, 23.7, 22.6, 14.0.

4.3.3.2 Molecular Rod Modification Example – Black Dye

Leeds Black 154 (**174**)
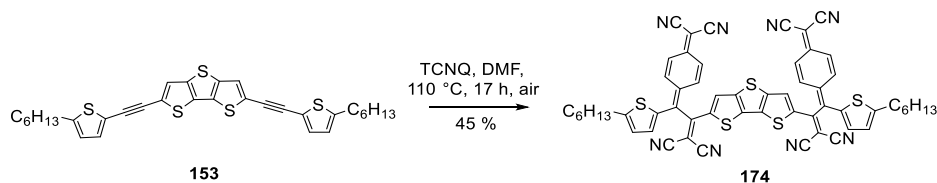
A mixture of 2,2'-dihexylthienylalkynyl-DTT (0.100 g, 0.173 mmol), 7,7,8,8-tetracyanoquinodimethane (0.106 g, 0.52 mmol) and dimethylformamide (10 mL) was stirred at 110 °C for 17 h in air. Once cool, the mixture was poured onto water (50 mL) and the aqueous phase extracted with ethyl acetate (150 mL × 3). The organic layers were collected together and washed with brine, dried and evaporated giving a dark crude residue. The crude was purified (silica, ethyl acetate) affording a dark green/turquoise solid (0.0391 g, 0.0397 mmol, 45 %); ^{1}H (500 MHz, CDCl$_3$): 7.96 (dd, J = 9.4, 1H), 7.80 (d, J = 4.1, 1H), 7.61 (s, 1H), 7.46 (dd, J = 10.1, 1H), 7.28 (dd, J = 1.8, 9.8, 1H), 7.01 (dd, J = 1.9, 9.6, 1H), 6.98 (d, J = 4.2, 1H).

Chapter 5

Results and Discussion

5.1 Charge Transfer for Acenes: The case for Air-Stable and Alternative Isomeric Candidates of Pentacene

5.1.1 Background

There has been great progress in the fields of materials chemistry and engineering in the last few decades for high-performing small-molecule charge-transfer materials[145–148] as the active component in optoelectronic devices which include light emitting diodes, photovoltaics and flexible display screens[11,149–152]. Charge-transfer materials need to overcome a number of diverse issues and further satisfy the increasing demand of greater performance, driven both by commercial growth and scientific inquest. Such macroscopic issues include industrial-scale device fabrication, the ease of processing each individual component layer, and overall device performance. While these are highly important, there are a number of microscopic issues at the molecular level which have yet to be addressed, and include air stability for ambient condition processing and efficient charge transfer across the active layer. Thus, suitable molecular structures are needed to bring together all the above concepts and provide the next generation of candidates for high-performing properties and device outputs.

Polycyclic aromatic hydrocarbons (PAHs) have been extensively investigated as organic semiconductors (OSCs) for the active layer in organic electronic devices. These are found to satisfy a large number of the above issues, yet there are few which have both air-stability and high charge-transfer properties. One line of inquiry is the investigation of the charge transfer mechanisms[24,46,153] for the improvement of organic-based devices. These investigations tend to focus on single-crystal OSC devices, where charge transfer mobility can reach as high as 35 cm^2 V^{-1} s^{-1} with a PAH molecule called pentacene[154–158]. Pentacene (**1**, Figure 24) is comprised of five fused benzene rings in a linear array of only carbon and hydrogen atoms.

1   **2**
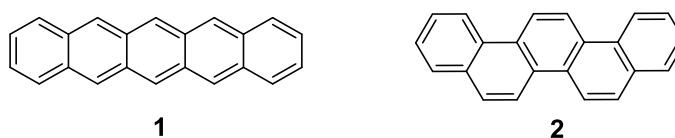
Figure 24. Structures of pentacene (**1**) and picene (**2**).

Single crystals of OSCs are commonly used because of their close-packing continuum of the organic molecules in the solid phase. On the other hand, the OSCs applied to organic electronics are in a thin-film state

and do not necessarily obey the same charge transport conduction mechanisms[47], even though they can still reach high transport mobilities, such as 3.0 cm^2 V^{-1} s^{-1} with a thin-film transistor of pentacene[4,156]. For this reason, more fundamental investigations, based solely on their molecular structures and not on the device architecture, are needed.

It was found that pentacene gave different values for the same charge-transfer and optoelectronic properties, depending on the applied experimental conditions. It was soon evident that pentacene is unstable in air[148] due to its small HOMO-LUMO gap (E_g = 1.8 eV), so is easily oxidised and difficult to operate under ambient conditions. Picene, an isomer of pentacene (**2**, Figure 24), is surprising in the sense that its charge transport benefits from oxygen doping[63,159,160], which is a well-known p-type doping phenomenon[161–163] with other OSCs. This suggests that picene with E_g = 4.21 eV has a superior stability over pentacene, imparted only from its molecular structure.

The stability can be explained with the aromatic sextet rule by Clar[164], which was described as being an important factor in the characterisation of PAHs; aromatic sextets are six localised π-electrons in a single six-membered carbon structure, such as benzene. Clar's rule is that a molecular structure with a given number of sextets is more stable than other resonance structures which have fewer sextets. This is illustrated with pentacene in Figure 25, which shows three possible Kekulé resonance structures in its closed shell form, each one having a π-sextet. If each resonance structure has the same number of sextets (*i.e.* one in a closed shell of pentacene), then a superposition of aromaticity is designated with an arrow, which shows the Clar structure and the rings it can migrate over.

Clar's Rule

Clar structure with a migrating π-sextet

Kekule resonance structures with π-sextets
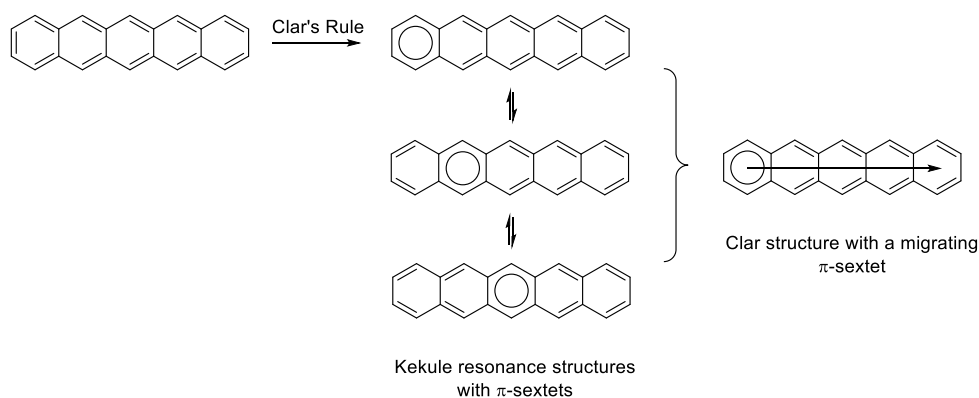
Figure 25. Kekulé resonance structures and the Clar structure of pentacene.

However, re-evaluation of Clar's rule suggests that pentacene may be more stable in an open shell singlet state[165], as shown in Figure 26. Two π-sextets are formed with two single radicals in the central ring at the *peri* positions. This explains why upon exposure to air, these two carbons readily oxidise into carbonyls or peroxides, disrupting the conjugation and thereby reducing the charge carrier mobility.
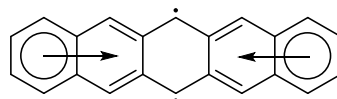
Figure 26. The Clar structure of pentacene in open shell state, having two π-sextets and two unpaired electrons localised on the central ring.

Applying Clar's rule to picene gives just one single Kekulé resonance structure, which has the greatest number of π-sextets (three); one and two π-sextet resonances are available but these are less stable than three. As no more than three π-sextets are possible, there is no possibility of generating the open shell singlet state, which explains why picene is less susceptible to oxygen than pentacene.
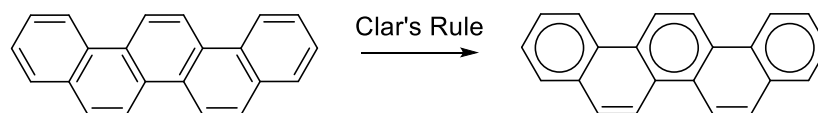
Figure 27. Application of Clar's rule to picene generates one closed-shell Kekulé resonance structure.

Although structure-property relationships were further explored through both experimental observations and theoretical calculations[160,166], the studies, however, focused on the charge-transfer properties of just these two isomers alone. There are twelve known isomers of (and including) pentacene[167–169], which have the formula $C_{22}H_{14}$. It is thus reasonable to continue this long line of investigation and probe the properties of the other isomers.

So far, their structures have only been explored with regards to their size[167] and aromatic nature[168,169]. To date, there are no known studies on the fundamental electronic and optical properties of the isomers of pentacene, even though there are reports of some being successfully synthesised, but not

subjected to charge-transfer investigations[170,171]. The identification and characterisation of these isomeric structures is paramount to develop this set of $C_{22}H_{14}$ PAHs and more importantly, determine which isomers are best suited for acene-based small-molecule technology.

This can be investigated with computational chemistry, where electronic and optical properties can be adequately modelled using a combination of molecular and quantum mechanics. Generally, a range of theories are tested and compared with experimental observations where possible or other theoretical calculations in the literature, then one is selected and applied to a wider range of structures. This approach has huge merit for materials chemistry and particularly small-molecule organic electronic devices, as large numbers of structures can be effectively screened for the active layer prior to any synthetic experiments undertaken and subsequently minimises both the resources and the time used in synthetic endeavours, as structures predicted to have high-performing properties can be specifically targeted out of a pool of potential candidates.

It is thus appropriate to deploy different theories which include density functional theory (DFT), Koopmans Theorem (KT) and Green's Function to calculate the physical properties of these isomers and identify suitable isomers as alternative candidates for the improvement of (1) their stability relative to pentacene, and (2) high charge-transfer properties for organic electronics. Their stability is investigated first by predicting the HOMO-LUMO gaps and ionisation energies of the twelve isomers and then probe their charge-transfer properties through the Marcus Theory, which involves the calculation of their internal reorganisation energies and using the 'splitting-in-dimer' method to calculate the transfer integrals across three intermolecular separations ($d = 3.0$, 3.5 and 4.0 Å); these parameters enable the rates of charge transfer to be determined and thus a deep understanding of the suitability of the isomers for organic electronic applications in comparison to pentacene. The overall purpose is to theoretically evaluate the properties of pentacene's isomers and determine if virtual screening is a worthy pursuit, prior to synthetic investigations, as a method of uncovering new and high-performing candidates and in turn highlight those which may have improved properties.

5.1.2 Virtual Screening of Pentacene's Properties

Different DFT functionals were screened against pentacene's FMO experimental properties, with other theories such as KT, OVGF and P3 deployed for comparison of the vertical ionisation energy. The charge-transfer properties, such as the internal reorganisation energy, transfer integral and rate of charge transfer, were then calculated and compared to experimental and theoretical literature values. Table 3 shows the hybrid functionals B3LYP and PBE0, which gave the closest HOMO, LUMO and E_g energies in comparison to the experimental energies[10,172] of -5.00 eV, -3.20 eV and 1.80 eV respectively, although the B3P86, BHandH and BHandHLYP functionals were off by more than 0.5 eV. While the pure functionals BLYP and PBEPBE proved exceptionally poor, the worst performing functionals were those of the long-range corrected or range-separated hybrids, namely LC-BLYP, LC-ωPBE, CAM-B3LYP and ωB97XD, with differences to experiment between 1-2 eV.

In stark contrast, the long-range corrected functionals gave some of the closest values to the experimental first vertical ionisation energy[173] of 6.59 eV, with LC-BLYP and LC-ωPBE proving the most accurate, except for CAM-B3LYP which has a difference of 0.76 eV. Interestingly, the ωB97XD gave a close under estimation of 6.42 eV, while the hybrid B3P86 over estimates at 6.84 eV. The widely-used Koopmans' Theorem underperformed by 0.53 eV, similar to the BLYP functional. The outer valence Green's function gave relatively similar values to the hybrid functionals B3LYP and PBE0, while the third order electron propagator, P3, was the most accurate, slightly beating LC-BLYP, at 6.51 eV.

Table 4 shows the calculated internal hole reorganisation energies (λ_h), hole transfer integral (t_h) and the rate of charge transfer (K_{CT}) for each functional; Grimme's third-order dispersion (D3) term were added for comparison of the intermolecular interactions. The lowest reorganisation energy were found with BLYP and PBEPBE (61 meV), followed closely by B3P86 (94 meV) and B3LYP (97 meV), which correlate well with both the experimental value[173] of 59 meV and theoretical calculations[135,174,175]. PBE0 gave a similar energy, 106 meV, while other hybrid functionals such as ωB97XD, BHandH and BHandHLYP are relatively higher at 171, 159 and 176 meV respectively. The largest reorganisation energies for pentacene were obtained with the long-range corrected functionals, including LC-BLYP (291 meV), CAM-B3LYP (189 meV) and LC-ωPBE (265 meV).

The spacing of $d = 3.3$-3.8 Å are reported in the literature[132,174,176] to be suitable for the transfer integrals of OSCs such as pentacene, although d was set to 3.0, 3.5 and 4.0 Å to determine how the functionals affect the electronic coupling over specific 0.5 Å differences of intermolecular separations. The first trend is the depreciation of both the transfer integral and the rate constant with increasing dimer spacings, across the range of functionals used, in agreement with the literature[48]. This is natural, as the intermolecular distances increase, *i.e.* the molecules in the dimer become further separated, their electronic coupling decreases and thus charge transfer would diminish. With each 0.5 Å increment, the hole transfer integrals decrease exponentially[174]

Table 3. HOMO, LUMO, E_g and vertical ionisation potential (IE_v) of pentacene, in electron volts (eV) with various functionals.

Functional	HOMO	LUMO	E_g	IE_v
BLYP	-4.26	-3.12	1.15	5.99
LC-BLYP	-7.16	-0.75	6.41	6.65
B3LYP	-4.94	-2.75	2.19	6.23
CAM-B3LYP	-6.04	-1.70	4.33	5.83
LC-ωPBE	-7.12	-0.89	6.23	6.65
PBEPBE	-4.45	-3.31	1.15	6.18
PBE0	-5.09	-2.64	2.45	6.27
ωB97XD	-6.57	-1.14	5.43	6.42
B3P86	-5.55	-3.36	2.19	6.84
BHandH	-5.57	-1.77	3.80	6.17
BHandHLYP	-5.59	-1.75	3.84	6.16
KT				6.06
OVGF				6.25
P3				6.51
Experimental	-5.00	-3.20	1.80	6.59

for the BLYP functionals, from 416 meV at 3.0 Å through 315 meV at 3.5 Å to 144 meV at 4.0 Å. Interestingly, there is little interaction of the Grimme's third-order dispersion across the dimer separations $d = 3.0\text{-}4.0$. The wB97XD, B3P86, BHandH and BHandHLYP functionals have exceedingly high hole transfer integrals for $d = 3.0$ Å at 804, 633, 764 and 745 meV respectively, similar to the long-range functionals such as LC-BLYP (826 meV), CAM-B3LYP (790 meV) and LC-ωPBE (806 meV). The majority of the hybrid functionals give relatively lower hole transfer integrals around 345-350 Å. Moreover, the integrals at 4.0 Å range between 140 and 190 meV for the uncorrected pure and hybrid functionals; interestingly that of B3LYP has excellent correlation with thin-film studies[177].

The charge-transfer rate constants are of the order $0.014\text{-}1.963\times10^{15}$ s^{-1} for the dimer distances $d = 3.0\text{-}4.0$ Å and functionals investigated in agreement with the literature[132,174]. The rates calculated at the 3.0 Å spacing were found to be relatively lower with long-range corrected functionals such as LC-BLYP ($K_{CT} = 0.199\times10^{15}$ s^{-1}) and CAM-B3LYP ($K_{CT} = 0.610\times10^{15}$ s^{-1}) than uncorrected pure BLYP ($K_{CT} = 1.04\times10^{15}$ s^{-1}) and hybrid B3LYP ($K_{CT} = 1.30\times10^{15}$ s^{-1}) respectively; this trend is reproducible with increasing d. The transfer integrals for long-range functionals approximately halve with each 0.5 Å angstrom increment, inferring a linear dependency, but the uncorrected pure and hybrid functionals show exponential decreases in accordance with the literature[174]. Having screened pentacene's properties with various functionals (Table 3), it is apparent that neither dispersion nor long-range functionals are appropriate for further investigations but rather the best performing one was B3LYP and therefore selected for the calculation of the electronic and optical properties of the remaining isomers.

Table 4. Internal hole reorganisation energy (λ_h / meV), hole transfer integral (t_h / meV) and the rate of charge transfer ($K_{CT} \times 10^{15}$ / s^{-1}) for each functional at d = 3.0, 3.5 and 4.0 Å dimer spacings for pentacene

		d=3.0 Å			d=3.5 Å		d=4.0 Å	
Functional	λ_h	t_h	K_{CT}	t_h	K_{CT}	t_h	K_{CT}
BLYP	61	416	1.04	315	0.595	144	0.124
BLYP-D3	61	418	1.04	315	0.594	144	0.124
LC-BLYP	291	826	0.199	419	0.051	200	0.012
B3LYP	97	624	1.30	345	0.397	159	0.084
B3LYP-D3	97	625	1.30	345	0.397	159	0.084
CAM-B3LYP	189	790	0.610	381	0.142	180	0.032
CAM-B3LYP-D3	169	791	0.786	381	0.183	180	0.041
LC-ωPBE	265	806	0.256	399	0.063	185	0.014
LC-ωPBE-D3	265	806	0.256	399	0.063	185	0.014
PBEPBE	61	413	1.02	315	0.592	142	0.120
PBEPBE-D3	61	414	1.03	315	0.592	141	0.120
PBE0	106	654	1.25	351	0.362	160	0.075
PBE0-D3	106	655	1.25	351	0.362	160	0.075
ωB97XD	171	804	0.791	383	0.179	181	0.040
B3P86	94	633	1.40	345	0.416	156	0.085
BHandH	159	764	0.832	404	0.233	190	0.051
BHandHLYP	176	745	0.638	176	0.176	183	0.039

5.1.3 Charge-Transfer Calculations for Pentacene's Isomers

The twelve known isomers of pentacene are illustrated in Figure 28, with selected bond lengths and angles. Their shapes vary from linear (pentacene, isomer **13**) to phenacene-like (picene, isomer **14**). Isomers benzo[*g*]chrysene **32** and dibenzo[*a,c*]anthracene **37** have a phenacene-like backbone with a phenyl ring appended in a *sec* and *tert* arrangement, respectively. The remaining isomers **33**-**36** and **38**-**41** have an end-on-end linear-array of phenyl rings, which includes the nonplanar structures benzo[*c*]chrysene **40** and dibenzo[*c,c'*]phenanthrene **41**. Isomer **41** is unusual, as it is a primitive or a 'half' helicene, making it a distinctive non-planar structure; there are four nonplanar structures in total, namely isomers **33**, **36**, **40** and **41**, as illustrated in Figure 29. **33** has a saddle-horse type structure, **36** and **40** have out-of-plane phenyl rings and **41** is half helical.

It is important to note the arrangements of the phenyl rings and the separation between the adjacent C-H units[178]. For example, pentacene has a zig-zag motif imparted by a 1,3 C-H arrangement, whereas picene has a chair motif from a 1,4 C-H arrangement. Structures which have 1,5 (**33**, **40**) or 1,6 (**41**) arrangements are found, as expected, to be non-planar, due to steric hindrance.

Pentacene	Picene	Benzo[*g*] chrysene
13	**14**	**32**

Benzo[*b*] chrysene	Dibenzo[*a,h*] anthracene	Dibenzo[*d,d'*] phenanthrene
33	**34**	**35**

Naphtho[*c*] phenanthrene	Dibenzo[*a,c*] anthracene	Dibenzo[*a,f*] anthracene
36	**37**	**38**

Benzo[*a*] tetracene	Benzo[*c*] chrysene	Dibenzo[*c,c'*] phenanthrene
39	**40**	**41**
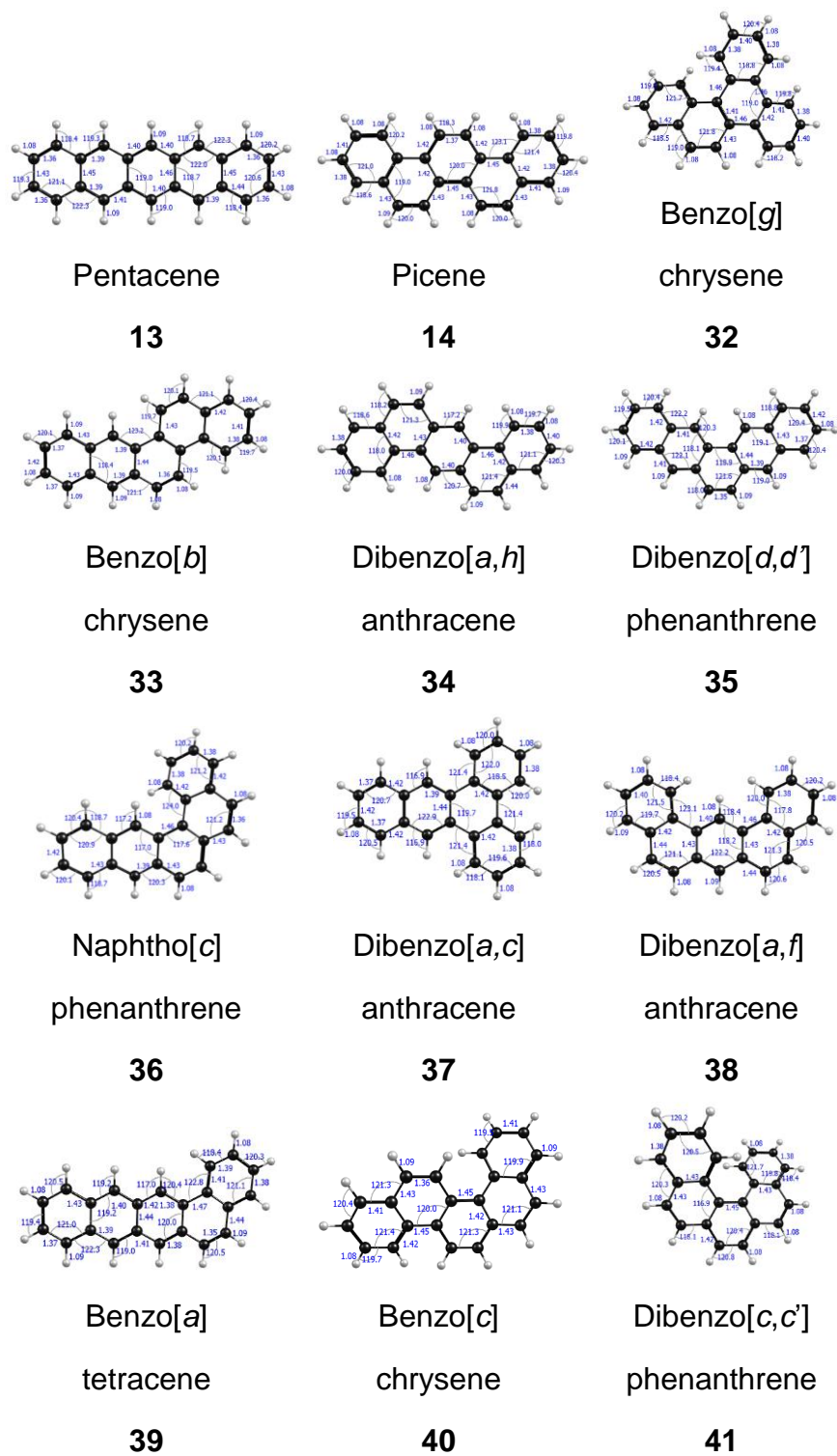
Figure 28. Structures of the twelve isomers with selected angles (°) and bond lengths (Å).

- 108 -

Benzo[*g*]chrysene

33

Naphtho[*c*]phenanthrene

36

Benzo[*c*]chrysene

40

Dibenzo[*c,c'*]phenanthrene

41
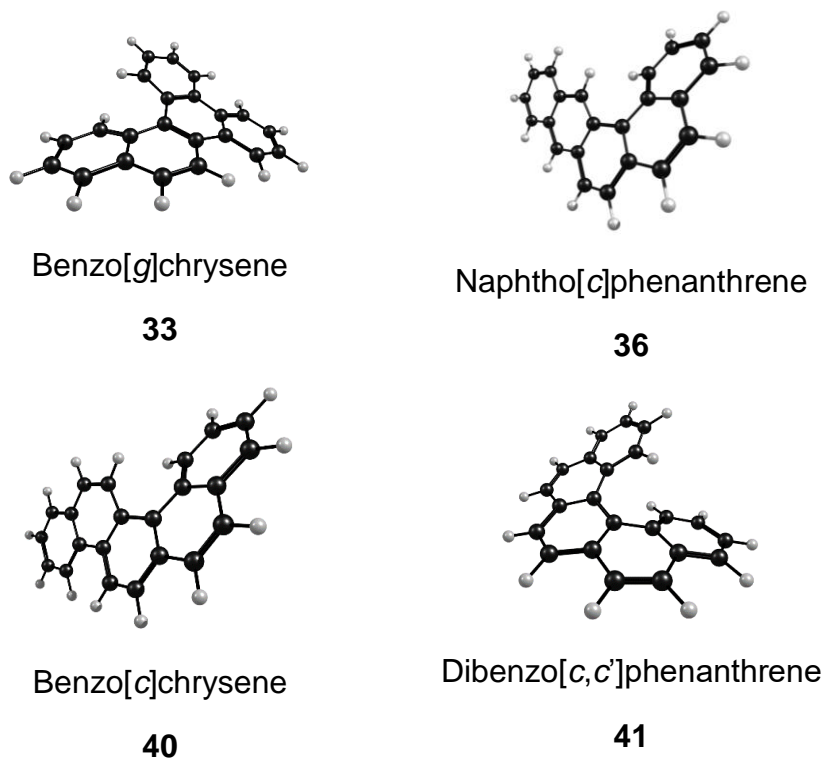
Figure 29. Structures of the four non-planar isomers.

The HOMO energy level of pentacene (-4.94 eV) is the highest out of all the isomers studied (Table 5); the relatively high HOMO energy is a known issue, which is considered to contribute to its instability[160,166]. By rearranging just one of the terminal rings, isomer **39** shows a relatively similar HOMO energy at -5.29 eV but significant improvement in stability, as evidenced by an increase in both the E_g and the optical gap energies, by more than 0.6 and 0.69 eV respectively; however **39** is the second least stable after pentacene out of all the isomers.

Other than picene, the remaining planar isomers **33-35** and **37** and **38** also have significantly improved stability and deeper HOMO levels than pentacene. Isomer **38** is one of the most stable planar structures (E_g = 3.89 eV) excluding picene; followed closely by isomers **34** and **37**, which have the same gap (E_g = 3.85 eV). The FMO energies of the non-planar **32**, **40** and **41** isomers are relatively similar to those of picene (**14**), with their deep HOMO levels centred at -5.85 eV, the LUMO at 1.70 eV and the E_g at 4.2 eV; **36** is the exception with values -5.52, -2.10 and 3.42 eV respectively, but not far from ideal. The HOMO-1 states for isomers **13** to **34** and **36** to **39** are relatively

Table 5. HOMO, LUMO, E_g, optical gap (S_0-S_1) with the oscillator strength in parenthesis of the optimised isomers at the B3LYP/6-311++G(d,p) level, in electron volts (eV).

Entry	H-1	H	L	L+1	E_g	S_0-S_1
13	-6.22	-4.94	-2.75	-1.33	2.19	1.90 (0.04)
14	-6.12	-5.85	-1.64	-1.59	4.21	3.55 (0.006)
32	-6.21	-5.80	-1.75	-1.38	4.05	3.60 (0.02)
33	-6.32	-5.55	-2.07	-1.32	3.48	3.10 (0.07)
34	-6.12	-5.72	-1.87	-1.56	3.85	3.36 (0.02)
35	-5.82	-5.66	-1.92	-1.90	3.75	3.11 (0.002)
36	-6.17	-5.52	-2.10	-1.36	3.42	3.02 (0.04)
37	-6.25	-5.76	-1.91	-1.32	3.85	3.43 (0.02)
38	-6.04	-5.76	-1.87	-1.56	3.89	3.38 (0.0004)
39	-6.28	-5.29	-2.37	-1.32	2.92	2.59 (0.04)
40	-5.95	-5.88	-1.67	-1.67	4.21	3.43 (0.002)
41	-5.97	-5.84	-1.72	-1.69	4.12	3.35 (0.001)

similar, focusing around -6.20 eV, suggesting this is a common and stable lower FMO energy; although no distinct trend is observed with the LUMO+1 states. The FMO levels are illustrated in Figure 30 and clearly shows the trends in stability between the planar and non-planar isomers, which correlate well with the literature[177,179–181].

These trends are reflected in the optical gap (S_0-S_1 / eV), determined from TD-DFT calculations. The excitation wavelengths of **34**, **37**, **40** and **41** are nearly doubled in comparison to pentacene (3.35-3.43 eV). **33** and **35** have moderate stability (3.10-3.11 eV), while the lowest is with isomer **39** at 2.59 eV. Interestingly, the non-planar isomer **3** is the most stable, more than picene by 0.05 eV.
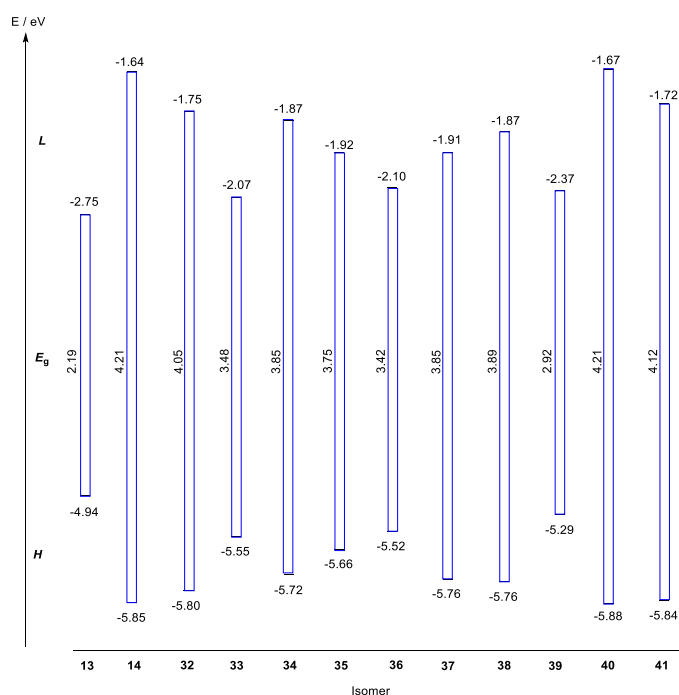
Figure 30. FMO energy diagram of HOMO (H), LUMO (L) and E_g (H-L separation drawn as bars) for all isomers with energies in electron volts (eV).

So far, the twelve isomers and their various optical properties have been probed, leading to trends in stabilities. Now, their ionisation energies are investigated with three different types of theories (two DFT, KT and Green's function with the P3 variant). The data in Table 3 implies that long-range functionals such as LC-BLYP overestimates, while pure BLYP underestimates, B3LYP is moderate and similar to that of OVGF, KT is poor and P3 is the most accurate with respect to the experimental value. With this understanding, these functionals are applied to calculate the vertical ionisation energies that are expected to bracket the experimental values.

Table 6 shows the vertical ionisation energy of the twelve isomers, and lists the pole strengths in parenthesis for OVGF and P3. All of the isomers **14** to **41** show relatively higher vertical ionisation energies than pentacene, with values reaching 7.24 eV with **40**, a difference of 1.11 eV. All reproduce the trend that pentacene has the lowest ionisation energy, followed closely by isomers **39** and then **33**. Except for pentacene, KT and OVGF give similar values for each isomer, which are on average 0.15 eV greater than the B3LYP functional; the LC-BLYP functional consistently gives the largest IE_vs, and has

- 111 -

a difference to B3LYP between 0.4 and 0.6 eV. The variation between the theories and the isomers are illustrated in Figure 31.

In general, the P3 functional gives values that are 0.2 eV greater than the commonly used OVGF functional. The IE_v for picene with P3 is 7.58 eV, which is in excellent agreement with the experimental value at 7.51 eV and suggests that P3 should be given more attention in future studies, particularly due to its level of accuracy over OVGF. The P3 values for isomers **32** (7.54 eV) and **41** (7.59 eV) are remarkably similar to that of picene, while those of **34**, **37** and **38** are similar to each other at 7.44 eV. Both isomers **33** and **35** have relatively low ionisation energies (P3) with 7.24 eV and 7.3 eV respectively. Isomer **40** has the greatest IE_v, only slightly larger than picene's theoretical value[177] by 0.06 eV, but significantly greater than pentacene with a difference of 1.11 eV. Isomer **39** is the second lowest at 6.94 eV, after pentacene, but the difference between them is a stabilising 0.43 eV.

Table 6. 1st Vertical ionisation energy (IE_v) in electron volts (eV), calculated with B3LYP, LC-BLYP, Koopmans' Theorem (KT), Outer Valence Green's Function (OVGF) and the Third Order Electron Propagator (P3) with their associated pole strengths (PS).

Entry	B3LYP	LC-BLYP	KT	OVGF	P3
13	6.23	6.65	6.06	6.25 (0.87)	6.51 (0.85)
14	7.20	7.82	7.42	7.37 (0.88)	7.58 (0.86)
32	7.16	7.67	7.31	7.28 (0.88)	7.54 (0.87)
33	6.88	7.44	6.98	7.01 (0.88)	7.24 (0.86)
34	7.07	7.65	7.24	7.20 (0.88)	7.42 (0.86)
35	6.99	7.57	7.16	7.14 (0.87)	7.35 (0.86)
36	6.87	7.40	7.03	6.98 (0.88)	7.29 (0.86)
37	7.12	7.71	7.29	7.25 (0.88)	7.48 (0.86)
38	7.10	7.71	7.28	7.23 (0.88)	7.46 (0.86)
39	6.62	7.11	6.64	6.71 (0.87)	6.94 (0.86)
40	7.24	7.85	7.43	7.39 (0.88)	7.62 (0.86)
41	7.21	7.79	7.38	7.35 (0.88)	7.59 (0.87)
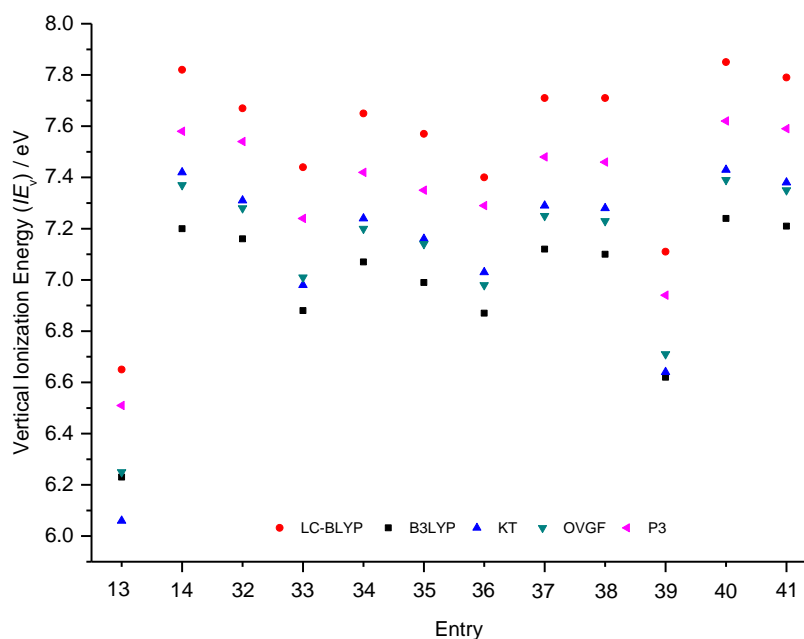
Figure 31. Vertical ionisation energies (IE_V) in electron volts (eV) calculated using different theories (LC-BLYP, B3LYP, KT, OVGF, P3) for all isomers.

The investigations now focus on (1) the structural relaxation ability of the isomers by calculating their internal hole reorganisation energies, (2) their electronic coupling transfer integrals and (3) their rates of charge transfer, for each dimer separation $d = 3.0$, 3.5 and 4.0 Å, as illustrated in Table 7. The internal hole reorganisation energies are overall relatively low, with isomers **33** and **36** to **40** being exceptional between 115 and 143 meV (Figure 7). Relatively high values are observed with **32** (188 meV), **34** (171 meV) and **35** (181 meV), which are similar to that of picene (188 meV); isomer **41** has the highest hole reorganisation energy with 212 meV.

Except for pentacene, the hole transfer integrals of the remaining isomers are largely unchanged between the $d = 3.0$ and 3.5 Å separation. The greatest difference is between the $d = 3.5$ and 4.0 Å separation, where the hole transfer integrals are approximately halved. At $d = 3.0$ Å, pentacene has the largest transfer integral at 624 meV, with relatively high values for isomers **33** (383 meV), **36** (284 meV), **37** (242meV) and **39** (486 meV). At $d = 3.5$ Å, these values for the same isomers remain largely unchanged with differences of < 20 meV. At $d = 4.0$ Å, the integral for **36** has decreased by 165 meV, although remarkably, those of isomers **37** and **39** are the same as pentacene

Table 7. Hole reorganisation energy (λ_h / meV) for each isomer and the hole transfer integral (t_h / meV) with the rate of charge transfer ($K_{CT} \times 10^{14}$ / s^{-1}) for each intermolecular separation of d = 3.0, 3.5 and 4.0 Å.

Entry	λ_h	t_h	K_{CT}	t_h	K_{CT}	t_h	K_{CT}
		d = 3.0 Å		d = 3.5 Å		d = 4.0 Å	
13	97	624	13.022	345	3.968	159	0.841
14	188	147	0.213	144	0.206	141	0.197
32	188	194	0.373	201	0.400	120	0.142
33	122	383	3.433	353	2.918	164	0.632
34	171	205	0.516	205	0.513	162	0.323
35	181	83	0.075	82	0.072	80	0.070
36	133	284	1.627	292	1.715	127	0.326
37	127	242	1.277	244	1.296	159	0.552
38	133	139	0.386	139	0.390	140	0.392
39	115	486	6.082	346	3.087	159	0.653
40	143	20	0.007	18	0.006	23	0.009
41	212	159	0.212	40	0.012	3	0.000

at 159 meV, with those of isomers **33** and **34** being even greater at 164 and 162 meV respectively. The relatively strong electronic coupling at this separation may be due to the isomers **34**, **34**, **37** and **39** being both planar and have linear anthracene segments in their structures, with the exceptions being **35** and **38.**

The rates of charge transfer at d = 3.0 Å for **33**, **36**, **37** and **39** are exceptional with K_{CT} = 3.43, 1.63, 1.28 and 6.08×10^{14} s^{-1} respectively, in comparison to that of pentacene's (13.0×10^{14} s^{-1}); at d = 3.5 Å, their rates are of the same order of magnitude at K_{CT} = 2.92, 1.72, 1.30 and 3.09×10^{14} s^{-1} respectively; those for d = 4.0 Å are significantly lower. It is clear these isomers out-perform all other isomers, except for pentacene, with increasing dimer separation. The non-planar isomer **32** has a transfer integral and rate constant of 301 meV and 0.400×10^{14} s^{-1} respectively, which is unexpected given its distorted structure. Those of the other two non-planar isomers **40** and **41** are much less so, with rates up to three orders of magnitude less. The
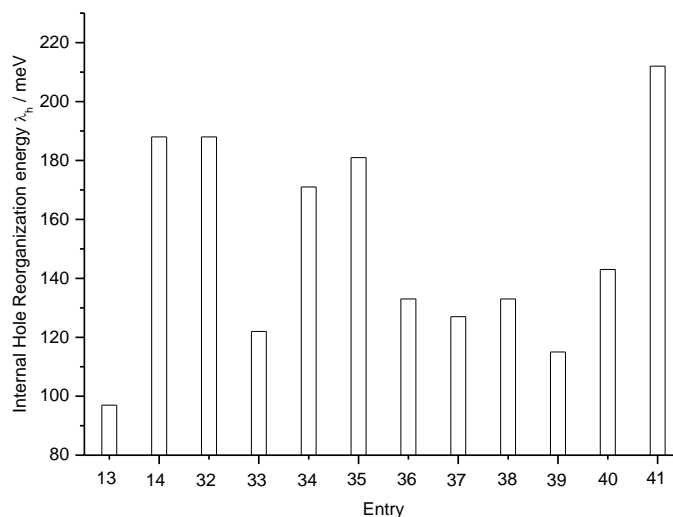
Figure 32. Internal hole reorganisation energy (λ_h) in millielectron volts (meV) for each isomer.
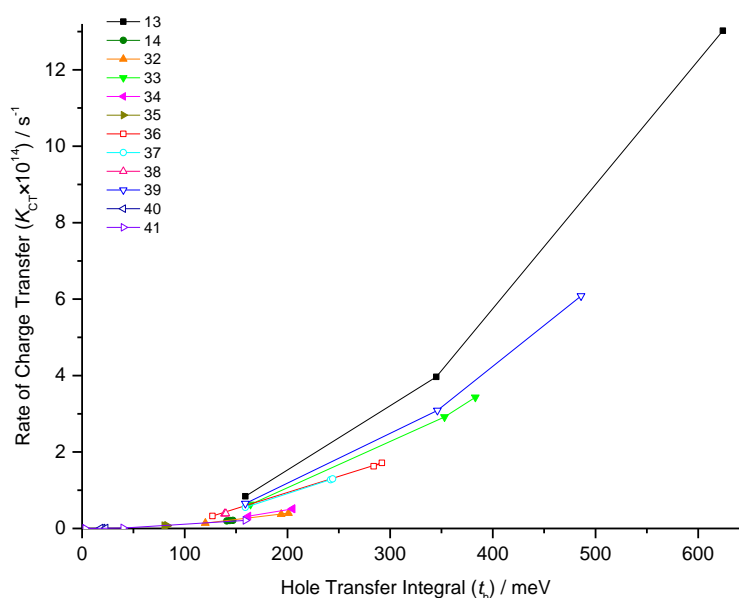
Figure 33. The rate of charge transfer (K_{CT}) versus the hole transfer integral (t_h) in electron volts (meV) for each intermolecular separation (d = 3.0, 3.5, 4.0 Å, decreasing separation with increasing transfer integral) for all isomers.

alternative contenders with regards to rates of charge transfer are easily identified from Figure 33, which shows the high-performing values of pentacene at each dimer separation (decreasing from 4.0 to 3.0 Å with increasing t_h) and those of isomers **33**, **36**, **37** and **39** being of the same order of magnitude.

5.1.4 Summary

The fundamental electronic and optical properties of pentacene's isomers were probed, for both their stability and charge transfer in organic electronic applications. Several pure and hybrid functionals were screened for pentacene's FMOs and charge-transfer properties, and the common B3LYP was found to perform the best in comparison to experimental values. Subsequently, the non-planar isomers **32**, **40** and **41** were found to have a relatively similar HOMO to that of picene, while their air stability is nearly two-fold to that of pentacene.

The third order electron propagator (P3) functional gives the most accurate first vertical ionisation energy, in comparison to the experimental values of pentacene and picene, and should be used over all other theories for excellent estimates of similar acenes. The isomer **40** was found to have the greatest increase in vertical ionisation in comparison to pentacene using P3, by 1.11 eV.

The internal hole reorganisation energies of picene and isomer **32** are identical at 0.188 eV, with those of isomers **33**, **36**, **37**, and **39** are less than 0.133 eV. The hole transfer integrals and the rates of charge transfer at three intermolecular separations were evaluated for all isomers and it is no surprise that **33**, **36**, **37**, and **39** have the same order of magnitude as those of pentacene at 3.5 Å, suggesting strong interactions in the solid phase for these molecules. The rates of charge transfer are also exceptional for isomers **33**, **36**, **37** and **39**. Combining these observations with their air stabilities, isomer **37** is the best all-round alternative candidate to pentacene, followed closely by the other three depending on the specific property of interest. Overall, these observations show that the isomers of pentacene deserve attention as potential air-stable and high-performing alternative candidates for organic electronic applications.

5.2 Design, Modelling and Synthesis of Fused-Ring Heteroacenes

5.2.1 Design and Modelling

Since the discovery of conducting polyacetylene[182], there has been a surge in research of π-conjugated systems, particularly concerning the development of high-performing materials through the rational design of the molecular structures. π-conjugated systems allow charge to be delocalised over the whole molecule, thereby imparting stability of the unpaired electron towards oxidative or reductive environments. Applications of π-conjugated systems include radio-frequency identification (RFID) tags[183], flexible displays[184], electronic papers[185] and sensors[186]. Yet, limitations still exist in terms of the underlying structure-property relationships for charge transfer. In addition to electronic properties, favourable optical responses are becoming increasingly sought after in materials chemistry. Nonlinear optical (NLO) investigations have led to a number of diagnostic applications, including the direct visualisation of carrier motion[187], the nucleation and growth of nanoparticles[188], second-harmonic generation of Langmuir-Blodgett films[189], surface structure and dynamics[190], protein detection[191] and more recently, optical switches[192]. Organic semiconducting[10] and NLO phenomena[192] are commonplace throughout the literature and yet there are no studies on the suitability of candidates for both fields.

Advances in the field of organic electronics tend towards specialisation, which may promote singular device functions and output responses. This is at odds with circuitry miniaturisation or downscaling devices to the molecular level where multi-response relays and outputs are highly desirable[193]. The rational design of multi-response systems to date tends to include multiple electron withdrawing or donating groups (EWGs or EDGs) on the molecular backbone, and are thus subject to chemical and environmental stability concerns. It is common practice, in the development of organic electronic materials, to design and synthesise a single molecular target. The performance of the synthesised material is characterised by fabrication and testing of an organic electronic device. Although this iterative synthetic/device fabrication and characterisation approach is capable of eventually arriving at a suitable candidate, it does have the disadvantage of high demand on time and resources, having to rely on costly device fabrication/testing exercise for each molecule synthesised. To increase the likelihood of arriving at a high-performing candidate without proportionally increasing the demand on time and resources, an alternative approach should be deployed to increase the number of structures investigated for a faster throughput of research. Thus,

a theoretical approach that virtually screens a number of structures *a priori* to any experimental undertaking can be adopted to save both time and resources.

To date, synthetic iteration has yielded a multitude of fused-ring compounds, of which only a small number[10] have charge carrier mobilities greater than $1.0 \, cm^2 \, V^{-1} \, s^{-1}$, such as dibenzodithienothiophen (DBDTT, **19**)[10,194,195] in Figure 34, with selected physical properties. DBDTT has a sufficiently stable optical gap (3.46 eV), permitting its application under ambient conditions. The internal hole reorganisation energy[196] of DBDTT is 0.117 eV, which is near ideal (0.1 eV) for organic semiconductors[54,197]. It is therefore of great interest to increase the number of fused rings on any high-performing structure to further improve its properties. Dibenzopentathiophene (B5TB, **42**)[198,199] is a heterocyclic homologue of DBDTT, which has two more thiophene rings in the core of the molecule, although its optical gap is lower. Disappointingly, B5TB has lower air-stability than DBDTT with a HOMO-LUMO gap (E_g) of 2.98 eV and relatively lower charge-transfer mobility by two orders of magnitude at $0.04 \, cm^2 \, V^{-1} \, s^{-1}$, which could be expected from its inferior reorganisation energy (0.240 eV), prompting the possibility that some isomers of the same formula of B5TB could yield better stability and charge-transfer properties.

$E_g = 3.46 \, eV$
$\mu_h = 1.8 \, cm^2 \, V^{-1} \, s^{-1}$
$\lambda_h = 0.117 \, eV$

DBDTT (**19**)

$E_g = 2.98 \, eV$
$\mu_h = 0.04 \, cm^2 \, V^{-1} \, s^{-1}$
$\lambda_h = 0.240 \, eV$
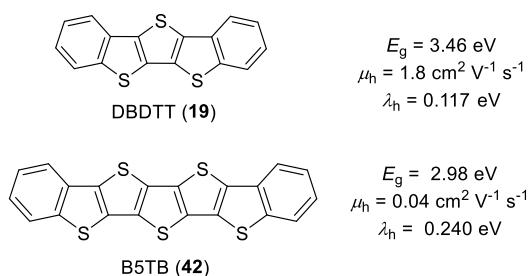
B5TB (**42**)

Figure 34. High-performing *p*-type organic semiconductors, DBDTT (**19**) and B5TB (**42**), with their experimentally-derived FMO optical gaps (E_g) from the literature and their internal hole reorganisation energies (λ_h).

Being a seven-membered compound with mixed heterocycles, B5TB can be isomerised to give the same core as DBDTT but with one thiophene unit fused to the terminal edge of each phenyl ring, as illustrated in Figure 35. As there are three faces and two possible orientations, there are six symmetric

isomers of B5TB, or virtual π–extended analogues of DBDTT, and as a result, six novel isomeric structures with DBDTT at its core can be created, called dithienodibenzodithienothiophene (DTBDTT). DTT-based heterocycles are of significant interest to organic electronics as once part of the core, it imparts high thermal stability[200] while the fused phenyl spacers extend the π-conjugation and permit better π-π stacking with adjacent molecules. Moreover, terminal thiophenes with internal phenyl fused-units have high thermal and photostability. These understandings give merit to the purpose of isomerising B5TB for improved properties. The benefit of virtually screening these isomers will (1) determine which one should be investigated synthetically and (2) aid the future development of structure-based design rules for heteroacenes.
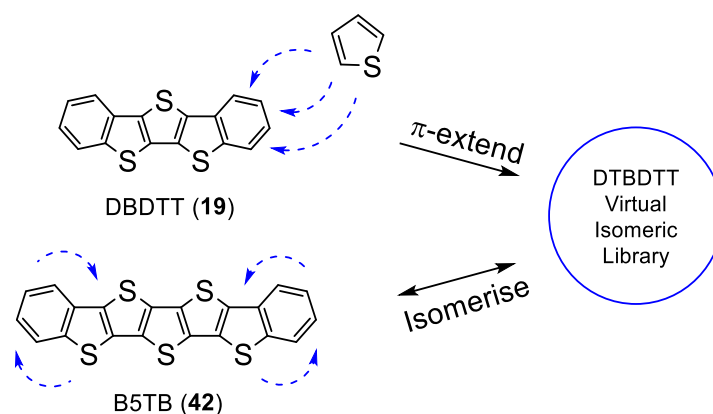
Figure 35. The process of generating the virtual isomeric library of heteroacenes through either π-extension of DBDTT or isomerisation of B5TB.

The structures of the six DTBDTT isomers from the π-expansion or isomerisation are illustrated in Figure 36. Together these diverse structures are theoretically screened with DFT to probe their properties and compare them to their parent isomer B5TB. They consist of the central DBDTT core with the thiophene heterocycles fused to the terminal phenyl edges in various arrangements, which in turn generates varying molecular shapes and sizes.
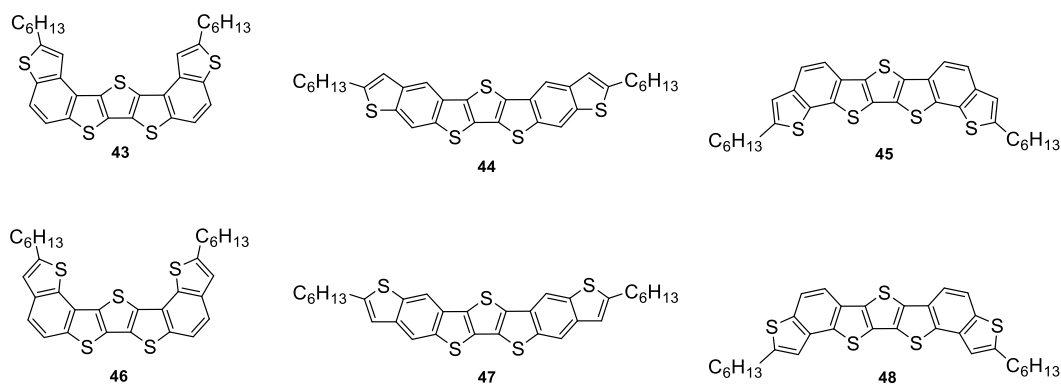
Figure 36. Structures of the six hepta-heteroacene DTBDTT isomers with solubilising hexyl chains (C_6H_{13}) in the virtual isomeric library.

Figure 37 shows that the isomer lengths vary between 13 and 17 Å. The isomers **43-45** have the terminal thiophene *anti* to the central thiophene in the DTT core, with those of **46-48** being *syn*. The most curved and smallest structures are **43** and **46**, with only 13.0 and 13.6 Å in length; the most linear are **44** and **47**, with lengths up to 16.9 Å, while **45** and **48** are phenacene-like and less than 16 Å.

Optical properties are of significant interest for organic electronics. Figure 38 shows the HOMO energy levels of **43** and **44** are almost identical in energy *ca.* -5.62 eV, with isomer **45** being exceptionally close at -5.60 eV; all isomers have remarkably similar HOMO energies to the experimentally determined value of -5.64 eV for B5TB. Both **43** and **47** have low LUMO energy levels of -2.03 eV and -2.08 eV respectively, similar to that of B5TB
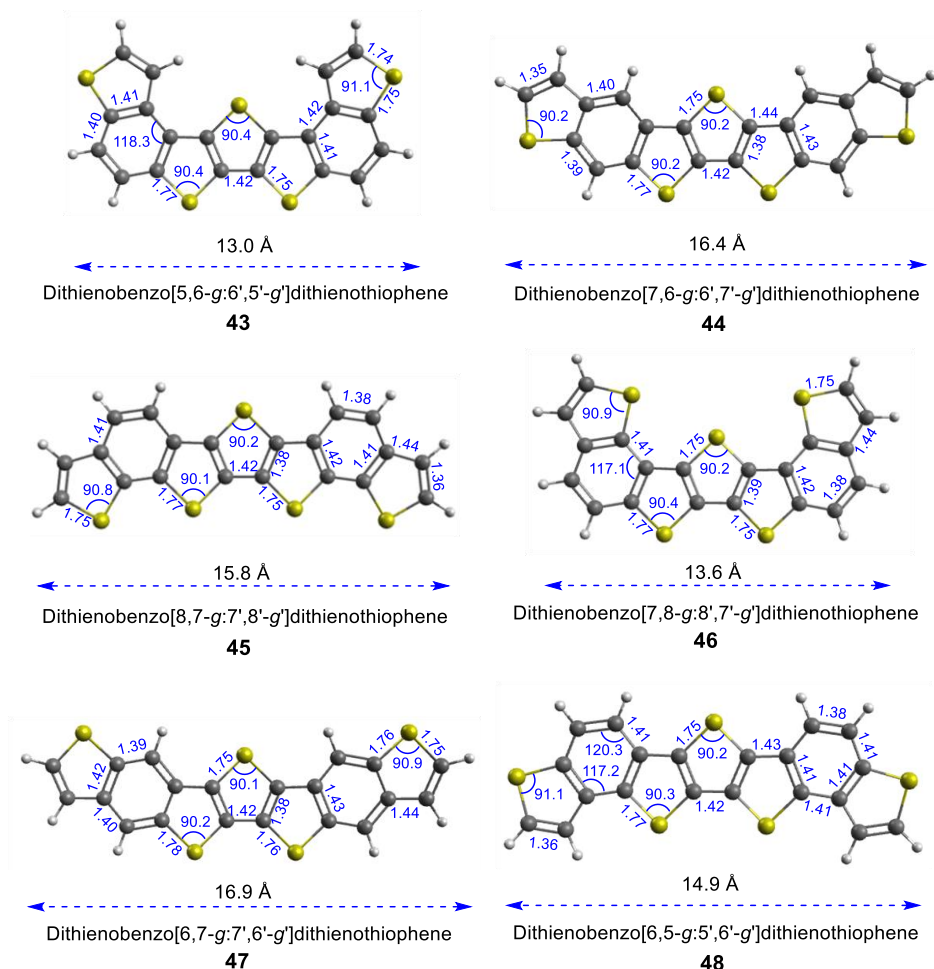
Figure 37. Structures of the isomeric virtual pool of symmetric fused-ring systems **43-48** based on the parent B5TB, with selected geometric parameters and hexyl chains omitted to reduce the computational cost.

(-2.66 eV theoretical and -2.08 eV experimental), whereas those of the others are higher between -1.72 and -1.95 eV.

Excluding **43** and **47**, the optical gaps (E_g) of the remaining candidates are relatively similar for their calculated values. If the theoretical value of E_g overestimates by 0.58 eV in comparison to the experimental B5TB, due to uncertainty in the LUMO state, then both **44** and **48** would still be more optically stable by as much as 0.3 eV than B5TB; suggesting that DTT does indeed stabilise the fused-ring structures.

The FMO energies and orbitals are illustrated in Table 8. The HOMO orbitals, in general, appear to align as expected across the double bonds of the thiophene units, forming a ladder-like array across the breadth of the molecules. This phenomenon is most noticeable in isomers **44**, **45**, **47** and **48**.

43, **44** and **46** are interesting with regards to the lack of orbital density on particular carbon atoms of the thiophene unit, noticeably at the connecting and fused carbon atoms with the phenyl ring for **43** and **46**, but on the terminal carbon of the thiophene with isomer **44**. This occurs evidently from the greater overlap with those of the phenyl ring for these isomers, where the molecular orbitals shared three fused atoms between both the thiophene and the phenyl ring; isomer **48** is a very close contender due to little orbital density on the terminal thiophene carbon.

In the LUMO state, the orbitals of **43** and **46** show the same phenomena, with **44** being the exception. Those which have orbitals in the same phase across the carbon atoms in a linear array, have a relatively stabilised LUMO energy, such as **43** (2.03 eV) and 5 (-2.08 eV), while those of **44** and **6** have a discontinuity at the peripheral thiophene carbons. The central orbitals around the DTT unit remain largely unchanged in both the HOMO and LUMO states.

It was understood from the ionisation calculations of pentacene's isomers (Section 5.1) that the DFT methods (B3LYP, LC-BLYP) bracketed the experimental values. However, the EPT methods gave the most accurate and particularly, the third order pole (P3). Table 9 and Table 10 show the ionisation and electron affinities for both DFT (B3LYP only), and EPT methods. The ionisation energy for should be relatively large *ca.* 5.0 eV such as with pentacene[10] or 5.81 eV with fluorinated acenes[201]. **43-48** all show exceptional stability, as high as 7.2 eV with the vertical ionisation of **48**, followed closely by that of **44** with 7.07 eV.

Table 8. Frontier molecular orbitals of the neutral isomers and their energies in electron volts (eV).

Entry	Ψ_H	Ψ_L
43	-5.62	-2.03
44	-5.62	-1.91
45	-5.60	-1.95
46	-5.66	-1.86
47	-5.56	-2.08
48	-5.67	-1.72
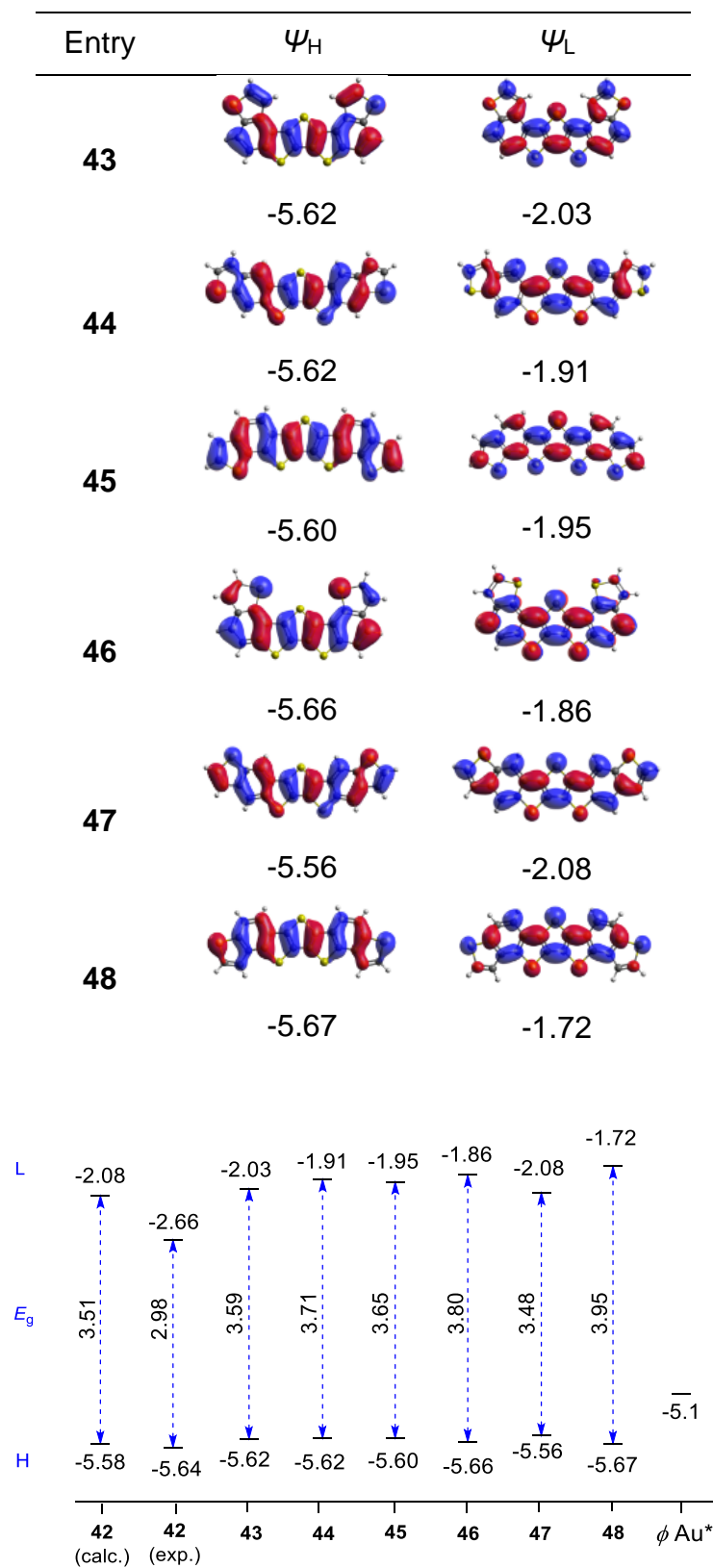
Figure 38. FMO diagram for the calculated and experimental values for parent B5TB (**42**) and isomers **43**-**48**, with the work function of gold.

Table 9. Calculated vertical ionisation energies (IE_V) in electron volts (eV) of B5TB (**42**) and isomers **43-48** using DFT (B3LYP) and EPT (KT, OVGF, P3).

| Entry | DFT | EPT | | |
	B3LYP	KT	OVGF	P3
42	6.79	7.15	6.72 (0.88)	7.39 (0.86)
43	6.85	7.25	6.81 (0.88)	7.43 (0.87)
44	7.07	7.30	6.77 (0.88)	7.38 (0.86)
45	6.82	7.19	6.73 (0.88)	7.41 (0.86)
46	6.89	7.28	6.85 (0.88)	7.43 (0.87)
47	6.75	7.17	6.76 (0.88)	7.35 (0.86)
48	7.25	7.33	6.82 (0.88)	7.45 (0.86)

Table 10. Calculated vertical electron affinities (EA_V) in electron volts (eV) of B5TB (**42**) and isomers **43-48** using DFT (B3LYP) and EPT (KT, OVGF, P3).

| Entry | DFT | EPT | | |
	B3LYP	KT	OVGF	P3
42	0.903	0.94	0.018 (0.90)	0.029 (0.88)
43	0.830	0.97	0.67 (0.98)	0.61 (0.98)
44	0.716	1.22	0.21 (0.90)	0.13 (0.89)
45	0.774	1.09	0.14 (0.90)	0.097 (0.88)
46	0.535	1.00	0.705 (0.98)	0.65 (0.98)
47	0.915	0.98	0.038 (0.89)	0.082 (0.88)
48	0.526	1.05	0.73 (0.98)	0.68 (0.98)

The hole (λ_h) and electron (λ_e) reorganisation energies were calculated for isomers **43-48** and presented in Table 11 and Table 12, along with the isomer B5TB (**42**) for comparison. Although the origin of small reorganisation energies are not known, Troisi reports[57] that the most significant relaxation contributions arise from C-C vibrational modes, *ca.* 800-1200 cm^{-1}, while Zhu

et al. reported 1500 cm^{-1} with reorganisation-frequency coupling calculations[202]. The internal hole reorganisation energy for **44** (84.2 meV) is relatively lower than those of tetracene (114 meV) and rubrene[203] (159 meV) and significantly lower than the calculated value for **42** (240 meV). Isomer **48** also has an ideal hole reorganisation energy (101 meV), while **44** and **45** are modest with 195 meV and 198 meV respectively (Figure 39). Isomers **43**, **45**, and the parent **42** in contrast, are not suitable for p-type organic semiconductor applications. It is known for n-types that the lower and upper limits[16] for electron affinity is 3.0 and 4.0 eV respectively, indicating that all the isomers and the parent **42** are not suitable for n-type devices. Interestingly, the λ_e energies of isomers **44** and **47** are not far from ideal with values comparable to n-type nitrogen substituted acenes[54].

In general, the hole transfer integrals (t_h) increase with intermolecular separation *d*, suggesting that the solid state packing of these structures may be wider than 4.0 Å as a maximum t_h was not reached, although the differences in t_h between 3.5-4.0 Å is less than those at 3.0-3.5 Å, suggesting the ideal intermolecular separation is just over 4.0 Å. **42** has the largest integral at *d* = 3.0 Å (113 meV), but relatively similar to isomers **45** (137 meV), **47** (135 meV) and **48** (138 meV) at *d* = 4.0 Å. Interestingly, isomers **43** and **46** have greater integrals than **42** for *d* = 4.0 Å at 152 meV and 156 meV respectively. The rates of charge transfer increase with *d*, and the largest rate was found for isomer **48** at *d* = 4.0 Å (0.602×10^{14} s^{-1}), followed closely by **44** (0.395×10^{14} s^{-1}), as illustrated in Figure 40 (Top). Moreover, the order of magnitude for all isomers including the parent isomer **42**, is of the same order as the previously studied pentacene's isomers (10^{14} s^{-1}), suggesting these fused-ring heteroacenes have significant potential as high-performing organic semiconductors.

The electron transfer integral is greatest with **42** at *d* = 3.0 Å (538 meV), followed closely by isomers **47** (491 meV) and **45** (448 meV). At *d* = 4.0 Å, all integrals between isomers **43-48** and **42** range between 169 meV and 178 meV (Figure 40 Bottom), further suggesting that *d* = 4.0 Å is the common intermolecular separations in the solid state for these structures.

Table 11. Hole reorganisation energy (λ_h / meV) for each isomer and the hole transfer integral (t_h / meV) with the rate of charge transfer ($K_{CT} \times 10^{14}$ / s^{-1}) for each intermolecular separation of d = 3.0, 3.5 and 4.0 Å.

Entry	λ_h	d = 3.0 Å		d = 3.5 Å		d = 4.0 Å	
		t_h	K_{CTh}	t_h	K_{CTh}	t_h	K_{CTh}
42	240	113	0.067	197	0.204	134	0.095
43	213	101	0.075	163	0.194	152	0.168
44	84	38	0.057	76	0.238	99	0.395
45	240	93	0.046	0.000	0.000	137	0.100
46	195	78	0.055	130	0.153	156	0.221
47	198	51	0.023	106	0.098	135	0.160
48	101	54	0.090	108	0.366	138	0.602

Table 12. Electron reorganisation energy (λ_h / meV) for each isomer and the electron transfer integral (t_h / meV) with the rate of charge transfer ($K_{CT} \times 10^{14}$ / s^{-1}) for each intermolecular separation of d = 3.0, 3.5 and 4.0 Å.

Entry	λ_e	d = 3.0 Å		d = 3.5 Å		d = 4.0 Å	
		t_e	K_{CTe}	t_e	K_{CTe}	t_e	K_{CTe}
42	248	538	1.393	366	0.643	175	0.148
43	238	417	0.940	361	0.705	171	0.158
44	214	322	0.748	316	0.721	177	0.225
45	230	448	1.193	0.000	0.000	178	0.189
46	357	389	0.210	359	0.178	169	0.039
47	220	491	1.613	363	0.884	173	0.201
48	230	199	0.235	189	0.212	173	0.178
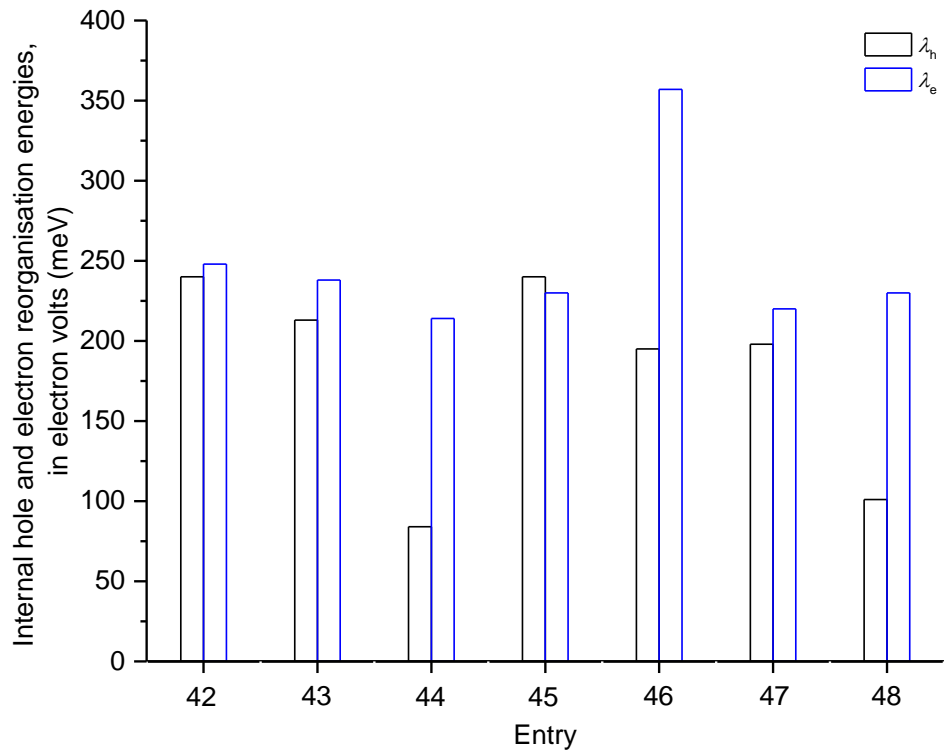
Figure 39. Internal hole (λ_h) and electron (λ_e) reorganisation energies in millielectron volts (meV) for each isomer.
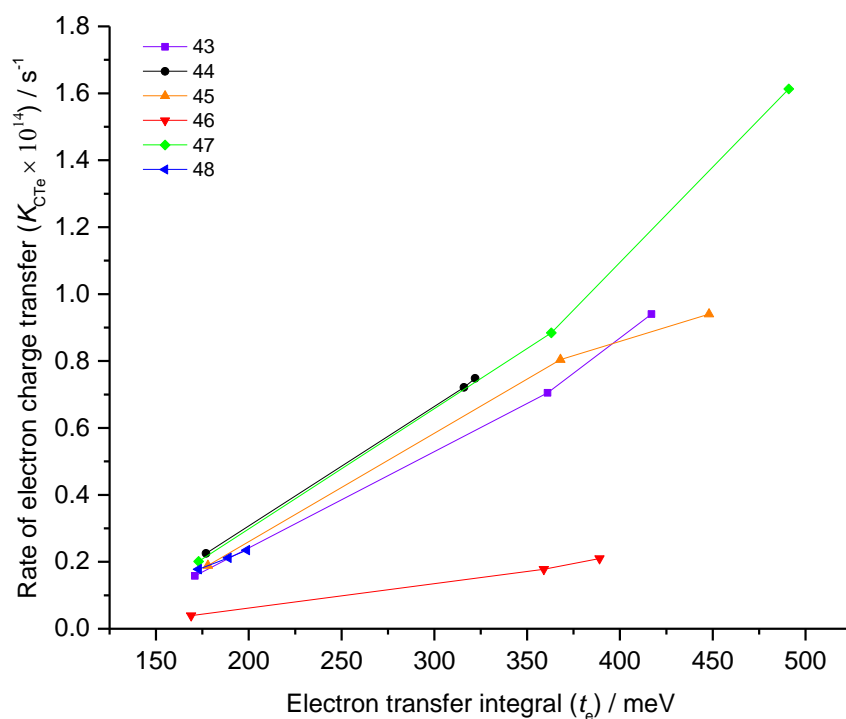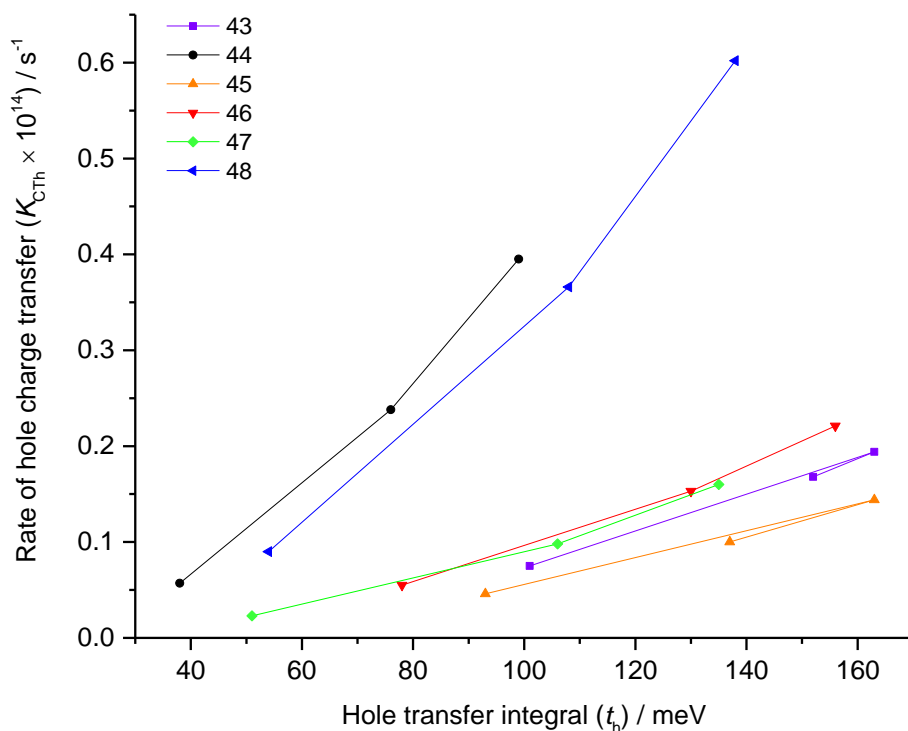
Figure 40. The rate of hole (Top) and electron (Bottom) charge transfer rate versus the hole and electron transfer integral (t_h) in millielectron volts (meV) for each intermolecular separation (d = 3.0, 3.5, 4.0 Å, decreasing separation with increasing transfer integral) for all isomers.

TD-DFT calculations are also of critical importance to ensure that an incident frequency does not interfere with molecular excitations for NLO second harmonic generation later in this study. **48** has the largest band gap (S_0-S_1) of 3.57 eV and **47** has the smallest (3.19 eV), second only to **42** (3.11 eV). Figure 41 shows the calculated UV-Vis spectra with normalised intensities for the neutral isomers in vacuum. All isomers have an intense absorption between 370-390 nm, corresponding to the S_1 band; some additional signals at higher energy centred at 304 nm, relating to S_2 or vibrational states. The decreasing intensities of this second band may originate from the frontier molecular orbital (FMO) phase overlap connecting the phenyl spacer and thiophene end-capping units (Table 8).
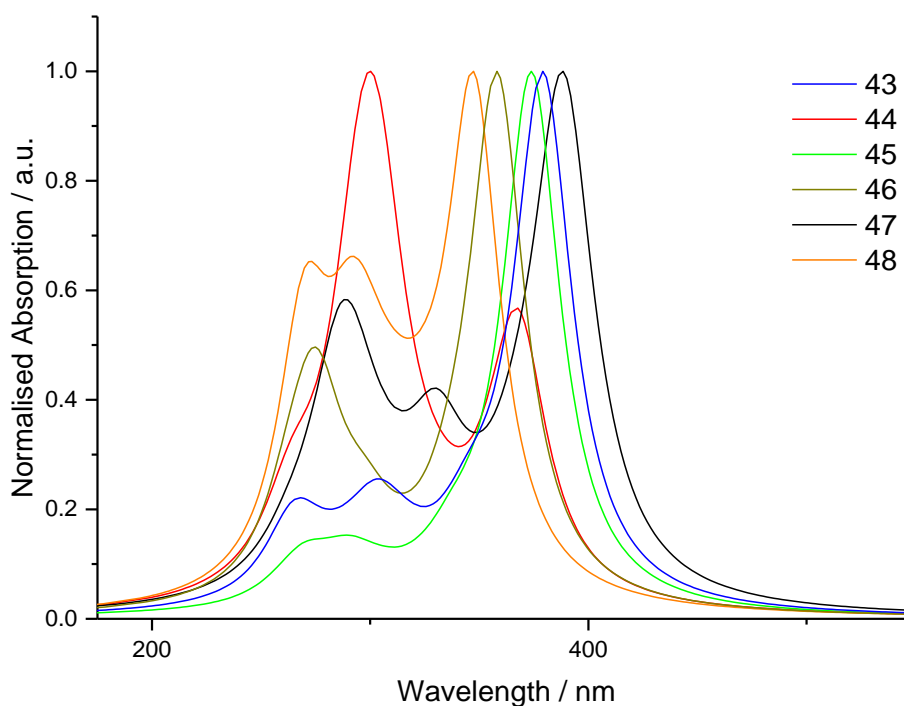
Figure 41. Simulated UV-Vis absorption spectra with normalised intensities of the vertically excited states for the neutral structures **43-48**.

Next, the nonlinear optic properties of the isomers are investigated, to see if these can be combined in a device application and compliment their electronic properties. What follows is a brief introduction to nonlinear optics, bearing in mind that in-depth discussion can be found elsewhere[204]. Nonlinear optics have two prominent fields of investigation, the electro-optic Pockels

effect $\beta(-w;w,0)$ and the second harmonic generation (SHG) $\beta(-2w;w,w)$; their applications which include the use of single finite electric fields have been given earlier.

Negative hyperpolarisabilities would suggest that the dipole vectors of the ground and excited states are antiparallel[205] and could promote splitting of the incident beam[206]. Moreover, two species co-crystallised with opposite hyperpolarisability signs constructively reinforce their antiparallel alignment for ideal electro-optic crystals[207]. To date, there has been a great deal of attention on the NLO properties of neutral molecules[208], Zwitter ions[207,209] and some on diradicals[210], but little on ground-state singularly-charged radical organic semiconductor systems. The significance is that organic molecules which loose or gain an electron to form a singularly charged radical cation or anion state do not have a closed-shell structure and can be thus subject to optical exploitation. Application of a frequency during such states provide NLO responses, such as first-order hyperpolarisability properties.

Table 13 and Table 14 show the NLO first-order hyperpolarizabilities of the optimised singularly-charged isomers (radical anions: A, cations: C) 1A-6C and the parent **42** for the electro-optic Pockels effect $\beta(-w;w0)$ and second harmonic generation (SHG) $\beta(-2w;w,w)$ respectively. The three largest contributory components (β_{zzz}, β_{zxx}, β_{zyy}) to the total hyperpolarizability parallel to the molecular z axis ($\beta_{\parallel}$) increase in the general order of $\beta_{zxx} < \beta_{zzz} < \beta_{zyy}$ for both the Pockels effect and SHG. The electric dipole of the molecular structure (μ^e) modulates the total hyperpolarizability $\beta_{\parallel}$ and thus the net effect is called the hyperpolarisability product $\mu^e\beta_{\parallel}$, which is experimentally measurable[34] and calculated at the frequency 1064 nm, in line with the wavelength of Nd-YAG lasers used in the experiments.

The $\beta_{\parallel}$ term shows no distinctive correlation between the anions and cations each isomer. The cationic forms of **43**, **44** and **46** exhibit large negative hyperpolarisability products, up to -8138×10^{-48} esu. The cation of B5TB is even smaller (54.1×10^{-48} esu), comparable to 6C. The anions of **45-48** have relatively low products, while those of 1A and **42** A are modest at 761 and 503×10^{-48} esu respectively.

Both anions and cations are found to possess positive and negative SHG hyperpolarisabilities, with outstanding values for 1A (-3016×10^{-48} esu) and 4C (-2488×10^{-48} esu), and good values for 1C (-484×10^{-48} esu), 2C (-487×10^{-48} esu) and 3A (-844×10^{-48} esu). **47** and **48** have very low

hyperpolarisabilities and hence not suitable for NLO applications. **42** follows those of isomer **48**, in respect to both the cation and anion magnitudes, considerably lower than the other isomers **44-46**, suggesting these DTBDTT isomers have superior NLO properties.

In addition, these theoretical results are of considerable significance in comparison to the asymmetric DTT-based structures synthesised by Kim and co-workers[211], which have electron donating and withdrawing groups, giving $\mu^e\beta_{II}$ values between -3000 to 5000×10^{-48} esu. Hyperpolarisabilities of these symmetric fused-ring organic structures **43-48** in their singularly charged radical states are found to exceed rationally-designed asymmetric molecular materials with push-pull electron groups.

Table 13. The NLO first-order hyperpolarisabilities β_{ijk} ($\times10^{-30}$ esu) the total hyperpolarisability parallel to the molecular z axis (β_{II}), the molecular electric dipole μ^e (Debye) and the net hyperpolarisability product $\mu^e\beta_{II}$ ($\times10^{-48}$ esu) for the frequency-dependent (1064 nm) electro-optic Pockels effect β(-w;w,0) of the optimised radical anionic (A) and radical cationic (C) isomers **42-48**.

Entry	β_{zzz}	β_{zxx}	β_{zyy}	β_{II}	μ^e	$\mu^e\beta_{II}$
42 A	20.1	-9.36	20400	7850	0.0641	503
42 C	1.01	-0.0992	-13.0	-41.0	1.32	54.1
43 A	86.0	-7.34	-555	892	0.853	761
43 C	-21.6	0.150	-1020	-1360	1.19	-1620
44 A	0.302	-137	131	3270	0.999	3270
44 C	-42.5	0.007	-10200	-4130	1.97	-8140
45 A	17.1	-8.38	-1270	87.3	1.37	120
45 C	1.45	-0.376	-84.9	89.5	2.03	182
46 A	5.79	-8.38	-77.1	112	1.89	212
46 C	-17.4	0.213	-1800	-12200	0.352	-4290
47 A	-0.947	-6.06	-135	57.0	1.09	62.1
47 C	9.54	0.173	-175	-65.5	0.277	-18.1
48 A	-6.00	27.0	19.9	6.31	1.47	9.28
48 C	87.2	-0.0308	535	260	0.348	90.5

Table 14. The NLO first-order hyperpolarisabilities β_{ijk} ($\times10^{-30}$ esu) the total hyperpolarisability parallel to the molecular z axis (β_{II}), the molecular electric dipole μ^e (Debye) and the net hyperpolarisability product $\mu^e\beta_{II}$ ($\times10^{-48}$ esu) for the frequency-dependent (1064 nm) second harmonic generation (SHG) β(-2w;w,w) of optimized radical anionic (A) and radical cationic (C) isomers **42**-**48**.

Entry	β_{zzz}	β_{zxx}	β_{zyy}	β_{II}	μ^e	$\mu^e\beta_{II}$
42 A	-22.2	-28.1	-13100	-2820	0.064	-181
42 C	1.85	-0.0702	-81.1	-7.700	1.32	10.2
43 A	398	51.4	-15800	-3540	0.853	-3020
43 C	19.4	0.128	-1990	-407	1.19	-484
44 A	14.4	-335	181	82.5	0.999	82.4
44 C	15.0	0.227	-1130	-247	1.97	-487
45 A	-0.366	-20.8	-323	-616	1.37	-844
45 C	5.81	-0.407	180	29.1	2.03	59.1
46 A	5.25	-18.9	-278	-77.4	1.89	-146.
46 C	6.14	0.120	-37500	-7070	0.352	-2490
47 A	-5.98	-10.6	-626	-291	1.09	-317
47 C	2.21	0.237	180	19.2	0.277	5.31
48 A	-16.2	226	-411	-97.2	1.47	-143
48 C	-55.9	-0.088	32.2	-55.3	0.35	-19.2

5.2.1.1 Summary

A small isomeric virtual pool of extended fused-ring heteroacene DTBDTT structures based on the parent isomer of B5TB were designed and then virtually screened for their optoelectronic properties prior to their synthesis. The regioposition of the end-capping thiophene is shown to have a strong effect on both the electronic and the optical properties of the molecule. Isomer candidates **44** and **48** have exceptional internal hole reorganisation and ionisation energies while candidates **43-46** show excellent NLO properties for both electro-optic and second harmonic generation. From these preliminary calculations, it is clear that **44** is worthy of investigation in both fields of organic semiconducting and nonlinear optics, with superior properties to the parent **42**. These findings highlight the merit of a theoretical screening approach to predict the fundamental properties of molecular structures, improve those of the parent structures, and aid the rational design of multi-functional optoelectronics.

5.2.2 Synthetic Strategy

The six isomeric candidates designed and modelled in section 5.2.1 should have the same chemical properties but different physical properties, such as air stability and charge transfer. It is therefore of great interest to discover their electronic and optical properties for high-performance thin-film transistors in molecular electronics. The physical properties of **44** and **45** were predicted from the virtual screening to be excellent and thus selected for experimental investigations; here **44** is probed while **45** is studied in section 5.2.3.

5.2.2.1 Retrosynthesis of Target 44

The approaches considered for the synthesis of the target isomers are categorised as divergent, convergent or hybrid, being a mixture of the two. Examples of the different approaches are illustrated in Figure 42, and show that neither convergence nor divergence are appropriate for the target isomers, due to (1) potential insolubilities of some intermediates; (2) low yields from relatively low reactivity of the terminal substituent positions; (3) instability under ambient conditions and during purification processes; (4) potential poor regioselectivity at the different substituent sites during each synthetic transformation to the final product. Thus, the hybrid approach was considered most appropriate, which involves the synthesis of two individual components, a core and a synthon molecular fragment. These fragments are identified,
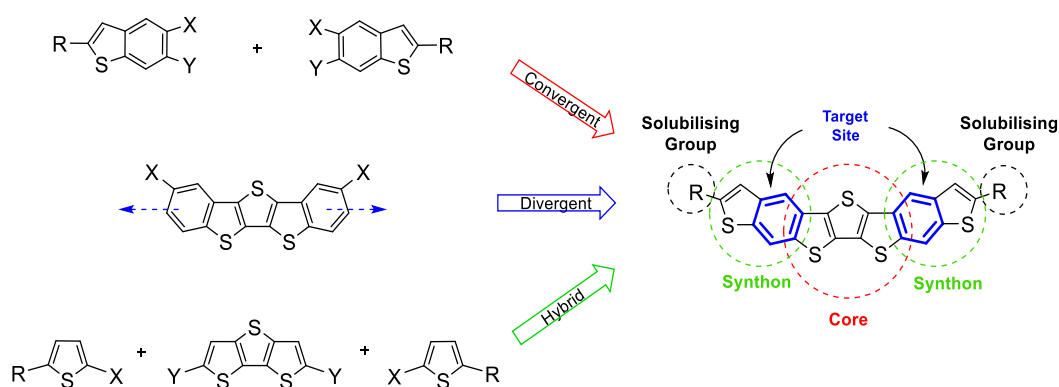
Figure 42. The convergent, divergent and hybrid approaches to isomer **44** with the core, synthon, solubilising groups and the target site for the synthetic transformations identified; R = C_6H_{13}, X/Y = functional groups.

along with the aromatic phenyl unit that fuses the core and synthon units together. This phenyl ring is the subject of the retrosynthesis until the core and synthons are obtained.

Chemistries for the formation of **44** could include benzannulation[212] or the pentacene method[213]. However, while benzannulations may be known, thiobenzannulations are not. In addition, neither the annulation nor the pentacene method would be able to ensure regioselectivity of the thiophene ring. Thus, the synthetic strategies for **44** must focus on some form of symmetric double cycloisomerisation. These can be achieved with Diels-Alder[214], Sigmatropic rearrangements[215] or acid-catalysed cyclation with Amberlyst 15[76,216] (Scheme 1). The Diels-Alder retrosynthesis requires the saturation of two bonds and the repositioning of one, giving intermediate **49**. Subsequent disconnections give an electron poor (vinyl-synthon, **50**) and an electron rich unit (DTT, **51**) and may be a regiospecific reaction in the forwards direction owing only to the vinyl reactivity at the 2-position of the synthon over the 3-position.
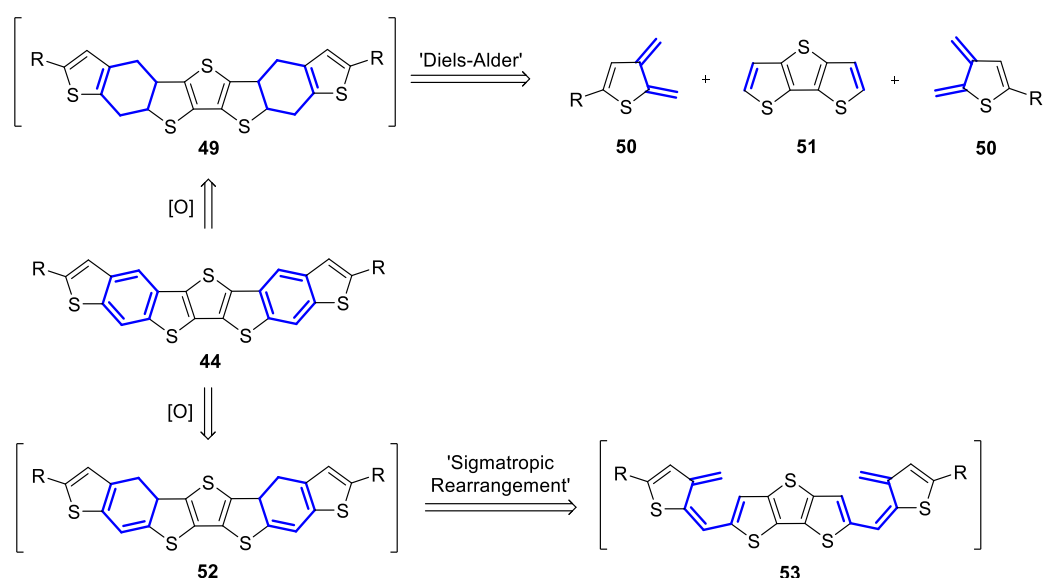
Scheme 1. Retrosynthetic Diels-Alder (Top) and Sigmatropic rearrangements (Bottom) with subsequent oxidation giving isomer **44**; R = C$_6$H$_{13}$.

The retrosynthetic Sigmatropic rearrangement saturates one double bond giving **52** and subsequent disconnections afford an intermediate **53**, where the synthons and core remain covalently tethered together. **53** can be divided into the synthon **50** and dibromo-DTT **54** from cut *i.*, which can be formed *via* a regioselective Heck reaction, as illustrated in Scheme 2. Cut *ii.* is the condensation between a vinyl intermediate **55**, through lithium-hydrogen exchange at its 2-position, and a diformylated-DTT **56**. Both vinyl synthons **50** and **55** may be challenging to make due to their terminal alkene carbons. In addition, the Diels-Alder and Sigmatropic routes (Scheme 1) require the oxidation of CH_2 and CH units, which may prove problematic due to the uneven stoichiometry of oxidant[217] needed per double bond and the sulfur centres may in turn be oxidised. This is without considering the potential of DTT to undergo such rearrangements as the aromaticity of DTT would have to be broken in both cases.

In contrast, the acid-catalysed retrosynthetic cycloisomerisation appears to have multiple routes for investigation, identified as the four steps A-D; step A is shown in Scheme 3. The first step A intermediate **57** consists of the DTT core unit covalently bound to the thiophene synthon with a methylene bridging unit and appended carbonyl derivative, namely an aldehyde (CHO).
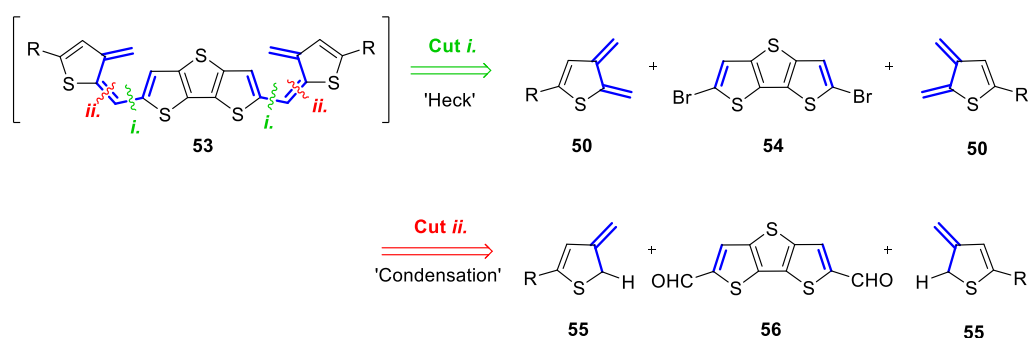
Scheme 2. Retrosynthesis of **53** with two divisions, a Heck (cut *i.*) and a condensation (cut *ii.*); R = C_6H_13.
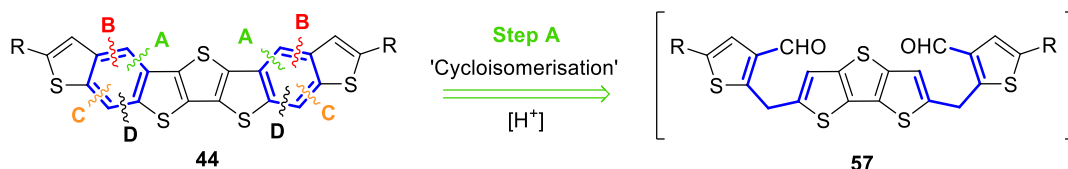
Scheme 3. Retrosynthetic step A of target **44**, giving the first step A intermediate **57**; R = C_6H_{13}.

For a rational retrosynthesis of **57**, both the reactivity and the position of the substituents must be taken carefully into consideration. Any C-C bond disconnections either side of the methylene bridge would result in a condensation reaction in the forward direction (Scheme 4). Interestingly, cut *i.* gives the core fragment **54** as generated from a literature procedure[144], but the synthon **58** has both an aldehyde at the 3-position and a methylene bromide at the 2-position, which may be competitive towards nucleophilic attack of the double-lithiated **54**. Cut *ii.* faces the same problem in reverse, where lithitation of the 2-position of **59** may attack its aldehyde, and in addition, the methylene bromide species **60** has no known synthetic preparation.

An alternative approach is to retrosynthetically reduce the oxidation state of the aldehyde group in **57** to eliminate the problem of the competing electrophilic groups towards nucleophilic attack. This is achieved with a functional group interconversion (FGI), where the aldehyde is converted into
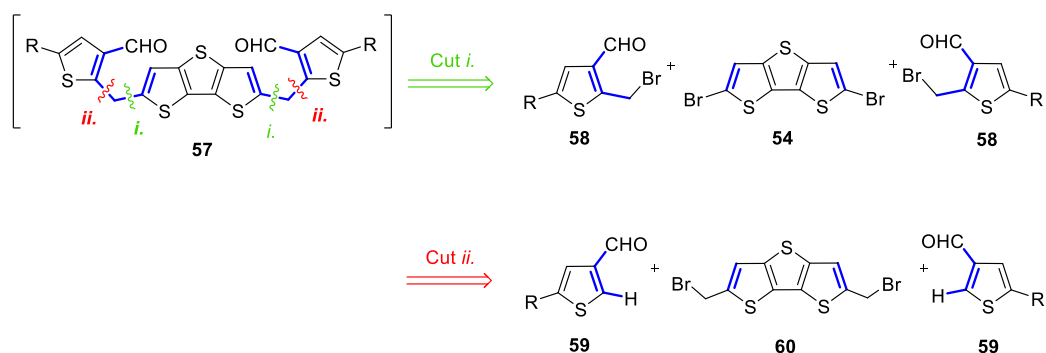
Scheme 4. Retrosynthesis of **57**, through the condensation of molecular fragments generated from cuts *i.* and *ii.*; R = C_6H_{13}.
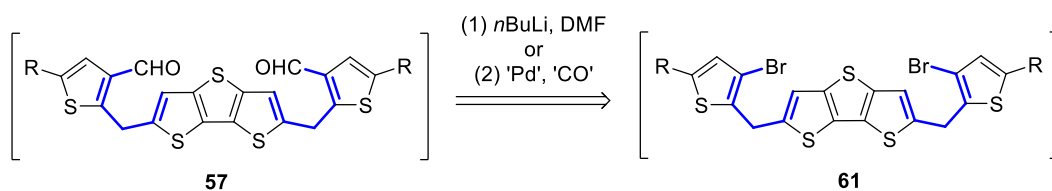
Scheme 5. Retrosynthetic function group interconversion of **57** through (1) lithium-halogen exchange and quench with electrophile transfer agent such as DMF, or (2) palladium-catalysed carbonylation[218]; R = C$_6$H$_{13}$.

an aryl-halide forming **61**, as illustrated in Scheme 5. There are two known possibilities for the forward synthetic direction, either (1) lithiation and quench with a carbonyl transfer agent such as DMF, or a palladium-catalysed 'carbonylation', which reductively inserts carbon monoxide and hydrogen.

The methylene position of **61** cannot be afforded easily and would still give the methylene-halide synthetic issue outline with Scheme 4. Therefore, a change in the oxidation state of the methylene bridge giving **62**, enables further retrosynthetic cuts at this site. While it is unreasonable to design a reaction's conditions involving oxidation in the forward direction due to the sulfur centres, it is entirely fine to do so retrosynthetically as the resulting forward conditions would be reduction, as illustrated in Scheme 6.

Scheme 7 shows the two possible cuts to the oxidised intermediate **62**. The first cut generates the core fragment with carbonyl substituents at the 2-position; this structure is only synthetically afforded from the core fragment **54** generated from cut *ii*. In contrast, the bifunctional synthon **64** is easily
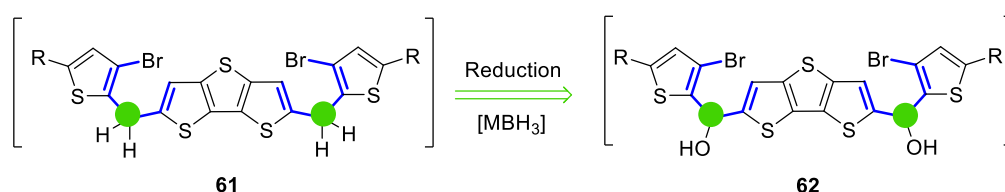
Scheme 6. Retrosynthesis of the intermediate **61**, *via* methylene oxidation (reduction with borohydride in the forward synthesis) giving a second A intermediate **62**; R = C$_6$H$_{13}$, M = Na, Li.
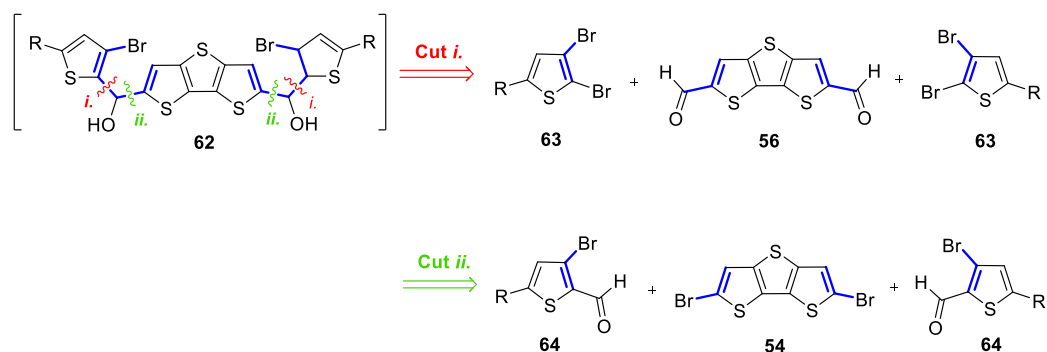
Scheme 7. Retrosynthesis of intermediate **62**, with two cuts either side of the methyleneoxy unit; R = C_6H_{13}.

afforded in two synthetic steps from hexylthiophene *via* a halogen dance reaction[219,220], and subsequently quenched with DMF, unlike that of cut *i*. (**63**) which needs polybromination.

In pursuit of alternatives, the remaining retrosynthetic steps of the phenyl ring are explored. Step B is the cleavage of the C-C bonds of target **44** between the 3-position of the thiophene synthon and the C-H unit at the phenyl target ring, as illustrated in Scheme 8. This may make the cycloisomerisation relatively easier due to the increase of the C-H reactivity at the 3-position of the resulting intermediate **65** rather than the DTT core as in Step A, Scheme 3, but could however, generate higher reactivity of the methylene bridge.

With the retrosynthetic understanding developed from step A, the aldehyde group of intermediate **65** is converted into a bromide substituent **66** (Scheme 9).
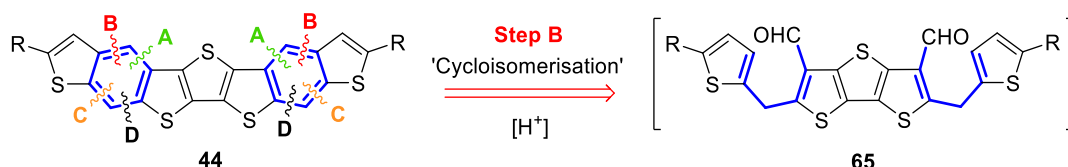
Scheme 8. Retrosynthetic step B of **44**; R = C_6H_{13}.
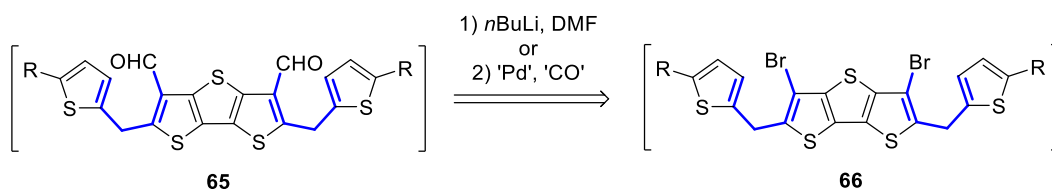
Scheme 9. Retrosynthetic function group interconversion of **65** through either (1) lithium-halogen exchange and quench with electrophile transfer agent such as DMF, or (2) palladium-catalysed carbonylation[218]; R = C$_6$H$_{13}$.

The retrosynthetic methylene reduction of **66** affords the intermediate **67** as shown in Scheme 10, with the bromine substituent on the DTT core and the C-H on the synthon, with the bridge oxidised to the methyleneoxy unit.

The first retrosynthetic cut of **67** (Scheme 11) gives the mono-formylated synthon **68** and a tetrabrominated-DTT (**69**), which needs one more step in the forward synthetic direction to the known literature preparation for dibrominated-DTT **54**, and the second cut gives hexylthiophene **70** and a bifunctional-DTT **71**, which requires additional steps after the formation of **54**.
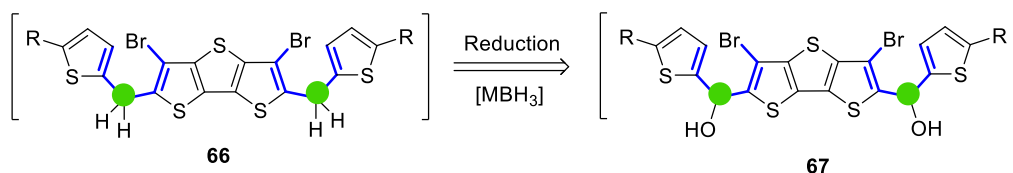
Scheme 10. Retrosynthesis of intermediate **66** *via* methylene oxidation (reduction in forwards synthesis with the carbon centre identified in green); R = C$_6$H$_{13}$, M = Na,Li.
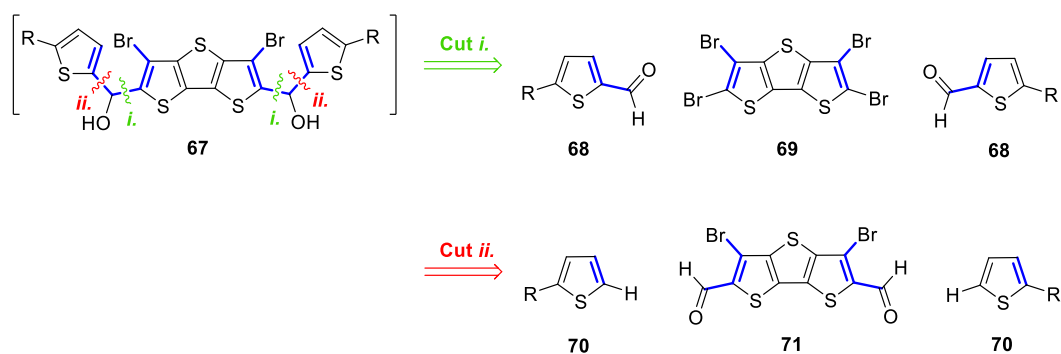
Scheme 11. Retrosynthesis of intermediate **67** with two cuts either side of the methyleneoxy bridging unit; R = C_6H_{13}.

Retrosynthetic step C of target **44** (Scheme 12) puts the methylene bridge in between the 3-positions of the synthon and the core units, with the aldehydes at the 2-position of DTT (**72**). The C-H of the 2-position of the synthon should be relatively more reactive than its 3-position as in steps A and B. However, inserting the methylene bridge into the 3-positions to afford the intermediate **72** may be more challenging.

The bromine substituent on the 2-position of **73** after an FGI may ensure greater reactivity than at the 3-position (Scheme 13).
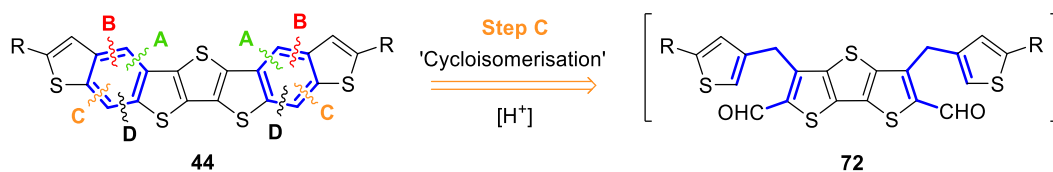
Scheme 12. Retrosynthetic step C of target **44**; R = C_6H_{13}.
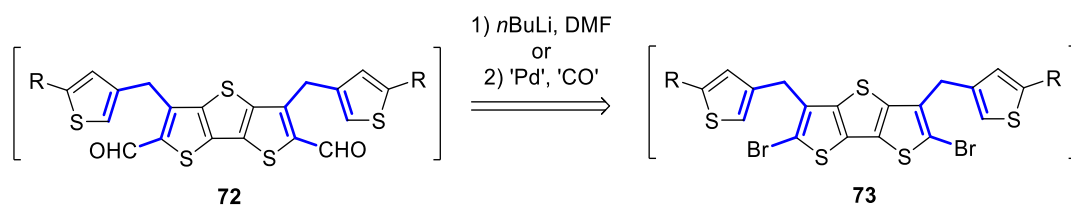
Scheme 13. Retrosynthetic functional group interconversion of **72**.

The retrosynthetic reduction of **73** to **74** may generate a relatively more stable methyleneoxy bridge due to its position at both 3-positions of the synthon and core and the hydrogen-bonding between the OH and the central S atom in DTT, forming two non-covalent intramolecular 6-membered rings (Scheme 14).

Cut *i.* of **74** would, under normal considerations, generate the tetrabromo-DTT core **69** and the aldehyde functional groups at the 3-position of the synthon **59** (Scheme 15). However, the 3-position is required to be more reactive than the 2-position of the core in this strategy and thus requires a more reactive halide towards lithiation, such as iodine; the resulting [2-bromo-3-iodo]$_2$-DTT (**75**) is challenging to synthesise. Cut *ii.* gives the bifunctional core fragment **77** which, as described above for its isomer **71**, requires several steps post the literature preparation of **54** to synthesise.
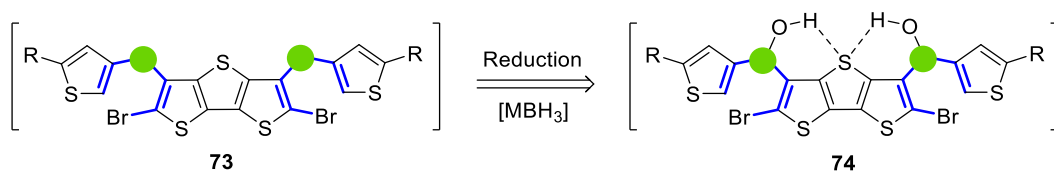
Scheme 14. Retrosynthesis of intermediate **73** *via* methylene oxidation (reduction in forwards synthesis); R = C$_6$H$_{13}$, M = Na, Li.

- 143 -
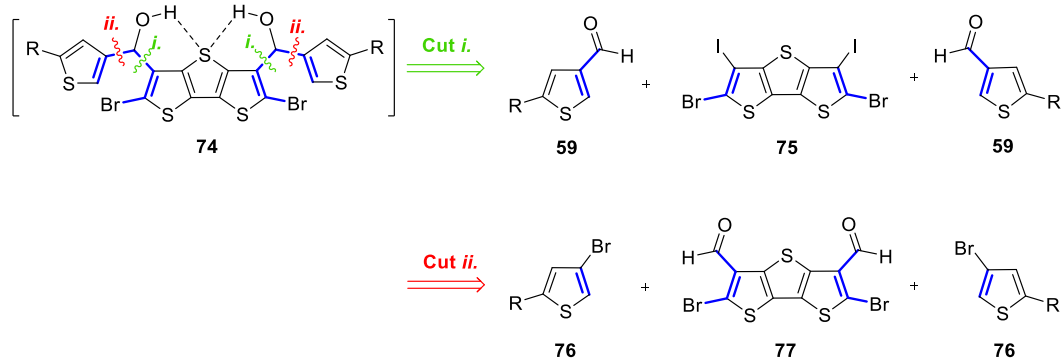
Scheme 15. Retrosynthesis of intermediate **74** with two cuts either side of the methyleneoxy bridging unit; R = C_6H_{13}.

The retrosynthetic step D in Scheme 16 gives intermediate **78** from C-C bond cleavage between the 2-position of DTT and the C-H of the methylene carbon. The benefit of this route is the increase in reactivity of both the C-H and CHO of **78** for acid-catalysed cycloisomerisation in the forward direction. The resulting methylene bridge is situated between the 3-positions of the thiophene and DTT units; its presence at this site may be challenging due to a decrease in reactivity.

A functional group interconversion of **78** to **79** (Scheme 17) should be readily achieved in the forward direction and the methylene bridge at the 3-position may be advantageous.
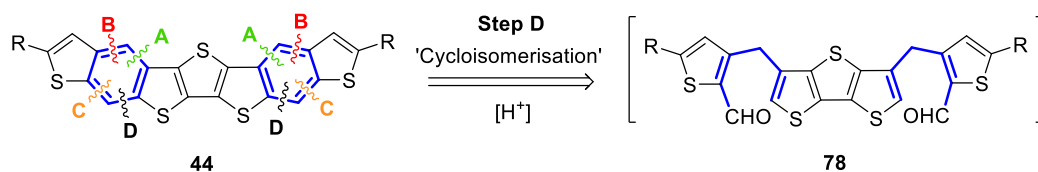
Scheme 16. Retrosynthetic step D of target **44** affording intermediate **78**; R = C_6H_{13}.
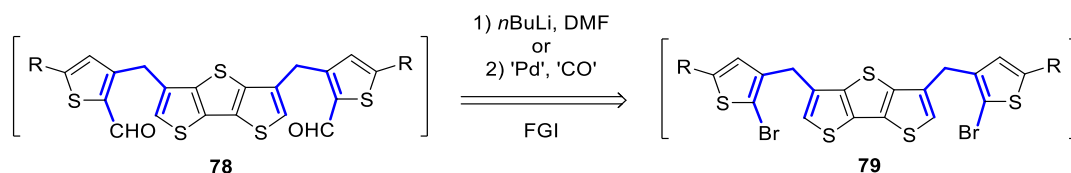
Scheme 17 Retrosynthetic functional group interconversion (FGI) of the aldehyde on the intermediate **78** giving a bromine substituent on the intermediate **79**; R = C_6H_{13}.

Formation of **80** from the reduction of **79** should proceed with relative ease in the forward direction due to no carbonyls at the 2-position but the methylene bridge would be relatively less reactive than step A and may require suitably stronger reducing agents; *i.e.* lithium borohydride over sodium borohydride (Scheme 18). The stability of the intermediate **80** may be relatively enhanced from possible hydrogen-bonding of the hydroxyl units to the central sulfur atom of the DTT core, forming two six-membered non-covalent intramolecular rings. In contrast, intermediates from steps A and B can only form five-membered rings.

The synthon from cut *i.* in Scheme 19 takes five steps, in contrast to two with that of cut *ii.*, which only needs double bromination from hexylthiophene. Both derivatised core units, however, will be challenging to synthesise, due to the substituents at the 3-positions.
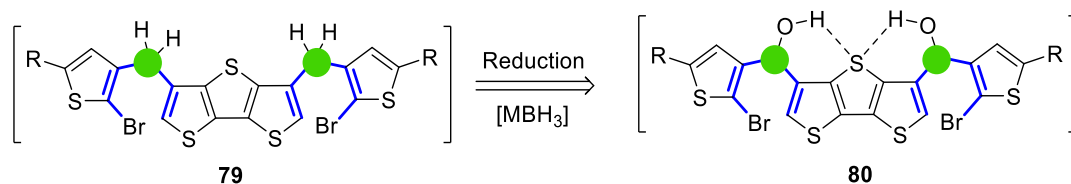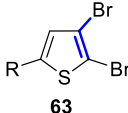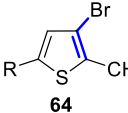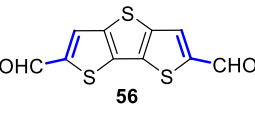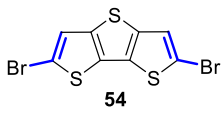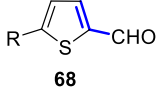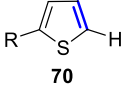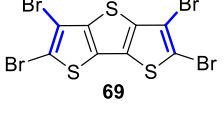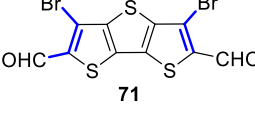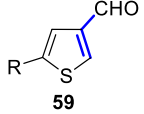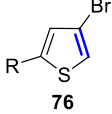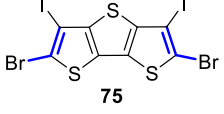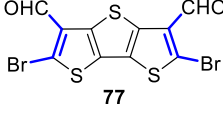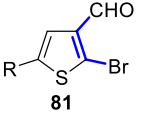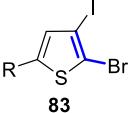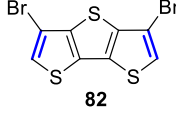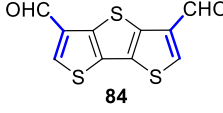
Scheme 18. Retrosynthesis of intermediate **79** *via* methylene oxidation (reduction in forwards synthesis); R = C_6H_{13}, M = Na, Li.

- 145 -
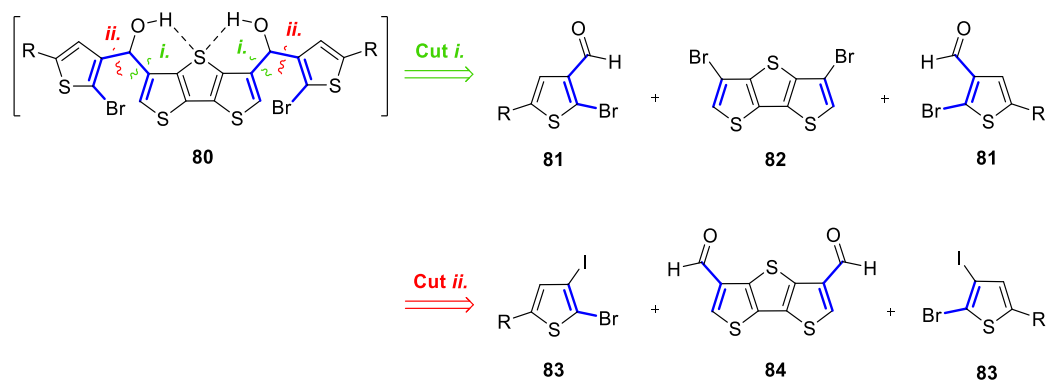
Scheme 19. Retrosynthesis of intermediate **80** with two cuts either side of the methyleneoxy bridging unit; R = C_6H_{13}.

Table 15 collects all the synthon and core molecular fragments from all four steps A-D. Here, the difficulty of the forward synthetic direction can be qualified from their complexity and foreseeable difficulty of these fragments. It is important to note that the core has less propensity for derivatisation than the thiophene synthons due partly for the need of double functionalisation over mono, but also partly to its high aromaticity, which significantly reduces its reactivity owing to its highly stable nature. Considering both the type and position of the functional groups, Steps C and D afford the most challenging fragments, while A and B give the simplest. Step A cut *ii.* also affords the dibromo-DTT (**54**) fragment which has a known synthetic procedure[144]. Overall, step A appears to be the most rational route to begin synthetic investigations.

Table 15. Collected synthon and core molecular fragments from the two cuts (*i., ii.*) of each four retrosynthetic steps (A-D); R = C_6H_{13}.

	Synthon Fragments		Core Fragments	
Step	Cut i.	Cut ii.	Cut i.	Cut ii.
A	**63**	**64**	**56**	**54**
B	**68**	**70**	**69**	**71**
C	**59**	**76**	**75**	**77**
D	**81**	**83**	**82**	**84**

5.2.2.2 Retrosynthesis of Target 45

The hybrid approach was selected for the retrosynthesis of **45**, as discussed with isomer **44**. The structure of **45** is a slight variant of **44**, where the 2-positions of the thiophene and the DTT core are directly C-C bonded, while their 3-postions are connected *via* an ethylene bridge and form half of the phenyl target ring. The core, synthon, solubilising groups and target ring formation are identified in Figure 43.
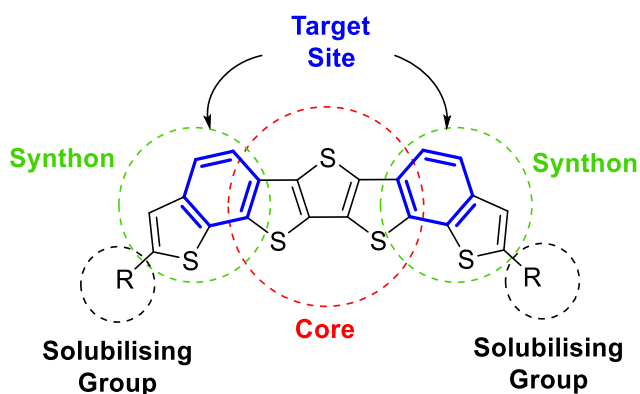
Figure 43. Target **45** with the core, synthon, solubilising groups and target ring identified, R = C_6H_{13}.

Scheme 20 illustrates a conventional ring formation of target **45** through Diels-Alder and Sigmatropic rearrangements. Unfortunately, the subsequent intermediates (**85**, **87**) would need oxidation of the newly formed bonds with unequal stoichiometries. Oxidation of the sulfur atoms may be avoided with specialist oxidants[217] but these cyclisations may not necessarily be clean, especially as they require the breaking of the strong aromaticity of DTT. Alternative cyclisations include the emerging and fast developing field of C-H activation, as detailed in steps A-D of Scheme 20.
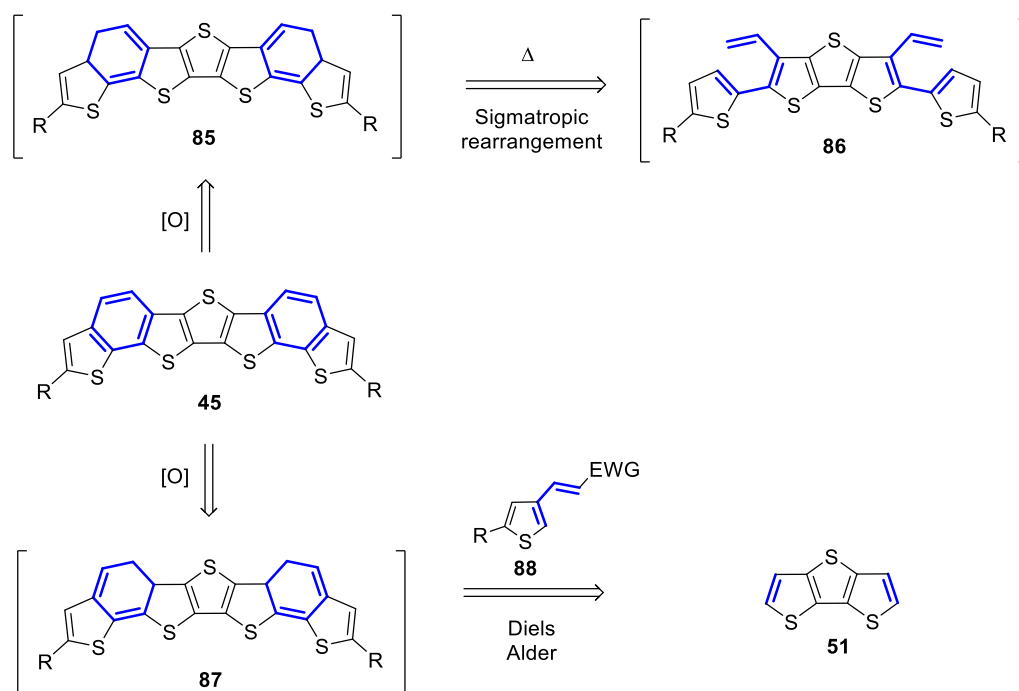
Scheme 20. Retrosynthesis of target **45** yielding sigmatropic and Diels-Alder chemistries gives rise to oxidation issues, R = C_6H_{13}.

The retrosynthetic cut A in Scheme 21 of **45** generates intermediate **89**, which consists of the core unit covalently bound at the 2-position to that of the synthon, which itself has an alkyne derivative at the 3-position and a hexyl (C_6H_{13}) unit at the 5-position. Cycloisomerisation with a metal or base forms the target phenyl ring and thus **45**, without the subsequent need for oxidation or reduction steps.

The intermediate **89** can be readily synthesised from two possible pairs of molecular fragments, as seen in Scheme 22. Retrosynthetic cut *i.* and *ii.* gives Suzuki and Sonogashira products, respectively. The literature-derived
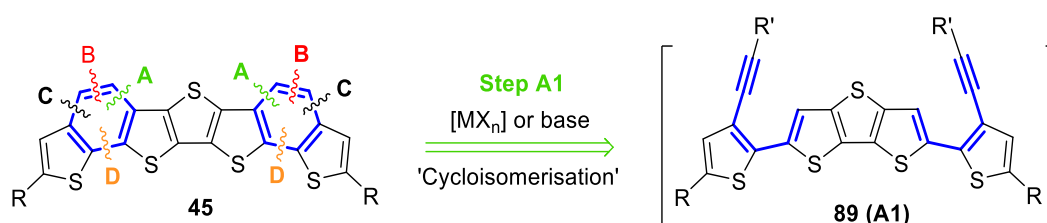
Scheme 21. Retrosynthetic step A1 of target **45**, formed from the metal-catalysed cycloisomerisation of intermediate **89** (A1); M = Pt, Ir, Au, X = Cl, R = C_6H_{13}, R' = H or C_4H_9.
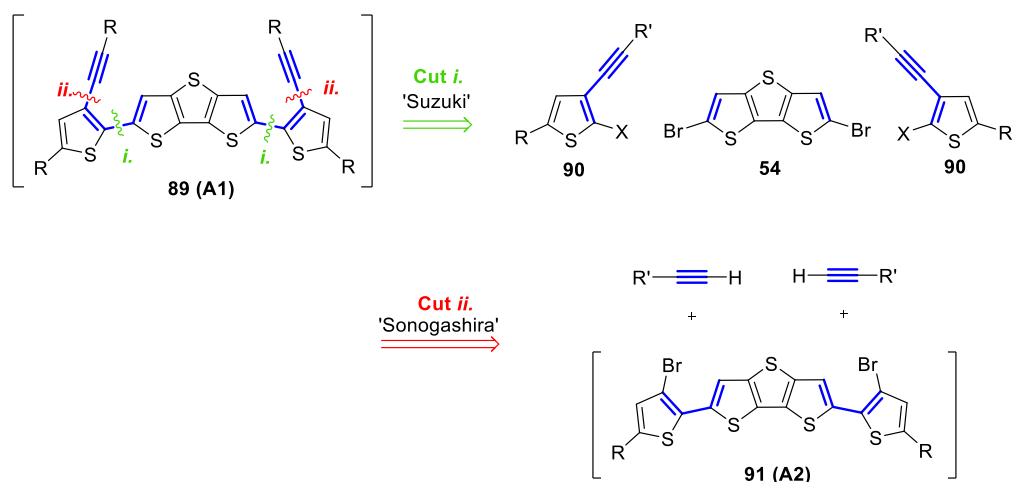
Scheme 22. Retrosynthesis of intermediate **89** giving Suzuki (cut *i.*) and Sonogashira (cut *ii.*) reagents, affording intermediate **91** (A2); X = BPin or SnMe$_3$, R = C$_6$H$_{13}$, R' = H or C$_4$H$_9$.

Br$_2$-DTT (**54**) is afforded with cut *i.*, although a highly derivatised synthon (**90**) is generated. Cut *ii.* gives the intermediate **91**, which consists of the synthon and DTT bound at their respective 2-positions with bromine substituents at the synthon's 3-position.

The retrosynthetic division of **91** (cut *i.*) gives **54** and a similar synthon (**92**) to previous structures seen with isomer **2**'s strategies, except that a C-C cross-coupling unit 'X' such as BPin or SnBu$_3$ is required at the 2-position and its presence with a bromine substituent on the same structure (**92**) may be unstable (Scheme 23). Cut *ii.* is a debromination giving the 'all-thiophene' intermediate **93**, which is a known species[221].
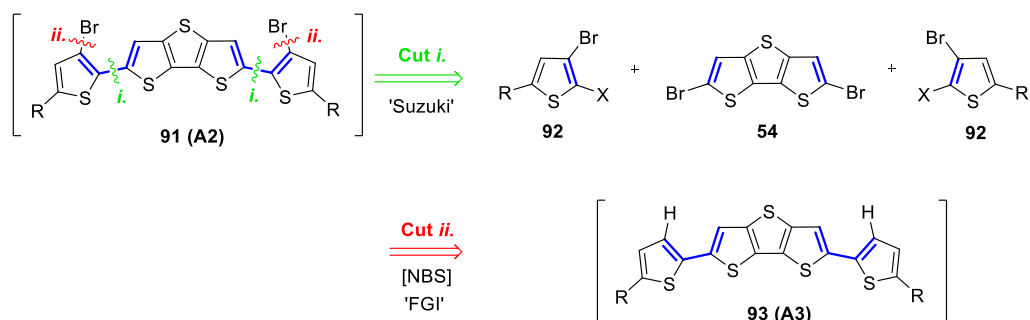
Scheme 23. Retrosynthetic cuts of **91** (A2) giving Suzuki products through cut 1, or a functional group interconversion *via* a double reduction at the 3-positions of the synthons giving the intermediate **93** (A3); X = BPin or SnBu$_3$, R = C$_6$H$_{13}$.
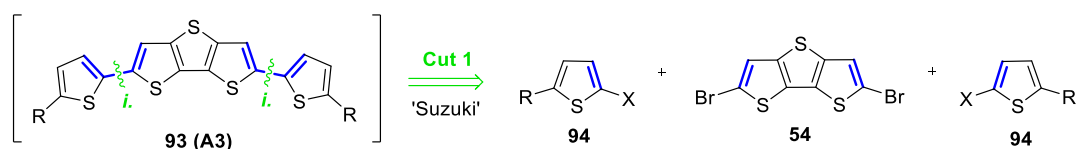
Scheme 24. Retrosynthetic division of intermediate **93** (A3), giving Suzuki reagents; X = BPin or SnBu$_3$, R = C$_6$H$_{13}$.

Intermediate **90** can be subdivided into its constituent synthon (**94**) and core (**54**) molecular fragments, as illustrated in Scheme 24, combined in a Suzuki reaction in the forward direction. These fragments are relatively simple and readily affordable, so suitable for synthetic investigations.

The retrosynthetic cut B divides the vinyl part of the phenyl ring giving to functional groups, possibly two aldehydes, which are known to undergo a McMurry coupling[222] in the forward direction with titanium tetrachloride (Scheme 25). The resulting intermediate **95** has four aldehydes across its backbone, which may hinder its stability.

The retrosynthetic division of **95** (Scheme 26) gives Suzuki products with only one single cut available between the 2 and 2' positions of the synthon and the core respectively. Both the afforded synthon (**96**) and the core (**77**) are bifunctional, which may be challenging to synthesise in the forward direction due to the carbonyls at the 3-positions, especially **96** which has a cross coupling group.
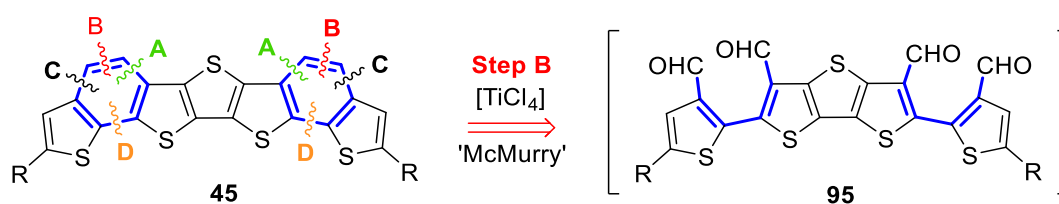
Scheme 25. Retrosynthesis of target **45** *via* step B, from the oxidative cleavage of the vinyl carbons at the two 3-positions, giving the McMurry intermediate **95**; R = C$_6$H$_{13}$.
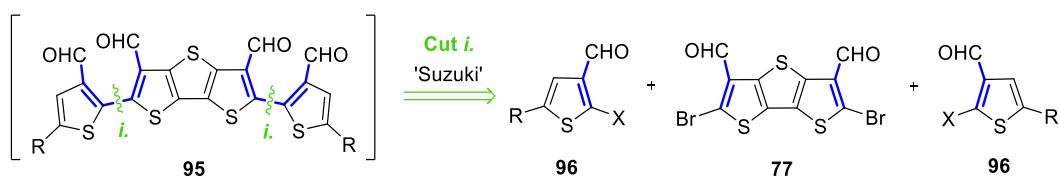
Scheme 26. Retrosynthesis of intermediate **95** *via* a Suzuki reaction giving the corresponding core and synthon molecular fragments, X = BPin or SnBu₃, R = C₆H₁₃.

The intermediate **97** (Scheme 27) generated from the retrosynthetic step C *via* cleavage of C-C bond between the 3-position of the synthon and the vinyl unit of the phenyl ring, consists of the linear thiophene backbone with two alkyne substituents on the 3-positions of the DTT core. The reactivity of the synthon's C-H at the 3-position is expected to differ to that of the core's in step A, where the structure may readily undergo cycloisomerisation but achieving the Sonogashira at the 3-position of the core may be more challenging.

The intermediate **97** can be divided by two cuts into molecular fragments, giving Suzuki (cut *i.*) and Sonogashira (cut *ii.*) reagents (Scheme 28). The resulting core (**98**) from cut *i.* will need several steps to synthesise while the synthons **94** are readily affordable. The Sonogashira reagents include intermediate **99**, which has bromine substituents at the 3-positions of the core, can be further divided as shown in.
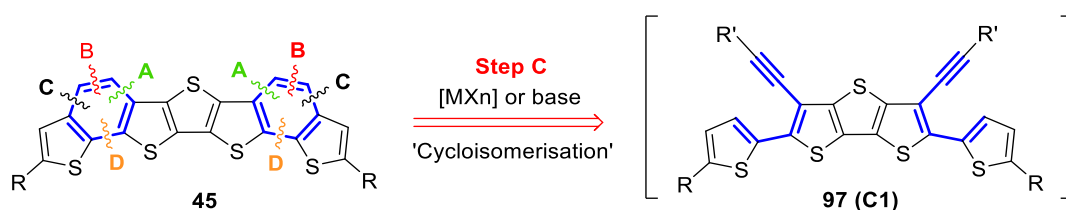
Scheme 27. Retrosynthesis of target **45** through step B, giving intermediate **97** (C1) in a reverse cycloisomerisation; R = C₆H₁₃, R = C₄H₉.
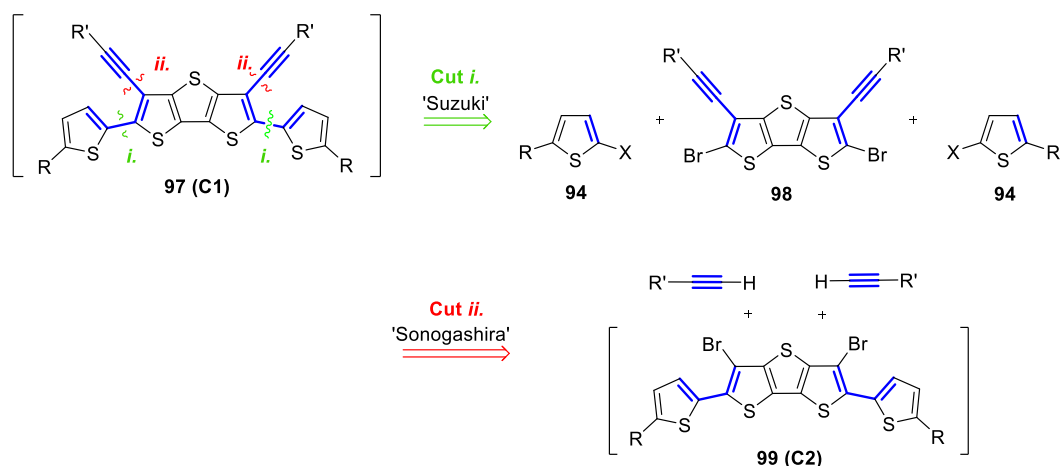
Scheme 28. Retrosynthesis of **97** (C1) yielding two cuts and affording Suzuki (cut *i.*) and Sonogashira (cut *ii.*) reagents; cut *ii.* gives intermediate **99** (C2) ; X = BPin or SnBu$_3$, R = C$_6$H$_{13}$, R' = H or C$_4$H$_9$.

Scheme 29 shows the retrosynthesis of **99** through two cuts, giving Suzuki (cut *i.*) reagents and a FGI (cut *ii.*) affords the intermediate **93**. Although the tetrabrominated DTT core fragment (**69**) is relatively simple, it needs an extra step after the formation of **54**. Cut *ii.* however, gives **93** as before through a FGI, although the bromine substitution is required to be regioselective to the 3-position of the DTT. **93** can be divided as illustrated above in Scheme 26.

Lastly, the retrosynthetic step D affords the intermediate **100** (Scheme 30), containing coupling agents on the synthon and bromine reagents on the
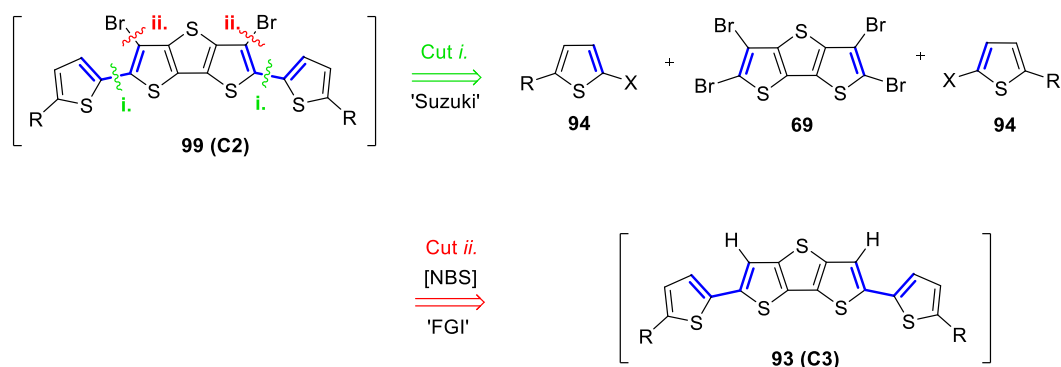
Scheme 29. Retrosynthesis of intermediate **99**, affording Suzuki reagents (cut *i.*) and intermediate **93** (cut *ii.*) through a double FGI; X = BPin or SnBu$_3$, R = C$_6$H$_{13}$.
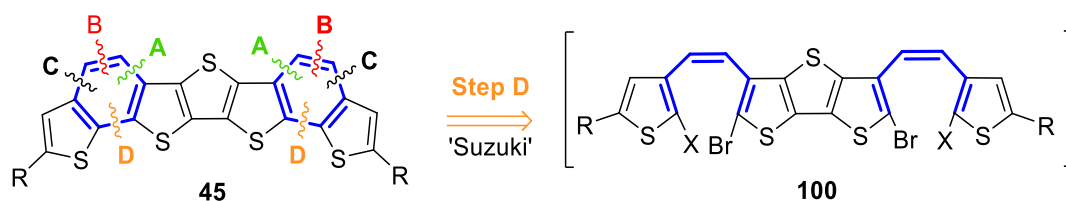
Scheme 30. Retrosynthesis of target **45**, *via* a Suzuki reaction affording intermediate **100**; X = BPin or SnBu$_3$, R = C$_6$H$_{13}$.

core components; their close proximity may destabilise the structure. The alternative intermediate (not shown) is to lithiate the 2-positions of the synthon and core and couple together[223] with CuCl$_2$, however, tetralithiated species would be extremely insoluble, even if stable.
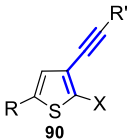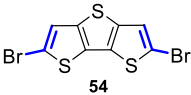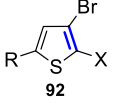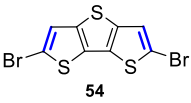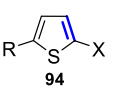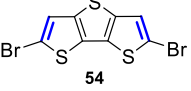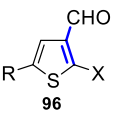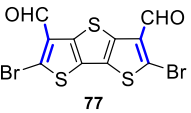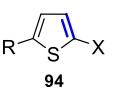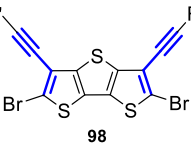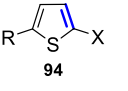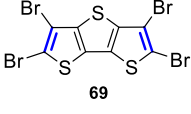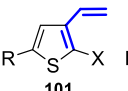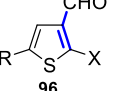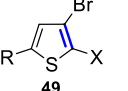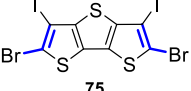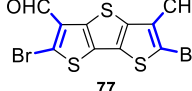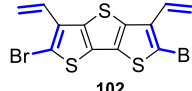
Nevertheless, the retrosynthesis of **100** (Scheme 31) gives three cuts, two Heck reactions[224] (cuts *i.* and *iii.*) and one McMurry reaction[222] (cut *ii.*). All of the resulting synthon and core units are bifunctional and thus challenging to synthesise in the forward direction, especially the synthons which have carbon or bromine substituents at the 3-positions but cross-coupling groups at the 2-positions and would thus be unstable on the single structure. While **75** and **75** have been described above, the fragment **102** is an unknown structure and potential unstable owing to its vinyl and bromine substituents.
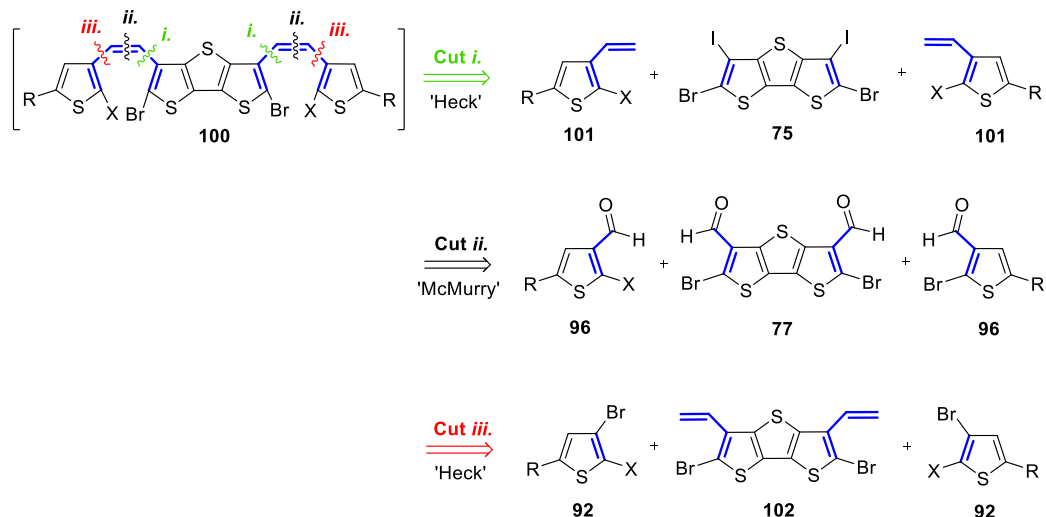
Scheme 31. Retrosynthesis of intermediate **100** through three cuts, affording Heck reagents (cuts *i.* and *iii.*) and McMurry reagents (cut *ii.*); X = BPin or SnBu$_3$, R = C$_6$H$_{13}$.

- 154 -

The core and synthon molecular fragments from all cuts and steps are collected together and presented in Table 16. Not all cuts generate fragments, but rather intermediates that need further division, resulting in several steps, such as A1, A2 and A3, for example. The dibromo-DTT (**54**) fragment is prevalent throughout all step A cuts, while its bifunctional derivatives are present with steps B-D. The fragments from both steps B and D may be unstable or relatively difficult to synthesise. The synthons of A and C steps are relatively simple and thus suitable for experimental investigations.

Table 16. Synthon and core molecular fragments from cuts *i.-iii.* and steps A-D; X = BPin or SnBu$_3$, R = C$_6$H$_{13}$, R' = C$_4$H$_9$.

Step	Synthon Fragments			Core Fragments		
	Cut i.	Cut ii.	Cut iii.	Cut i.	Cut ii.	Cut iii.
A1	**90**	-	-	**54**	-	-
A2	**92**	-	-	**54**	-	-
A3	**94**	-	-	**54**	-	-
B	**96**	-	-	**77**	-	-
C1	**94**	-	-	**98**	-	-
C2	**94**	-	-	**69**	-	-
D	**101**	**96**	**49**	**75**	**77**	**102**

- 155 -

5.2.2.3 Summary

Considering the well-established approaches of divergence or convergence towards a synthetic target, a hybrid approach was considered, as a combination of the two, to have the most stable and synthetically viable structures with regards to the reaction steps, conditions and coupling techniques. Out of three possible retrosynthetic strategies considered with regards to the hybrid approach, which involved the pentacene method, thiobenzannulation and cycloisomerisation, only the latter option was deemed appropriate for the target **44**. Of which, three cycloisomerisation chemistries were probed: Diels-Alder, Sigmatropic rearrangement and acid-catalysed cylcoisomerisation. Due to the potential synthetic challenges in generating the required starting fragments, the reactivity of the groups and unequal stoichiometric oxidation issues, the acid-catalysed cycloisomerisation was considered to be the best route in terms of reaction conditions and stability with regards to the resulting derivatives.

The hybrid approach was therefore applied through cycloisomerisation to **44** and the structure was broken down into its constituent parts, such as the core and the synthon molecular fragments, with the phenyl ring identified to be the focus of the synthetic investigations. These fragments were collected together and those which were the most synthetically viable from relatively low-cost commercial starting materials were highlighted as preferential for the forward synthetic investigations.

The hybrid approach was also considered to offer the best variation, in both structural derivatives and synthetic conditions for isomer **45**. For similar reasons as described with **44**, the phenyl ring was identified as the target site for the retrosynthetic strategy to focus on. The conventional techniques such as Diels-Alder and Sigmatropic rearrangements were applied to isomer **3** and deemed unfeasible. The pentacene method and annulation would not give the target isomer nor be regioselective. Thus, a C-H activated cycloisomerisation catalysed by transition metal or organic base was the focus of the strategy. Retrosynthetic cuts generated the synthon and core molecular fragment derivatives. Each structure and associated forward conditions were scrutinised for stability, reactivity and ease of synthesis, which resulted in the steps A and C with their corresponding molecular fragments selected for forward synthetic investigations of **45**.

The synthon and core molecular fragments identified from the retrosynthetic strategies are relatively similar for both isomers and small enough to not undergo further structural division, but rather, an evaluation of their synthetic background, structural nature and reaction conditions. These considerations are met by deploying computational chemistry to gain a deeper understanding for the mechanism of the synthesis of the synthon fragment in section 5.2.3, while reaction conditions are developed for the synthesis of the core fragment in section 5.2.4.

5.2.3 Modelling the Mechanism of the Synthon Molecular Fragment

The thiophene synthon (**64**) identified from the synthetic strategy for target **44** is shown in Figure 44; the bromine and aldehyde groups can be repositioned to give synthon **81**, which could be used for the synthesis of target **45**. Both structures have the solubilising hexyl chain at the 5-position, with the bromine and aldehyde substituents differing between the 2- and 3-positions. The aldehyde functional group purpose is to add a carbon atom to form one of the methylene units of the phenyl ring formed between the thiophene synthon and the DTT core; that of the bromine is to be converted into an aldehyde group for the same purpose.
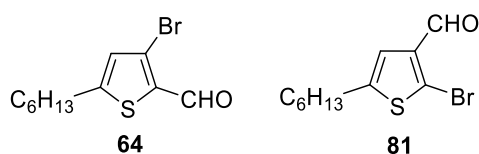
Figure 44. Two synthons, showing the bromine and aldehyde (CHO) functional groups at the 2- and 3-positions of the thiophene, with the hexyl chain (C_6H_{13}) at the 5-position.

5.2.3.1 Background

Halogen dance (HD) reactions are intermolecular rearrangements of halogen substituents on aromatic rings. The reaction class is a widely useful tool in the synthesis of materials for a range of applications from organic semiconductors to chiral drug scaffolds[225–229]. HD reactions have been observed for diverse substrates including thiophene[230,231], phenyl[232,233], furan[234,235], thiazole[236], oxazole[237] and pyridine[238] units.

Scheme 32 illustrates the HD reaction with 2-bromo-5-hexylthiophene (**1**) and LDA affording 3-bromo-2-formyl-5-hexylthiophene (**2**) in 88% yield[239]. The reaction shows the repositioning of the bromine atom on the thiophene ring and the addition of a formyl transfer agent, 1-formylpiperidine, immediately quenching the lithium salt and yielding **64**. This scheme illustrates how the HD reaction can generate a useful multi-functional product in high yield from a mono-functional starting reagent.

i. LDA, -78 °C, 30 min;
rt, 15 h
ii. 1-formylpiperidine,
0 °C, 15 min; rt, 30 min

88 %
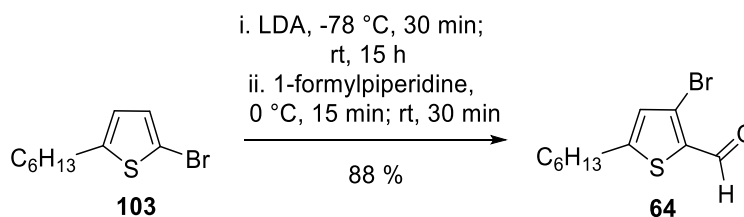
Scheme 32. The Synthesis of the HD mediated-3-bromo-2-formyl-5-hexylthiophene product.

The base which led to the discovery of the HD reaction (in 1951) was sodium acetylide in liquid ammonia[240]. The generality of the reaction was confirmed two years later by the same research group using sodium amide[231]. For these reactions mixtures of polybrominated species were observed in the products. Subsequent work using bases such as potassium anilide[230] and lithium diisopropylamine (LDA)[239] has, however, shown that the conditions of the HD reaction can be adjusted to produce a relatively clean product.

The conditions of the reaction are typically low temperatures (-78 °C) for a short time (30 min), after which the mixture is allowed to warm to room temperature and stirred overnight. These conditions are 'promotive' of an HD reaction[219], but give little indication as to the likely mechanism.

Proposed mechanisms have been difficult to test because the multiple intermediates are highly reactive and hard to observe directly. However, infrared absorption spectroscopy has been used to monitor organolithium intermediates in cryogenic reactors[241]. Very fast rates were observed for the lithiation of 2- and 3-bromothiphene by LDA in THF at -86 °C, in which a steady state was reached within *ca.* a minute. The relatively faster reaction of the 3-bromo compound was attributed to a stronger inductive effect of the bromine substituent compared to 2-bromothiophene (no reaction was observed for thiophene at -86 °C although metalation was observed at -40 °C). IR absorption cannot be applied to follow the subsequent steps of the HD as the spectral profiles of the species under investigation overlap.

5.2.3.2 Evaluation of the Four-Centre Model

The mechanism behind the HD reaction is generally believed to consist of a cascade of deprotonation (metal-hydrogen exchange) and metal-halogen exchange reactions[219]. Scheme 33 shows the possible first steps, as they might apply to the synthesis of 3-bromo-2-formyl-5-hexylthiophene. In the model we only consider the lithiation and bromination possibilities for the 2, 3 and 4 positions around thiophene because in the "real" chemistry the 5 position is blocked by alkyl chains or other derivatives (Scheme 33). The proton abstraction of 2-bromothiophene (**103**) at the 3 (**104**) or 4 positions (**105**), or lithium halogen exchange at the 2 position (**106**), are labelled as steps 1a, 1b and 1c respectively.

The reactivity of the protons and bromine substituent was evaluated by considering the Gibbs energies of their respective anions in THF using the default polarisable continuum model. The Gibbs free energy of the anion deprotonated at position 3 (step 1a) is found to be lower than the other two positions, and hence the proton at this position would be preferentially abstracted. This conclusion is confirmed with atomic charge analysis.

$R_{exp} = C_6H_{13}$; $R_{DFT} = H$
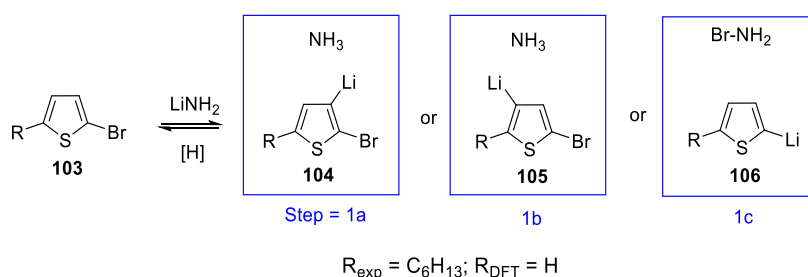
Scheme 33. Lithiation of 2-bromothiophene (**103**); the possible products of each of the reactions (**104**, **105**, and **106**) are the associated reactions of step 1a, 1b and 1c respectively.

Table 17. Internal and free Gibbs energies in THF[a]

Anion	U / a.u.	ΔG / a.u.
104	-3126.067706	-3126.055707
105	-3126.062513	-3126.050591

[a] Calculated using IEFPCM

Atomic charges were calculated and shown in Table 18. All the methods except for MK show the H^3 atom is relatively more positive than H^4 and thus in the model HD reaction the H^3 atom would be expected to be attacked by the lithium amide preferentially. All methods show that the H^3 atom is more positive than the bromine atom (Br) thus the bromine is unlikely to be attacked.

Table 18. Atomic charges (eV) with various methods
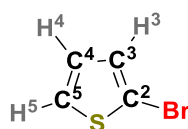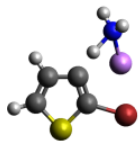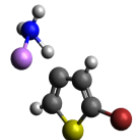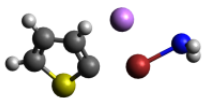
Atom	Mulliken	MK	NBO	AIM
S	-0.18	0.10	0.45	0.25
C^2	-0.078	-0.21	0.35	-0.26
C^3	0.16	0.083	0.28	0.030
C^4	-0.56	-0.25	-0.24	0.013
C^5	0.13	-0.18	-0.39	-0.20
H^3	0.19	0.099	0.23	0.055
H^4	0.15	0.17	0.22	0.044
H^5	0.25	0.19	0.23	0.071
Br	-0.051	0.0047	0.13	-0.011

While it is known that reagents like alkyl lithium aggregate in ether-based solvents, there is uncertainty with regards to the degree[242]. pKa values and lithium equilibria have been investigated by Streitwieser[243] who found that solvation continuum models were inadequate for the study of lithiated species (in THF), which are believed to exist as tetramers at low temperatures in solution. On the other hand NMR studies[244] find the binding of explicit solvent molecules to lithiated reagents is under kinetic rather than thermodynamic control. It is also known that there are large interaction energies associated with ethers which may determine the degree of aggregation[245].

Due to the uncertainty in the literature over the role of solvent, the lithiation possibilities were calculated in vacuum and those of the first step are summarised in Table 19 (see Appendix B for Cartesian structures); the singular imaginary frequencies for the transition states correlate well with those of phenyl lithium-proton stretches[246]. Both the barrier and the Gibbs reaction energies of 1a were the smallest (9.81 and 22.51 kJ mol^{-1}) while 1c is the largest (110.11 and 115.53 kJ mol^{-1}).

Once the transition states for the three possibilities of the first step of the dance were located, the reaction energy profiles along their IRCs were calculated. Due to the deep dipole-dipole wells in both the entrance and exit channels the reaction was unable to be followed to completion in either direction. The IRC paths 1a-c are referenced to the sum of the energy of the

Table 19. Transition states, frequencies, activation energies and Gibbs reaction energies for steps 1a-c.

Step	TS‡	Vibration / cm^{-1}	U_a / kJ mol^{-1}	$\Delta_r G$ / kJ mol^{-1}
1a		1325i	9.81	22.51
1b		1366i	30.26	51.05
1c		229.1i	110.11	115.53

individually optimised reagents, shown as the filled triangle (labelled 1a OR) on the left-hand side of Figure 45. The sum of energies of the individually optimised products for the three reactions is shown on the right-hand side of the diagram.

The striking difference between the lithium-hydrogen exchange reactions and the lithium-halogen exchange reaction is the nature of their transition states. Both reaction steps 1a and 1b have tight transition states, while 1c is relatively loose. All three reactions exhibit deep wells in both entrance and exit channels. These are due to dipole-dipole interactions between the reactants and products. For both lithium-halogen exchange reactions the well on the product side is significantly more stable than that on
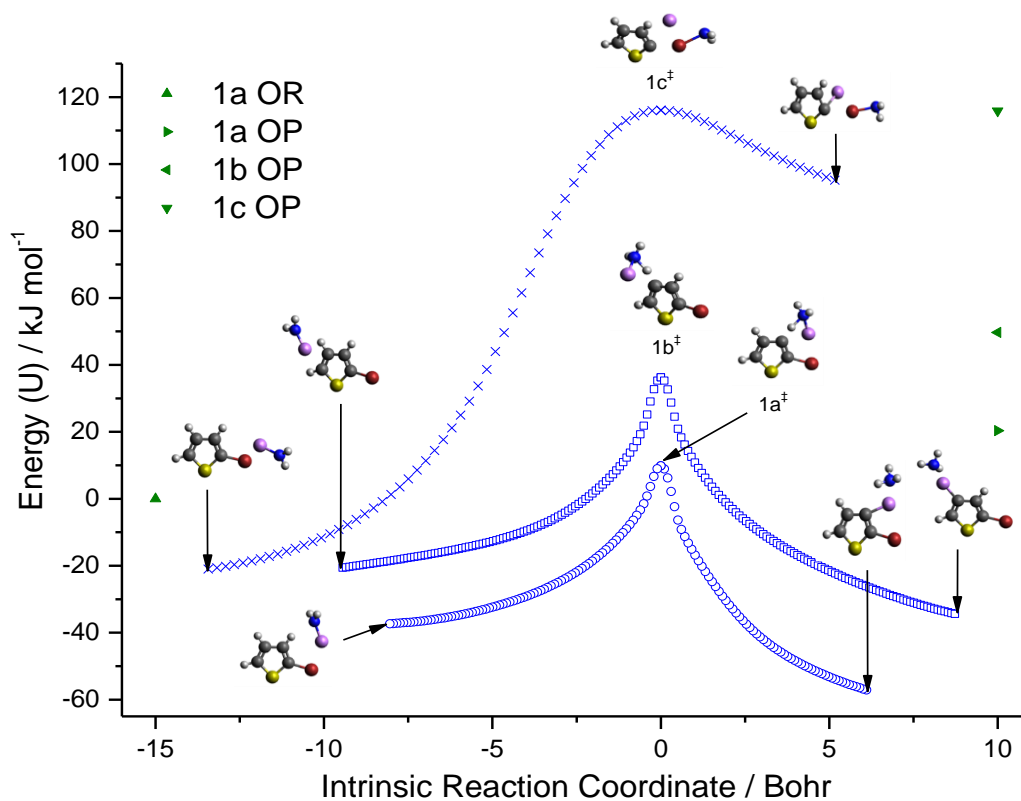
Figure 45. Minimum energy path along the forward and reverse intrinsic reaction coordinates of steps 1a-c, relative to the energy of the starting materials; the optimised reagents (OR) and optimised products (OP) are shown as single data points (green triangles). The potential energy wells in the entrance and exit channels are due to strong dipole-dipole interactions between the reactants and products; 1a has deeper potential energy wells than 1b or 1c due to a dipole alignment at the 3 position of thiophene.

the reactant side, so despite the fact that reactions 1a and 1b are both predicted to be endothermic ($\Delta_r U_g$ of +20.4 and +49.7 kJ mol^{-1} respectively) the complex on the product side is predicted to be thermodynamically favoured.

Both lithium-hydrogen exchange reactions 1a and 1b have modest barriers in the forward direction, 9.81 kJ mol^{-1} and 30.26 kJ mol^{-1} respectively. At -78 °C, reaction 1a is expected to be kinetically favoured over 1b by a factor of order 2.3×10^5. However, the reaction rate at low temperature may also be enhanced by quantum mechanical tunnelling through the narrow barrier between the entrance and exit channel complexes. Thus the most likely product of the first step of the dance is a lithium-proton exchange reaction, probably favouring the production of 3-lithio-2-bromothiophene (**104**) over 4-lithio-2-bromothiophene (**105**).

The reaction of step 2 is now investigated, which involves the lithium-halogen exchange between **103** and **104**, as shown in Scheme 34. While **106** was found to be kinetically and thermodynamically unfavourable from the reaction of **103** and lithium amide, **106** has now to be produced from the forward reaction of step 2.

Species **106** and **63** must then undergo a transmetallation between the thiophene partners (Scheme 35) to produce the target lithium species **107**. To achieve this, the lithium and bromine atoms of **106** and **63** exchange places thereby reforming the starting reagent **103**; the cooperative exchange of substituents is called a "do-si-do" reaction. The reformation of **103** suggests the overall mechanism is autocatalytic or pseudo-clock type.
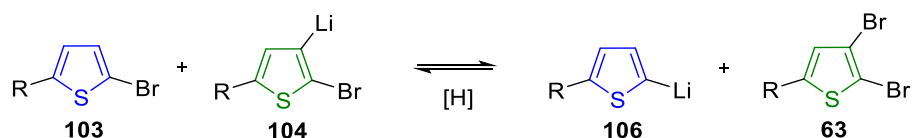
Scheme 34. Reaction step 2, the generation of the 2,3-dibromothiophene **63**; the colours indicate the substrate transformation.
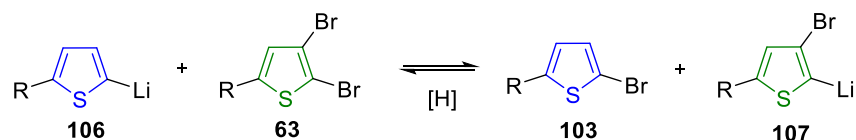
Scheme 35. Reaction step 3, the "do-si-do"; the colours indicate the substrate transformation.

It is also possible for reagent **104** and product **63** species from step 2 to cross couple and undergo their own lithium-halogen exchange to furnish an alternative or bromide catalysis, also giving **107** (Scheme 36). If this were the case, it must be an additional step (step 4), only possible once some 2,3-dibromothiophene (**63**) has been formed from step 2. Since **63** is both a reagent and product it could also be influential in the HD as an auto catalyst.
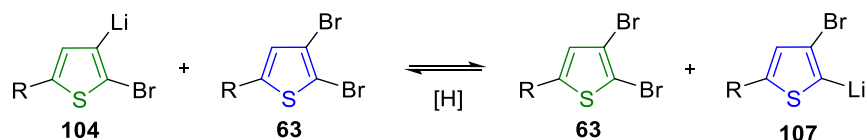
Scheme 36. Bromide catalysis (step 4), generating major lithium species **107**; the colours indicate the substrate transformation.

The four-centre type transition states were found for the lithium-halogen exchange steps 2, 3 and 4 *via* the STQN method and their stationary nature was confirmed with frequency and IRC calculations (see Figure 46) and summarised in Table 20. Step 2 is only slightly endothermic (11.05 kJ mol^{-1}) but is predicted to proceed over a substantial barrier of 202.2 kJ mol^{-1}. Steps 3 and 4 have similarly high barriers but are exothermic (-49.3 and -38.3 kJ mol^{-1} respectively). The transmetallation of lithium between the two thiophenes in the transition states appears to occur by a cradle-like structure, as illustrated in Figure 47.
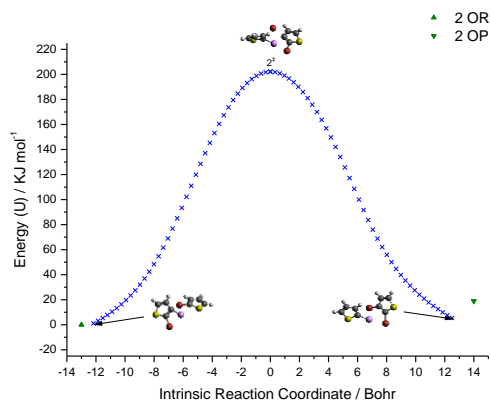
Step 2
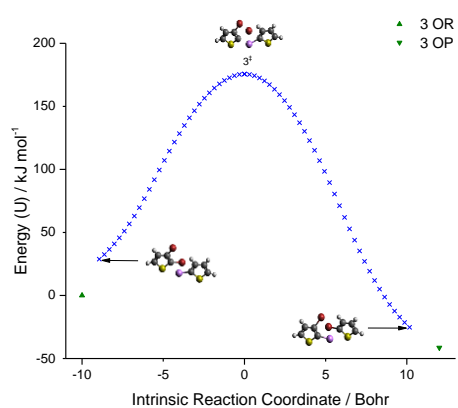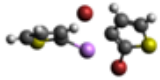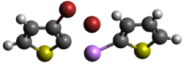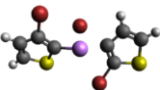
Step 3
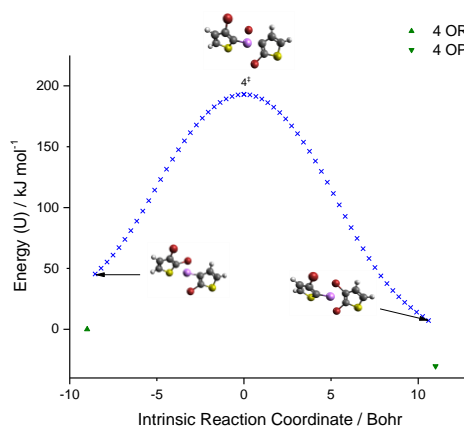
Step 4

Figure 46. Minimum energy path along the forward and reverse intrinsic reaction coordinates of steps 2, 3 and 4 (four-centre type); referenced to the optimised starting reagents (OR).

Table 20. Transition states (four-centre type), frequencies, activation energies and Gibbs reaction energies for steps 2-4.

Step	TS‡	Vibration / cm^{-1}	U_a / kJ mol^{-1}	$\Delta_r G$ / kJ mol^{-1}
2		265.0i	202.2	11.05
3		266.2i	175.6	-49.29
4		272.5i	193.1	-38.25
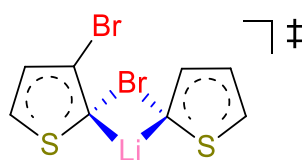
Figure 47. The four-centre geometry of the lithium-halogen exchange transition state 3; the lithium atom is directly bound to both carbanions.

The relatively large energy barriers in the reverse direction and the deeper energy wells on the product side of steps 3 and 4 essentially traps the target lithium species **107**. The build-up of **107** over time ensures **64** is produced as the major product upon quenching with an electrophile.

Thus far, the rearrangement of the lithium, proton and bromine atoms on a thiophene substrate are studied, linking the suspected steps in the halogen-dance mechanism through four-centre type lithium-bromine exchange steps. Yet the activation energies presented from these studies suggest each reaction step to be improbable, even at room temperature. Therefore, the model could be improved by (1) long range correction to the potentials, swapping B3LYP for LC-ωPBE[247] and LC-BLYP, (2) dispersion-corrected functionals[248], and (3) explicit and continuum solvation models[249] of THF.

Long-range corrected functionals gave four-centre type transition states with single imaginary frequencies, but only at the lower basis set of 6-31+G(d). Grimme's dispersion-corrected functionals resulted in transition states that gave the expected reagents and products at the

B3LYP/6-311++G(d,p) level. The resulting activation energies were reduced by 30-40 kJ mol^{-1}, in comparison to the non-dispersion corrected functionals (activation energies are shown in Table 21 and Table 22). The overall result, however, is that while the barriers are somewhat lower when dispersion terms are considered, the resultant barrier heights are still far too high to be consistent with experiment.

Post-HF calculations of the transition states proved to be computationally challenging, but the thermodynamics was successfully investigated at the 'chemically accurate' MP2 and CCSD levels of theory (Table 23). CCSD gives almost identical endo- and exothermicities to the B3LYP-D3BJ and D2 functionals (*i.e.* to within chemical accuracy of *ca.* 3 kJ mol^{-1}).

Table 21. Activation energies (kJ mol^{-1}) for steps 1a-4 at various theory levels, in vacuum with no Grimme's dispersion terms; lithium-proton exchanges and the lithium-halogen (four-centre type) exchange steps; [-] no activation energy available due to the transition state being unobtainable after multiple attempts.

Step	HF/ 6-31G(d)	B3LYP/ 6-31+G(d)	B3LYP/ 6-311++G(d,p)
1a	15.40	-4.896	9.810
1b	63.25	22.93	30.26
1c	162.1	98.29	110.1
2	298.4	180.5	202.2
3	-	165.0	175.6
4	299.2	173.9	193.1

Table 22. Activation energies (kJ mol^{-1}) for steps 1a-4 at various theory levels, in vacuum with Grimme's dispersion terms; lithium-proton exchanges and the lithium-halogen (four-centre type) exchange steps.

B3LYP-D2/ 6-311++G(d,p)	B3LYP-D3/ 6-311++G(d,p)	B3LYP-D3BJ/ 6-311++G(d,p)	wB97XD/ 6-311++G(d,p)
-27.33	0.5300	-6.14	-2.100
1.260	21.92	17.02	19.46
85.99	98.33	95.60	116.2
163.0	177.0	174.8	230.8
140.8	146.6	146.4	217.6
151.1	158.0	160.3	221.5

Table 23. Internal energies of reaction (kJ mol^{-1}) for steps 1a-4 at the MP2 and CCSD theory levels, in vacuum; lithium-proton exchanges and the lithium-halogen (four-centre type) exchange steps.

Step	MP2/ 6-311++G(d,p)	CCSD/ 6-311++G(d,p)
1a	12.92	11.68
1b	39.90	40.93
1c	134.5	120.9
2	4.120	8.640
3	-44.06	-47.48
4	-39.95	-38.84

Even though dispersion-corrected functionals give a significant improvement, the activation energies for steps 3 and 4 remain high. An attempt to improve the calculations using an explicit solvation model, using steps 1a and 2 as suitable test-case transition states (Table 24) was conducted. An explicit THF molecule coordinated to the lithium atom (calculated in vacuum) increases the barrier heights by ~9 and ~21 kJ mol^{-1} respectively. This suggests, that adding electron density to the lithium atom weakens the lithium-carbon bonds and destabilises the transition state. Although Streightweiser[243] suggests explicit solvation models to be the most appropriate, continuum models were also investigated, namely the default Integral Equation Formalism Polarisable Continuum Model (IEFPCM)[249] in G09, Truhlar's and co-workers solvation model incorporating electron density (SMD)[108] which is a variant of IEFPCM and the Conductor Polarisable Continuum Model (CPCM)[110]. It was found that all of these models increased the barriers by varying degrees (of order 10-25 kJ mol^{-1}).

Table 24 Activation energies (kJ mol-1) considering explicit and continuum solvation models at the B3LYP-D2/6-311++G(d,p) level.

Step	THF[a]	IEFPCM[b]	SMD[c]	CPCM[d]
1a	18.59	26.15	18.47	25.96
2	222.9	215.5	195.5	215.1
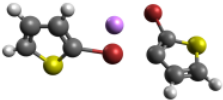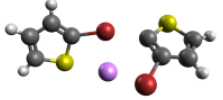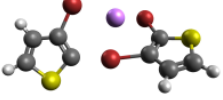
[a] Explicit THF molecule, [b] the default Integral Equation Formalism Polarisable Continuum Model (IEFPCM) in G09, [c] solvation model incorporating electron density (SMD), [d] Conductor Polarisable Continuum Model (CPCM); [a] is at the B3LYP/6-311++G(d,p) and [b-d] is B3LYP-D2/6-311++G(d,p) levels

5.2.3.3 Evidence for an S_N2 Model

It was clear that solvation models (explicit and continuum) do not explain how the reaction can proceed smoothly in THF because the predicted activation barriers are relatively large and kinetically unfavourable. This suggests that an alternative lithium-halogen exchange mechanism needs investigating to locate reasonable energy barriers for the HD reaction. Multiple attempts at locating a 'bromate' type transition state were not successful as they also resulted in the formation of bithiophene products and the release of lithium bromide - clearly incorrect.

Alternatively, S_N2 type transition states were investigated. Such transition states were found for all the lithium-halogen exchange steps 2-4, with a single imaginary frequency each (Table 25) and confirmed with IRC calculations. The S_N2 transition states show the lithium coordinated in between the bromine atoms (Figure 48) and the sulfur of the thiophene (step 3). The barrier for step 2 is reduced from *ca.* 200 to 45 kJ mol^{-1}, and steps 3 and 4 become barrierless (-12.22 and -20.89 kJ mol^{-1}), where 4 was the most favourable reaction.

Table 25. Transition states (S_N2 type), frequencies and activation energies for steps 2, 3 and 4.

Step	TS‡	Vibration / cm^{-1}	U_a / kJ mol^{-1}
2		112.7i	44.93
3		143.4i	-12.22
4		72.35i	-20.89
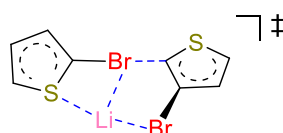
Figure 48. The S_N2 geometry of the lithium-halogen exchange transition state 3; the lithium atom coordinates between the bromine atoms (and partially to sulfur with state 3).
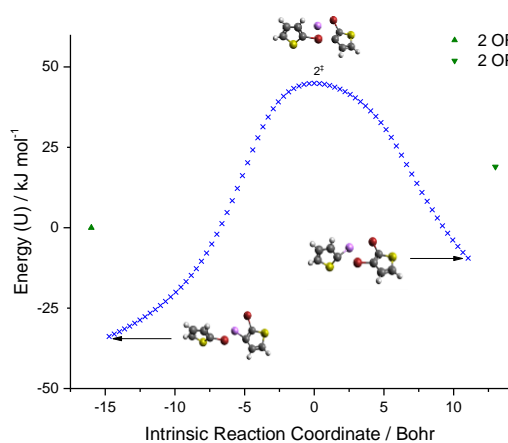
Step 2
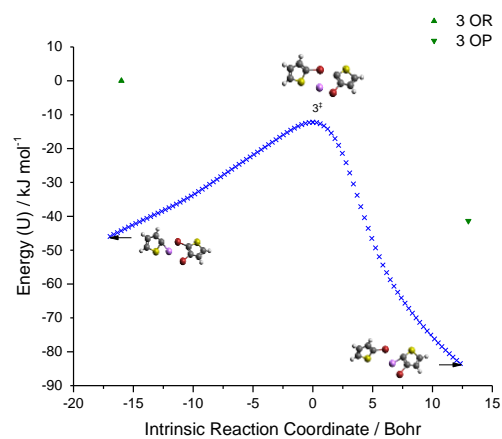
Step 3
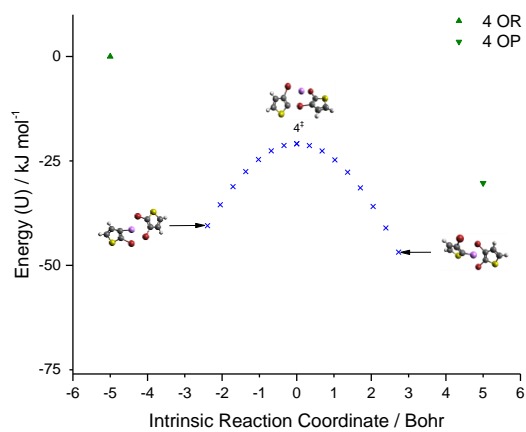
Step 4

Figure 49. Minimum energy path along the forward and reverse intrinsic reaction coordinates of steps 2-4 (S_N2 type), referenced to the optimised starting reagents (OR).

The overall Gibbs energy profile for the S_N2 mechanism is illustrated in Figure 50 and Figure 51 for steps 2-3 and 4 respectively. Figure 50 suggests that step 2, proceeding *via* an S_N2 type transition state, is the rate determining step in the halogen dance reaction. As shown in the supporting information, the minimum energy paths also all exhibit deep wells on both sides of the transition state for all the S_N2 type reactions. Reactions 3 and 4 show 'submerged' transition states which lie below the energies of the optimised starting materials, but flanked on either side by deep attractive wells due to the dipole-dipole interactions between both the reactant and product species. This suggests that the entire reaction sequence from the initial lithiation step to the halogen exchange occurs between the same sets of molecules which are strongly confined by the electrostatic forces between them.

A plausible mechanism, similar to that proposed in the literature[239], for the model halogen dance reaction is outlined in Scheme 37. One proton abstraction at the 3 position and two lithium-halogen exchanges can afford the target lithium species (**107**) in just three steps. Step 2 is predicted to be the rate limiting step with a barrier of *ca.* 45 kJ mol^{-1}. Steps 3 and 4 are predicted
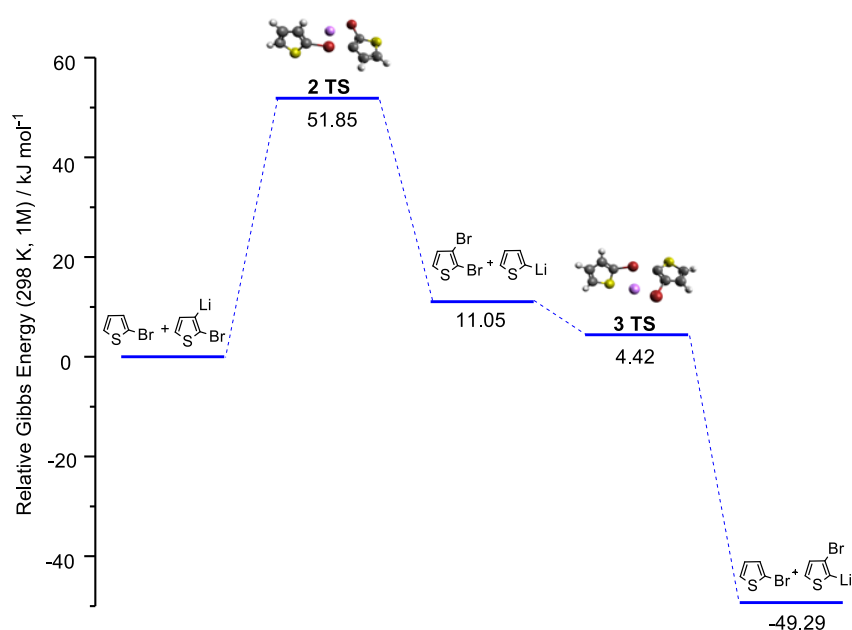
Figure 50. The relative Gibbs energy profile for the S_N2 mechanism steps 2 and 3. For clarity, the wells in the entrance and exit channels are not shown.
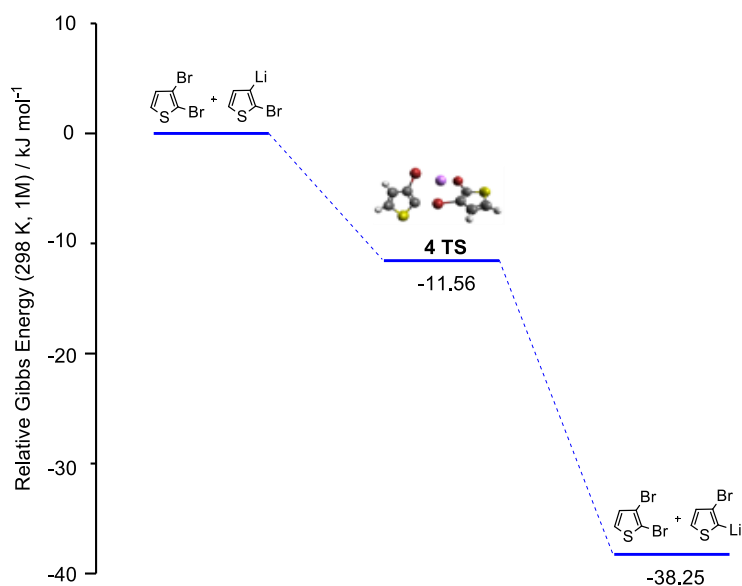
Figure 51. The relative Gibbs energy profile for the S_N2 mechanism step 4. For clarity, the wells in the entrance and exit channels are not shown.
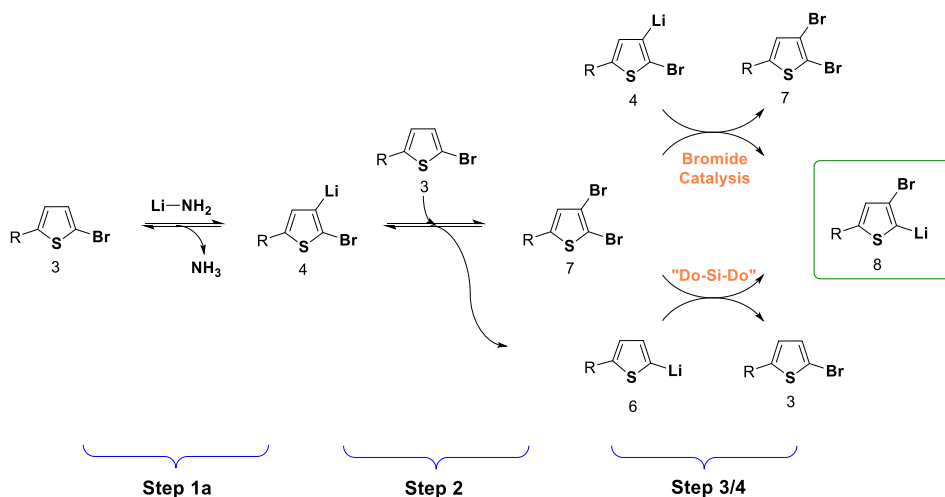
Scheme 37. A plausible mechanism for the model HD reaction; R=C_6H_{13} experimentally and R=H in model.

to be barrierless with submerged transition states (*i.e.* exhibit negative barriers with potential wells in the entrance and exit channels). This conclusion is consistent with the two key requirements for the HD reaction originally outlined by Frohlich[239], that (a) the HD reaction is promoted by base and (b) the formation of 2,3-dibromothiophene is needed.

5.2.3.4 Summary

DFT was deployed to investigate the potential energy landscape and overall reaction mechanism of a model HD reaction for the formation of the thiophene synthon. Two types of transition state were located for the lithium-halogen exchanges, which is central to the overall HD mechanism; the S_N2 type was favoured over the four-centre type. The four-centre transition state was found to lead to activation barriers which are inconsistent with experimental observation that the reaction proceeds smoothly and quite rapidly at room temperature after the initial low temperature lithiation of the halogenated substrate. The S_N2 lithium-bromide transition states are barrierless, except the second which is the limiting step.

The rate determining step is the reaction of the substrate with lithiated product to generate a 2,3-dibromothiophene *via* an S_N2 type transition state. The 2,3-dibromothiophene subsequently reacts with lithiated product *via* two barrierless paths, connected by submerged S_N2 type transition states, leading to exchange of the halogen and lithium substituents. Although the overall driving force was thermodynamics, the kinetic factors tightly control the reaction path through temperature. While dibromothiophenes may act to catalyse the reaction, the reformation of 2-bromothiophene suggests the HD reaction of 5-alkyl-2-bromothiophene is a pseudo-clock type.

This investigation has proved highly useful and generated practical understanding with regards to experimental conditions. It has also developed more in-depth knowledge of the lithium-bromide exchange which is highly deployed for synthetic functional group interconversions.

5.2.4 Method Development for the Core Molecular Fragment

The fused-thiophene core molecular fragment is widely used as a constituent in high-performing, flexible and smart organic electronic technology such organic thin-film transistors[250] and organic light emitting diodes[251], even though it retails at a relatively high commercial cost. In addition, several methods, as outlined below, have been developed for its synthesis and yet the reagents as well as the intermediates are relatively unstable and thus the synthetic procedures face (1) low-scale production due to the degradation of the starting materials, which require in-house preparations with immediate use; and (2) some methods use lithiation chemistry, which is efficient for synthetic transformations, but gives scaling issues due to the cryogenic nature of the reaction and highly reactive nature of the lithiation reagents. These issues warrant an investigation into an alternative route to this highly useful molecular fragment.

5.2.4.1 Background

There are four well-published routes in the literature to date. The first synthesis of dithienothiophene was published by Stoyanovich *et al.*[42] in 1965, however limited spectroscopic characterisation was reported. Jong[43] and Janssen[44] reported an improved route for the synthesis of DTT in 1970, with an adaption of the procedure for sulfur insertion using freshly prepared bis(phenylsulfonyl)sulfide. Lithiation of 3-bromothiophene (**108**) swaps the bromine group for lithium and turns the 3 position into a reactive carbanion. Insertion of sulfur by bis(phenylsulfonyl)sulfide gives intermediate **109** and ring closure between the 2 and 2' positions is afforded by lithiation and copper chloride giving DTT (**51**) in overall yield of 35 %. A disadvantage is the use of the odorous and toxic bis(phenylsulfonyl)sulfide, which is normally prepared fresh due to its relatively high commercial cost and long-term storage instability.
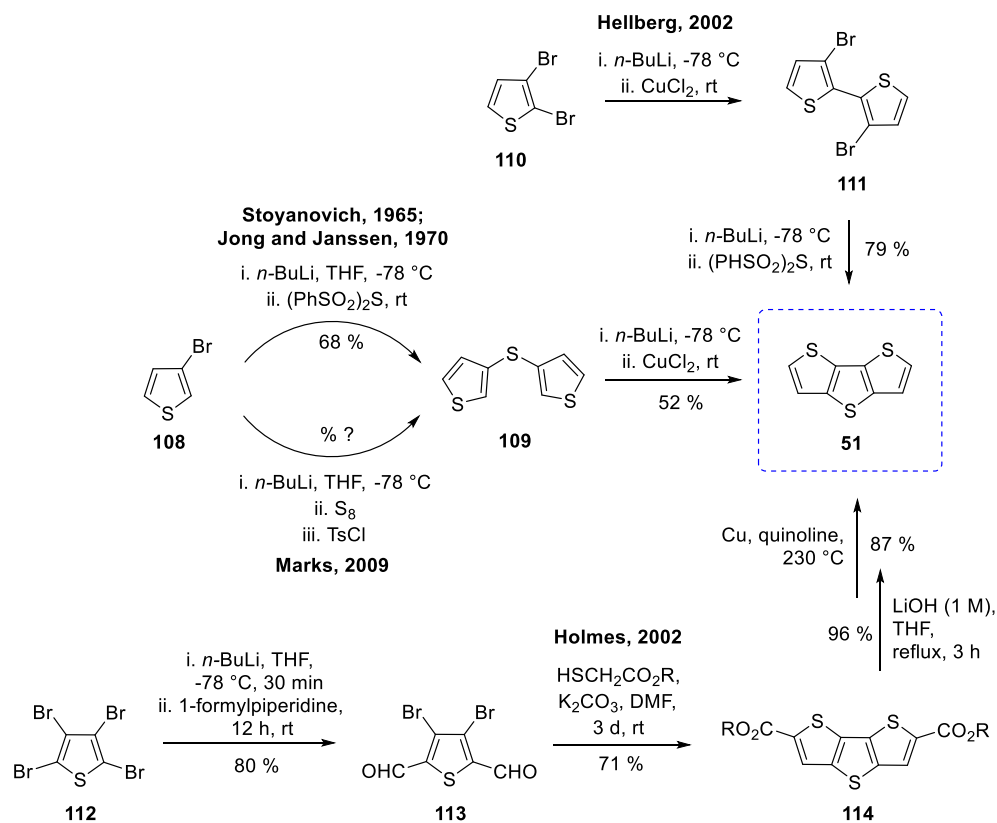
Scheme 38. Synthetic routes to DTT.

In 2002, two very different and alternative routes were published. The approach by Hellberg *et al.*[223] used 2,3-dibromothiophene (**110**) as the starting reagent. Regioselective lithiation of the 2-bromo position using *n*-butyl lithium and oxidative coupling gave the 3,3'-dibromo-2,2'-bithiophene (**111**) in 79 % yield and DTT 55.3 % total yield after purification. This method is similar to the previous method by Jong and Janssen, whereby the order of the steps has been reversed and affording 20 % more of the total yield than the previous method.

The second alternative route was developed by Holmes *et al.*[252], due to challenges with scaling up. This approach builds the two external thiophenes around the central ring. Dilithiation of tetrabromothiophene (**112**) and quenching with 1-formylpiperidine gives 3,4-dibromothiophene-2,6--dicarboxylic acid (**113**). Reaction with ethylmercaptoacetate in potassium carbonate base and DMF gave **114**. Hydrolysis with 1 M lithium hydroxide in THF affords the corresponding carboxylic acid and an *in situ* reduction of the carboxylic groups with copper in quinoline gave DTT in 47 % overall yield. The advantages of this route are that all intermediates can be purified by

crystallisation, synthesised on a 5-10 g scale and the initial derivatised groups at the 2 and 3 positions can be used to introduce further functionalities. However, its main disadvantage is the long reaction time scale, with four reaction steps and three days for the second step. Another significant difficulty, is the homo-polymerisation of **113** upon quenching the dilithiated species with DMF, which occurs readily as one lithiated thiophene anion can attack any newly formed carbonyl; to overcome this, very high stirring speeds and fast addition of s single aliquot of DMF was added which ensures scaling up to industrial production is highly challenging.

In 2009 Chen and Marks[253] reported a revision of the one-pot synthesis of DTT. Insertion of sulfur between two 3-bromothiophene molecules giving a sulfide intermediate which undergoes subsequent ring-closure with a lithiating reagent and copper (II) chloride giving DTT in 36 % yield. The advantages of this route include relatively cheap reaction conditions, no need for the preparation of fresh reagents and a one-pot reaction. However, the disadvantages are purification and difficult work-up. These may be due to poor lithiation selectivity generating numerous by-products, but this disadvantage also occurs with the previous routes.

Overall, the most common factor is the lithiation chemistries, while the biggest difference lies with the type and use of the sulfur reagent. Interestingly, the approaches to date involve the thiophene as a nucleophile and the sulfur reagent as an electrophile. It is possible to reverse these affinities such that the sulfur is a nucleophile and the thiophene is an electrophile. This novel approach is developed in section 5.2.4.2 and avoids the use of cryogenic temperatures and lithiated reagents.

5.2.4.2 Method Development for DTT

Considering the four literature routes to the DTT core molecular fragment, there is significant scope for method development, using relatively low-cost and commercially available reagents which are stable under ambient conditions. Initial attempts aimed at generating a novel multistep route to DTT *via* a divergent approach as illustrated in Scheme 39; the key step is a double sulfide insertion with subsequent cyclisation.

Previous thioether and fused thiophene products synthesised through homo- or cross-coupling which use the copper/sulfide system were focused on substrates with iodine substituents[254], which are normally favoured due to their higher reactivity than bromine. However, this chemistry is developed using bromine substituents due to their relatively cheaper cost and commercial availability. Motivation for this investigation was further realised from a comprehensive review of DTT synthesis[255], where up until now, the thiophene substrate has been used as a nucleophile through dilithiation and the sulfur inserted as an electrophile. Upon inversing the chemistry[256–260], such that the bithiophene substrate becomes the electrophile and the sulfur becomes the nucleophile, an alternative method to DTT can be considered. The present procedure also avoids the use of lithiation and sulfur tosyl/anhydrides for the ring-closing step, in comparison to other routes.

Starting with tetrabromothiophene **112**, a double regioselective Sonogashira reaction successfully gave the bis(2-trimethylsilylalkynyl-3-bromo)thiophene (**115**) in 87 % yield. The next step involved the addition of the nucleophilic reagent, sodium sulfide nonahydrate, in DMSO for 18 h at 180 °C; although this only gave DTT in trace amounts.
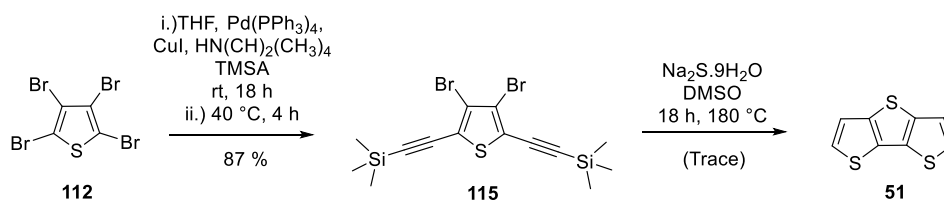
Scheme 39. Initial convergent approach with novel conditions for the synthesis of DTT, involving a double sulfide insertion and cyclisation.

The method was adapted to a convergent approach, which involves a single insertion of a sulfur atom and cyclisation to the 3,3-dibromo-2,2'-bithiophene substrate (**111**); the central thiophene is formed, fused in between the adjacent two thiophene rings, as illustrated in Scheme 40.

Table 26 shows the selected entries which led to the optimised conditions. Entry 1 shows the sulfur insertion with thiourea and cesium carbonate as base, but only giving trace amounts of DTT product after 20 h at 130 °C. Entry 2 specifies sodium sulfide nonahydrate and carbonate as the sulfur reagent and base respectively, while the solvent and catalyst was DMF and $C^{II}O$, again giving similar yields. Entries 3 and 4 combine different conditions from those of 1 and 2, but give no observable DTT in the absence of base. Increasing the reaction time and varying the ratio of the sulfur reagent
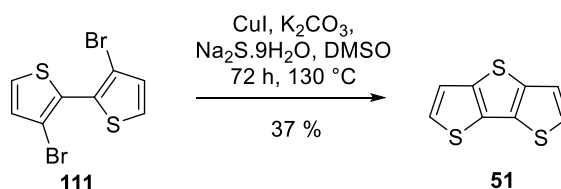
Scheme 40. Synthesis of unsubstituted DTT through a C-S coupling and ring closing 'one pot' step.

Table 26. Selected entries for the C-S ring closing conditions; a) microwave reaction, b) with 3,3'-diiodo-2.2'-bithiophene, *trace amounts.
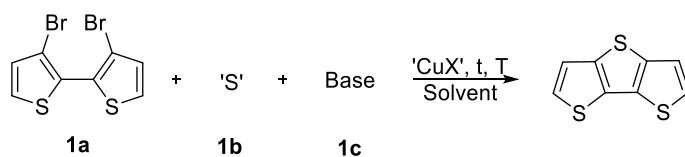
Entry	1a:1b:1c	'S'	Base	Solvent	CuX	t / h	T / °C	%
1	1:1.2[b]:2	thiourea	Cs_2CO_3	DMSO	CuI	20	130	t*
2	1:1.2:2	$Na_2S.H_2O$	K_2CO_3	DMF	$Cu^{II}O$	20	130	t*
3	1:1.2:0	$Na_2S.H_2O$	K_2CO_3	DMSO	CuI	24	130	0
4	1:3.6:0	$Na_2S.H_2O$	K_2CO_3	DMSO	CuI	24	130	0
5	1:1.2:2	$Na_2S.H_2O$	K_2CO_3	DMSO	CuI	65	130	15
6	1:3.6:2	$Na_2S.H_2O$	K_2CO_3	DMSO	CuI	72	130	23
7	1:3.6:4	$Na_2S.H_2O$	K_2CO_3	DMSO	CuI	24	130	33
8	1:3.6:4	$Na_2S.H_2O$	K_2CO_3	DMSO	CuI	48	130	39
9	1:3.6:4	$Na_2S.H_2O$	K_2CO_3	DMSO	CuI	72	130	42
10	1:3.6:4	$Na_2S.H_2O$	K_2CO_3	Diglyme	CuI	72	130	0
11	1:3.6:4	$Na_2S.H_2O$	K_2CO_3	Toluene	CuI	72	130	t*
12	1:3.6:4	$Na_2S.H_2O$	K_2CO_3	DMF	CuI	72	130	20
13	1:3.6:4	$Na_2S.H_2O$	K_2CO_3	DMAc	CuI	72	130	41
14	1:3.6:4	$Na_2S.H_2O$	K_2CO_3	DMSO/ H_2O (1:1)	CuI	72	130	0
15	1:3.6:4	$Na_2S.H_2O$	K_2CO_3	DMSO	CuI	72	60	0
16	1:3.6:4	$Na_2S.H_2O$	K_2CO_3	DMSO	CuI	72	90	17
17	1:3.6:4	$Na_2S.H_2O$	HK_2PO_4	DMSO	CuI	72	130	24
18	1:3.6:4	$Na_2S.H_2O$	KOH	DMSO	CuI	72	130	28
19	1:3.6:4	$Na_2S.H_2O$	Net_3	DMSO	CuI	72	130	31
20	1:3.6:4	$Na_2S.H_2O$	KOAc	DMSO	CuI	72	130	27
21	1:3.6:4	$Na_2S.H_2O$	Cs_2CO_3	DMSO	CuI	72	130	0
22[a]	1:1.2:2	Na_2S	K_2CO_3	DMSO	CuI	3	130	96
23[a,b]	1[i]:3.6:4	Na_2S	K_2CO_3	DMSO	CuI	3	130	97

and base to the bithiophene substrate, gave noticeable product in 15-42 % yields between 20 and 72 h (Entries 5-9).

Lower boiling point solvents were briefly screened to determine if polarity has a significant effect. A small selection of solvents with different polaroty (determined by dielectric constant) such as diglyme, toluene, DMF, DMAc and water mixtures were investigated (Entries 10-14); only DMF and DMAc gave product formation but in low yields.

Lower temperatures such as 60 °C and 90 °C were investigated but gave no observable target product and only oligomeric mixtures observed from the oil-like products (Entries 15 and 16). Next, the effect of base was probed, where bases such as hydrogen dipotassium phosphate and potassium hydroxide gave lower yields (Entries 17 and 18), while triethylamine and potassium acetate gave 31 % and 27 % yields respectively and caesium carbonate afforded zero yield (entries 18, 19 and 20). Lower equivalents and a significantly reduced reaction time was observed with microwave synthesis (entry 21), affording near quantitative yields of the target DTT (96 %); the iodo substituent gave similar yields (97 %).

The successful formation of DTT after purification for each condition was inferred from ^{1}H-NMR, with a typical spectrum shown in Figure 52. Two doublet signals are observed, one for a proton at the 2 position (a) (7.32 ppm) and the other at the 3 position (b) (7.39 ppm). The structure of DTT was confirmed from its single-crystal x-ray structure obtained with the microwave conditions, as illustrated in Figure 53. DTT was found to have close (< 4 Å) intermolecular separations, which is ideal for the core component in organic semiconductors.
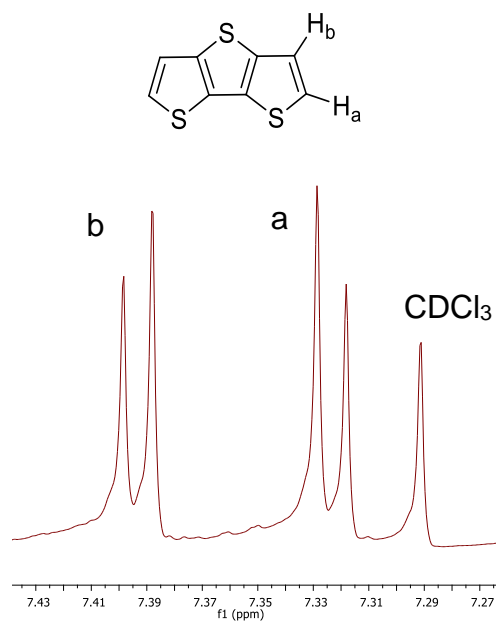
Figure 52. ^{1}H-NMR Spectrum of DTT (**51**).
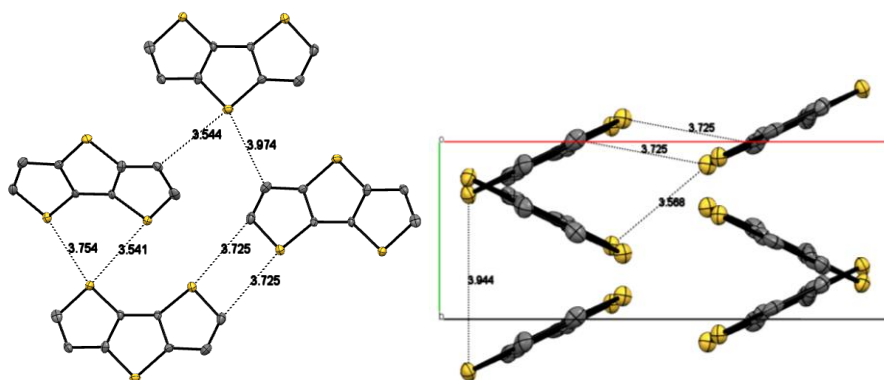
Figure 53. Single crystal x-ray structure of DTT, showing the close intermolecular distances between adjacent DTT molecules.

Scheme 41 shows a plausible mechanism for the sulfide insertion into the 3,3'-dibromo-2,2'-bithiophene substrate. Copper is coordinated to one of the thiophene-bromine bonds and thus makes nucleophilic attack more likely at the 3 position. Although minimised by the anhydrous solvents, the addition of sulfide must generate a thiol in the presence of the hydrate adducts and thus the requirement of a base. The mechanism is plausible but needs further investigations considering (1) the effect of absolute anhydrous conditions; (2) fine tuning the conditions to understand the cause of the side product formation and how this could be reduced to improve the yields for other solvents.
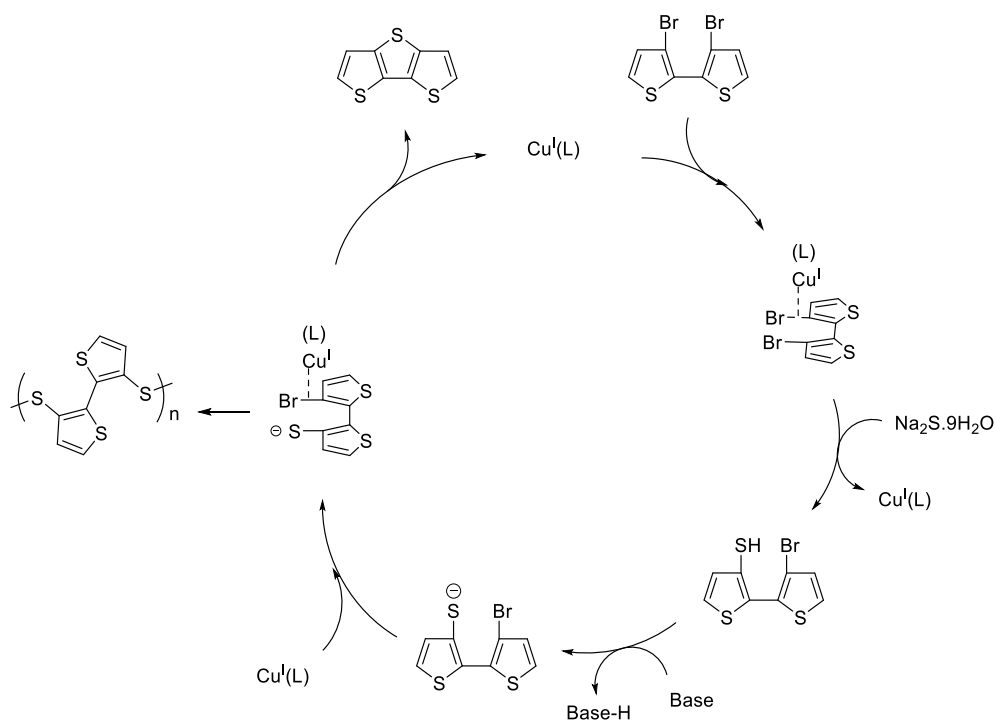
Scheme 41. A plausible mechanism for the formation of DTT with the novel sulfide insertion conditions; including a stage for potential side product generation (as homo-coupled polythiophene-thioethers).

5.2.4.4 Summary

In summary, a one-pot route was developed for the synthesis of DTT using relatively mild conditions and stable starting reagents, which were selected for their commercial availability and relatively low-cost. The conditions developed are absent of lithiation chemistry and cryogenic temperatures and thus have a greater potential for scaling up. The reactions times are significantly reduced, to under 1 h, which is an advantage for high throughput production.

5.2.5 Forward Synthesis

5.2.5.1 Target 44

The synthetic strategy devised in section 5.2.2 for target **44** is investigated here, with the focus on the synthesis of the final target from the core and synthon molecular fragments. Scheme 42 shows the retrosynthetically-designed forward route towards **44**, starting with a regioselective lithiation of the DTT core (**54**) and subsequent reaction with the derivatised thiophene synthon **64** giving the condensate intermediate (**116**). The hydroxy groups are reductively removed then the 3,3'-bromine substituents on **117** are exchanged for an aldehyde functionality (**118**) and the subsequent acid-catalysed (Amberlyst-15) cycloisomerisation gives the target molecule **44**.
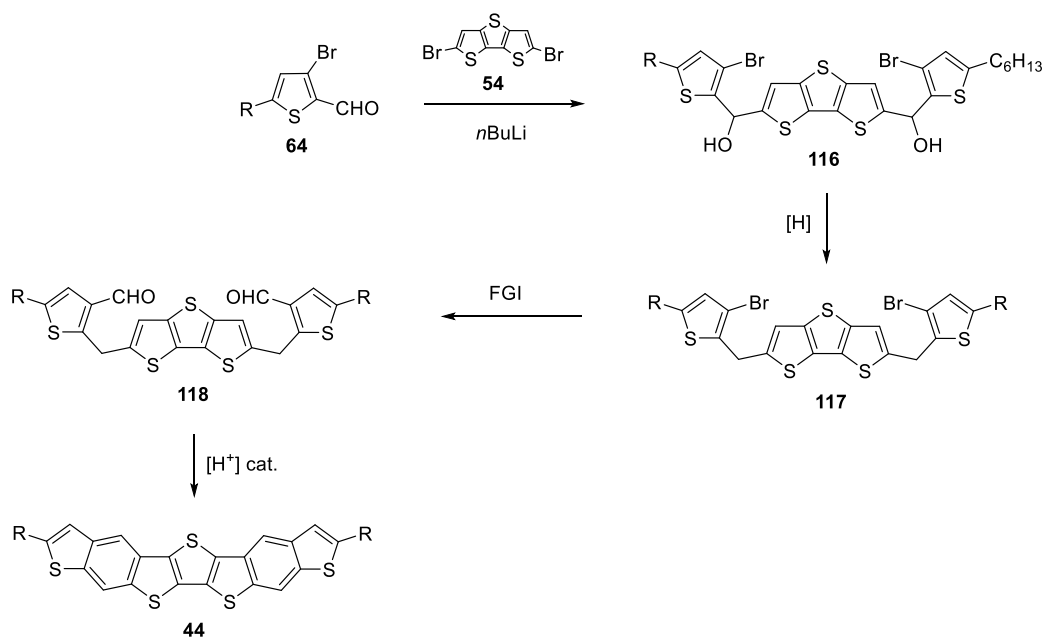
Scheme 42. Retrosynthetically-designed forward synthesis of **44**, starting with the molecular fragments that were identified from the synthetic strategy; R = C$_6$H$_{13}$.

5.2.5.1.1 Synthon Molecular Fragment

The two synthons outlined in Section 5.2.3 (Figure 44) were synthetically investigated. Compound **81** was first probed due to the difficulty of positioning the aldehyde and bromine groups at the 3- and 2-positions respectively. Scheme 43 shows a potential route to **81** *via* a lower oxidation approach of a primary alcohol. The first step is dibromination of thiophene-3-methanol (**119**) giving 2,5-dibromothiophene-3-methanol (**120**). Once this initial intermediate is formed, substitution at the 5 position gives **121** *via* a selective Sonogashira coupling and subsequent oxidation could afford **81**.
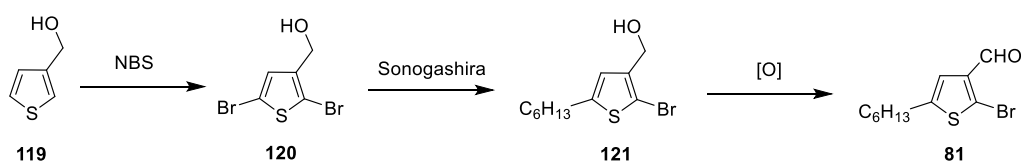
Scheme 43. A potential route to **48** *via* a lower oxidation state.

Initial efforts were successful with the addition of NBS to **119** in THF after 16 h at room temperature (Scheme 44) which gave the dibromo product (**120**) in 57 % yield.
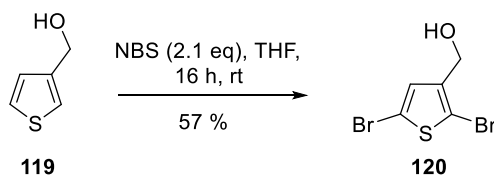
Scheme 44. Synthesis of 2,5-dibromothiophene methanol (**50**).

An attempt to synthesise **121** was made *via* a Sonogashira cross-coupling reaction between **120** and trimethylsilylacetylene (Scheme 45), however this was not successful; only multiple unidentifiable impurities were observed. This may be due to poor regioselectivity of the five position of the thiophene ring. An alternative approach is to perform the HD reaction with 2-bromo-5-hexylthiophene and quench with water, giving 3-bromo-5-hexylthiophene. However, the lithiation-bromine exchange would
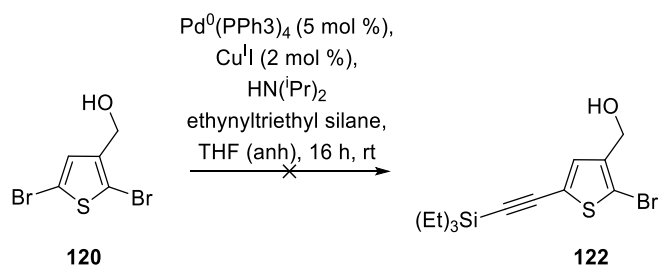
Scheme 45. Unsuccessful regioselective Sonogashira reaction of 2,5-dibromothiophene-3-methanol (**120**).

be out-competed by the available proton at the 2-position. Thus, the synthon **64** with the substituents in the opposite positions was investigated.

The synthesis of the formyl functionality at the 2 position (**123**) with bromine at the 3-position of a thiophene is easily afforded through regioselective lithiation of 2,3-dibromthiophene (**110**) giving the desired product (Scheme 46). This is because the bromine substituent at the 2-position is more reactive towards 1 equivalent of *n*-butyl lithium than the 3-position; another option is to use LDA with 3-bromothiophene.
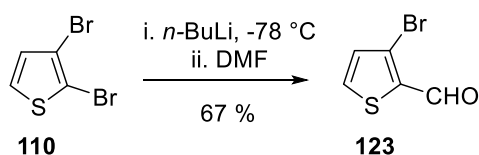
Scheme 46. Synthesis of 2-formyl-3-bromothiophene (**123**).

The overall issue with Scheme 46, is that **123** does not have a solubilising alkyl chain and thus the synthesis needs to be carefully reconsidered from the synthetic strategy section 5.2.2. This was deployed and illustrated in (Scheme 47), which shows the pathways followed to synthesise the thiophene synthons.

These structures were challenging because of their asymmetric nature with three different functional groups, resulting in a careful consideration of the design of the reaction route. The efforts for the synthesis of the synthon **64** were initially focused on the preparation of 3-bromo-5-hexylthiophene[55] (**76**) which was successfully formed in 73 % yield, from the isomerisation of

bromine from the 2 to the 3-position *via* a halogen-dance reaction (HDR)[220] (Scheme 47); the HDR is vital for the synthesis of the synthon, such that the kinetics and thermodynamics of the reaction mechanism was investigated in Chapter 5.2.3. Proton abstraction at the 2-position of **76** and quenching with a carbonyl transfer agent such as 1-formylpiperidine[51] afforded **64** in 55 % yield and 37 % total yield. One possibility for the low yield is a proton abstraction at the 4 position rather than the intended 2-position by the LDA; another reason could be a lithium-halogen exchange and quench at the 3-position. A second option is to consider the previous chemistry presented in Scheme 46 with 2,3-dibromothiophene (**110**) but undergo a HDR initially to give **125**, then alkylation affording **76** in two steps.

The key intermediate **76** is particularly useful as it can afford the asymmetric three-functional thiophene (**64**) with two of the groups, bromine and formyl, in the desired regiopositions. The advantages for the first option is a relatively low-cost starting material (**124**) and one high-yielding HDR; the disadvantage is four steps to the target synthon. The advantage for the second option starting with **110** is only three steps to **76**, however the disadvantages include a low-yielding HDR and the selective alkylation of a lithium-halogen exchange at the 2-position of **125** resulting in the removal of butylbromide *in situ*; this may lead to loss of product through a secondary HD reaction. Thus, the first route starting with thiophene appears to be the most desirable and robust towards **64**.
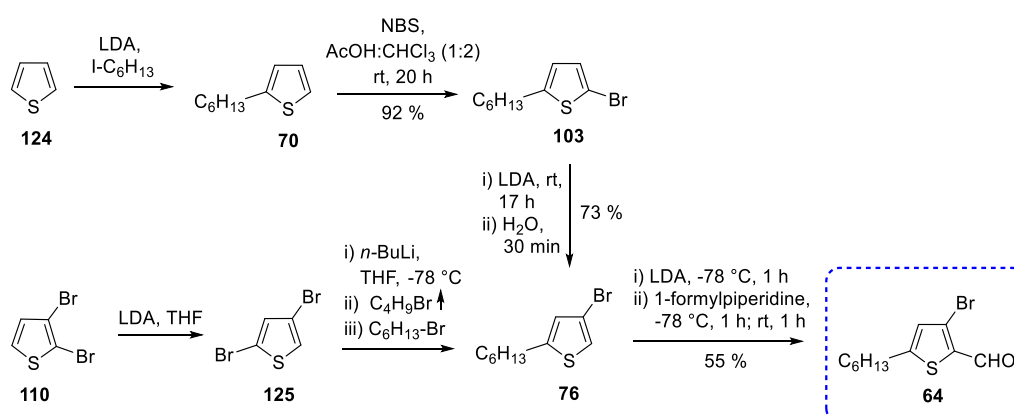
Scheme 47. An alternative strategy to the target thiophene synthon (**64**).

It was determined that the isolation of **76** was not needed, because **64** could be directly trapped from the active lithium salt (**107**) with an electrophile other than water. For example, quenching the HDR with 1-formylpiperidine gave **64** in 88 % yield and 81 % total yield. Although the literature presents examples of trapping lithium salts with different electrophiles after halogen dance reactions, there are only few examples of the direct formation of an aldehyde[56]. Nevertheless, the route illustrated in Scheme 48 shows the novel synthon can be formed in two steps starting from 2-*n*-hexylthiophene with significantly improved total yield.

The stacked proton spectra in Figure 54 show how the signals in the aromatic and aldehyde regions can be used to verify the product formation of **70**, **103** and **64**. The first spectrum shows three peaks, two are doublets (7.07 ppm, H_a; 6.76 ppm, H_c) and the third a multiplet (6.89 ppm, H_b). Upon bromination of the 2 position, the spectrum of **103** is simpler with two doublet signals (6.83 ppm, H_a; 6.52 H_b). Halogen dance and formylation gives **64** with two singlet signals as a thiophene proton (6.88ppm, H_a) and an aldehyde proton (9.90 ppm, H_d).
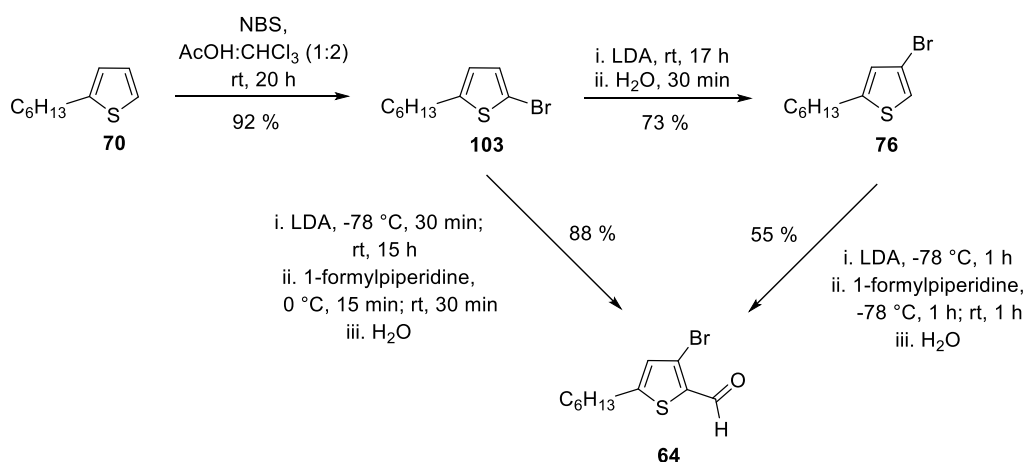
Scheme 48. Synthesis of the target synthon (**64**).
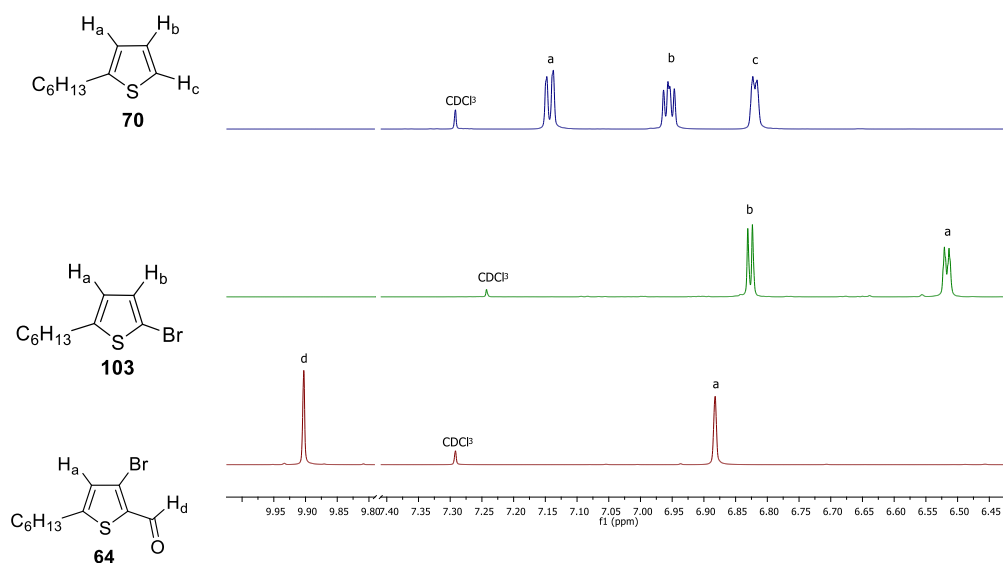
Figure 54. Stacked ^{1}H Spectra of **70**, **103** and **64** showing the aldehyde and thiophene protons only.

A clear indication of the formyl group in **64** can be seen with the infrared spectrum in Figure 55. A sharp peak for the aldehyde carbonyl group is observed at 1698 cm^{-1} and expected hydrogen bonding as a broad stretch between 3560 – 3080 cm^{-1}. Other signals are observed for single bonds to hydrogen (CH, alkyl) at 2927 cm^{-1}, aromatic double bonds (C=C) at 1439 cm^{-1} and a broad peak thought to consist of aromatic bromide (C-Br) and aromatic sulfide (C-S) stretches at 1037 cm^{-1}.
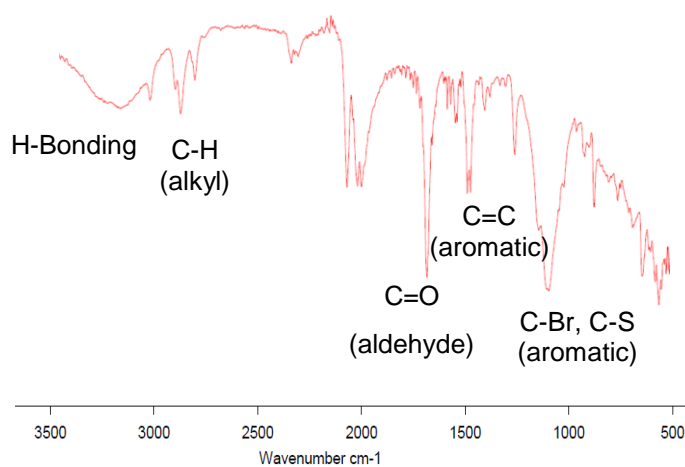
Figure 55. Infrared spectrum of neat **64** at 21 °C.

5.2.5.1.2 Core Molecular Fragment

The successful method development of DTT in Section 5.2.4.2 enabled its use in synthetic developments of the target isomer. However, the DTT fragment requires the additional step of double bromination, and production on the small scale due to microwave conditions; although the conditions developed are a huge improvement over the other routes with regards to time, reagent stability and lithiation chemistries involved. Therefore, the longer but large-scale route by Holmes *et al.*[252] (reproduced in Scheme 49) was deployed for the target **44** synthesis.
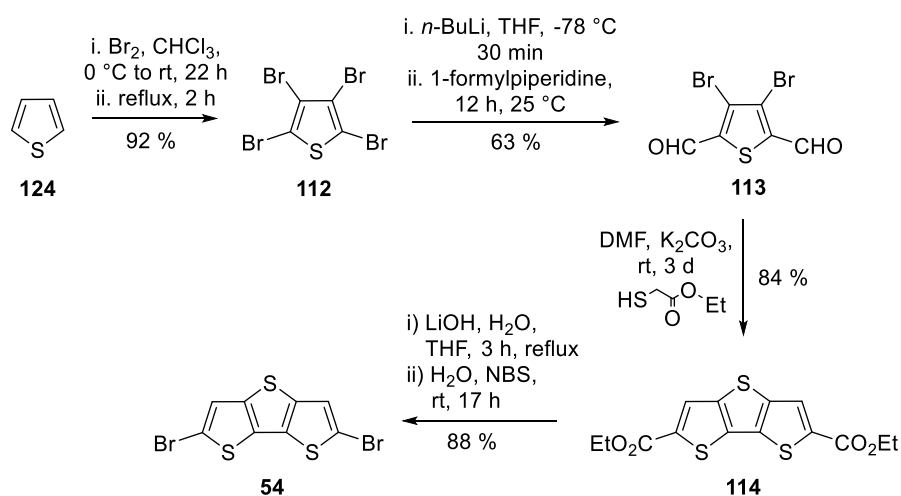
Scheme 49. Holmes route to DTT-Br$_2$ (**54**).

5.2.5.1.3 Condensate Intermediates

The synthesis of the target **44** was continued (Scheme 50) utilising the core **54** and synthon molecular fragments **64**, for the condensate (**116**) to be investigated[41,69]. The carbanions from the dilithiation of DTT-Br$_2$ (**54**) *via* lithium-halogen exchange reacts with the aldehyde of the synthon forming hydroxy lithium salts; quenching with water gives **28**. This compound exists as an oily residue where solvent and excess synthon was observed to still be present which could not be removed under strong vacuum or with freeze-drying using liquid nitrogen. Purification with flash column chromatography using either silica or alumina resulted in product decomposition; even once the column was deacidified with base such as triethylamine. This could be explained from the oxy groups of the silica promoting dehydration of the product leading to unstable cations. Indeed, the procedure[41,69] for the synthesis of similar analogues do not purify this type of intermediate, but instead use the crude directly in the next reaction, whereby the yield is stated over both the reaction steps. Surprisingly, **116** was unable to be purified over alumina, only yielding significant breakdown of product. Although there is no certain explanation, one reason may be the strong electrostatic interactions or coordination between the hydroxyl groups of the intermediate and the aluminium metal centres thereby polarising the C-O bond and thus activating that particular carbon site (11) enabling reactivity.

Intermediate **116** was confirmed from the inspection of the crude ^{1}H (Figure 56) and ^{13}C{^{1}H} NMR (Figure 57) spectra. First, the proton spectrum clearly shows three singlet peaks for the aromatic protons a (7.00 ppm) b (6.14 ppm) and c (6.48 ppm). Apart from residual solvent such as dichloromethane (DCM), diethyl ether (†) and water signals, there are only two unidentified peaks designated with * possibly arising from impurities; no signals are observed for the labile OH protons.
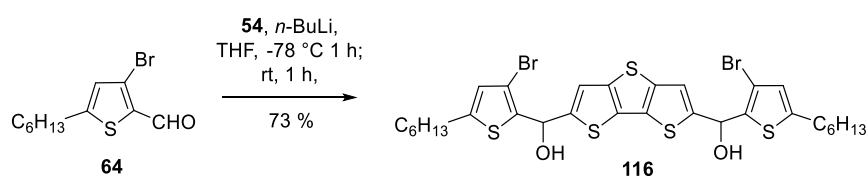
Scheme 50. Synthesis of the condensate intermediate **116**.
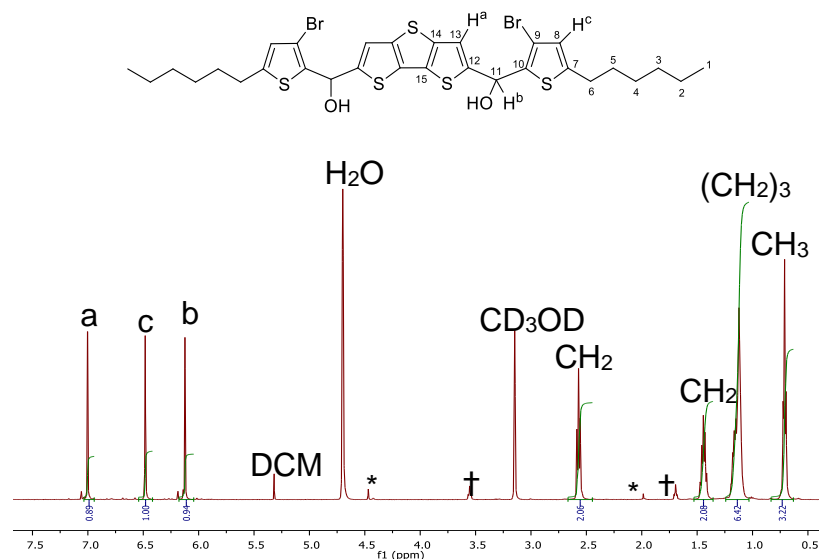
Figure 56. Crude ^{1}H spectrum of **116**, in deuterated methanol.

The ^{13}C{^{1}H} spectrum (Figure 57) of **116** shows signals in the alkyl region (0-50 ppm) for the hexyl chain with carbon atoms 1-6, a signal for the methoxy carbon 11 at 68.9 ppm, and signals for the thiophene and DTT segments between 107-150 ppm with carbons 7,8-15. The signals for 8 and 13 were easily assigned from inspection of the HMQC spectrum (Figure 58), while 9 is characteristic for thiophene bromides; the remaining signals were assigned from comparison of starting materials.
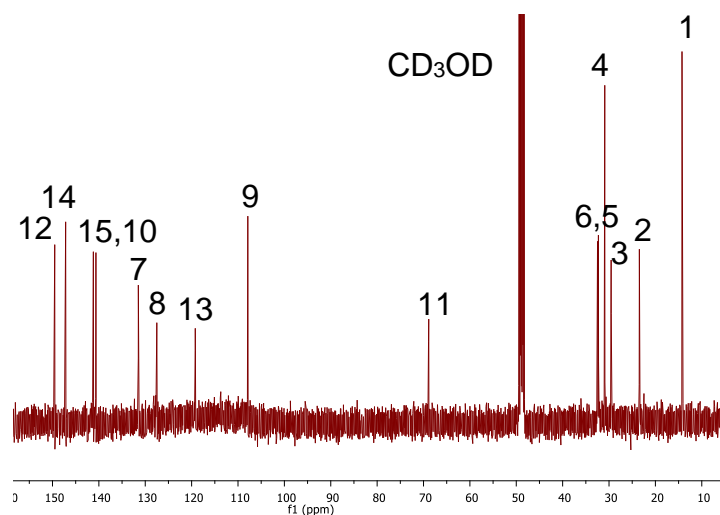
Figure 57. ^{13}C{^{1}H} NMR spectrum of condensate (**116**), in deuterated deuterated methanol.
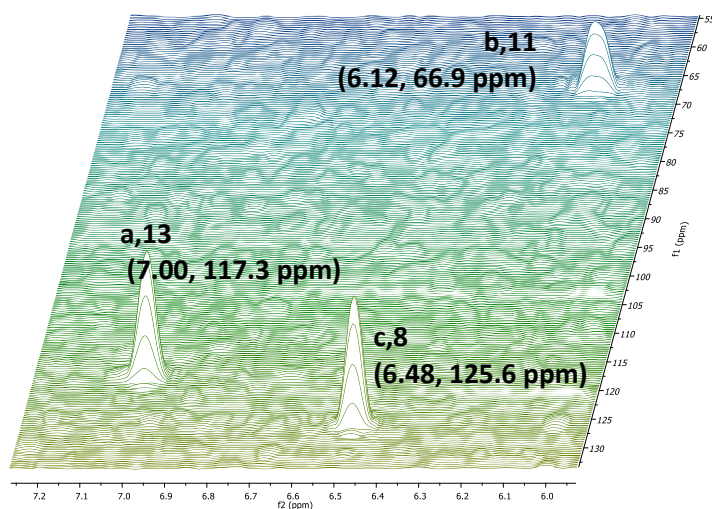
Figure 58. White-wash stacked HMQC spectrum of condensate **116**, showing the aromatic and methine protons only, in deuterated chloroform.

Interestingly, the expected m/z signal for **116** of 745.9686 was observed only between 250-320 °C with a low error of 14.5 ppm (a) as illustrated in Figure 59. The most intense peak with m/z at 748 ppm is considered to be the condensate (M+H) and other lower m/z signals were observed, most probably for a mono (730) and double dehydration (712) in a step-wise formation, with extended conjugation in the dehydrate to satisfy valency; these possible structures are shown in Figure 60.
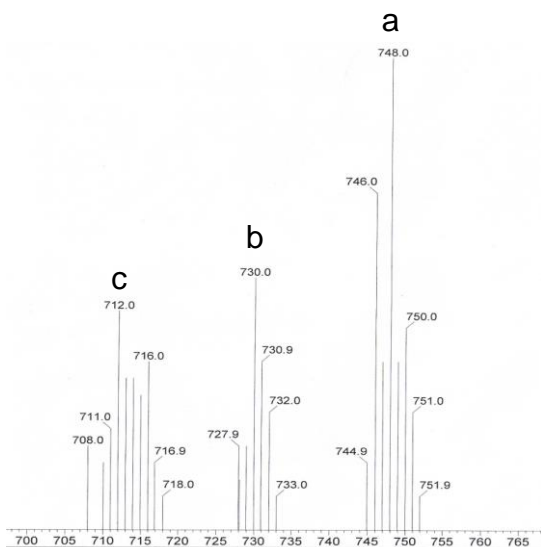
Figure 59. Time of Flight Positive Electron Impact Mass Spectrum (TOF MS EI+) of a) the condensate (**116**), b) monohydrate cation and c) dehydrate cation**.**
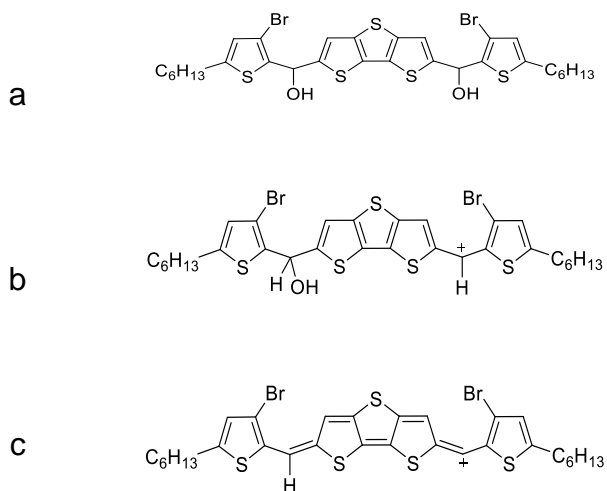
Figure 60. Illustration of possible structures from the MS data.

As a result of the instability, crude **116** was used in the next step without purification. The reduced intermediate (**117**) was synthesised (Scheme 51) from a relatively weak reducing agent, sodium cyanoborohydride. **117** was clearly identified from the signal at 4.32 ppm in the ^{1}H spectrum corresponding to the methylene groups (Figure 61).
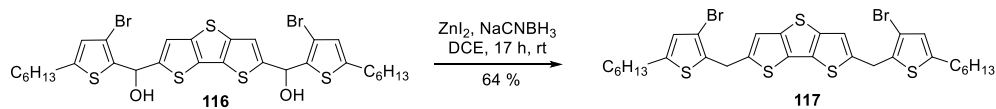
Scheme 51. Synthesis of the reduced intermediate (**117**).
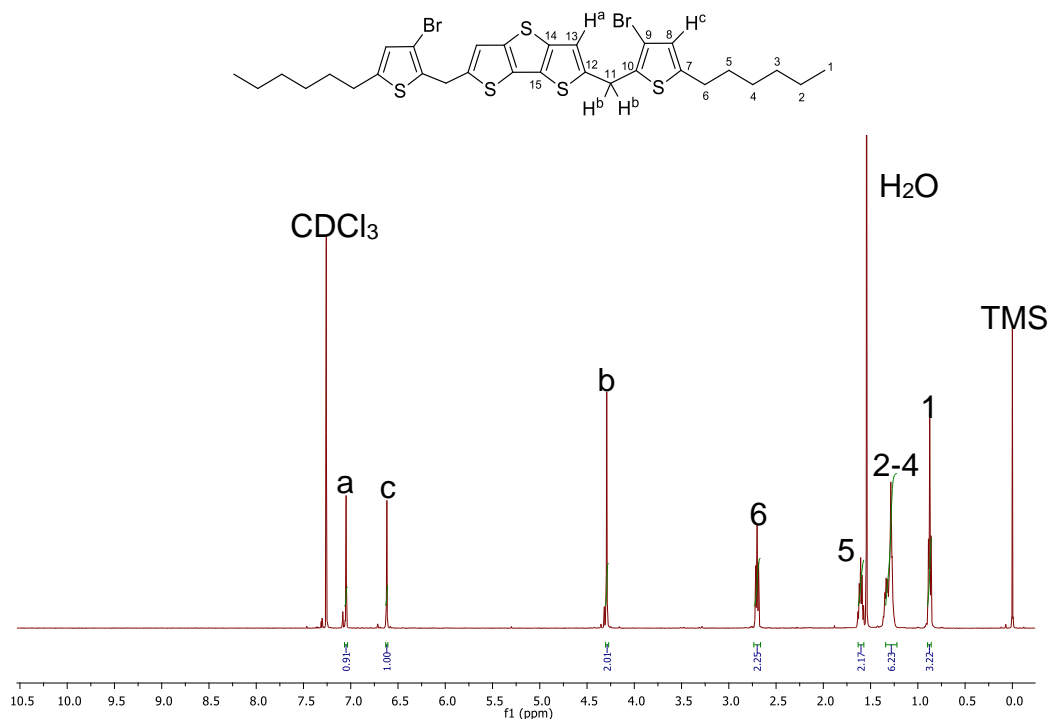
Figure 61. ^{1}H-NMR spectrum of the condensate (**117**), showing aromatic and methylene protons only, in deuterated chloroform.

The product was confirmed with ^{13}C{^{1}H} NMR, HMQC spectra and mass-spectrometry. Furthermore, the ^{13}C DEPT 135 spectra clearly shows the CH signal for the condensate and the disappearance of the CH$_2$ signal for the dehydrate, as illustrated in Figure 62. The signal arising from carbon 11 on **116** at 69.1 ppm not only has a significant chemical shift from the C-O ether/hydroxy region to 30.7 ppm in the C-C alkyl-aromatic region on **117**, but also changes phase indicating the addition of a proton to that carbon centre.
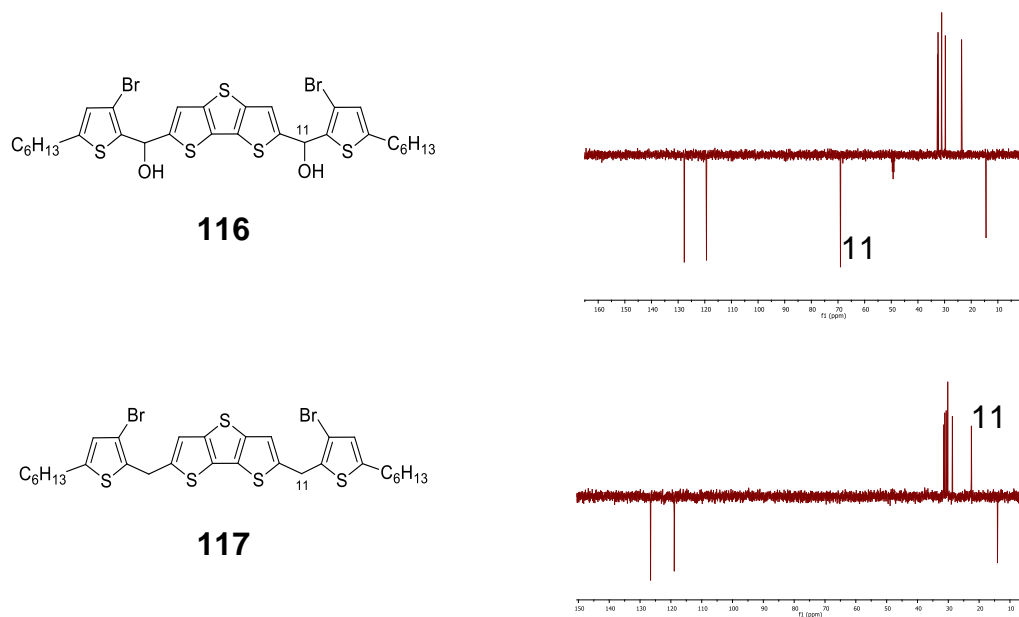
Figure 62. ^{13}C DEPT 135 spectra of condensate (**116**) and dehydrate (**117**), in deuterated chloroform.

The next step involved the conversion of the bromine substituent to the aldehyde functional group, as illustrated in Scheme 52. The first condition attempted (Method A), involved a lithium-halogen exchange and quench with 1-formylpiperidine. This was unsuccessful and no identifiable products were isolated. Observations include (1) the immediate change in colour of the reaction mixture from colourless/pale yellow to pink and then to dark purple, upon the addition of the *n*-butyl lithium; (2) the subsequent colour change from purple to green upon quenching with 1-formylpiperidine. These observations are not consistent with lithium-halogen exchanges[220] which are not immediate and do not normally result in bright colours. One possibility could be a lithium-proton exchange with one of the methylene protons, generating the pink and purple colours, followed by quenching with the 1-formylpiperidine, as illustrated in Scheme 53. The reactivity of the methylene protons could not have been easily predicted. Moreover, the potential products produced during the reaction could include oligomer/polymer structures, due to impartial quenching and self-condensation. It is unlikely that this would occur of double lithiation occurred at the 3-position of thiophene, as thiophene does not lend itself to bimolecular nuclear substitution.
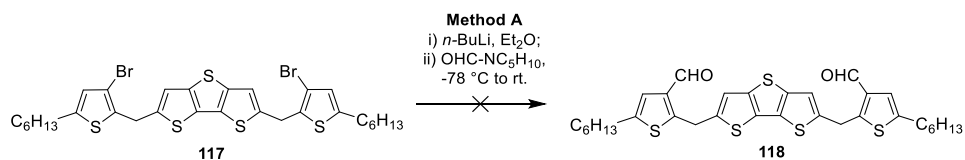
Scheme 52. Synthesis of the final intermediate **118** towards the target **44** *via* method A.
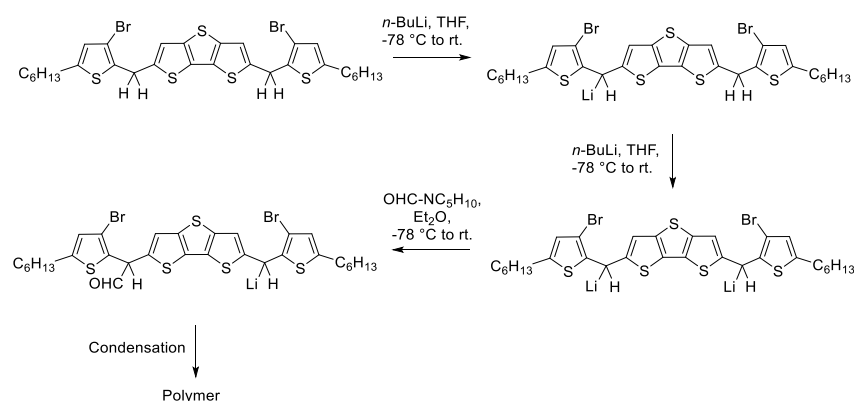
Scheme 53. Possible methylene lithiation reaction and self-condensation.

Method B (Scheme 54) consisted of a palladium-catalysed carbonylation. This involved the oxidative insertion of carbon monoxide from a carbonyl-transfer agent (*e.g.* DMF) and the reductive elimination of the final intermediate. Unfortunately, only the debrominated species was isolated, suggesting that the double palladium insertion occurred, even though the carbon monoxide could not be inserted. Several experiments were run with varied equivalents of the N-formyl saccharide, the reaction time and the reaction temperature; all of which gave the same debrominated product. These observations show that metal insertion at the C-Br sites are viable and could be suitable towards Grignard chemistry in future investigations.
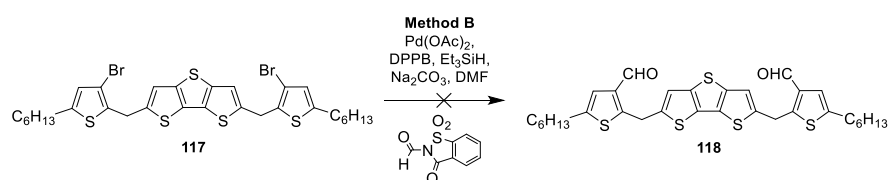
Scheme 54. Synthesis of the final intermediate **118** towards the target **44** *via* method B.

5.2.5.1.4 Summary

The synthon, core and intermediates were fully characterised for both isolated and crude compounds. The route to the synthon was developed and simplified through the use of a HDR. The retrosynthetically-designed forward synthesis was successful until the penultimate step, where the dehydrate intermediate could not undergo a functional group interconversion between bromine and an aldehyde substituent. Unforeseen stability issues arose with the condensate intermediate, which was used as a crude in the next step to generate the dehydrate. The double lithiation of the penultimate step and may be due to the reactivity of the methylene protons.

An alternative condition using palladium-catalysed carbonylation resulted in the debromination of the dehydrate intermediate but no carbonyl insertion. This suggests (1) there is reactivity at the C-Br sites towards transition metal catalysis and (2) double metal insertion is synthetically viable, thus prompting the possibility of Grignard chemistry in future investigations. One alternative route, a slight variant of the designed route, also has potential for the synthesis of the target in future work. The majority of issues are considered to arise from the high stability and aromaticity of the DTT core, which were unforeseen but may be overcome. Overall, the synthesis of **44** is ongoing but shows promise, with different chemistries, to form the novel fused-ring heteroacene in only five steps.

5.2.5.2 Target 45

The total forward synthesis for **45,** based on the A3 retrosynthetic strategy, is illustrated in Scheme 55, following the hybrid approach. The borylated synthon (**126**) is readily achieved from hexyl thiophene and the dibromo-DTT (**54**) core unit from literature preparations. These are combined and the subsequent intermediates (**93**[261], **91**, and **89**) undergo an FGI, Sonogashira then a metal- or base-catalysed cycloisomerisation respectively, giving the target **45**. The inclusion of solubilising units, such as alkanes, ensure high solubility of both the final target and the intermediates throughout both the synthesis and characterisation. The greatest challenges in this proposed total synthesis are the regioselective double bromination (FGI) of **93** and the cycloisomerisation of **89**, which may need optimising. Finally, Scheme 55 shows a relatively simple forward route that was retrosynthetically designed to give the target in moderate to high yields and few synthetic steps.
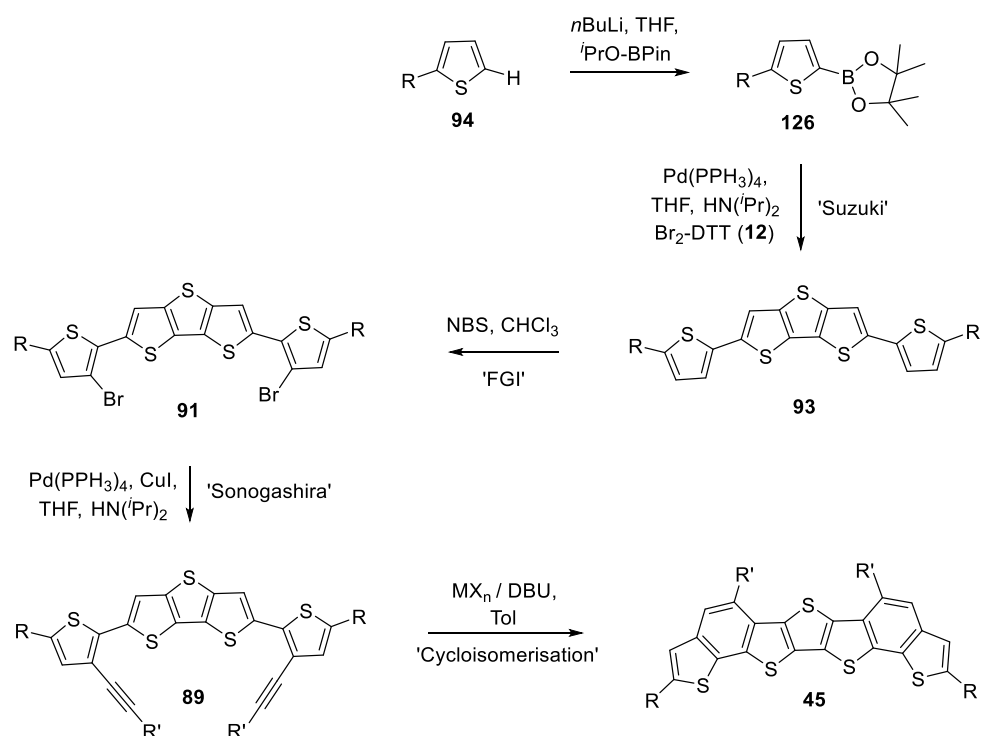
Scheme 55. Synthesis of **45**; R = C_6H_{13}, R' = H or C_4H_{13}, M = Ir, Pt, Au, X = Cl.

5.2.5.2.1 Synthon Molecular Fragment

Scheme 56 shows the synthesis of the thiophene synthon molecular fragment **127** towards the target **45** through a simple and facile route, as devised in the synthetic strategy (section 5.2.4.1). The hexyl chain ensures solubility in the final target **44**, with added solubility imparted from the *n*-butyl chain in the ethynyl unit of **127**. A monobromination of *n*-hexylthiophene (**70**) gives 2-bromo-5-hexylthiophene (**103**) in 82 % yield. Standard HDR of **103** to rearrange the bromine substituent to the 3-position gives **76** in 81 % yield as previously discussed. Subsequent Sonogashira with *n*-Hex-1-yne affords the target thiophene synthon (**127**) in 95 % yield.

The next stage involves the functionalisation of the synthon fragment with a C-C transfer group for coupling to **54**, such as with boron and tin. Scheme 57 shows the synthesis of the derivatised synthons through standard Stille coupling reaction[262] (Method A) and Suzuki[263] (Method B) towards 2-(tri-butylstannyl)-3-hexynyl-5-hexylthiophene (**128**) and 2-(Boropinacol)-3-hexynyl-5-hexylthiophene (**129**) respectively. Only the crude products were isolable, as both the borolated and stanylated synthons were unstable on silica and alumina during flash column chromatography purification. This could be due to the electron density being withdrawn into the alkyne bond making the functional group labile.
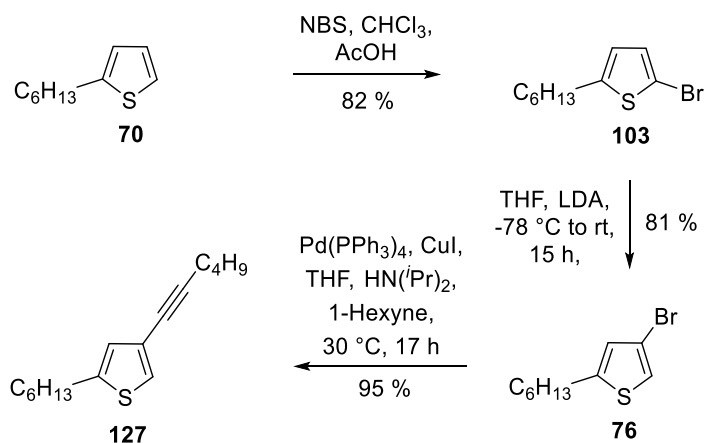
Scheme 56. Synthesis of the alkyne derivatised synthon **127**.
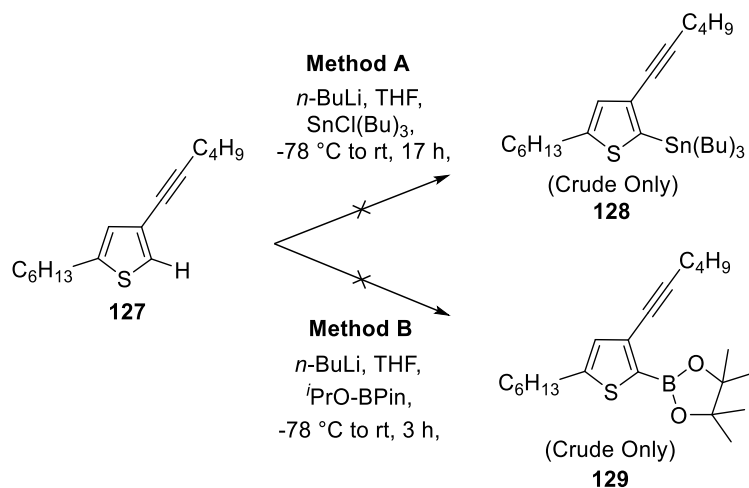
Scheme 57. Attempted synthesis to synthon molecular fragments derivatised with tin (**128**) and boron (**129**) coupling groups.

5.2.5.2.2 Core Molecular Fragment

The DTT-Br$_2$ (**54**) route by Holmes *et al.*[144] is suitable for the synthesis of the core molecular fragment of target **45**.

5.2.5.2.3 Condensate Intermediates

Unfortunately attempts to use the crude to synthesise intermediate **89** were unsuccessful (Scheme 58); any unreacted boryl or stannyl reagents could have interfered with the reaction.
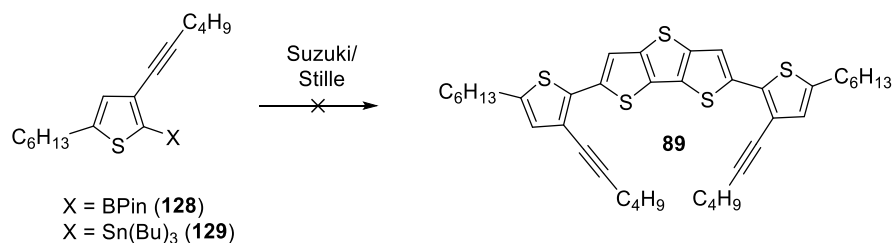
Scheme 58. Unsuccessful Suzuki and Sonogashira synthesis of the intermediate **89** *via* the crude synthons **128** (X = BPin) and **129** (Sn(Bu)₃).

Considering the instability of the functionalised synthons **128** and **129**, an alternative route was investigated (Scheme 59), which consisted of the borylation of a pre-brominated thiophene. 2-bromo-5-hexylthiophene underwent a HDR and the resulting lithium salt at the 2-position was quenched with isopropxy-boropinacol to give the functionalised fragment **130**. Although unsuccessful, the reason is most likely due to the lithiated thiophene being a poor nucleophile towards boroesters, as well as esters in general, owing to only the protonated product (**76**) being isolated.

The synthetic strategy was re-addressed and a regioselective double bromination route was adopted. The resulting synthon is the borylated thiophene **126**, synthesised from hexylthiophene in 74 % yield (Scheme 60). Suzuki coupling with **54** gave the linear all-thiophene intermediate **93**, isolated on alumina rather than silica due to its instability, in 69 % yield. The regioselective double bromination *via* sequential addition of two
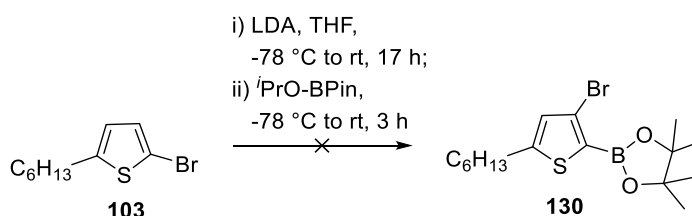
Scheme 59. Attempted synthesis of derivatised synthon **130**.

one-equivalent aliquots of NBS gave the substituted intermediate **91** in 47 % yield; found to be stable on silica and in air. Successful double Sonogashira to **91** with *n*-Hex-2-yne gave **89** in 81 % yield and found to be highly stable.

The final step is the C-H activated ring-closing cyclisation to give the target **45**. The first type of condition attempted was metal catalysed (Method A), using platinum[264] and iridium chlorides[265,266] in toluene at 80 °C. There was no consumption of **89** with various reaction times, nor the formation of **45** with either catalyst, suggesting alternative conditions are needed. Thus, base-catalysed cyclisation with DBU was attempted, as reported for similar fused-ring thiophene substrates[264,267]. Unfortunately, this was unsuccessful and resulted in de-ethynylation of intermediate **89** rather than ring-closure. These observations infer the C-H unit of DTT is extremely stable towards cyclisation, particularly with substituted thiophenes at the 2-positions.
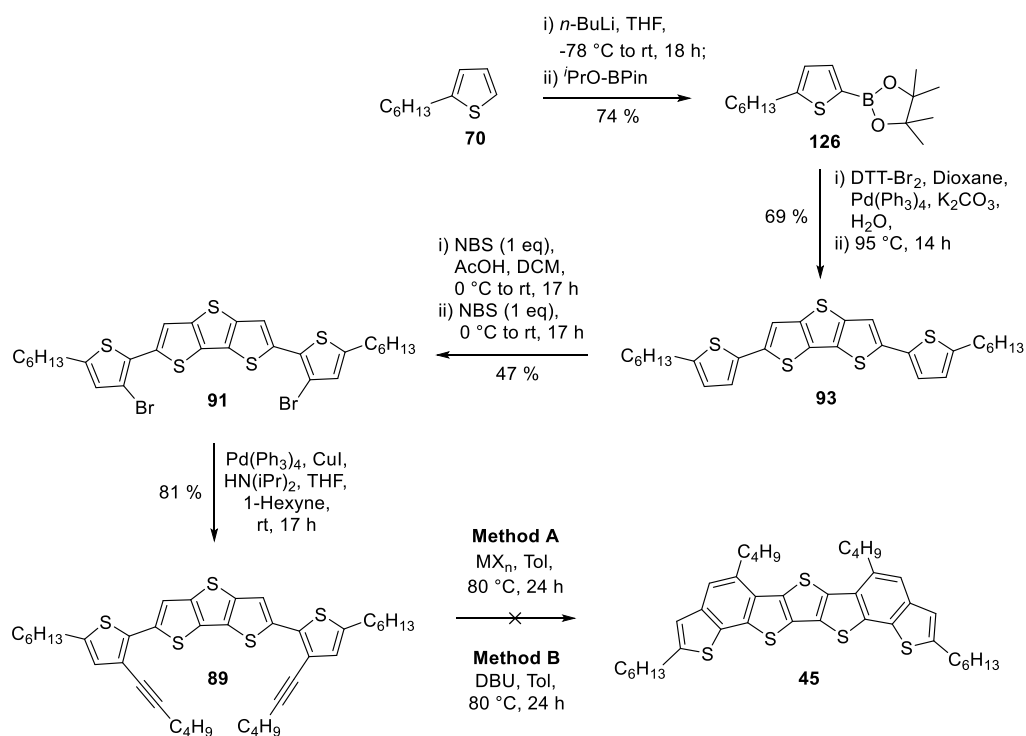
Scheme 60. Attempted synthesis of **45** from intermediate **89**, with two additional *n*-butyl solubilising chains on the phenyl ring *via* metal chlorides MX$_n$ (Pt and Ir) and organic base (DBU) catalysis.

5.2.5.2.4 Summary

The synthon molecular fragment to target **45** proved challenging, owing only to the functionalised group being highly unstable during purification; no desired intermediate was observed when the synthon was used as crude. However, a regioselective double-bromination followed by a double Sonogashira successfully gave the derivatised substrate as the final intermediate and found to be highly stable. This substrate proved too stable unfortunately, particularly with regards to the subsequent C-H activation and intramolecular cyclisation under two metal-catalysed and one base-catalysed conditions.

5.2.6 Alternative Routes

One option for future synthetic investigations of **44** is to utilise the Vilsmeier-Haack (VH) reaction, requiring a minor re-design of the overall forward synthetic route, to incorporate a simpler synthesis of the thiophene synthon. The VH conditions generates the carbonyl from DMF *in situ* as an electrophile, and activates the C-H of an aromatic ring for substitution. Such conditions have been reported for both the 2- and the 3-positions of a thiophene substrate[268], but there is still the possibility for the C-H methylene units to participate in the reaction.
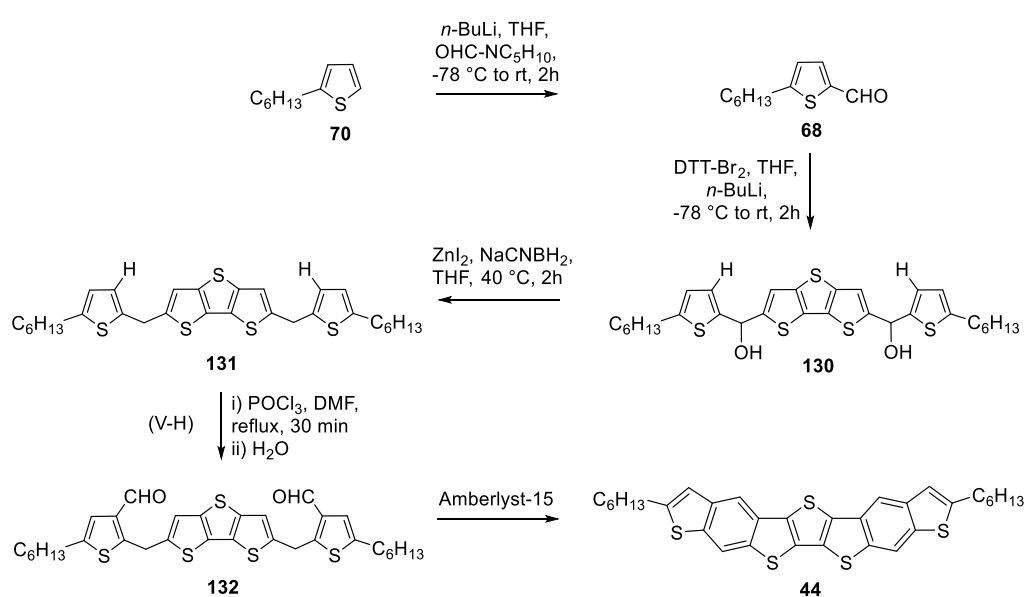
Scheme 61. Alternative route to target **44**, utilising the Vilsmeier-Haack reaction (V-H).

Conditions for the synthesis of **45** could be investigated with H and methyl-terminated alkynes in future work, accompanied by other catalyst such as gold chlorides[269] (Method C). Other options could include a double-bromination of the C-H units of DTT, with ring-closure by palladium catalysis (Method D) or ICl-induced cyclisation[270] with the removal of the resulting iodine substituents on **b** by lithiation and quench with water giving isomer **3** (Method E), as shown in Scheme 62.
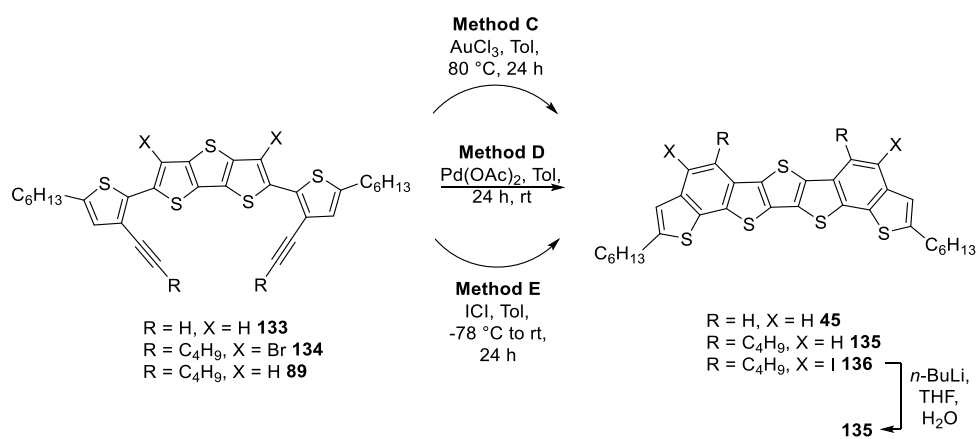
Scheme 62. Three potential conditions for the cyclisation of **89**-type derivatives and the final synthetic step of target **45**.
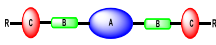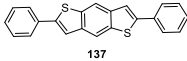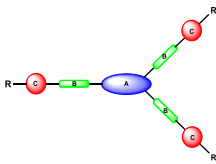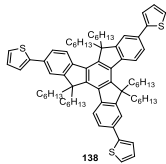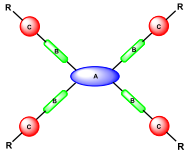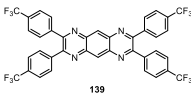
5.3 Design, Modelling and Synthesis of Oligo-Fused Heteroacenes

5.3.1 Design and Modelling

As outlined in the project plan (Chapter 3), a second type of structure was designed that has similarities with the fused-ring heteroacenes (Section 5.2) in terms of its small molecular nature and its constituent molecular fragments, but structural differences in terms of the way the fragments are bonded together. This structural variation was achieved by the incorporation of unsaturated 'oligomeric' bonds such as alkynes between the aromatic rings, *i.e.* spacer units which allow rotation and stretches. Not only does this permit a high degree of solubility in common organic solvents, due to the increased level of entropy, but also a simplification of the synthetic routes.

Through the combination of the core, synthon and spacer units, a great number of structural variations can be achieved. The diversity is further increased with the consideration of the number of reactive sites at the core and synthon units. Table 27 illustrates three generic molecular shapes, with selected examples from the literature. The entries increase in structural terms with the number of derivatives; designated by the motif as linear, trigonal and tetragonal. Interestingly, the linear motif gives rise to more than one type of molecular packing in the solid state of thin film, namely variations between slipped-stack and herringbone. The trigonal and tetragonal structures uniquely give discotic packing, which is columnar in nature. The molecular shapes can thus be broken down into molecular fragments, such as the core (A), spacer (B), and synthon (C) units. The identification and understanding of these unit combinations greatly enhances retrosynthetic strategies and forward synthetic investigations. The corresponding examples are found to have charge transfer, with that for the linear structure **137** having greater mobility[271] (0.044 cm^2 V^{-1} s^{-1}) than either the trigonal[272] (**138**, 0.001 cm^2 V^{-1} s^{-1}) or tetragonal[273] (**139**, 0.012 cm^2 V^{-1} s^{-1}).

Table 27. The motif, packing array and the general molecular shape of selected structures with their observed mobilities (μ_{TF} / cm^2 V^{-1} s^{-1}).

Motif	Packing	Shape	Example	μ_{TF}
Linear	Herringbone, Slipped Stack		137	0.044
Trigonal	Discotic		138	0.001
Tetragonal	Discotic		139	0.012

Moreover, the alkyne spacer unit has been realised as not just a structural component in the final targets, but also as an intrinsic functional group due to its propensity for conversion through transformations such as carboxylation[274], hydro-amination[275] and addition to electrophiles[276]. Electron-rich alkyne substrates enable the construction of drug scaffolds[277,278] normally unavailable from conventional synthetic approaches and a number of catalytic systems have been developed[279–282] to synthesise polycyclic heterocycles from alkynes as enhanced fluorescence probes. Single alkynes can furnish heterocycles such as triazoles[283,284], furans[285] and oxazoles[286] while two alkynes in close array can undergo domino reactions to afford poly-fused aromatics[287], thereby yielding complex products from simple building blocks.

A careful selection of the core, capping and fine-tuning units for alkyne molecular substrates[288] is critical for the improvement of physical properties. By structural and heteroatom variation of the derivative, the properties can be fine-tuned for a given application, or used to selectively control the reactivity of the alkyne bond towards further functionalisation. For example, the functionalised products presented in Figure 63 are structurally diverse but are all derived from the same rod-like substrate. The resulting donor-acceptor
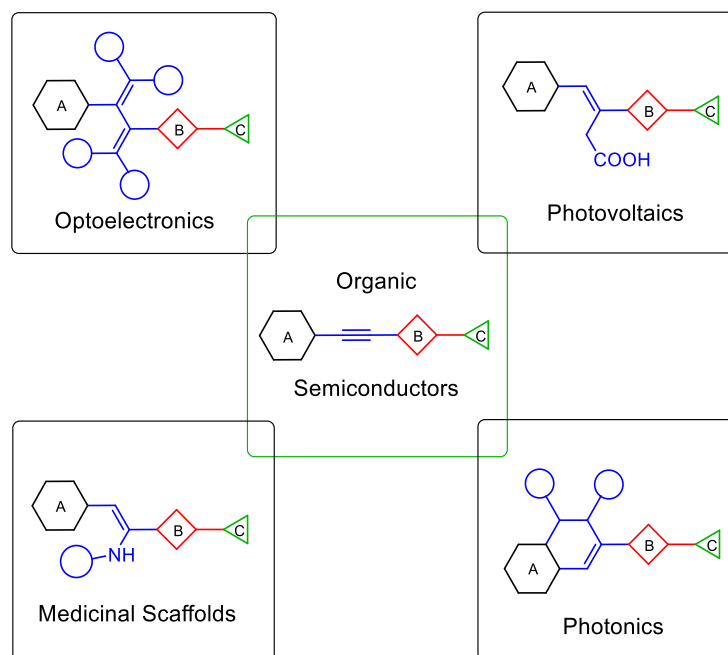
Figure 63. Modification and application of alkyne substrates; [A] core, [B] end-capping and [C] fine-tuning derivative units.

structures[276,289] with strongly-conjugated organic substituents, have a number of applications other than medicinal scaffolds and include optoelectronics, photovoltaics, and photonics; partly due to their electron-rich structures but also partly due to their structural diversity, facilitating both nonlinear[290] optical (NLO) phenomena and charge-transfer properties. Indeed, their rod-like alkyne substrates have a tendency to promote charge transfer and such intrinsic organic semiconductor behaviour is realised as molecular wires[291] and transistors in organic electronics.

Some leading examples of molecular rods are shown in Figure 64, which have thiophene as the central core unit sandwiched between two alkyne derivatives. These structures present the thiophene-based homologous series of diethynyl molecular rods. Naturally, the monothiophenyl molecular rods have been extensively explored in the literature, from alkyl[292] (**140**) and silyl[292] groups (**141**) through aromatic[292–294] (**143**), heteroatomic aromatic substituents such as pirydyl[295] (**142**), anisyl[296] (**144**) and methoxy[297] (**145**), to bulky aromatic pyrene[298] (**146**) units. Due to the challenging multi-step synthesis of the next fused-ring homologue, thienothiophene (TT), a limited number of structures are reported and include tertiary-butyl (**147**),

Label	Homologue	R
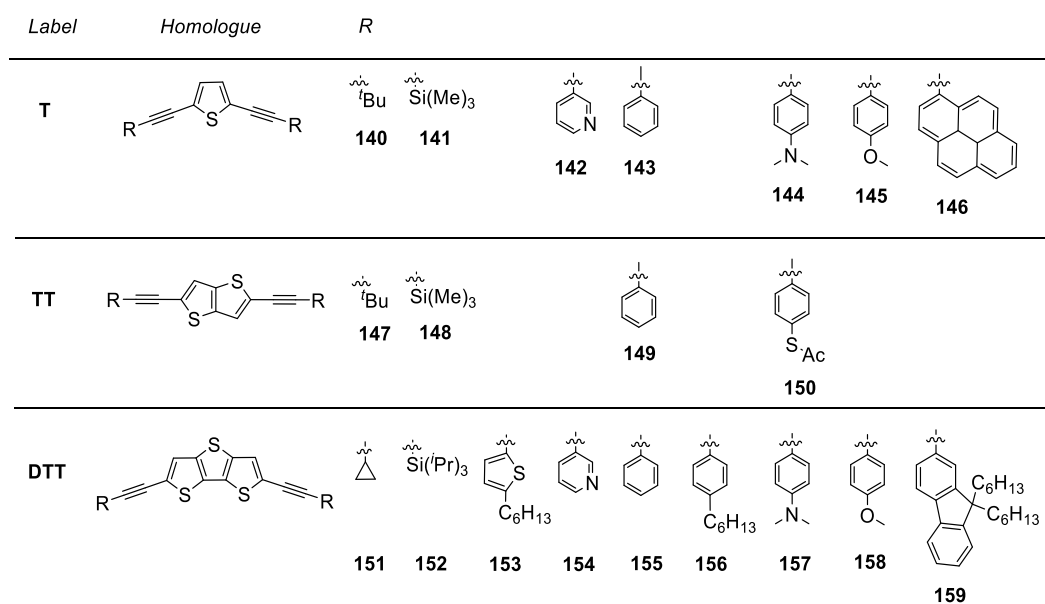
Figure 64. Leading examples of heterocyclic π-extended molecular rods with ethylene spacer units and fused-ring thiophenyl (T and TT) cores, and novel derivatives with the DTT core.

trimethylsilane[299] (**148**), phenyl[294] (**149**) and phenylthioacetate[300] (**150**). Following this trend, the next homologue in the series is dithienothiophene (DTT), which has yet to be fully explored in the literature and is the focus of the present study. To date, there are only a few reports on DTT alkyne derivatives[255,277,301,302] that present a thorough characterisation of a range of structurally diverse units. These include metalated alkynes such as iron[301], gold[299], platinum[303] and ferrocene[301], while DFT modeling[304] was reported for structures yet to be prepared in the literature, for applications such as molecular wires.

The DTT units are known to be highly stable[10] and impart closer intermolecular interactions in the solid state that facilitate greater physical properties for electronic device applications. Interestingly, there are no reports on heteroatoms (silicon, nitrogen, oxygen) located at the periphery of the DTT-alkyne moieties.

The FMO energy levels for the HOMO and LUMO states are presented in Figure 65 and include the work function of a gold electrode, one of the most commonly used[73,305–307] (-5.1 eV). The silyl **152** and pyridyl compounds **154** have the lowest HOMO levels at -5.68 and -5.69 eV respectively, whereas the methoxy derivative **158** has the highest (-4.49 eV). The smallest optical
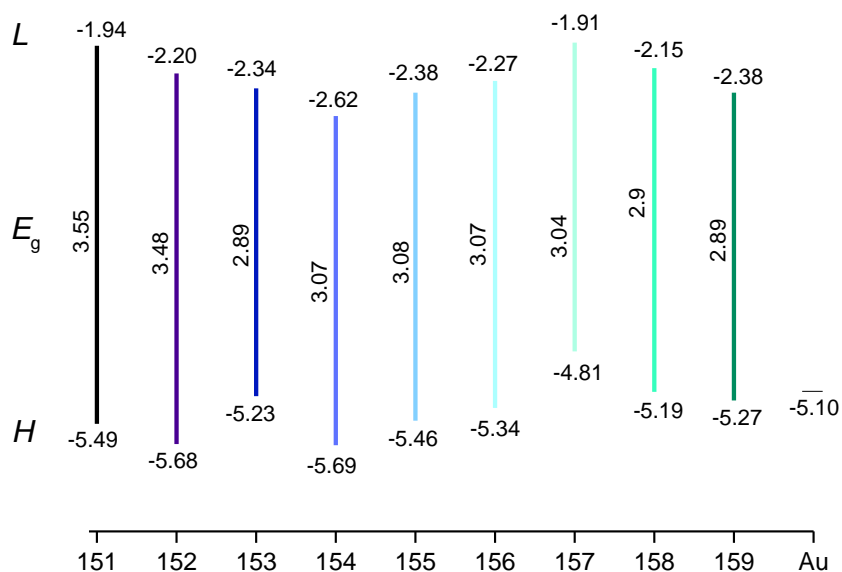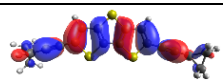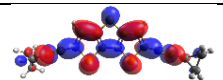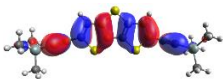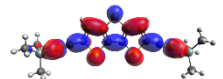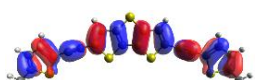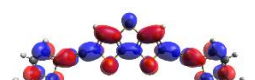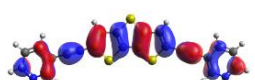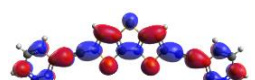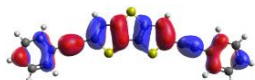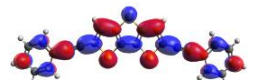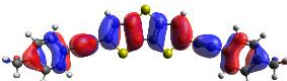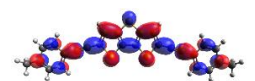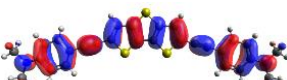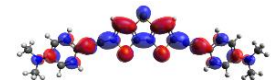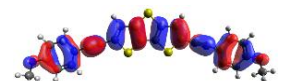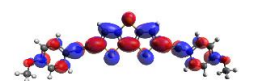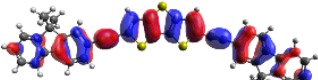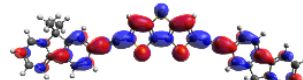
Figure 65. FMO plots (eV) of compounds 151-159 and the work function of a gold electrode.

energy gaps E_g are with **153** and **157** at 2.89 and 2.90 eV, while the largest is with the cyclopropyl **151** (3.55 eV) and silyl **152** compounds (3.48 eV); the pyridyl **154** and phenyl-based compounds **156**-**158** all have similar gaps between 3.04-3.08 eV. The relatively close energies between the HOMO levels and the work functions for all compounds makes them suitable for OTFT applications[308–311], while their relatively large HOMO-LUMO gap makes them air-stable for ambient processing conditions in organic electronic device fabrication.

The FMOs are plotted in Table 28. Relatively little orbital density is observed on the derivatives of compounds **151** and **152**, yet significant greater density is observed on the ethynyl bonds than on the other compounds. Compound **153** has orbitals across all carbon atoms in the thiophene unit, yet **154** and **155** lack orbitals on two atoms of their six-membered ring derivatives. In contrast, orbitals are present on all atoms of the phenyl unit and the methyl, methoxy and dimethylamine units, showing the HOMO state can be π-extended across and beyond the aromatic derivatives. Except for **151** and **152**, all LUMO states for compounds **153**-**159** show extensive orbitals of similar pattern across the breadth of the structures.

Table 28 Frontier molecular orbital plots of the highest occupied and lowest unoccupied with their energies in electron volts (eV).

Entry	Ψ_H	Ψ_L
151		
	-5.49	-1.94
152		
	-5.68	-2.20
153		
	-5.23	-2.34
154		
	-5.69	-2.62
155		
	-5.46	-2.38
156		
	-5.34	-2.27
157		
	-4.81	-1.91
158		
	-5.19	-2.15
159		
	-5.27	-2.38

5.3.1.1 Summary of the Design and Modelling

A second type of linear structure for experimental investigation is rationally-designed to diversify the molecular targets from fused-ring structures to include an oligomeric bonding unit which imparts close-packing and charge transfer properties, namely an alkyne unit. The resulting structures complement investigations into optoelectronics by providing a greater degree of structural and heteroatomic variation, which gives rise to different physical properties such as solubility, thermal stability and charge transfer. Their linear molecular shapes are to enable cooperative herring-bone type packing interactions to facilitate relatively high charge-transfer properties.

A novel molecular library was conceived as a rational progression and the next analogue in the fused-thiophene series, utilising DTT as the core and other derivatised moieties for the synthons. The library consists of components which vary the electronic and optical properties of the ethynyl-DTT fragments through heteroatomic structural diversity of the synthon, and could potentially give rise to both p- and n-type organic semiconductors. In summary, a second type of structure was conceived with candidates designed for soluble and air-stable thin-film organic transistors.

5.3.2 Synthetic Strategy

5.3.2.1 General Reterosynthesis

The retrosynthesis of the oligo-fused heterocyclic molecular rods *via* a hybrid approach is comprised of two cuts, both affording Sonogashira reagents. Scheme 63 shows the general retrosynthesis of one particular target (**66**) which has a phenyl based synthon. Cut *i.* gives the dibromo-DTT molecular fragment (**12**) and a derivatised alkyne (**70**), while cut *ii.* gives a diethynyl-DTT structure (**71**) which may be unstable, and a brominated phenyl ring (**72**). A large majority of the molecular fragments identified with the first cut of the retrosynthesis are commercially available, or can be readily synthesised, suggesting they are stable and can fast-track experimental investigations, which is a significant advantage.
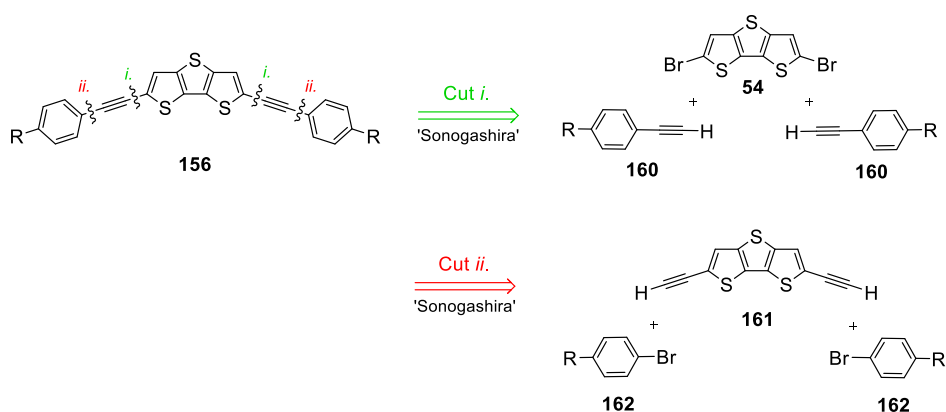
Scheme 63. General retrosynthesis of target **156**, giving Sonogashira reagents from both cuts; R = C$_6$H$_{13}$.

5.3.2.2 Summary of the Synthetic Strategy

Although the retrosynthesis is relatively simple, one strategy was revealed to result in the synthesis of the potentially unstable core fragment diethynyl-DTT **161**; this can now be avoided to ensure stability and solubility throughout synthesis to utilise **54** as identified for the fused-ring structures in the section 5.2. Sonogashira chemistry was identified to be suitable for the target structures, with the most stable synthons containing the ethynyl unit. Such synthons are either synthetically or commercially viable, which ensures the ease of the target synthesis.

5.3.3 Forward Synthesis

The hybrid synthetic strategy adopted for these molecular rods start with the synthesis of the synthon units and then C-C coupling to the core DTT fragment (Scheme 64). Raithby *et al.*[299] also found isolated diethynyl-DTT to be unstable (cut *ii.* of the General Retrosynthesis 5.3.2.1) and thus unsuitable for this study. Dibromo-DTT (**54**) was synthesised according to the latest route reported by Holmes *et al.*, which is a facile, high-yielding three-step route starting from commercially available tetrabromothiophene[144].

Except for compounds **153**, **156** and **159**, the derivatised alkynes were used as bought at high-purity grades (98-99+ %); these were synthesised *via* a Sonogashira coupling[312] of a brominated substrate with trimethylsilylacetylene, followed by deprotection with TBAF affording the H-terminated alkyne in high yield. Subsequent addition to **54** using a second Sonogashira reaction gave the target products in exemplary yields of 61-67 %, compared to the TT analogues[294,299,300]. The alkyne derivatives were chosen for their structural and heteroatom variation, while also designed to ensure good solubility in common organic solvents, an important factor in solution-processed thin-film transistors[10,46].

Single-crystal X-ray structures of the individual molecules and the unit cell packing for compounds **152**, **155**, **156**, **157** and **158** are presented in Figure 66; compounds **151**, **153**, **154** and **159** did not crystallise. Compound
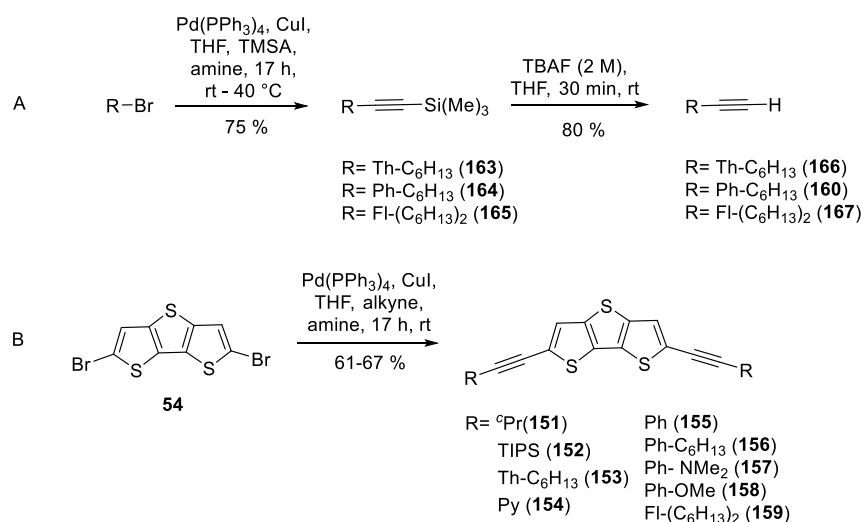
Scheme 64. Facile synthesis of symmetric dithienothiophenyl ethynyl derivatives under mild Sonogashira conditions using readily available alkynes.

152 crystallised in a monoclinic cell and was solved in the *I*2/*a* space group, with half a molecule in the asymmetric unit. There is an in-plane bending distortion between the TIPS groups and the DTT core of the single molecular structure. The isopropyl units lock the molecules together into an ideal brick-weave type motif.

The phenyl derivative, compound **155**, crystallised in an orthorhombic cell and solved in the $P2_12_12_1$ space group. The unit cell is remarkably different from all other crystallised compounds in Figure 66, due to the layers stacking perpendicular to each other. The phenyl-hexyl derivative **156**, crystallised in a triclinic unit cell and the *P*-1 space group. The hexyl units stack cooperatively, varying significantly from the unit cell of compound **155**. The phenyl rings of 6 have a herringbone type arrangement along the crystallographic *a*-axis, with the adjacent molecules bound through S-S (3.400 Å) and S-π (3.213 Å) interactions. The aniline derivative **157** was crystallised as yellow-green plates in a monoclinic unit cell in the $P2_1/c$ space group with one molecule in the asymmetric unit from the slow diffusion of hexane into dichloromethane, which remained trapped in the single-crystal in between the layers and located in Figure 3 on the edges of the unit cell.

The methoxy derivative **158** was crystallised from the same conditions as **157** as yellow-green plates in the orthorhombic space group $Cmc2_1$ with half a molecule in the asymmetric unit. Interestingly, both **157** and **158** show remarkable structural distortions, where **157** displays an inflection of curvature across the whole molecule, while 8 exhibits a large out-of-plane bend of 34.7 ° (Figure 67). This phenomenon suggests these structures have a relatively high degree of flexibility, rather than rigid scaffolds, in the solid state.
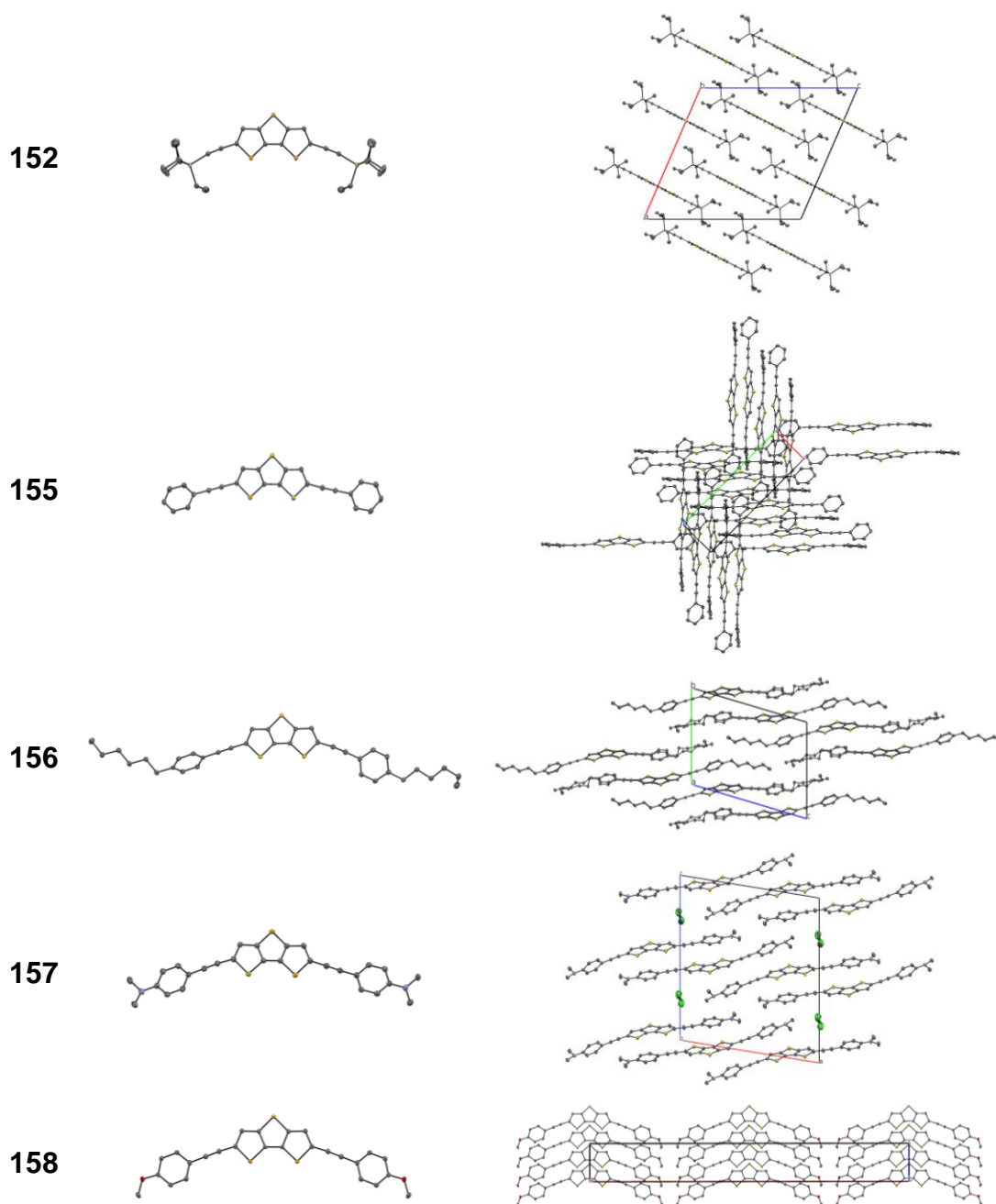
Figure 66. Single crystal X-ray ORTEP plots with thermal ellipsoids at the 50 % level of the single molecules and their packing in the unit cell; hydrogen atoms removed for clarity.

The distances between the adjacent molecules and layers were compared to those in a single-crystal structure of pure DTT. Figure 68 shows several intermolecular distances between the sulfur atoms of the thiophene rings. The sulfur or carbon atoms of the each thiophene in DTT has intermolecular distances with the corresponding ring or to the adjacent
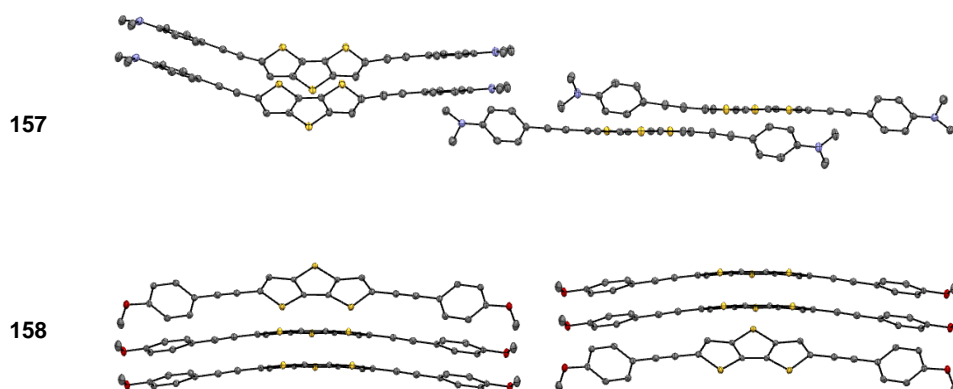
Figure 67. Single crystal X-ray ORTEP plots with thermal ellipsoids at the 50 % level showing an inflection of curvature across **157** and a large out-of-plane bending distortion with **158**.

molecule of 3.54-3.75 Å. In comparison, all four of the single-crystal structures presented in this work have very similar intermolecular distances, regardless of the large out-of-plane bends, twisted phenyl rings or solvent incorporation. These distances correlate well with the literature for TT analogues[299], suggesting these could be ideal candidates for organic semiconductors.

Selected structural parameters from the single-crystal data are presented in Table 29; DFT[313] calculations were performed for all compounds and the Cartesian coordinates are available in the Appendix B2. The DFT values show exceptional correlation to the single-crystal bond lengths (< 0.02 Å) and angles (< 3 °) and can thus be used with confidence for a reliable structural prediction. The table shows C2-C6 bond length is less than the C3-C4 bond in DTT, suggesting significant aromaticity concentrated in the central thiophene ring. This is corroborated with the differences between the C-S bonds, such that S5-C6 < S5-C4. The alkyne bonds are noticeably longer for the single-crystal structures **152** and **157** than for **156** and **158**, possibly owing to the strength in their electron donating power and thus slightly weakening the triple bond; the corresponding DFT calculations for the alkyne bond lengths correlate well, in comparison to the single-crystal data. The bond angle C4-S5-C6 is 91 ° for the terminal thiophene, reproduced across all structures and 111-112 ° for the C=C-C intra-ring angles. The angle C7-C4-S5 between the alkyne bond and

DTT (**51**)

TIPS (**152**)

Ph-C$_6$H$_{13}$ (**156**)

Ph-NMe$_2$ (**157**)

Ph-OMe (**158**)
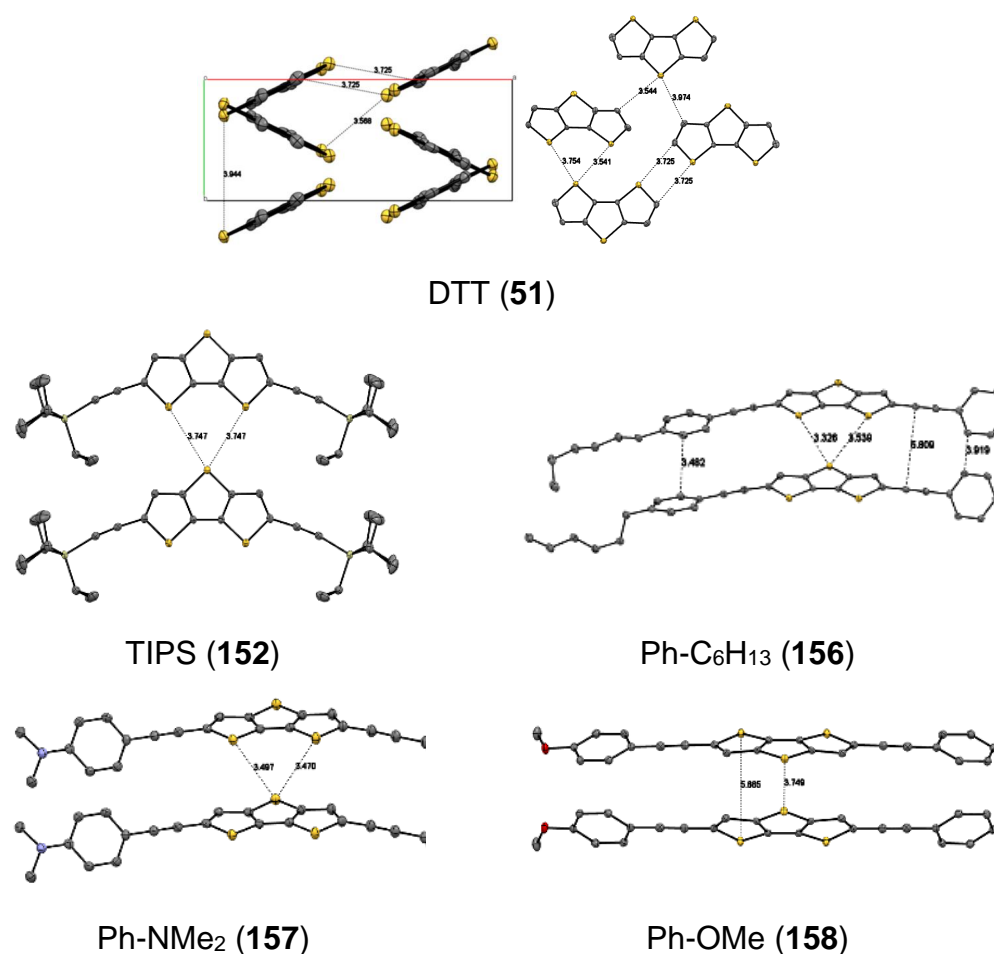
Figure 68. Single crystal packing of a pure DTT molecule (reproduced from Section 5.2.4.2) and the compounds **152**, **156**, **157** and **158**, showing the intermolecular distances between the sulfur atoms of the central and outer thiophene rings between the adjacent molecules; presented as single crystal X-ray ORTEP plots with thermal ellipsoids at the 50 % level.

thiophene ring varies between 117-119 °, due to the different structural distortion phenomena.

The optical properties of the compounds were probed using UV-Vis spectroscopy (Figure 69) and clearly shows the diversity of their electronic structure. In general, the optical-gap decreases with increasing aromaticity of the derivative, where the silyl **152** has the largest (338 nm) and the dimethylamine derivative **157** has the smallest (468 nm). The split in the absorption peaks of **151** and **152** is not reproduced by the other compounds and although uncommon in the literature, the phenomenon is present for some oligo-fused thiophenes[311]. The pyridyl derivative **154** has an absorption curve that is highly similar to that of compounds **155** and **158**, suggesting there is

little difference in terms of electron density or donating and withdrawing power amongst these derivatives. Except for **152**, there is relatively little absorption in the 200-300 nm region, although low-intensity peaks are centred on 300 nm, while other peaks at lower wavelengths centred on 250 nm arising from deep energy levels.

Thermal decomposition profiles were investigated with thermal gravimetric analysis (TGA) as seen in Figure 70. The profiles for all compounds exhibited two thermal decomposition temperatures, with the second onset being around 381 °C for all. This reproducible temperature suggests the origin is the decomposition of the DTT core unit. All compounds show relatively good thermal stability, with the first and lowest decomposition onset of **153** at 89.0 °C followed closely by **152** and **154** at 121.1 and 149.4 °C respectively. Interestingly, compound **5** decomposes at 252.7 °C, whereas compound **156** decomposes at 381.5 °C, being a 128.8 °C difference. This suggests strong electron donation highly stabilises the alkyne bond and overall structure.

Table 29. Selected bond lengths (Å) and angles (°) from single crystal structures.
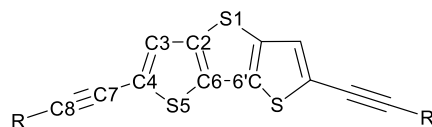
Bond Length	152	155	156	157	158
S1-C2	1.744	1.745	1.749	1.744	1.759
S5-C6	1.720	1.719	1.721	1.724	1.738
C6-C6'	1.418	1.418	1.411	1.413	1.415
C2-C6	1.384	1.386	1.388	1.391	1.395
C2-C3	1.418	1.417	1.410	1.415	1.411
C3-C4	1.367	1.376	1.374	1.373	1.382
C4-C7	1.424	1.417	1.410	1.417	1.399
C4-S5	1.751	1.747	1.756	1.752	1.777
C7-C8	1.208	1.201	1.206	1.201	1.214
Angle					
C4-S5-C6	90.9	91.0	91.1	91.1	90.0
S5-C6-C2	111.4	111.3	110.9	110.9	111.1
C2-C6-C6'	112.4	112.5	112.7	112.3	112.6
C6-C2-S1	112.4	112.6	112.0	112.6	112.4
C2-C3-C4	111.2	110.9	111.2	111.0	112.1
C7-C4-S5	117.2	117.3	117.3	118.0	120.0
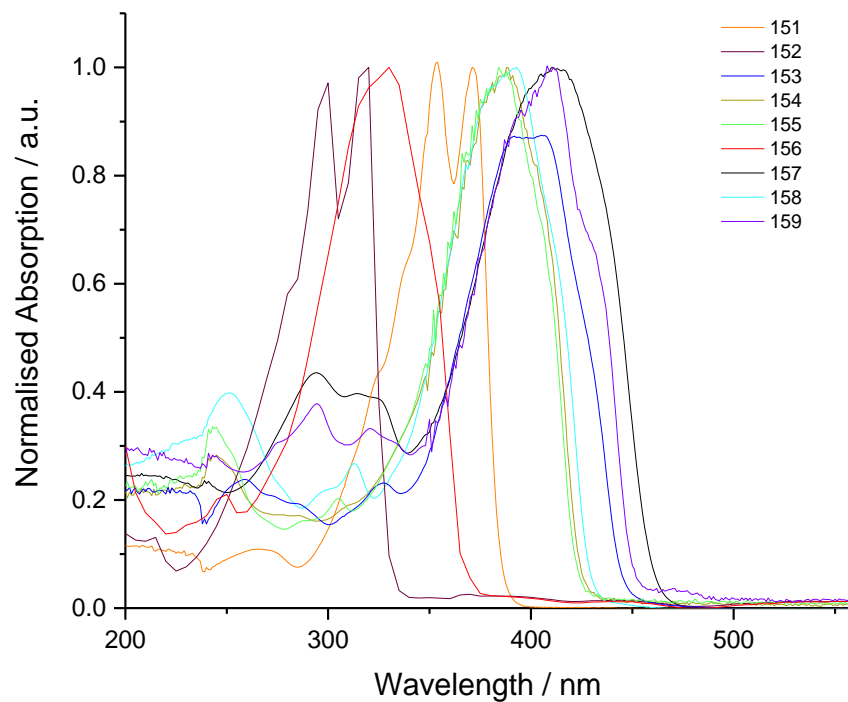
Figure 69. Normalised UV-Vis spectra in chloroform at 21 °C.
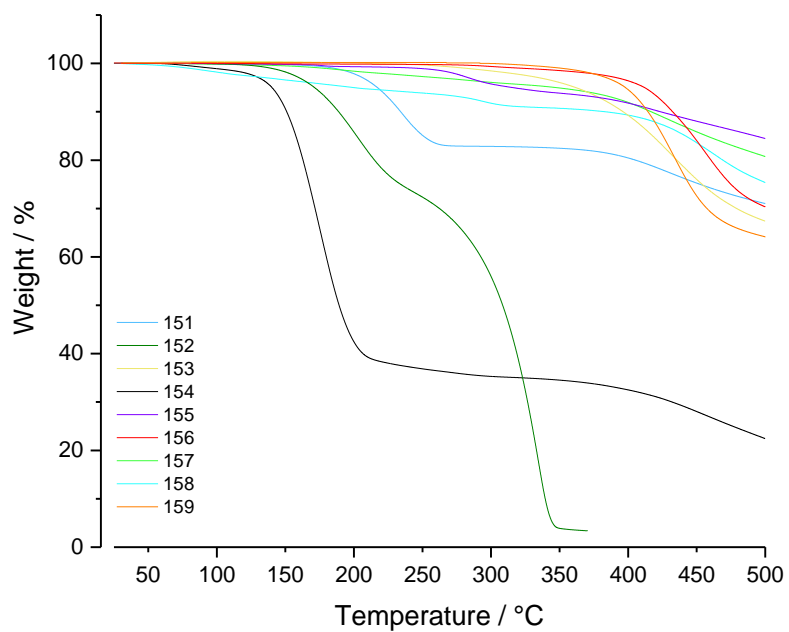
Figure 70. Thermal gravimetric analysis (TGA) of the sample weight (%) under nitrogen between 25 °C and 500 °C.

5.3.3.1 Summary of Forward Synthesis

In summary, electron rich molecular rods containing a DTT core and capped with a structural variety of derivatised alkynes were synthesised and fully characterised, including optical, electronic, thermal and DFT analysis. It was found that all have excellent solubility in common organic solvents and show ideal packing in the solid state, while compound **156** and **159** are thermally stable up to 381 °C. These high stabilities and solid-state interactions are suitable for charge-transfer applications in OTFTs.

5.3.4 Synthetic Modification Example for Optoelectronics

The successful synthesis and characterisation of the oligo-fused heterocyclic molecular rods in section 5.3.3 enabled the generation of a highly stable small library of compounds for charge transfer applications in solution-processed OTFTs. Compound **153** was selected and developed further with investigations into its use as light-scavenging structure, by synthetic conversion into a strongly absorbing chromophore; such applications include dye sensitized solar cells. There is a growing interest in black dyes and pigments[314,315] as there are few chromophores that give a truly black colour and these can be split into inorganic and organic structures. To date, the inorganic complexes are based either on chromium[316,317] (**168**) or ruthenium[314,318] (**169**), as illustrated in Figure 71A. These consist of a metal centre and various derivatised aromatic ligands. Due to toxicity concerns, there has been a shift towards metal-free or purely organic structures, which acquire their black colour from strong electron-donating or withdrawing groups.

There are two common types of organic chromophores, as shown in Figure 71B and include i) the azo species Acid Black 1[319] (**170**) and substituted amino-arylazothiazoles[320] (**171**) and ii) the indoline-thiazole Indoline Dye 4[321] (**172**) and phenoxazine-thiazole[322] TH304 (**173**); these structures are strongly inter-related. The Acid Black-based dyes are widely used throughout industrial colouration and solar cell technology, while the least designed and worst performing are the amino-arylazothiazoles, in strong contrast to the rationally-designed Indoline Dye 4. Acid Black 1 has a typical diazo-based dye structure with electron donating NH_2/OH groups and SO_3Na/NO_2 withdrawing groups, while the substituted amino-arylazothiazoles mixes azo and thiazole units. The Indoline Dye 4 utilises electron-rich phenyl units for the donating group with the highly conjugated thiazoline units for the withdrawing group. The TH304 is only a slight variant of Indoline Dye 4, with a different electron-donating octyl-phenoxazine unit. These typical structures and their many derivatives are widely reported for the design of strongly-absorbing chromophores.
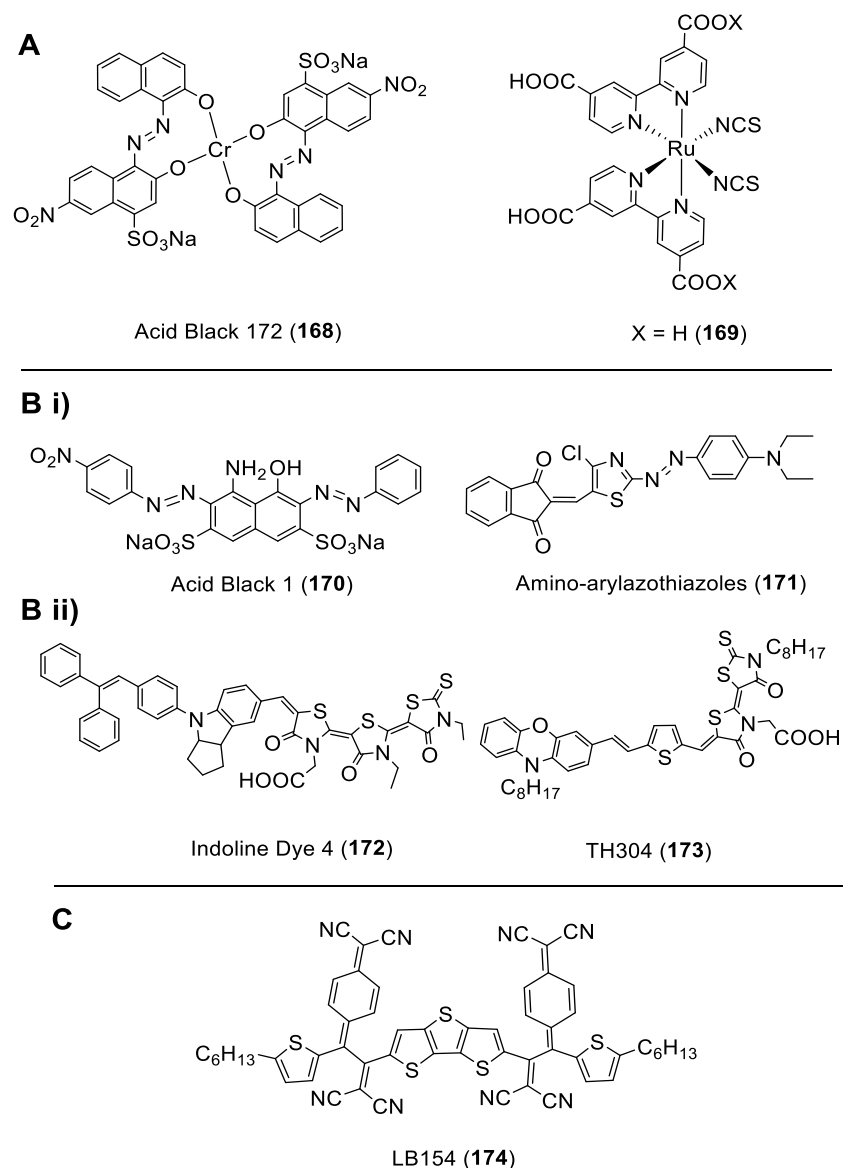
Figure 71. Selected black pigments and their structures, a) conventional inorganic, b) typical organic and c) novel organic chromophore.

Many derivatives of both the inorganic and organic structures in Figure 71 A and B, include sulfate or acidic groups that have a second role of binding to a given substrate. Their polar nature and acidity enables the colorants to be water soluble, and unfortunately, extremely hygroscopic once in the solid state or thin-film. While water solubility is desirable for eluent processing in dyeing textiles or thin-film formation on a substrate, it has significant disadvantages in organic electronic device applications. It is highly desirable for structures to operate on substrates or in devices such as dye-sensitised solar cells without them being sensitive to environment variables. The

challenge is to synthesise a strongly-conjugated chromophore that absorbs light across hundreds of nanometers and be soluble in the solvent of choice. In stark contrast to the structures presented in Figure 1, the pigment synthesised in this study, designated as Leeds Black 154 or (LB154, Figure 71C, **174**), has a unique chromophore, comprised of dithienothiophenyl (DTT), 7,7,8,8-tetracyanoquinodimethane (TCNQ), and two hexylthiophenes which facilitate excellent solubility in common organic solvents and optoelectronic properties. Herein, we report a bifunctional smart material consisting of a water-repellent organic black pigment with a novel and strongly-absorbing panchromatic chromophore.

5.3.4.1 Synthesis and Characterisation

Scheme 65 shows the synthesis of **174**. Compound **153** was designed for organic transistor applications[323] but its electron-rich nature and high stability is perfectly suited to electron-poor adducts such as nitriles. Following the extensive work by Diederich[289] and Shoji[276,324,325] on single and double alkyne cycloadditions with nitrile adducts *via* a ring-opening of tetracyanocyclobutene intermediates, TCNQ was added in a similar fashion to the electron-rich molecular rod and afford the target material in moderate yield (45 %).

The chromophore absorption is strong enough to absorb all incident light in solution, as illustrated in Figure 72A, which shows total opacity of the pigment in acetonitrile. Figure 72 B and C) shows the excellent thin-film formation on both glass and paper substrates respectively.
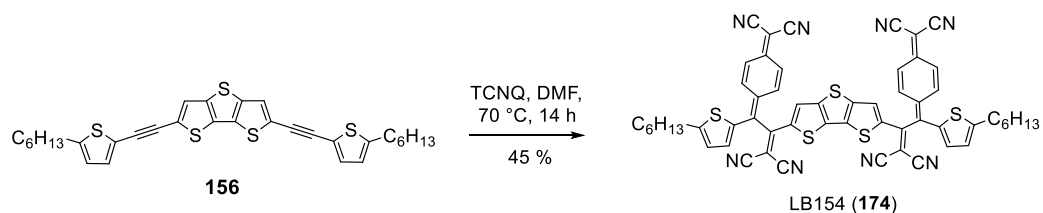
Scheme 65. Synthesis of **174** from molecular rod **156**.
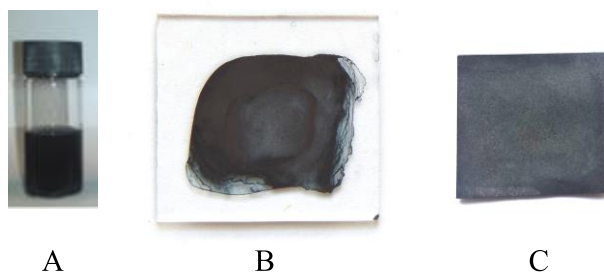
Figure 72. The strong absorption of the compound **174** as A) total opacity in acetonitrile solution (10.6 mg in 10 mL) and examples of the pigment on B) glass and C) paper showing excellent thin-film formation.

The unique chromophore of LB154 ensures a strong 600 nm absorption across the visible and ultraviolet regions between 200 and 800 nm (Figure 73). The broad lower intensity peak at longer wavelengths (650 nm) is considered to arise from a TCNQ excitation while the sharp intense peak at lower wavelengths (250 nm) and broad shoulder absorption up to 400 nm is due to the DTT absorption unit. This is confirmed with the comparison of the UV-Vis absorption spectrum of **153**, which shows the most intense peak centred at 400 nm and contains vibrational modes at 250 nm. Moreover, **174** still retains absorption at its lowest intensity around 500 nm, ensuring the structure does not yield any colour in this region.
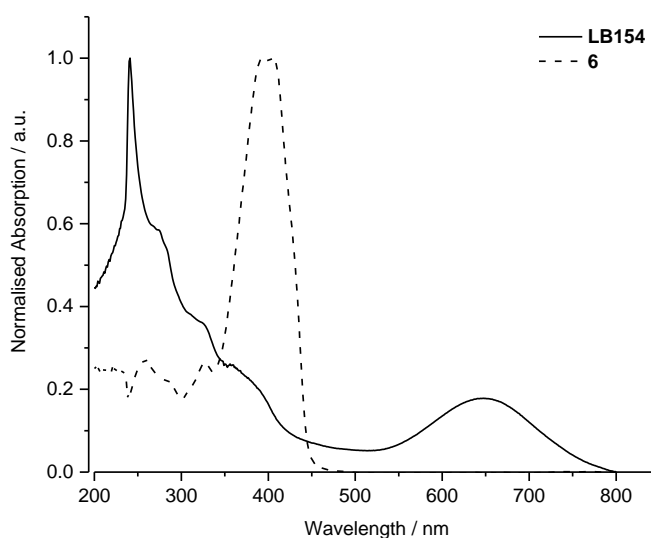
Figure 73. UV-Vis absorption spectra of pure 1**56** and **174** in chloroform at 20 °C.

Density functional theory (DFT) calculations were performed to probe the energy gap of the highest occupied and lowest unoccupied molecular orbitals (HOMO and LUMO respectively) and elucidate orbital contributions (Figure 74). **174**'s strong optical HOMO energy level is localised to one of the TCNQ adducts. The LUMO energy level spreads across the breadth of the backbone of the structure. The overlap of the low energy HOMO/LUMO orbital densities may be a large contributing factor for the strong panchromatic absorption. Moreover, the HOMO-LUMO gap is 2.04 eV, which is greater than that of pentacene[148], by 0.204 eV, proving **174** has strong air stability for processing under ambient conditions.
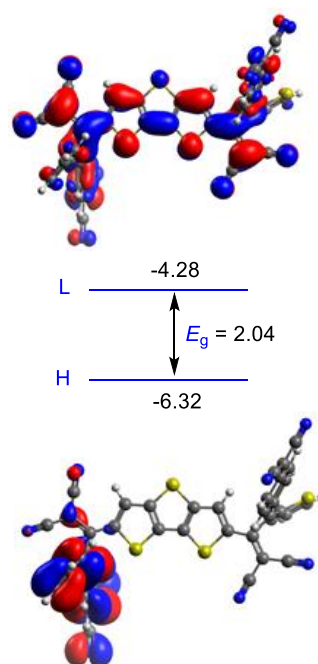
Figure 74. HOMO-LUMO orbital plots and associated energies of **174** in eV. The overlapping of the low energy HOMO and LUMO orbital densities across the structure and low energy gap suggest significant suitability for both light scavenging and charge-transfer applications. The hexyl units were omitted for computational time.

Figure 75 shows the reflectance spectra of dyed paper, and shows an inflection at 560 nm, correlating well with the UV-Vis absorption. It is important to note that the reflectance does not achieve higher than 14.1 % at 700 nm, clearly indicating the strength of the chromophore. The K/S strength value was found to be 4.283 and the colour of the sample was measured in the CIELAB colour space, giving 35.75, -0.22 and -1.56 for L*, a* and b* respectively, in agreement with the literature[326].
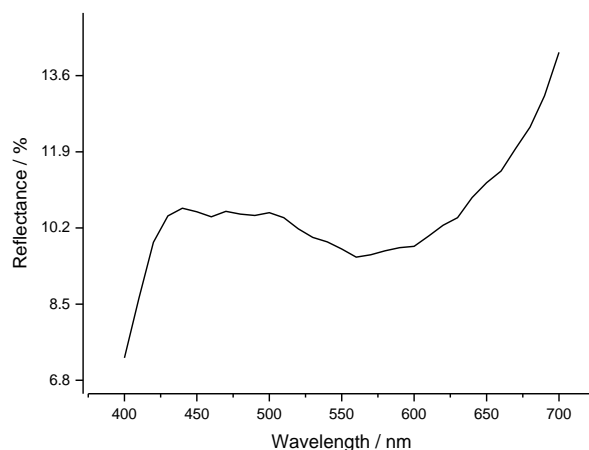
Figure 75. The reflectance spectrum of dyed paper with **174** showing an inflection at 560 nm.

Figure 76 illustrates the thermal gravimetric profile of **174**, and shows the first decomposition onset at 101.4 °C and a second at 370.5 °C. Even at 150 °C, the weight still remains at 96.7 %, showing good thermal stability. The first onset could be due to the removal of the outer hexyl and nitrile units from the structure, followed by the slow decomposition of the highly conjugated core of the molecule, which may explain the long and gradual weight loss, with the second onset due to the final decomposition of the core DTT unit.
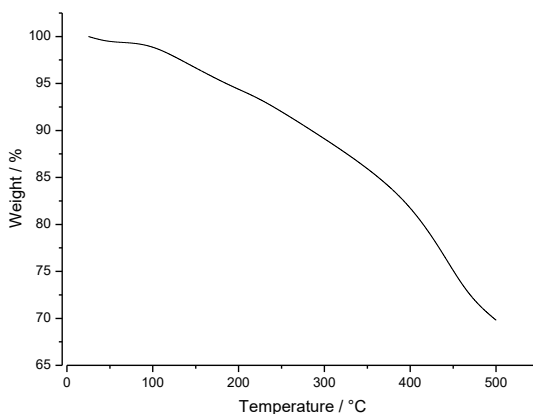
Figure 76. Thermal gravimetric profile of **174** operated under nitrogen as sample weight (%) between 25 and 500 °C; first decomposition onset at 101.4 °C and second at 370.5 °C.

5.3.4.2 Summary of the Synthetic Modification Example

In summary, a novel black organic pigment has been synthesised that contains a unique donor-acceptor chromophore. The material was found to be panchromatic and absorbs over a 600 nm window between 200 and 800 nm. The thin-films form excellent adhesion to both glass and paper substrates and in acetonitrile the solution is rendered completely opaque, with complete solvation in other common organic solvents. These results suggest the solution-processable and air-stable structure will have wide-ranging applications in organic optoelectronics. Furthermore, this example illustrates the propensity for an alkyne spacer unit between two electron rich aromatic groups to be synthetically converted and transform the organic electronic substrate to an organic optoelectronic structure, thereby bridging these two fields.

Chapter 6

Conclusions

In conclusion, a wide range of phenomena for two target structure types and their associated properties were thoroughly investigated, including the mechanisms of formation and condition optimisation towards their molecular fragments. These structures were rationally designed and their charge transfer properties were calculated. Overall, the approach of the virtual screening followed by synthetic investigations was advantageous in the pursuit of novel and high-performing organic semiconductors, with some candidates selected and probed for organic electronic applications, while others were found to be relatively lower performing and thus not pursued, thereby saving both time and resources. These results suggest that the solution-processable and air-stable fused-ring and oligo-fused heteroacene structures will have wide-ranging applications in organic optoelectronics. The multi-functional fused-ring target **44** has the theoretical suitability for use in both the electronic and optical fields, and a potential device which incorporates both. Finally, the electron rich DTT-based molecular rods have strong potential as organic semiconductors for organic electronic applications. The following sections concludes the findings in more detail with respect to each section, but begins by outlying the theoretical methodology used.

6.1 Theoretical Methodology

Exceptionally high levels of accuracy for all structures and property calculations was ensured from deploying a mixed methodology. This comprised of optimising the structures from (1) molecular mechanics and (2) quantum mechanics, through DFT; all subsequent property calculations were performed with DFT. The level of theory deployed was selected to be appropriate for the atoms in the molecular structures investigated, and as structures such as the thiophene synthon include bromine, a row two element, the appropriate complete basis set called 6-311G was chosen. Due to the varied properties investigated, both polarisation and diffuse functions were included to yield the 6-311++G(d,p) basis set that is ideal for organic semiconductor calculations. This is in contrast to the commonly used 6-31+G(d) basis set, as a number of challenging structures were investigated, many of which are either novel or have unknown crystal structures and thus small and incomplete basis sets are inappropriate. In addition, all calculations were compared to either experimental observations or 'chemically accurate' theories such as CCSD, which was deployed in the synthon reaction

mechanism to confirm the exergonic nature of the las two steps in absence of experimental values.

From a wide choice of DFT functional to choose from, a number of which were screened against the experimentally observed properties of pentacene, one of the most famous acene p-type organic semiconductor. It was found that the B3LYP functional proved to be the best across all properties investigated and thus used for subsequent calculations for both acenes and heteroacenes.

To perform the high-accuracy calculations with efficiency and in parallel, the latest computational chemistry software called Gaussian 09 was used, and operated on a HPC computer system, enabling multiple calculations to run continuously until completion.

With regards to the semiconductor properties, FMOs such as the HOMO, LUMO and their energy differences (E_g) and Marcus Theory were probed for air-stability and charge transfer, respectively. Those of charge transfer include the ionisation energy, electron affinity, internal reorganisation energy, the transfer integral and the rate of charge transfer. Theories other than that of Marcus for the calculation of the ionisation energy include the Koopman's Theorem (KT), the Outer Valence Green's Function (OVGF), and a variant, the third-order electron propagator (P3).

For the molecular synthon fragment studies, location for the transition state structures proved key, and acquired through the synchronous transit-guided quasi-Newton (STQN) method. Once located, the transition states were confirmed by performing intrinsic reaction coordinate calculations (IRCs) in both the forwards and reverse direction, which gave the starting reagents and products. The difference between the optimised reagents and products gave the reaction step energies, and confirmed with the chemically accurate CCSD theory as described above.

Numerous solvation methods were deployed but none gave satisfactory results; these calculations were hindered by the lack of correlation in the literature with regards to aggregation or dispersion. Hence, all calculations for structures and properties of both the molecular fragments and the organic semiconductors were performed in vacuum rather than solution or solid state. Reliability of the results was determined by comparison to experimental results or theoretical calculations in the literature.

6.2 Pentacene's Isomers

Through DFT, it was found that at least four of pentacene's eleven known isomers are highly suited as potential organic semiconductors and alternative candidates to pentacene itself. Their air-stabilities are on average higher, due to their E_g being 1-2 eV greater than pentacene. Interestingly, those four isomers, namely benzo[b]chrysene, naphtha[c]phenanthrene, dibenzo[a,c]anthracene and benzo[a]tetracene, are relatively less stable than the remaining isomers, yet have the highest rates of charge transfer of the order 1.3-2.9 × 10^{14} s^{-1} for the 3.5 Å intermolecular spacing. This is significant considering (1) that of pentacene is 4.0 × 10^{14} s^{-1} and (2) isomer dibenzo[a,c]anthracene is a non-planar structure and thus breaks the rule-of-thumb of planarity for high charge transfer candidates.

The remarkable differences in air-stability between pentacene and picene and the similarities between four other isomers to picene suggests these are worth of experimental investigations. Moreover, the rate of charge-transfer of these isomers tend to out-perform picene by an order of magnitude. Such structures have yet to be experimentally investigated and the calculations give merit to a theoretical approach which minimises the time and resources used to produce high-performing organic semiconducting materials. In addition, the third-order electron propagator (P3) was found to give the most accurate ionisation energies and should thus be used over other theories, including DFT, KT and pure OVGF.

6.3 Fused-Ring Heteroacenes

From the understandings generated from the studies on pentacene's isomers, investigations into heteroacenes were conducted for dual-purpose device applications, such as charge transfer and nonlinear optics. These began by comparing the charge transfer properties of two well-known structures. It was evident that the larger heterocyclic homologue, B5TB, with two more thiophenes in the core, performs relatively worse than the smaller homologue. This is in contrast with the general rule that the charge transfer properties increase with conjugation. It was clear that this rule does not necessarily apply to homologues, but could still work for the B5TB chemical formula if it was re-arranged to give a new structure. In fact, isomerisation of B5TB generated

six fused-ring isomers, which could also be generated from the heterocyclic π-expansion of DBDTT.

In an attempt to determine if these new six structures could indeed have improved properties, their air-stabilities and charge transfer properties were investigated with DFT. Although somewhat expected, the isomers did not show suitability for n-type devices, but did show remarkable application for p-type devices, owing to (1) air-stability, with all six isomers showering equal or greater stability than B5TB; (2) relatively high vertical ionisation energies; (3) ideal internal hole reorganisation energies, < 0.1 eV; (4) relatively good transfer integrals (t_h ~ 100 meV) with associated rates of hole charge transfer between $0.02\text{-}0.168 \times 10^{14}\,s^{-1}$, which is the same order of magnitude as pentacene (**13**).

The calculated UV-Vis spectra revealed interesting line shapes that correlated with the HOMO levels of the isomers, and suggested that although all gave a broad absorption between *ca.* 200 and 450 nm, the isomers **2** and **3** gave the most intense absorption centred on 300 and 400 nm respectively. It would therefore be of great interest to synthesise and compare the optical properties of these structures. In addition, their NLO properties were probed. The first-order hyperpolarisabilities were calculated at the experimentally applied frequency of 1064 nm for (1) the Pockels effect, which has applications in two-photon microscopy and quantum key security by the polarisation of light in Pockel cell devices, and (2) second harmonic generation with applications in optical switches. It was found that one isomer (**2**) gave exceptional hyperpolarisabilities for both effects and had excellent charge transfer properties, thus inferring that the structure would be suitable as a multi-response material for both electronic and NLO applications. There is the potential for the NLO outputs to be generated by the ionised form of **44** in a typical OTFT device and thus enhancing electronic miniaturisation.

Having theoretically characterised the properties of the six isomers, two were selected and underwent retrosynthesis to determine the molecular fragments to start in the forward direction. It was considered that both the divergent and convergent routes would give rise to challenging reactive conditions or unstable structures and thus a hybrid approach was deemed the most appropriate in terms of stability. The phenyl ring was selected for synthetic manipulation due to the availability of known chemistries. Ring-formation conditions for **44** such as Diels-Alder reactions and Sigmatropic rearrangements gave rise to potentially unstable starting

reagents and intermediates that would be challenging to oxidise in the final step. An acid-catalysed route was realised to give molecular fragments of differing functional groups and thus a small library of fragments were generated. Th retrosynthesis of **45** suggested that C-H activated cyclisation *via* a transition metal catalysis or organic base was preferential. Considering these fragments and their associated forward conditions, a retrosynthetically-designed forward route was selected for both **44** and **45**.

The synthon molecular fragment was first investigated and it was immediately observed that the Halogen Dance reaction was key to the success with this structure. Initial efforts found the reaction to give the target synthon in modest yield but after realising there was little evidence in the literature to support the reported reaction mechanism, a DFT study was undertaken with a high level of theory to give a deeper understanding into this highly useful reaction. Among numerous discoveries, it was found that the first step needed to be cryogenically cooled for a short period of time (*i.e.* 1-2 h) then allowed to warm to room temperature and stirred overnight; this insight led to higher yields in excess of 88 % for the synthon. These conditions were finally understood from the discovery that the lithiation of the other positions on the thiophene ring are highly sensitive to temperature, and need to be carefully controlled; the remaining reaction steps are exergonic and occur readily after the first successful lithiation step.

Next, the DTT core molecular fragment was investigated. There are four well-known routes to DTT in the literature, but all of which involve lithiation chemistry and some include unstable reagents and intermediates. Thus, there was significant room for improvement, by developing alternative conditions that were relatively cheap, commercially available, stable with long shelf lives, and did not involve lithiation chemistry. This was achieved once it was realised that the four literature routes to date insert the sulfur atoms as electrophiles, being attacked by the lithiated anions as the nucleophiles. Reversing this chemistry generated the new conditions such that the sulfur became the nucleophile and the thiophene substrate the electrophile. Multiple conditions were probed and it was found that sodium sulfate, potassium carbonate and copper iodide gave the best yields, although these were on average below 50 %. Application of microwave synthesis in sealed vials gave significant improvement, to near-quantitative yields (96-97 %); the product formation was confirmed from NMR and single-crystal structures.

The synthon and core molecular fragments were synthesised in the forward direction towards **44**, using the understandings from the DFT work and conditions developed, and then these fragments were combined and gave the condensed intermediate towards the target isomer. It was found this intermediate was challenging to purify, but was successfully used as crude in the next step and gave the reduced structure; this intermediate was well characterised. Unfortunately, the penultimate step, of converting the bromine into a carbonyl substituent, was not successful; neither the lithiation and quench nor the palladium-catalysed carbonylation gave the desired intermediate. It was considered that this intermediate was too stable, especially the bromine substituent, and the DTT core unexpectedly increased the reactivity of the methylene protons; alternative conditions were suggested for future work. **45** was then investigated, and it was found that the functionalisation of the 3-ethynylthiophene synthon proved unstable during purification, probably owing to the withdrawing nature of the alkyne bond which made the stannyl and boryl cross-coupling groups labile. Nevertheless, the synthetic route was re-addressed to add the ethynyl units to the thiophene backbone of the target. The all-thiophene linear substrate was successfully synthesised and the subsequent steps of (1) double bromination *via* one-equivalent aliquot additions and (2) double Sonogashira gave the final intermediate. Once more, this structure proved too stable for all attempted cyclisation conditions, as recommended widely in the literature; alternative conditions and structural modifications were considered for future work.

6.4 Oligo-Fused Heteroacenes

As outlined in the project plan, a second type of structure was investigated, to compliment the organic electronic device applications of interest but to also contrast in terms of molecular structure; this second type of structure may induce varied physical properties. The structure consisted of oligomeric bonds and fused-ring segments, such that the overall structure would impart greater solubility not just from the alkyl chains, but also from its greater degree of entropy from potential rotation and stretches of the oligomeric bonds. Single and double bonds were immediately ruled out due to their extensive coverage in the literature, which highlighted alkyne bonds as a potential point of exploration, and did indeed have a gap in the literature, especially for the incorporation of DTT fragments. The molecular shape of the targets were

considered to be linear, owing to the poorly performing nature of the trigonal and tetragonal shapes giving rise to discotic packing and thus poor mobilities.

Once the bonding nature and the linear shape was determined, a small library of molecular rod-like compounds was designed from the consideration of (1) the derivative structure such as alkyl or aromatic unit; (2) the type of aromatic, *i.e.* thiophene, piridyl, phenyl, and fluoryl; (3) alkyl and heteroatomic substituents. The DFT modelling revealed their HOMO levels to bracket the work function of a gold electrode, and their E_g to be as stable as the fused-ring heteroacene isomers, with energy gaps between 2.89-3.55 eV.

Their retrosynthesis proved to be relatively simple, with a single disconnection utilising Sonogashira conditions in the forward direction; one instability issue highlighted was the double ethynyl-substituent on the DTT fragment from one retrosynthetic cut, which enabled this route to be avoided. The forward synthesis involved the derivatisation of some alkynes and the direct addition of others which were commercially available. The total number of synthetic steps did not exceed three and the relatively high-yielding Sonogashira conditions meant the route was efficient and desirable for the production of novel organic semiconductors.

The single crystals of five of the compounds, namely the silyl, phenyl, hexyl-phenyl, dimethylamine-phenyl and the methoxy-phenyl derivatives were obtained. The TIPS derivative gave a highly regular packing motif, while the phenyl derivative gave interpenetrating layers where the molecules were perpendicular to each other; such an arrangement is not ideal for organic semiconductors due to the low probability of charge transfer from one molecule to another in the perpendicular direction, especially under the influence of an applied field in an OFET type device. Interestingly, the remaining hexyl-phenyl, dimethlamin-phenyl and methoxy-phenyl derivatives gave the desired interlayer slipped-stack array in the solid state. These observations suggest derivatised alkynes may have a greater propensity for charge transfer due to electrostatic and π-π interactions between the derivatised groups. Moreover, all of the derivatives regardless of their bulkyl or linear nature, proved to pack with similar or better intermolecular distances between the DTT cores (3.5-3.7 Å), in comparison to the crystal structure of pure and unmodified DTT. These distances are ideal for the packing of organic semiconductors and suggest high-performance in the solid state.

These compounds exhibited good thermal stability, with some (thiophenyl, hexyl-phenyl, and fluoryl) having stabilities as high as 381 °C. Their excellent solubility, high thermal stability and ideal solid state packing suggests suitability for operation in organic transistor devices.

In addition, one compound was selected and synthetically modified to show the interconvertive nature of the alkyne bond and thus transform the potential organic semiconductor into a strongly absorbing chromophore for light-scavenging applications, such as dye-sensitised solar cells. A strong electrophile such as 7,7,8,8-tetracyanoquinodimethane (TCNQ) was added in DMF and gave a novel pigment, considered to be only the fifth organic black pigment known, and the first to consist of an unconventional panchromatic chromophore spanning 600 nm that does not contain a diazo or indoline-based substrate. The synthesised air-stable compound is also hydrophobic and thus ideal for operation under ambient conditions in optoelectronic applications such as solar cells.

Chapter 7

Future Work

Due to the success of the DFT work deployed for modelling the structures and properties of both acenes and heteroacenes, a greater structural diversity could be probed in the future, considering non-planar three-dimensional structures such as Mobiüs-type molecules, short nanotubes and fullerene-like structures, for the development of the next generation of candidates for optoelectronic applications. Reaction mechanisms for ring-closing cyclisations could be explored, catalysed by both, acid, transition metal and organic base. Charge transfer calculations on the oligo-fused heterocycle single crystals would give a deep and highly accurate understanding of the process in the solid state for these structures.

The synthesis of the fused-ring heterocycle isomers is to continue, with emphasis on the alternative routes and conditions as described in the Section 5.2.6. Other options include the potential use of a convergent or divergent approach with retrosynthetic strategies and DFT modelling to deduce a suitable forward route.

The successful synthesis and characterisation of a diverse library of oligo-fused heterocycles has provided insight into which alkyne derivatives provide the most thermally stable structures and a selected example was shown to readily undergo synthetic modification of the alkyne into a panchromatic chromophore for light-scavenging applications. These observations could be developed by extending the length of the compounds with additional oligo-fused units to determine how their length affects their stability, solubility and charge-transfer properties.

The focus of the work to date is on symmetric targets, and thus one novel approach would be to design, model and synthesise asymmetric organic semiconductor candidates. Such structures may have unique alignments in the solid state and thus additional applications in organic magnetic materials and memory devices. These could be comprised of a mixture of the fused and oligomeric bonding nature investigated and yield a diverse library of new materials for optoelectronic applications.

List of References

1   K. Gupta, Organic Electronics, http://www.engineeringapps.net/contributions/details/organic-electronics, (accessed 30 June 2017).

2   UK semiconductor pioneer sets its sights on China | Printed Electronics World, http://www.printedelectronicsworld.com/articles/9788/uk-semiconductor-pioneer-sets-its-sights-on-china, (accessed 30 June 2017).

3   Mobile Devices | Applications | Flexible Electronics | FlexEnable - FlexEnable, http://www.flexenable.com/applications/mobile-devices/, (accessed 30 June 2017).

4   Y. Yamashita, *Sci. Technol. Adv. Mater.*, 2009, **10**, 24313.

5   J. Mei, Y. Diao, A. L. Appleton, L. Fang and Z. Bao, *J. Am. Chem. Soc.*, 2013, **135**, 6724–6746.

6   David Terraso, New Transistor for Plastic Electronics Exhibits the Best of Both Worlds, http://www.news.gatech.edu/2011/01/27/new-transistor-plastic-electronics-exhibits-best-both-worlds, (accessed 30 June 2017).

7   H. Klauk, *Chem. Soc. Rev.*, 2010, **39**, 2643–2666.

8   H. Sirringhaus, *Proc. IEEE*, 2009, **97**, 1570–1579.

9   D. Xiang, X. Wang, C. Jia, T. Lee and X. Guo, *Chem. Rev.*, 2016, **116**, 4318–4440.

10   C. Wang, H. Dong, W. Hu, Y. Liu and D. Zhu, *Chem. Rev.*, 2012, **112**, 2208–2267.

11   H. Klauk and John Wiley & Sons., *Organic electronics : materials, manufacturing and applications*, Wiley-VCH, 2006.

12   M. Faraday, *Experimental Researches in Electricity*, J. M. Dent & Sons Ltd., Second Ed., 1922.

13   L. de Forest, *Trans. Am. Inst. Electr. Eng.*, 1906, **25**, 735–763.

14   US 1745175 A, 1926.

15   P. R. Morris, *A History of the World Semiconductor Industry*, IEE History of Technology Series 12, 1989.

16   H. Xiao, *Introduction to semiconductor technology*, SPIE, Second Ed., 2012.

17   The Nobel Prize in Physics 1956, http://www.nobelprize.org/nobel_prizes/physics/laureates/1956/, (accessed 4 May 2017).

18   A. Tsumura, H. Koezuka and T. Ando, *Appl. Phys. Lett.*, 1986, **49**, 1210–1212.

19   A. R. Murphy and J. M. J. Fréchet, *Chem. Rev.*, 2007, **107**, 1066–1096.

20   A. Facchetti, *Mater. Today*, 2007, **10**, 28–37.

21   Y. M. Sun, Y. Q. Liu, D. B. Zhu, H. Tada, R. Schmechel, H. von Seggern, L. L. Miller, C. D. Frisbie, H. E. Katz, F. P. Cuomo, B. K. Greening and J. West, *J. Mater. Chem.*, 2005, **15**, 53–65.

22   P. Strohriegl and J. V. Grazulevicius, *Adv. Mater.*, 2002, **14**, 1439–1452.

23   A. Mishra, C.-Q. Ma and P. Bäuerle, *Chem. Rev.*, 2009, **109**, 1141–1276.

24   J. L. Brédas, J. P. Calbert, D. A. da Silva Filho and J. Cornil, *Proc. Natl. Acad. Sci. U. S. A.*, 2002, **99**, 5804–9.

25   D. Eley, *Nature*, 1948, **162**, 819.

26   H. Akamatu and H. Inokuchi, *J. Chem. Phys.*, 1950, **18**, 810–811.

27   H. Akamatu and H. Inokuchi, *J. Chem. Phys.*, 1952, **20**, 1481–1483.

28   R. G. Kepler, *Phys. Rev.*, 1960, **119**, 1226–1229.

29   O. H. LeBlanc, *J. Chem. Phys.*, 1960, **33**, 626–626.

30   O. H. LeBlanc, *J. Chem. Phys.*, 1961, **35**, 1275–1280.

31   D. M. Burland, *Phys. Rev. Lett.*, 1974, **33**, 833–835.

32   R. R. Chance and C. L. Braun, *J. Chem. Phys.*, 1973, **59**, 2269–2272.

33   R. R. Chance and C. L. Braun, *J. Chem. Phys.*, 1976, **64**, 3573–3581.

34   W. Warta, R. Stehle and N. Karl, *Appl. Phys. A Solids Surfaces*, 1985, **36**, 163–170.

35   N. Karl, R. Stehle and W. Warta, *Mol. Cryst. Liq. Cryst.*, 1985, **120**, 247–250.

36   W. Warta and N. Karl, *Phys. Rev. B*, 1985, **32**, 1172–1182.

37   L. B. Schein, *Chem. Phys. Lett.*, 1977, **48**, 571–575.

38   L. B. Schein, C. B. Duke and A. R. McGhie, *Phys. Rev. Lett.*, 1978, **40**, 197–200.

39   L. B. Schein, W. Warta, A. R. McGhie and N. Karl, *Chem. Phys. Lett.*, 1983, **100**, 34–36.

40   C. L. Braun and T. W. Scott, *J. Phys. Chem.*, 1983, **87**, 4776–4778.

41   P. E. Parris, V. M. Kenkre and D. H. Dunlap, *Phys. Rev. Lett.*, 2001, **87**, 126601.

42   V. M. Kenkre, J. D. Andersen, D. H. Dunlap and C. B. Duke, *Phys. Rev. Lett.*, 1989, **62**, 1165–1168.

43   V. M. Kenkre and D. H. Dunlap, *Philos. Mag. Part B*, 1992, **65**, 831–841.

44 H. Scher and M. Lax, *Phys. Rev. B*, 1973, **7**, 4491–4502.

45 H. Scher and E. W. Montroll, *Phys. Rev. B*, 1975, **12**, 2455–2477.

46 V. Coropceanu, J. Cornil, D. A. da S. Filho, Y. Olivier, R. Silbey and J.-L. Bredas, in *Chem. Rev.*, Am. Chem. Soc., 2007, vol. 107, pp. 926–952.

47 G. Horowitz, *Adv. Mater.*, 1998, **10**, 365–377.

48 W. Helfrich and W. G. Schneider, *Phys. Rev. Lett.*, 1965, **14**, 229–231.

49 E. Silinsh and V. Capek, *Organic Molecular Crystals: Interaction, Localization, and Transport Phenomena*, American Institute of Physics, New York, 1994.

50 R. Silbey and R. W. Munn, *J. Chem. Phys.*, 1980, **72**, 2763–2773.

51 S. Fratini and S. Ciuchi, *Phys. Rev. Lett.*, 2003, **91**, 256403.

52 T. Holstein, *Ann. Phys. (N. Y).*, 1959, **8**, 325–342.

53 R. A. Marcus, *J. Chem. Phys.*, 1956, **24**, 966–978.

54 M. Winkler and K. N. Houk, *J. Am. Chem. Soc.*, 2007, **129**, 1805–1815.

55 G. Horowitz, R. Hajlaoui, R. Bourguiga and M. Hajlaoui, *Synth. Met.*, 1999, **101**, 401–404.

56 J. H. Schön, C. Kloc and B. Batlogg, *Phys. Rev. Lett.*, 2001, **86**, 3843–3846.

57 A. Troisi, *Chem. Soc. Rev.*, 2011, **40**, 2347–2358.

58 H. Usta, G. Lu, A. Facchetti and T. J. Marks, *J. Am. Chem. Soc.*, 2006, **128**, 9034–9035.

59 A. Mishra, D. Popovic, A. Vogt, H. Kast, T. Leitner, K. Walzer, M. Pfeiffer, E. Mena-Osteritz and P. Bäuerle, *Adv. Mater.*, 2014, **26**, 7217–7223.

60 S. Subramanian, S. K. Park, S. R. Parkin, V. Podzorov, T. N. Jackson, J. E. Anthony, K. P. Sung, S. R. Parkin, V. Podzorov, T. N. Jackson and J. E. Anthony, *J. Am. Chem. Soc.*, 2008, **130**, 2706–2707.

61 G. R. Llorente, M.-B. Dufourg-Madec, D. J. Crouch, R. G. Pritchard, S. Ogier, S. G. Yeates and Z. Bao, *Chem. Commun.*, 2009, **18**, 3059.

62 A. M. Hiszpanski, Y.-L. Loo, A. L. Briseno, A. J. Crosby, S. Yu, Y. Hou, B. Zou, T. Cui, G. Zou, B. Sundqvist, Z. Luo, H. Li, Y. Li, J. Liu, S. Chen, G. Wang and Y. Liu, *Energy Environ. Sci.*, 2014, **7**, 592–608.

63 H. Okamoto, N. Kawasaki, Y. Kaji, Y. Kubozono, A. Fujiwara and M. Yamaji, *J. Am. Chem. Soc.*, 2008, **130**, 10470–10471.

64 O. D. Jurchescu, M. Popinciuc, B. J. van Wees and T. T. M. Palstra, *Adv. Mater.*, 2007, **19**, 688–692.

65 T. W. Kelley, D. V. Muyres, P. F. Baude, T. P. Smith and T. D. Jones, *MRS Proc.*, 2003, **771**, L6.5.

66 Y. Zhang, H. Dong, Q. Tang, Y. He and W. Hu, *J. Mater. Chem.*, 2010, **20**, 7029–7033.

67 Y. Wang, R. Kumashiro, R. Nouchi, N. Komatsu and K. Tanigaki, *J. Appl. Phys.*, 2009, **105**, 124912.

68 P. Gao, D. Beckmann, H. N. Tsao, X. Feng, V. Enkelmann, M. Baumgarten, W. Pisula and K. Müllen, *Adv. Mater.*, 2009, **21**, 213–216.

69 T. Uemura, Y. Hirose, M. Uno, K. Takimiya and J. Takeya, *Appl. Phys. Express*, 2009, **2**, 111501.

70 H. Ebata, T. Izawa, E. Miyazaki, K. Takimiya, M. Ikeda, H. Kuwabara and T. Yui, *J. Am. Chem. Soc.*, 2007, **129**, 15732–15733.

71 K. Takimiya, H. Ebata, K. Sakamoto, T. Izawa, T. Otsubo and Y. Kunugi, *J. Am. Chem. Soc.*, 2006, **128**, 12604–12605.

72 N. Miyaura and A. Suzuki, *Chem. Rev.*, 1995, **95**, 2457–2483.

73 T. Yamamoto and K. Takimiya, *J. Am. Chem. Soc.*, 2007, **129**, 2224–2225.

74 J. J. H. Gao, R. J. R. Li, Q. Li, Q. Meng, H. Jiang, H. X. H. Li, W. W. P. Hu, L. Q. Li, Q. Meng, H. Jiang, H. X. H. Li and W. W. P. Hu, *Adv. Mater.*, 2007, **19**, 3008–3011.

75 P.-Y. Huang, L.-H. Chen, Y.-Y. Chen, W.-J. Chang, J.-J. Wang, K.-H. Lii, J.-Y. Yan, J.-C. Ho, C.-C. Lee, C. Kim and M.-C. Chen, *Chem. - A Eur. J.*, 2013, **19**, 3721–3728.

76 B. Wex, B. R. Kaafarani and D. C. Neckers, *J. Org. Chem.*, 2004, **69**, 2197–2199.

77 L. Zhang, L. Tan, Z. Wang, W. Hu and D. Zhu, *Chem. Mater.*, 2009, **21**, 1993–1999.

78 M. He and F. Zhang, *J. Org. Chem.*, 2007, **72**, 442–451.

79 J. E. Anthony, *Chem. Rev.*, 2006, **106**, 5028–5048.

80 M. M. Payne, S. R. Parkin, J. E. Anthony, C.-C. Kuo and T. N. Jackson, *J. Am. Chem. Soc.*, 2005, **127**, 4986–4987.

81 M.-H. Yoon, S. A. DiBenedetto, A. Facchetti and T. J. Marks, *J. Am. Chem. Soc.*, 2005, **127**, 1348–1349.

82 M. H. Yoon, C. Kim, A. Facchetti and T. J. Marks, *J. Am. Chem. Soc.*, 2006, **128**, 12851–12869.

83 D. Kumaki, S. Ando, S. Shimono, Y. Yamashita, T. Umeda and S. Tokito, *Appl. Phys. Lett.*, 2007, **90**, 53506.

84 D. Shukla, S. F. Nelson, D. C. Freeman, M. Rajeswaran, W. G. Ahearn, D. M. Meyer and J. T. Carey, *Chem. Mater.*, 2008, **20**, 7486–7491.

85 H. E. Katz, *Chem. Mater.*, 2004, **16**, 4748–4756.

86	H. E. Katz, a. J. Lovinger, J. Johnson, C. Kloc, T. Siegrist, W. Li, Y.-Y. Lin and A. Dodabalapur, *Nature*, 2000, **404**, 478–481.

87	A. Afzali, C. D. Dimitrakopoulos and T. L. Breen, *J. Am. Chem. Soc.*, 2002, **124**, 8812–8813.

88	A. N. Sokolov, S. Atahan-Evrenk, R. Mondal, H. B. Akkerman, R. S. Sánchez-Carrera, S. Granados-Focil, J. Schrier, S. C. B. B. Mannsfeld, A. P. Zoombelt, Z. Bao and A. Aspuru-Guzik, *Nat. Commun.*, 2011, **2**, 437.

89	T. Cramer, T. Steinbrecher, T. Koslowski, D. A. Case, F. Biscarini and F. Zerbetto, *Phys. Rev. B*, 2009, **79**, 155316.

90	S. R. Yost, L.-P. Wang and T. Van Voorhis, *J. Phys. Chem. C*, 2011, **115**, 14431–14436.

91	W. D. Cornell, P. Cieplak, C. I. Bayly, I. R. Gould, K. M. Merz, D. M. Ferguson, D. C. Spellmeyer, T. Fox, J. W. Caldwell and P. A. Kollman, *J. Am. Chem. Soc.*, 1995, **117**, 5179–5197.

92	T. A. Halgren, *J. Comput. Chem.*, 1996, **17**, 490–519.

93	A. K. Rappe, C. J. Casewit, K. S. Colwell, W. A. Goddard and W. M. Skiff, *J. Am. Chem. Soc.*, 1992, **114**, 10024–10035.

94	C. Froese Fischer, *Comput. Phys. Commun.*, 1987, **43**, 355–365.

95	E. Schrödinger, *Phys. Rev.*, 1926, **28**, 1049–1070.

96	M. A. Abdulsattar and K. H. Al-Bayati, *Phys. Rev. B*, 2007, **75**, 245201.

97	M. J. S. Dewar and W. Thiel, *J. Am. Chem. Soc.*, 1977, **99**, 4899–4907.

98	M. J. S. Dewar, E. F. Healy and J. J. P. Stewart, *J. Chem. Soc. Faraday Trans. 2*, 1984, **80**, 227.

99	R. G. Parr, D. P. Craig and I. G. Ross, *J. Chem. Phys.*, 1950, **18**, 1561–1563.

100	L. C. Allen and A. M. Karo, *Rev. Mod. Phys.*, 1960, **32**, 275–285.

101	C. Møller and M. S. Plesset, *Phys. Rev.*, 1934, **46**, 618–622.

102	J. W. Strutt, *Theory of Sound*, Macmillan, 2nd Editio., 1894.

103	H. J. Monkhorst, *Int. J. Quantum Chem.*, 2009, **12**, 421–432.

104	J. A. Pople, M. Head- Gordon and K. Raghavachari, *J. Chem. Phys.*, 1987, **87**, 5968–5975.

105	M. Caffarel and P. Claverie, *J. Chem. Phys.*, 1988, **88**, 1088–1099.

106	J. F. Corney and P. D. Drummond, *Phys. Rev. Lett.*, 2004, **93**, 260401.

107	A. D. Becke, *J. Chem. Phys.*, 2014, **140**, 18A301.

108	A. V. Marenich, C. J. Cramer and D. G. Truhlar, *J. Phys. Chem. B*, 2009, **113**, 6378–6396.

109   J. B. Foresman, T. A. Keith, K. B. Wiberg, J. Snoonian and M. J. Frisch, *J. Phys. Chem.*, 1996, **100**, 16098–16104.

110   V. Barone and M. Cossi, *J. Phys. Chem. A*, 1998, **102**, 1995–2001.

111   M. Cossi, N. Rega, G. Scalmani and V. Barone, *J. Comput. Chem.*, 2003, **24**, 669–681.

112   S. Miertuš and J. Tomasi, *Chem. Phys.*, 1982, **65**, 239–245.

113   J. L. Pascual-ahuir, E. Silla and I. Tuñon, *J. Comput. Chem.*, 1994, **15**, 1127–1138.

114   M. D. Hanwell, D. E. Curtis, D. C. Lonie, T. Vandermeersch, E. Zurek and G. R. Hutchison, *J. Cheminform.*, 2012, **4**, 17.

115   M. J. Frisch, G. W. Trucks, H. B. Schlegel, G. E. Scuseria, M. A. Robb, J. R. Cheeseman, G. Scalmani, V. Barone, G. A. Petersson, H. Nakatsuji, X. Li, M. Caricato, A. Marenich, J. Bloino, B. G. Janesko, R. Gomperts, B. Mennucci, H. P. Hratchian, J. V. Ortiz, A. F. Izmaylov, J. L. Sonnenberg, D. Williams-Young, F. Ding, F. Lipparini, F. Egidi, J. Goings, B. Peng, A. Petrone, T. Henderson, D. Ranasinghe, V. G. Zakrzewski, J. Gao, N. Rega, G. Zheng, W. Liang, M. Hada, M. Ehara, K. Toyota, R. Fukuda, J. Hasegawa, M. Ishida, T. Nakajima, Y. Honda, O. Kitao, H. Nakai, T. Vreven, K. Throssell, J. A. Montgomery, J. E. P. Jr., F. Ogliaro, M. Bearpark, J. J. Heyd, E. Brothers, K. N. Kudin, V. N. Staroverov, T. Keith, R. Kobayashi, J. Normand, K. Raghavachari, A. Rendell, J. C. Burant, S. S. Iyengar, J. Tomasi, M. Cossi, J. M. Millam, M. Klene, C. Adamo, R. Cammi, J. W. Ochterski, R. L. Martin, K. Morokuma, O. Farkas, J. B. Foresman, D. J. Fox, Gaussian, Inc. and Wallingford, 2016.

116   A. D. Becke, *J. Chem. Phys.*, 1993, **98**, 5648–5652.

117   Y. Hu, J. Yin, K. Chaitanya and X.-H. Ju, *Croat. Chem. Acta*, 2016, **89**, 81–90.

118   L. Viani, Y. Olivier, S. Athanasopoulos, D. A. da Silva Filho, J. Hulliger, J.-L. Brédas, J. Gierschner and J. Cornil, *ChemPhysChem*, 2010, **11**, 1062–1068.

119   B. Baumeier, J. Kirkpatrick and D. Andrienko, *Phys. Chem. Chem. Phys.*, 2010, **12**, 11103–11113.

120   S. R. Langhoff, *J. Phys. Chem.*, 1996, **100**, 2819–2841.

121   Y. Hosoi, K. Okamura, Y. Kimura, H. Ishii and M. Niwano, *Appl. Surf. Sci.*, 2005, **244**, 607–610.

122   S. Refaely-Abramson, R. Baer and L. Kronik, *Phys. Rev. B*, 2011, **84**, 75144.

123   P. Sjoberg, J. S. Murray, T. Brinck and P. Politzer, *Can. J. Chem.*, 1990, **68**, 1440–1443.

124   T. Koopmans, *Physica*, 1934, **1**, 104–113.

125   N. Kishimoto, Y. Hagihara, K. Ohno, S. Knippenberg, J.-P. François

and M. S. Deleuze, *J. Phys. Chem. A*, 2005, **109**, 10535–10546.

126   G. Onida, L. Reining and A. Rubio, *Rev. Mod. Phys.*, 2002, **74**, 601–659.

127   T. A. Niehaus, M. Rohlfing, F. Della Sala, A. Di Carlo and T. Frauenheim, *Phys. Rev. A*, 2005, **71**, 22508.

128   D. Danovich, *Wiley Interdiscip. Rev. Comput. Mol. Sci.*, 2011, **1**, 377–387.

129   O. Dolgounitcheva, M. Díaz-Tinoco, V. G. Zakrzewski, R. M. Richard, N. Marom, C. D. Sherrill and J. V. Ortiz, *J. Chem. Theory Comput.*, 2016, **12**, 627–637.

130   H. H. Corzo, A. Galano, O. Dolgounitcheva, V. G. Zakrzewski and J. V. Ortiz, *J. Phys. Chem. A*, 2015, **119**, 8813–8821.

131   M. D?az-Tinoco, O. Dolgounitcheva, V. G. Zakrzewski and J. V. Ortiz, *J. Chem. Phys.*, 2016, **144**, 224110.

132   J. C. Sancho-García and A. J. Pérez-Jiménez, *Phys. Chem. Chem. Phys.*, 2009, **11**, 2741–2746.

133   G. Cappellini, G. Malloci and G. Mulas, *Superlattices Microstruct.*, 2009, **46**, 14–18.

134   G. Malloci, G. Mulas, G. Cappellini and C. Joblin, *Chem. Phys.*, 2007, **340**, 43–58.

135   G. Malloci, G. Cappellini, G. Mulas and A. Mattoni, *Chem. Phys.*, 2011, **384**, 19–27.

136   S. C. B. Mannsfeld, A. Virkar, C. Reese, M. F. Toney and Z. Bao, *Adv. Mater.*, 2009, **21**, 2294–2298.

137   J. Cosier, A. M. Glazer and IUCr, *J. Appl. Crystallogr.*, 1986, **19**, 105–107.

138   CrysAlisPro, Rigaku Oxford Diffraction | Rigaku - X-ray analytical instrumentation, http://www.rigaku.com/en/rigakuoxford, (accessed 16 April 2017).

139   G. M. Sheldrick, *Acta Crystallogr. Sect. A Found. Crystallogr.*, 2008, **64**, 112–122.

140   G. M. Sheldrick, *Acta Crystallogr. Sect. A Found. Adv.*, 2015, **71**, 3–8.

141   G. M. Sheldrick, *Acta Crystallogr. Sect. C Struct. Chem.*, 2015, **71**, 3–8.

142   O. V. Dolomanov, L. J. Bourhis, R. J. Gildea, J. A. K. Howard and H. Puschmann, *J. Appl. Crystallogr.*, 2009, **42**, 339–341.

143   C. F. Macrae, I. J. Bruno, J. A. Chisholm, P. R. Edgington, P. McCabe, E. Pidcock, L. Rodriguez-Monge, R. Taylor, J. van de Streek and P. A. Wood, *J. Appl. Crystallogr.*, 2008, **41**, 466–470.

144   T.-H. H. Kwon, V. Armel, A. Nattestad, D. R. MacFarlane, U. Bach, S. J. Lind, K. C. Gordon, W. Tang, D. J. Jones and A. B. Holmes, *J. Org.*

Chem., 2011, **76**, 4088–4093.

145 F. Liu, L.-H. Xie, C. Tang, J. Liang, Q.-Q. Chen, B. Peng, W. Wei, Y. Cao and W. Huang, *Org. Lett.*, 2009, **11**, 3850–3853.

146 S. Sergeyev, W. Pisula and Y. H. Geerts, *Chem. Soc. Rev.*, 2007, **36**, 1902.

147 H. Xia, D. Liu, X. Xu, Q. Miao, J.-L. Brédas, K. Matsumoto, H. Kurata, T. Kubo, S. Shinamura, H. Mori, E. Miyazaki and K. Takimiya, *Chem. Commun.*, 2013, **49**, 4301–4303.

148 Y.-C. Chang, M.-Y. Kuo, C.-P. Chen, H.-F. Lu and I. Chao, *J. Phys. Chem. C*, 2010, **114**, 11595–11601.

149 M. Bendikov, F. Wudl and D. F. Perepichka, *Chem. Rev.*, 2004, **104**, 4891–4946.

150 S. R. Forrest, *Nature*, 2004, **428**, 911–918.

151 S. Logothetidis, *Mater. Sci. Eng. B*, 2008, **152**, 96–104.

152 J. Lewis, *Mater. Today*, 2006, **9**, 38–45.

153 X.-Y. Zhu, Q. Yang and M. Muntwiler, *Acc. Chem. Res.*, 2009, **42**, 1779–1787.

154 O. D. Jurchescu, J. Baas and T. T. M. Palstra, *Appl. Phys. Lett.*, 2004, **84**, 3061–3063.

155 S. F. Nelson, Y. Y. Lin, D. J. Gundlach and T. N. Jackson, *Appl. Phys. Lett.*, 1998, **72**, 1854–1856.

156 H. Klauk, M. Halik, U. Zschieschang, G. Schmid, W. Radlik and W. Weber, *J. Appl. Phys.*, 2002, **92**, 5259–5263.

157 D. J. Gundlach, Y. Y. Lin, T. N. Jackson, S. F. Nelson and D. G. Schlom, *IEEE Electron Device Lett.*, 1997, **18**, 87–89.

158 Y.-Y. Lin, D. J. Gundlach, S. F. Nelson and T. N. Jackson, *IEEE Electron Device Lett.*, 1997, **18**, 606–608.

159 R. Mitsuhashi, Y. Suzuki, Y. Yamanari, H. Mitamura, T. Kambe, N. Ikeda, H. Okamoto, A. Fujiwara, M. Yamaji, N. Kawasaki, Y. Maniwa and Y. Kubozono, *Nature*, 2010, **464**, 76–79.

160 Y. Wang, S. Di Motta, F. Negri and R. Friedlein, *J. Am. Chem. Soc.*, 2011, **133**, 10054–10057.

161 O. Mitrofanov, D. V. Lang, C. Kloc, J. M. Wikberg, T. Siegrist, W.-Y. So, M. A. Sergent and A. P. Ramirez, *Phys. Rev. Lett.*, 2006, **97**, 166601.

162 C.-K. Lu and H.-F. Meng, *Phys. Rev. B*, 2007, **75**, 235206.

163 H. Najafov, D. Mastrogiovanni, E. Garfunkel, L. C. Feldman and V. Podzorov, *Adv. Mater.*, 2011, **23**, 981–985.

164 E. Clar, *Polycyclic Hydrocarbons*, Springer Berlin Heidelberg, Berlin, Heidelberg, 1964.

165 M. Solà, *Front. Chem.*, 2013, **1**, 22.

166 T. P. Nguyen, J. H. Shim and J. Y. Lee, *J. Phys. Chem. C*, 2015, **119**, 11301–11310.

167 K. Pelzer, L. Greenman, G. Gidofalvi and D. A. Mazziotti, *J. Phys. Chem. A*, 2011, **115**, 5632–5640.

168 J. Aihara, *Bull. Chem. Soc. Jpn.*, 2008, **81**, 241–247.

169 T. Matsumoto, U. Nagashima, K. Tanabe and S. Ono, *J. Comput. Chem. Japan*, 2003, **2**, 63–70.

170 D. Vasu, H. Yorimitsu and A. Osuka, *Angew. Chemie Int. Ed.*, 2015, **54**, 7162–7166.

171 M. Iwasaki, Y. Araki, S. Iino and Y. Nishihara, *J. Org. Chem.*, 2015, **80**, 9247–9263.

172 P. I. Djurovich, E. I. Mayo, S. R. Forrest and M. E. Thompson, *Measurement of the lowest unoccupied molecular orbital energies of molecular organic semiconductors*, 2009, vol. 10.

173 N. E. Gruhn, D. A. da Silva Filho, T. G. Bill, M. Malagoli, V. Coropceanu, A. Kahn and J.-L. Br?das, *J. Am. Chem. Soc.*, 2002, **124**, 7918–7919.

174 R. Cardia, G. Malloci, A. Bosin, G. Serra and G. Cappellini, *Chem. Phys.*, 2016, **478**, 8–13.

175 J. C. Sancho-García, *Chem. Phys.*, 2007, **331**, 321–331.

176 J. C. Sancho-García and A. J. Pérez-Jiménez, *J. Chem. Phys.*, 2014, **141**, 134708.

177 A. Modelli and L. Mussoni, *Chem. Phys.*, 2007, **332**, 367–374.

178 D. S. Sabirov, *Comput. Theor. Chem.*, 2014, **1030**, 81–86.

179 S. Kivelson and O. L. Chapman, *Phys. Rev. B*, 1983, **28**, 7236–7243.

180 M. Nendel, K. N. Houk, L. M. Tolbert, E. Vogel, H. Jiao and P. von Ragué Schleyer, *Angew. Chemie Int. Ed. English*, 1997, **36**, 748–750.

181 M. Bendikov, H. M. Duong, K. Starkey, K. N. Houk, E. A. Carter and F. Wudl, *J. Am. Chem. Soc.*, 2004, **126**, 7416–7417.

182 C. K. Chiang, C. R. Fincher, Y. W. Park, A. J. Heeger, H. Shirakawa, E. J. Louis, S. C. Gau and A. G. MacDiarmid, *Phys. Rev. Lett.*, 1977, **39**, 1098–1101.

183 V. Subramanian, P. C. Chang, J. B. Lee, S. E. Molesa and S. K. Volkman, *IEEE Trans. Components Packag. Technol.*, 2005, **28**, 742–747.

184 G. H. Gelinck, H. E. A. Huitema, E. van Veenendaal, E. Cantatore, L. Schrijnemakers, J. B. P. H. van der Putten, T. C. T. Geuns, M. Beenhakkers, J. B. Giesbers, B.-H. Huisman, E. J. Meijer, E. M. Benito, F. J. Touwslager, A. W. Marsman, B. J. E. van Rens and D. M. de Leeuw, *Nat. Mater.*, 2004, **3**, 106–110.

185 J. Jacobson, B. Comiskey, J. D. Albert and H. Yoshizawa, *Nature*, 1998, **394**, 253–255.

186 A. N. Sokolov, M. E. Roberts and Z. Bao, *Mater. Today*, 2009, **12**, 12–20.

187 T. Manaka, E. Lim, R. Tamura and M. Iwamoto, *Nat. Photonics*, 2007, **1**, 581–584.

188 J. Butet, J. Duboisset, G. Bachelier, I. Russier-Antoine, E. Benichou, C. Jonin and P.-F. Brevet, *Nano Lett.*, 2010, **10**, 1717–1721.

189 G. J. Ashwell, R. C. Hargreaves, C. E. Baldwin, G. S. Bahra and C. R. Brown, *Nature*, 1992, **357**, 393–395.

190 K. B. Eisenthal, , DOI:10.1021/CR0403685.

191 R. D. Wampler, D. J. Kissick, C. J. Dehen, E. J. Gualtieri, J. L. Grey, H.-F. Wang, D. H. Thompson, J.-X. Cheng and G. J. Simpson, *J. Am. Chem. Soc.*, 2008, **130**, 14076–14077.

192 B. Champagne, A. Plaquet, J.-L. Pozzo, V. Rodriguez and F. Castet, *J. Am. Chem. Soc.*, 2012, **134**, 8101–8103.

193 L. Zhu, Y. Zhao, Q.-C. Wang, X. Ma, Z.-F. Chen, H. Tian, Y. Zhao, Y. Geerts, U. Scherf, K. Müllen and B. Z. Tang, *J. Mater. Chem. C*, 2013, **1**, 1059–1065.

194 L. H. Klemm, D. R. Mccoy and D. R. Olson, *J. Heterocycl. Chem.*, 1970, **7**, 1347–1352.

195 F. N. Bilheri, A. L. Stein and G. Zeni, *Adv. Synth. Catal.*, 2015, **357**, 1221–1228.

196 S. Canola, C. Pecoraro and F. Negri, *Theor. Chem. Acc.*, 2016, **135**, 33.

197 G. R. Hutchison, M. A. Ratner and T. J. Marks, *J. Am. Chem. Soc.*, 2005, **127**, 2339–2350.

198 Toshihiro Okamoto, Kenichi Kudoh, and Atsushi Wakamiya, S. Yamaguchi*, T. Okamoto, K. Kudoh, A. Wakamiya and S. Yamaguchi, *Org. Lett.*, 2005, **7**, 5301–5304.

199 X. Qi, S. Zou, X. Liu, W. Hao, H. H. Zhang, Z. Zang, H. H. Zhang, J. Gao and W. Hu, *New J. Chem.*, 2015, **39**, 1045–1050.

200 Y. Liu, C. Di, C. Du, Y. Liu, K. Lu, W. Qiu and G. Yu, *Chem. - A Eur. J.*, 2010, **16**, 2231–2239.

201 M. L. Tang, A. D. Reichardt, P. Wei and Z. Bao, *J. Am. Chem. Soc.*, 2009, **131**, 5264–5273.

202 R. Zhu, Y.-A. Duan, Y. Geng, C.-Y. Wei, X.-Y. Chen and Y. Liao, *Comput. Theor. Chem.*, 2016, **1078**, 16–22.

203 C. W. Dirk, R. J. Twieg and G. Wagniere, *J. Am. Chem. Soc.*, 1986, **108**, 5387–5395.

204 D. P. Shelton and J. E. Rice, *Chem. Rev.*, 1994, **94**, 3–29.

205 J. Abe, Y. Shirai, N. Nemoto and Y. Nagase, *J. Phys. Chem. B*, 1997, **101**, 1910–1915.

206 M. Nakano and K. Yamaguchi, *Chem. Phys. Lett.*, 1993, **206**, 285–292.

207 F. Pan, M. S. Wong, V. Gramlich, C. Bosshard and P. Günter, *J. Am. Chem. Soc.*, 1996, **118**, 6315–6316.

208 H.-C. Lin, W.-Y. Lin, H.-T. Bai, J.-H. Chen, B.-Y. Jin and T.-Y. Luh, *Angew. Chemie Int. Ed.*, 2007, **46**, 897–900.

209 C. Lambert, S. Stadler, G. Bourhill and C. Bräuchle, *Angew. Chemie Int. Ed. English*, 1996, **35**, 644–646.

210 S. Ohta, M. Nakano, T. Kubo, K. Kamada, K. Ohta, R. Kishi, N. Nakagawa, B. Champagne, E. Botek, A. Takebe, S. Umezaki, M. Nate, H. Takahashi, S. Furukawa, Y. Morita, K. Nakasuji and K. Yamaguchi, *J. Phys. Chem. A*, 2007, **111**, 3633–3641.

211 O.-K. Kim, A. Fort, M. Barzoukas, M. Blanchard-Desce, J.-M. Lehn, G. Puccetti, I. Ledoux, J. Zyss and J. Zyss, *J. Mater. Chem.*, 1999, **9**, 2227–2232.

212 N. Asao, T. Nogami, S. Lee and Y. Yamamoto, *J. Am. Chem. Soc.*, 2003, **125**, 10921–10925.

213 J. Luo and H. Hart, *J. Org. Chem.*, 1987, **52**, 4833–4836.

214 A. Criado, D. Peña, A. Cobas and E. Guitián, *Chem. - A Eur. J.*, 2010, **16**, 9736–9740.

215 A. G. Lvov, V. Z. Shirinian, A. V. Zakharov, M. M. Krayushkin, V. V. Kachala and I. V. Zavarzin, *J. Org. Chem.*, 2015, **80**, 11491–11500.

216 B. Wex, F. M. Jradi, D. Patra and B. R. Kaafarani, *Tetrahedron*, 2010, **66**, 8778–8784.

217 L. Liu and P. E. Floreancig, *Org. Lett.*, 2010, **12**, 4686–9.

218 S. T. Gadge and B. M. Bhanage, *RSC Adv.*, 2014, **4**, 10367.

219 M. Schnürch, M. Spina, A. F. Khan, M. D. Mihovilovic and P. Stanetty, *Chem. Soc. Rev.*, 2007, **36**, 1046–1057.

220 L. Jones and B. J. Whitaker, *J. Comput. Chem.*, 2016, **37**, 1697–1703.

221 M. Melucci, L. Favaretto, C. Bettini, M. Gazzano, N. Camaioni, P. Maccagnani, P. Ostoja, M. Monari and G. Barbarella, *Chem. - A Eur. J.*, 2007, **13**, 10046–10054.

222 J. E. Mcmurry, *Acc. Chem. Res*, 1983, **16**, 405–411.

223 F. Allared, J. Hellberg and T. Remonen, *Tetrahedron Lett.*, 2002, **43**, 1553–1554.

224 Y. Suzaki, K. Shimada, E. Chihara, T. Saito, Y. Tsuchido and K. Osakada, *Org. Lett.*, 2011, **13**, 3774–3777.

225 M. Ashizawa, T. Niimura, Y. Yu, K. Tsuboi, H. Matsumoto, R. Yamada,

S. Kawauchi, A. Tanioka and T. Mori, *Tetrahedron*, 2012, **68**, 2790–2798.

226   J. L. Brusso, O. D. Hirst, A. Dadvand, S. Ganesan, F. Cicoira, C. M. Robertson, R. T. Oakley, F. Rosei and D. F. Perepichka, *Chem. Mater.*, 2008, **20**, 2484–2494.

227   S. Y. Kang, K.-S. Song, J. Lee, S.-H. Lee and J. Lee, *Bioorg. Med. Chem.*, 2010, **18**, 6069–6079.

228   M. Ohtawa, S. Ogihara, K. Sugiyama, K. Shiomi, Y. Harigaya, T. Nagamitsu and S. Ōmura, *J. Antibiot. (Tokyo).*, 2009, **62**, 289–294.

229   P. Schuisky, H.-J. Federsel and W. Tian, *J. Org. Chem.*, 2012, **77**, 5503–5514.

230   C. E. Moyer Jr. and J. F. Bunnett, *J. Am. Chem. Soc.*, 1963, **85**, 1891–1893.

231   A. Vaitiekunas and F. F. Nord, *J. Am. Chem. Soc.*, 1953, **75**, 1764–1768.

232   X. Duan, X.-F. Duan and Z.-B. Zhang, *Heterocycles*, 2005, **65**, 2005.

233   T. Kojima and S. Hiraoka, *Org. Lett.*, 2014, **16**, 1024–1027.

234   J. Frohlich and C. Hametner, *Monatshefte fur Chemie Chem. Mon.*, 1996, **127**, 435–443.

235   F. Sauter, J. Frolich and K. Blasl, *Heterocycles*, 1994, **37**, 1879.

236   E. L. Stangeland and T. Sammakia, *J. Org. Chem.*, 2004, **69**, 2381–2385.

237   P. Stanetty, M. Spina and M. D. Mihovilovic, *Synlett*, 2005, **2005**, 1433–1434.

238   M. J. Pieterse and H. J. Denhertog, *Recl. des Trav. Chim. des Pays-Bas*, 1962, **81**, 855–863.

239   J. Fröhlich, C. Hametner and W. Kalt, *Monatsh. Chem.*, 1996, **127**, 325–330.

240   A. Vaitiekunas and F. F. NORD, *Nature*, 1951, **168**, 875–876.

241   D. Lumpi, C. Wagner, M. Schöpf, E. Horkel, G. Ramer, B. Lendl and J. Fröhlich, *Chem. Commun.*, 2012, **48**, 2451–2453.

242   G. Fraenkel, S. Subramanian and A. Chow, *J. Am. Chem. Soc.*, 1995, **117**, 6300–6307.

243   A. Streitwieser, J. R. Reyes, T. Singhapricha, S. Vu and K. Shah, *J. Org. Chem.*, 2010, **75**, 3821–3830.

244   A. Corruble, D. Davoust, S. Desjardins, C. Fressigné, C. Giessner-Prettre, A. Harrison-Marchand, H. Houte, M.-C. C. Lasne, J. Maddaluno, H. Oulyadi and J.-Y. Y. Valnot, *J. Am. Chem. Soc.*, 2002, **124**, 15267–15279.

245   C. Fressigné, A. Corruble, J.-Y. Valnot, J. Maddaluno and C.

Giessner-Prettre, *J. Organomet. Chem.*, 1997, **549**, 81–88.

246   M. Tacke, *Eur. J. Inorg. Chem.*, 1998, **1998**, 537–541.

247   O. A. Vydrov and G. E. Scuseria, *J. Chem. Phys.*, 2006, **125**, 234109.

248   S. Grimme, S. Ehrlich and L. Goerigk, *J. Comput. Chem.*, 2011, **32**, 1456–1465.

249   J. Tomasi, B. Mennucci and R. Cammi, *Chem. Rev.*, 2005, **105**, 2999–3094.

250   Y. S. Yang, T. Yasuda, H. Kakizoe, H. Mieno, H. Kino, Y. Tateyama and C. Adachi, *Chem. Commun. (Camb).*, 2013, **49**, 6483–5.

251   J. Li, H.-S. Tan, Z.-K. Chen, W.-P. Goh, H.-K. Wong, K.-H. Ong, W. Liu, C. M. Li and B. S. Ong, *Macromolecules*, 2011, **44**, 690–693.

252   J. Frey, A. D. Bond and A. B. Holmes, *Chem. Commun.*, 2002, 2424–2425.

253   M.-C. Chen, Y.-J. Chiang, C. Kim, Y.-J. Guo, S.-Y. Chen, Y.-J. Liang, Y.-W. Huang, T.-S. Hu, G.-H. Lee, A. Facchetti and T. J. Marks, *Chem. Commun.*, 2009, 1846–1848.

254   W. You, X. Yan, Q. Liao and C. Xi, *Org. Lett.*, 2010, **12**, 3930–3933.

255   T. Ozturk, E. Ertas and O. Mert, *Tetrahedron*, 2005, **61**, 11055–11077.

256   H. Yu, M. Zhang and Y. Li, *J. Org. Chem.*, 2013, **78**, 8898–8903.

257   P. Oechsle and J. Paradies, *Org. Lett.*, 2014, **16**, 4086–4089.

258   M. Kuhn, F. C. Falk and J. Paradies, *Org. Lett.*, 2011, **13**, 4100–4103.

259   P. Zhao, H. Yin, H. Gao and C. Xi, *J. Org. Chem.*, 2013, **78**, 5001–5006.

260   L.-L. Sun, C.-L. Deng, R.-Y. Tang and X.-G. Zhang, *J. Org. Chem.*, 2011, **76**, 7546–7550.

261   M. Melucci, L. Favaretto, C. Bettini, M. Gazzano, N. Camaioni, P. Maccagnani, P. Ostoja, M. Monari and G. Barbarella, *Chem. - A Eur. J.*, 2007, **13**, 10046–10054.

262   W. Yue, A. Lv, J. Gao, W. Jiang, L. Hao, C. Li, Y. Li, L. E. Polander, S. Barlow, W. Hu, S. Di Motta, F. Negri, S. R. Marder and Z. Wang, *J. Am. Chem. Soc.*, 2012, **134**, 5770–5773.

263   K.-T. Wong, T. S. Hung, Y. Lin, C.-C. Wu, G.-H. Lee, S.-M. Peng, C. H. Chou and Y. O. Su, *Org. Lett.*, 2002, **4**, 513–516.

264   K. Mitsudo, H. Sato, A. Yamasaki, N. Kamimoto, J. Goto, H. Mandai and S. Suga, *Org. Lett.*, 2015, **17**, 4858–4861.

265   T. Yasukawa, T. Satoh, M. Miura and M. Nomura, *J. Am. Chem. Soc.*, 2002, **124**, 12680–12681.

266   H. Aramoto, Y. Obora and Y. Ishii, *J. Org. Chem.*, 2009, **74**, 628–633.

267   R. Rieger, D. Beckmann, W. Pisula, M. Kastler and K. Müllen, *Macromolecules*, 2010, **43**, 6264–6267.

268   B. Liu, R. Wang, W. Mi, X. Li and H. Yu, *J. Mater. Chem.*, 2012, **22**, 15379–15387.

269   G. Dyker, D. Hildebrandt, J. Liu and K. Merz, *Angew. Chemie Int. Ed.*, 2003, **42**, 4399–4402.

270   T. Yao, M. A. Campo and R. C. Larock, *J. Org. Chem.*, 2005, **70**, 3511–3517.

271   K. Takimiya, Y. Kunugi, H. Ebata and T. Otsubo, *Chem. Lett.*, 2006, **35**, 1200–1201.

272   Y. M. Sun, K. Xiao, Y. Q. Liu, J. L. Wang, J. Pei, G. Yu and D. B. Zhu, *Adv. Funct. Mater.*, 2005, **15**, 818–822.

273   H. Wang, Y. Wen, X. Yang, Y. Wang, W. Zhou, S. Zhang, X. Zhan, Y. Liu, Z. Shuai and D. Zhu, *ACS Appl. Mater. Interfaces*, 2009, **1**, 1122–1129.

274   M. Beesu and M. Periasamy, *J. Organomet. Chem.*, 2012, **705**, 30–33.

275   H. Siebeneicher and S. Doye, *European J. Org. Chem.*, 2002, **2002**, 1213–1220.

276   T. Shoji, S. Ito, K. Toyota, M. Yasunami and N. Morita, *Chem. - A Eur. J.*, 2008, **14**, 8398–8408.

277   K. A. Leonard, M. I. Nelen, L. T. Anderson, S. L. Gibson, R. Hilf and M. R. Detty, *J. Med. Chem.*, 1999, **42**, 3942–3952.

278   S. Altomonte, G. L. Baillie, R. A. Ross and M. Zanda, *RSC Adv.*, 2015, **5**, 13692–13701.

279   S. Hiraoka, M. Shiro and M. Shionoya, *J. Am. Chem. Soc.*, 2004, **126**, 1214–1218.

280   M. Yamashita, K. Hirano, T. Satoh and M. Miura, *Org. Lett.*, 2009, **11**, 2337–2340.

281   Z. Shi, S. Ding, Y. Cui and N. Jiao, *Angew. Chemie Int. Ed.*, 2009, **48**, 7895–7898.

282   J.-R. Huang, Q.-R. Zhang, C.-H. Qu, X.-H. Sun, L. Dong and Y.-C. Chen, *Org. Lett.*, 2013, **15**, 1878–1881.

283   V. D. Bock, H. Hiemstra and J. H. van Maarseveen, *European J. Org. Chem.*, 2006, **2006**, 51–68.

284   B. R. Buckley, S. E. Dann, D. P. Harris, H. Heaney and E. C. Stubbs, *Chem. Commun.*, 2010, **46**, 2274–2276.

285   G. Zeni and R. C. Larock, *Chem. Rev.*, 2004, **104**, 2285–2310.

286   R. Ding, Y. Li, C. Tao, B. Cheng and H. Zhai, *Org. Lett.*, 2015, **17**, 3994–3997.

287   T. P. Willumstad, P. D. Boudreau and R. L. Danheiser, *J. Org. Chem.*, 2015, **80**, 11794–11805.

288   N. S. Baek, S. K. Hau, H.-L. Yip, O. Acton, K.-S. Chen and A. K.-Y.

Jen, *Chem. Mater.*, 2008, **20**, 5734–5736.

289 T. Michinobu, C. Boudon, J.-P. P. Gisselbrecht, P. Seiler, B. Frank, N. N. P. Moonen, M. Gross and F. Diederich, *Chem. - A Eur. J.*, 2006, **12**, 1889–1905.

290 F. Nisic, A. Colombo, C. Dragonetti, E. Garoni, D. Marinotto, S. Righetto, F. De Angelis, M. G. Lobello, P. Salvatori, P. Biagini and F. Melchiorre, *Organometallics*, 2015, **34**, 94–104.

291 W. Hong, D. Z. Manrique, P. Moreno-Garc??a, M. Gulcur, A. Mishchenko, C. J. Lambert, M. R. Bryce, T. Wandlowski, P. Moreno-García, M. Gulcur, A. Mishchenko, C. J. Lambert, M. R. Bryce and T. Wandlowski, *J. Am. Chem. Soc.*, 2012, **134**, 2292–2304.

292 R. J.-P. Corriu, T. Deforth, W. E. Douglas, G. Guerrero, T. Deforth and W. S. Siebert, *Chem. Commun.*, 1998, **0**, 963–964.

293 X. Qu, T. Li, P. Sun, Y. Zhu, H. Yang and J. Mao, *Org. Biomol. Chem.*, 2011, **9**, 6938.

294 G. García, J. M. Granadino-Roldán, A. Garzón, M. Moral, T. Peña-Ruiz, A. Navarro, M. P. Fernández-Liencres and M. Fernández-Gómez, *J. Phys. Chem. C*, 2010, **114**, 12325–12334.

295 E. Paegle, S. Belyakov, M. Petrova, E. Liepinsh and P. Arsenyan, *European J. Org. Chem.*, 2015, **2015**, 4389–4399.

296 J. G. Rodriguez, A. Lafuente, L. Rubio and J. Esquivias, *Tetrahedron Lett.*, 2004, **45**, 7061–7064.

297 K. Kishikawa, M. C. Harris and T. M. Swager, *Chem. Mater.*, 1999, **11**, 867–871.

298 R. Mishra and J. Sankar, *RSC Adv.*, 2013, **3**, 10658.

299 P. Li, B. Ahrens, N. Feeder, P. R. Raithby, S. J. Teat and M. S. Khan, *Dalton Trans.*, 2005, 874–83.

300 A. Seidler, J. Svoboda, V. Dekoj, J. V. Chocholoušová, J. Vacek, I. G. Stará and I. Starý, *Tetrahedron Lett.*, 2013, **54**, 2795–2798.

301 H. H. Shah, R. A. Al-Balushi, M. K. Al-Suti, M. S. Khan, C. H. Woodall, K. C. Molloy, P. R. Raithby, T. P. Robinson, S. E. C. Dale and F. Marken, *Inorg. Chem.*, 2013, **52**, 4898–4908.

302 T. Okujima, A. Toda, Y. Miyashita, A. Nonoshita, H. Yamada, N. Ono and H. Uno, *Heterocycles*, 2012, **86**, 637.

303 L. Sudha Devi, M. K. Al-Suti, N. Zhang, S. J. Teat, L. Male, H. A. Sparkes, P. R. Raithby, M. S. Khan and A. Köhler, *Macromolecules*, 2009, **42**, 1131–1141.

304 M. Jothi and P. Kumaradhas, *Comput. Theor. Chem.*, 2012, **1000**, 10–18.

305 K. W. J. Heard, J. J. Morrison, L. Weston, C. H. Lo, L. Pirvu, J. Raftery, M. S. Little, J. J. W. McDouall, S. G. Yeates and P. Quayle, *Chem. Commun.*, 2015, **51**, 6115–6118.

306 H. Klauk, U. Zschieschang, R. T. Weitz, H. Meng, F. Sun, G. Nunes, D. E. Keys, C. R. Fincher and Z. Xiang, *Adv. Mater.*, 2007, **19**, 3882–3887.

307 R. J. Chesterfield, J. C. McKeen, C. R. Newman, P. C. Ewbank, D. A. da Silva Filho, J.-L. Brédas, L. L. Miller, K. R. Mann and C. D. Frisbie, *J. Phys. Chem. B*, 2004, **108**, 19281–19292.

308 V. T. T. Huong, T. B. Tai and M. T. Nguyen, *Phys. Chem. Chem. Phys.*, 2012, **14**, 14832–14841.

309 C. R. Newman, C. D. Frisbie, D. A. da S. Filho, J.-L. Brédas, P. C. Ewbank and K. R. Mann, *Chem. Mater.*, 2004, **16**, 4436–4451.

310 C. Wang, Z. Wei, Q. Meng, H. Zhao, W. Xu, H. Li and W. Hu, *Org. Electron. physics, Mater. Appl.*, 2010, **11**, 544–551.

311 M. E. Cinar and T. Ozturk, *Chem. Rev.*, 2015, **115**, 3036–3140.

312 K. Sonogashira, *Development of Pd–Cu catalyzed cross-coupling of terminal acetylenes with sp2-carbon halides*, 2002, vol. 653.

313 R. S. Sánchez-Carrera, V. Coropceanu, D. A. da Silva Filho, R. Friedlein, W. Osikowicz, R. Murdey, C. Suess, W. R. Salaneck and J.-L. Brédas, *J. Phys. Chem. B*, 2006, **110**, 18904–18911.

314 M. Grätzel, *J. Photochem. Photobiol. C Photochem. Rev.*, 2003, **4**, 145–153.

315 M. Grätzel, *J. Photochem. Photobiol. A Chem.*, 2004, **164**, 3–14.

316 L.-N. Du, Y.-Y. Yang, G. Li, S. Wang, X.-M. Jia and Y.-H. Zhao, *Int. Biodeterior. Biodegradation*, 2010, **64**, 566–573.

317 W. Chai and M. Liebman, *J. Urol.*, 2004, **172**, 953–957.

318 M. K. Nazeeruddin, S. M. Zakeeruddin, R. Humphry-Baker, M. Jirousek, P. Liska, Vlachopoulos, N. V. Shklover, C.-H. Fischer and M. Grätzel, *Inorg. Chem.*, 1999, **38**, 6298–6305.

319 J. Grzechulska and A. W. Morawski, *Appl. Catal. B Environ.*, 2002, **36**, 45–51.

320 J. Griffiths and R. Marsden, *Chem. Commun.*, 1998, **6**, 1349–1350.

321 T. Horiuchi, H. Miura, K. Sumioka and S. Uchida, *J. Am. Chem. Soc.*, 2004, **126**, 12218–12219.

322 H. Tian, X. Yang, R. Chen, A. Hagfeldt and L. Sun, *Energy Environ. Sci.*, 2009, **2**, 674.

323 CN105646528A, 2016.

324 T. Shoji, S. Ito, K. Toyota, T. Iwamoto, M. Yasunami and N. Morita, *European J. Org. Chem.*, 2009, **2009**, 4316–4324.

325 T. Shoji, J. Higashi, S. Ito, T. Okujima, M. Yasunami and N. Morita, *Chem. - A Eur. J.*, 2011, **17**, 5116–5129.

326 J. Ryu, J. Dai, K. Koo and T. Wakida, *J. Soc. Dye. Colour.*, 1992, **108**,

278–282.

Appendix A

Single-Crystal X-Ray Structure Refinement Data

Table 30. Crystal data and structure refinement for the core molecular fragment **51**.
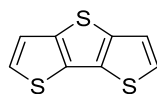
Identification code	LJ171214_Mo
Empirical formula	$C_8H_4S_3$
Formula weight	196.29
Temperature/K	120.01(11)
Crystal system	monoclinic
Space group	$P2_1/c$
a/Å	10.2883(12)
b/Å	3.9439(4)
c/Å	19.3432(18)
α/°	90.00
β/°	102.647(10)
γ/°	90.00
Volume/Å^3	765.84(14)
Z	4
ρ_{calc}g/cm^3	1.702
μ/mm^{-1}	0.883
F(000)	400.0
Crystal size/mm^3	0.36 × 0.13 × 0.07
Radiation	MoKα (λ = 0.71073)
2Θ range for data collection/°	6.54 to 56.52
Index ranges	-13 ≤ h ≤ 12, -5 ≤ k ≤ 5, -17 ≤ l ≤ 25
Reflections collected	4494
Independent reflections	1897 [R_{int} = 0.0708, R_{sigma} = 0.0807]
Data/restraints/parameters	1897/0/100
Goodness-of-fit on F^2	1.229
Final R indexes [I>=2σ (I)]	R_1 = 0.1067, wR_2 = 0.2699
Final R indexes [all data]	R_1 = 0.1174, wR_2 = 0.2749
Largest diff. peak/hole / e Å^{-3}	1.28/-0.76

Table 31. Crystal data and structure refinement for the oligo-fused heteroacene compound **152**.
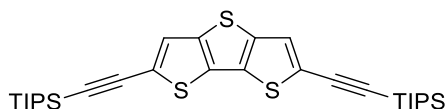
Identification code	LJ48iii_Mo
Empirical formula	$C_{30}H_{44}S_3Si_2$
Formula weight	557.01
Temperature/K	120.03(10)
Crystal system	monoclinic
Space group	I2/a
a/Å	21.1832(17)
b/Å	6.8954(3)
c/Å	23.3507(15)
α/°	90.00
β/°	113.436(9)
γ/°	90.00
Volume/Å^3	3129.4(4)
Z	4
ρ_{calc}g/cm^3	1.182
μ/mm^{-1}	0.331
F(000)	1200.0
Crystal size/mm^3	0.21 × 0.16 × 0.13
Radiation	MoKα (λ = 0.71073)
2Θ range for data collection/°	6.2 to 52.74
Index ranges	-26 ≤ h ≤ 22, -8 ≤ k ≤ 8, -29 ≤ l ≤ 29
Reflections collected	11120
Independent reflections	3191 [R_{int} = 0.0482, R_{sigma} = 0.0476]
Data/restraints/parameters	3191/0/165
Goodness-of-fit on F^2	1.044
Final R indexes [I>=2σ (I)]	R_1 = 0.0371, wR_2 = 0.0792
Final R indexes [all data]	R_1 = 0.0464, wR_2 = 0.0840
Largest diff. peak/hole / e Å^{-3}	0.33/-0.25

Table 32. Crystal data and structure refinement for the oligo-fused heteroacene compound **155**.
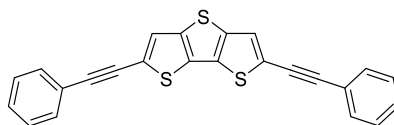
Identification code	LJ236_Cu_c
Empirical formula	$C_{24}H_{12}S_3$
Formula weight	396.52
Temperature/K	120.00(10)
Crystal system	orthorhombic
Space group	$P2_12_12_1$
a/Å	5.13090(6)
b/Å	17.0690(2)
c/Å	20.4378(3)
α/°	90
β/°	90
γ/°	90
Volume/Å^3	1789.93(4)
Z	4
ρ_{calc}g/cm^3	1.471
μ/mm^{-1}	3.816
F(000)	816.0
Crystal size/mm^3	0.34 × 0.12 × 0.09
Radiation	Cu Kα (λ = 1.54184)
2Θ range for data collection/°	6.746 to 147.904
Index ranges	-6 ≤ h ≤ 6, -20 ≤ k ≤ 21, -24 ≤ l ≤ 21
Reflections collected	17205
Independent reflections	3555 [R_{int} = 0.0409, R_{sigma} = 0.0254]
Data/restraints/parameters	3555/0/244
Goodness-of-fit on F^2	1.067
Final R indexes [I>=2σ (I)]	R_1 = 0.0243, wR_2 = 0.0619
Final R indexes [all data]	R_1 = 0.0256, wR_2 = 0.0630
Largest diff. peak/hole / e Å^{-3}	0.22/-0.20
Flack parameter	-0.003(7)

Table 33. Crystal data and structure refinement for the oligo-fused heteroacene compound **156**.
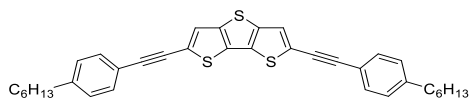
Identification code	MG054_d_Cu
Empirical formula	$C_{36}H_{36}S_3$
Formula weight	564.83
Temperature/K	99.9(4)
Crystal system	triclinic
Space group	P-1
a/Å	11.58459(13)
b/Å	15.8530(2)
c/Å	19.0367(2)
a/°	100.6239(11)
ß/°	102.3467(10)
γ?/°	110.7141(12)
Volume/Å3	3062.41(7)
Z	4
ρ_{calc}mg/mm^3	1.225
m/mm-1	2.373
F(000)	1200
Crystal size/mm3	0.18 × 0.16 × 0.1
Radiation	CuKa (λ = 1.54184)
2 Θ range for data collection	6.22 to 133.18°
Index ranges	-13 = h = 13, -18 = k = 18, -22 = l = 22
Reflections collected	58533
Independent reflections	10441 [Rint = 0.0318, Rsigma = 0.0199]
Data/restraints/parameters	10441/0/707
Goodness-of-fit on F2	1.028
Final R indexes [I>=2s (I)]	R1 = 0.0324, wR2 = 0.0887
Final R indexes [all data]	R1 = 0.0405, wR2 = 0.0968
Largest diff. peak/hole / e Å^{-3}	0.28/-0.25

Table 34. Crystal data and structure refinement for the oligo-fused heteroacene compound **158**.
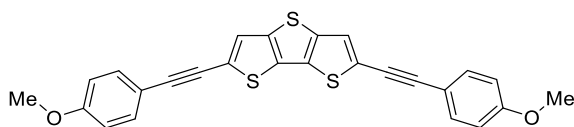
Identification code	LJ168ii_Mo
Empirical formula	$C_{26}H_{16}O_2S_3$
Formula weight	456.57
Temperature/K	120.01(10)
Crystal system	orthorhombic
Space group	Cmc21
a/Å	49.998(2)
b/Å	7.3008(4)
c/Å	5.9467(4)
a/°	90
ß/°	90
γ /°	90
Volume/Å3	2170.7(2)
Z	4
ρ_{calc}g/cm^3	1.397
µ/mm-1	0.363
F(000)	944
Crystal size/mm^3	0.29 × 0.25 × 0.05
Radiation	MoKa (λ = 0.71073)
2 Θ range for data collection/°	6.91 to 62.368
Index ranges	-56 = h = 70, -9 = k = 10, -8 = l = 7
Reflections collected	7607
Independent reflections	3016 [R_{int} = 0.0313, R_{sigma} = 0.0387]
Data/restraints/parameters	3016/1/143
Goodness-of-fit on F2	1.064
Final R indexes [I>=2s (I)]	R1 = 0.0345, wR2 = 0.0832
Final R indexes [all data]	R1 = 0.0365, wR2 = 0.0845
Largest diff. peak/hole / e Å^{-3}	0.34/-0.34
Flack parameter	0.06(4)

Table 35. Crystal data and structure refinement for the oligo-fused heteroacene compound **157**.
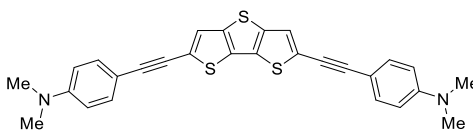
Identification code	LJ164ii_Cu
Empirical formula	$C_{28.4}H_{22.8}Cl_{0.8}N_2S_3$
Formula weight	516.63
Temperature/K	120.01(10)
Crystal system	monoclinic
Space group	$P2_1/c$
a/Å	19.2742(3)
b/Å	5.92056(9)
c/Å	22.4913(3)
α/°	90
β/°	99.3220(13)
γ/°	90
Volume/Å^3	2532.67(6)
Z	4
$\rho_{calc}g/cm^3$	1.355
μ/mm^{-1}	3.603
F(000)	1075.0
Crystal size/mm^3	0.19 × 0.11 × 0.09
Radiation	CuKα (λ = 1.54184)
2Θ range for data collection/°	7.968 to 148.634
Index ranges	-23 ≤ h ≤ 16, -7 ≤ k ≤ 7, -27 ≤ l ≤ 28
Reflections collected	18715
Independent reflections	5100 [R_{int} = 0.0441, R_{sigma} = 0.0378]
Data/restraints/parameters	5100/2/320
Goodness-of-fit on F^2	1.039
Final R indexes [I>=2σ (I)]	R_1 = 0.0532, wR_2 = 0.1422
Final R indexes [all data]	R_1 = 0.0584, wR_2 = 0.1474
Largest diff. peak/hole / e Å^{-3}	0.88/-0.90

Appendix B1

Molecular Modelling - Energies

Charge Transfer Modelling for Acenes

Table 36. Optimised and single-point energies of the neutral, anionic and cationic isomers, in Hartree (atomic energy units); calculated at the B3LYP/6-311++G(d,p) level.

Entry	E(M$_{OPT}$)	E(M$^+_{OPT}$)	E(M$^+_{SP}$)
13	-846.9971	-846.7698	-844.3460
14	-847.0235	-846.7623	-847.0200
32	-847.0117	-846.7519	-847.0082
33	-847.0189	-846.7683	-847.0166
34	-847.0237	-846.7669	-847.0205
35	-847.0175	-846.7640	-847.0142
36	-847.0028	-846.7498	-847.0007
37	-847.0094	-846.7595	-847.0070
38	-847.0196	-846.7601	-847.0172
39	-847.0233	-846.7647	-847.0209
40	-847.0127	-846.7714	-847.0106
41	-847.0137	-846.7506	-847.0112

Table 37. Reorganisation energies and vertical ionization and electron affinities, in electron volts; calculated at the B3LYP/6-311++G(d,p) level.

Entry	λ_1	λ_2	IE_V
13	0.049	0.05	6.23
14	0.09	0.10	7.20
32	0.09	0.09	7.16
33	0.06	0.06	6.88
34	0.08	0.09	7.07
35	0.09	0.09	6.99
36	0.06	0.06	6.94
37	0.07	0.07	6.87
38	0.06	0.06	7.12
39	0.07	0.07	7.10
40	0.06	0.06	6.62
41	0.08	0.07	7.24

Frequency Data

Table 38. Frequency Data of Optimized Pentacene (**13**) at different theoretical levels.

BLYP/6-311++G(d,p)		BLYP-D3/6-311++G(d,p)		LC-BLYP/6-311++G(d,p)		B3LYP/6-311++G(d,p)	
Frequencies (cm⁻¹)	Intensity (Km mol⁻¹)	Frequencies (cm⁻¹)	Intensity (Km mol⁻¹)	Frequencies (cm⁻¹)	Intensity (Km mol⁻¹)	Frequencies (cm⁻¹)	Intensity (Km mol⁻¹)
37.1504	0.405104	36.7728	0.403913	38.727	0.437084	38.3943	0.463931
68.0469	0	67.4176	0	74.0331	0	71.2587	0
98.0992	0	97.2381	0	105.24	0	101.929	0
116.119	0.946125	117.606	0.951891	121.746	1.11344	119.1	1.15668
142.437	0	141.332	0	151.797	0	148.079	0
186.861	1.28581	185.62	1.28716	199.44	1.2156	193.78	1.42459
231.411	0	230.01	0	244.419	0	238.12	0
232.154	0	235.64	0	248.22	0	239.006	0
255.943	0	256.833	0	269.98	0	263.194	0
285.327	0	283.816	0	296.584	0	294.901	0
335.905	0	334.361	0	361.334	0	348.506	0
352.953	0.246005	359.704	0.247983	370.754	0.0538951	361.752	0.212916
367.371	0.00148196	365.604	0.00211861	394.479	0.0918644	381.123	0.00375474
442.421	0	448.204	0	465.895	0	453.994	0
454.877	30.1833	453.641	29.7521	486.651	47.1186	472.413	39.3274
457.486	0	456.193	0	487.803	0	473.798	0
460.828	0	459.136	0	501.29	7.851	479.465	6.13812
462.348	8.05096	460.813	8.67941	502.31	0.0189361	480.168	0
477.284	10.3485	478.906	10.5457	509.003	0	490.185	10.5833
499.323	0	504.807	0	525.436	0	512.562	0
509.234	0	508.146	0	536.113	0	523.746	0
534.454	0	533.265	0	564.16	0	550.502	0
564.706	1.99927	565.007	2.05283	588.138	5.02399	579.057	3.12196
600.697	0	600.83	0	626.193	0	615.668	0
623.004	4.89714	622.391	4.77397	649.818	5.07876	638.496	5.61179
629.809	0	629.181	0	661.074	0	646.107	0
685.182	0	684.281	0	741.413	0	709.682	0
705.263	0	706.3	0	743.957	3.8619	724.765	0
720.532	88.1594	719.182	88.1788	744.139	0	743.723	3.29136
720.926	2.51594	720.958	2.39604	773.256	93.5886	747.441	97.5764
724.337	0	723.291	0	778.84	0	748.578	0
725.65	0	724.353	0	783.747	0	752.81	0
734.66	0	734.044	0	796.066	0	761.404	0
745.77	0	744.675	0	800.699	0	768.324	0
748.873	0	747.718	0	810.656	0	772.257	0
768.668	0	774.139	0	824.971	0	794.54	0
811.506	0	810.139	0	858.793	0.165472	837.049	0.18597
813.051	17.6234	811.883	17.6871	871.288	0	841.031	0
813.397	0.181328	815.351	0.215251	875.759	0	846.653	0
817.378	0	816.195	0	899.121	18.263	847.82	19.5533
840.979	0	839.995	0	920.166	0	872.993	0
857.822	0	856.812	0	924.008	0.199557	888.463	0.432789
858.854	0.529483	863.559	0	943.44	3.56494	895.375	0
864.328	0	872.989	0.753907	950.921	0	898.782	0
877.75	0	877.089	0	955.051	0	912.97	0
889.825	88.7107	888.921	88.4665	957.126	0	921.79	2.59596
896.708	1.75655	896.93	1.79097	981.351	0	929.919	100
910.91	0	912.243	0	989.106	100	936.08	0
933.705	0	932.763	0	1005.7	4.08097	978.25	0
934.685	10.1655	933.754	10.2683	1034.62	0	979.091	9.93438
949.06	0	948.334	0	1043.44	0	992.117	0
949.493	0	948.774	0	1043.88	6.68202	992.275	0
989.647	13.2357	992.771	13.0349	1054.56	0	1015.31	12.5398
991.289	0	994.278	0	1054.62	0	1017.99	0
1107.94	7.54116	1111.07	7.02001	1062.08	8.05056	1133.9	1.18738
1123.31	0	1127.5	0	1176.46	12.7607	1142.6	9.45918
1125.96	0.610462	1129.85	0.562914	1187.67	0	1157.25	0
1154.66	0	1166.52	0	1200.91	0	1184.38	0
1157.32	0.236055	1168.54	0.253597	1205.22	0.0777837	1187.93	0.165209
1167.98	0	1173.7	0	1218.6	0	1199.66	0
1175.98	0	1183.55	0	1227.71	0	1206.79	0
1177.58	2.75782	1185.08	2.72887	1229.58	4.22838	1209.62	3.20578
1205.13	0	1210.67	0	1268.61	0	1241.12	0
1213.52	1.17202	1220.71	1.27508	1277.03	6.6491	1250.03	1.73955
1257.31	0	1262.27	0	1317.08	0.0254424	1294.63	0.00419647
1259.47	0.00698638	1269.94	3.6081	1322.89	0	1294.79	0
1274.58	0	1277.38	17.415	1329.54	13.4058	1312.17	0
1275.2	20.475	1289.63	0	1349.3	0	1317.33	20.729
1288.2	0	1291.76	0	1365.15	11.6853	1331.66	0
1331.62	2.17001	1332.6	1.92137	1376.52	0	1358.11	12.9669
1335.81	13.8526	1341.75	14.9926	1414.48	2.14551	1374.81	2.60954
1359.38	0	1360.96	0	1442.4	0	1409.55	0
1359.46	1.33503	1361.35	1.59213	1461.39	0	1416.03	1.18064
1369.96	6.3448	1374.89	4.98996	1483.4	2.31865	1417.93	0
1373.26	0	1375.81	0	1487.13	0.00631203	1425.99	7.14737
1378.61	0	1380.06	0	1528.48	0	1432.67	0
1427.78	0.597759	1427.99	0.574672	1529.89	0.532639	1475.46	0.0670332
1431.48	0.00127025	1436.31	0.0281775	1532.35	0	1475.93	0.526768
1447.22	0	1449.76	0	1536.53	0.194119	1491.4	0
1484.48	2.10745	1487.26	2.11395	1626.05	1.97518	1540.22	2.75145
1489.16	0	1490.5	0	1661.74	0	1555.95	0
1512.05	0	1513.23	0	1673.82	0	1573.65	0
1512.57	3.01229	1513.47	2.99359	1675.65	11.4302	1576.14	4.49674
1528.83	0	1530.33	0	1688.08	0	1590.75	0
1558.1	0	1561.7	0	1736.88	0.190332	1631.66	0
1574.09	0.152113	1575.65	0.266521	1752.47	0	1638.65	0.260954
1598.28	7.04534	1600.03	6.96778	1781.16	0	1668.88	0
1599.94	0	1601.05	0	1787.96	8.48454	1670.21	8.76986
3071.67	3.1443	3068.76	2.92008	3212.51	0.850571	3153.86	2.35754
3073.36	0	3070.5	0	3213.95	0	3155.46	0
3073.45	0	3070.69	0	3214.04	0	3155.53	0
3075.45	4.17256	3072.75	4.25417	3215.67	2.19931	3157.46	4.00454
3076.52	14.1207	3073.9	18.3342	3215.77	3.24157	3158	3.30439
3077.93	0	3075.52	0	3216.52	0	3159.08	0
3078.53	57.4814	3076.05	53.9415	3217.32	10.5755	3160.14	49.5445
3079.36	0	3076.79	0	3218.6	0	3161.01	0
3082.33	4.33304	3080.13	4.31433	3220.94	4.46562	3163.53	4.65787
3083	0	3080.76	0	3221.44	0	3164.28	0
3095.43	0	3094.07	0	3235.03	0	3176.72	0
3095.46	76.3245	3094.1	76.0123	3235.04	26.2615	3176.74	66.664
3107.63	100	3106.96	100	3245.46	25.3653	3188.5	82.9821
3107.8	0	3107.12	0	3245.53	0	3188.64	0

Table 1. Continued.

B3LYP-D3/6-311++G(d,p)		CAM-B3LYP/6-311++G(d,p)		CAM-B3LYP-D3/6-311++G(d,p)		LC-ωPBE/6-311++G(d,p)	
Frequencies (cm⁻¹)	Intensity (Km mol⁻¹)	Frequencies (cm⁻¹)	Intensity (Km mol⁻¹)	Frequencies (cm⁻¹)	Intensity (Km mol⁻¹)	Frequencies (cm⁻¹)	Intensity (Km mol⁻¹)
38.0366	0.458777	38.3446	0.449923	38.0936	0.450974	37.8683	0.445701
70.8952	0	72.8995	0	72.6652	0	72.7766	0
101.055	0	103.298	0	102.775	0	103.053	0
120.484	1.15055	120.186	1.16744	121.255	1.1734	119.047	1.12161
147.228	0	150.423	0	149.986	0	149.125	0
192.711	1.41507	196.29	1.32938	195.59	1.33727	195.389	1.20833
239.392	0	240.695	0	242.518	0	238.917	0
241.446	0	243.121	0	243.238	0	242.129	0
263.972	0	266.106	0	266.754	0	266.324	0
293.031	0	295.876	0	295.078	0	290.642	0
347.594	0	354.727	0	354.028	0	355.887	0
368.222	0.209361	365.362	0.128416	370.301	0.126555	362.05	0.0722947
379.836	0.00098497	386.501	0.0278356	385.761	0.0259121	383.898	0.0720958
459.887	0	459.104	0	463.791	0	454.991	0
470.353	39.5298	479.664	45.6082	479.035	45.7568	478.066	47.693
472.471	0	480.261	0	479.625	0	478.771	0
478.292	4.79659	488.635	0.707067	487.886	0.721185	490.702	0.0257556
478.633	0	492.213	0	491.376	0	493.568	8.16274
491.644	10.6529	494.909	8.9995	496.092	9.11597	497.601	0
517.644	0	518.341	0	522.004	0	513.921	0
524.388	0	529.99	0	529.505	0	524.841	0
550.009	0	557.917	0	557.371	0	555.816	0
579.413	3.14589	583.506	4.03389	583.771	4.08063	578.399	4.59683
615.986	0	620.249	0	620.588	0	614.467	0
638.293	5.44196	643.522	5.3342	643.458	5.25642	636.83	4.90769
645.99	0	652.665	0	652.679	0	646.444	0
708.686	0	724.357	0	723.925	0	726.872	0
725.615	0	732.216	0	732.868	0	729.745	0
743.67	3.14611	750.033	3.62091	749.874	3.5455	744.304	3.51549
746.448	97.4271	758.824	94.5332	758.312	94.7649	764.099	92.0788
748.791	0	762.854	0	762.378	0	766.734	0
751.746	0	764.432	0	763.914	0	770.07	0
760.721	0	777.421	0	776.901	0	786.454	0
769.85	0	781.975	0	781.453	0	787.213	0
773.793	0	787.095	0	786.535	0	793.72	0
799.498	0	807.556	0	811.227	0	817.376	0
838.768	0.21538	846.691	0.17167	848.045	0.195999	844.843	0.148766
840.324	0	854.451	0	854.085	0	861.847	0
846.195	0	859.566	0	859.226	0	865.657	0
847.234	19.2665	868.472	19.127	868.136	19.1171	883.436	18.9849
873.095	0	891.903	0	891.634	0	903.432	0
894.639	0	904.007	0.299362	913.949	0.410758	914.135	0.217083
898.87	0	918.366	0	918.042	0	926.597	3.20394
901.572	0.611448	921.885	0	921.679	0	934.367	0
914.145	0	931.669	3.06482	931.815	3.11235	934.994	0
921.993	2.61324	939.212	0	939.039	0	939.801	0
928.592	100	945.638	0	946.59	0	954.489	0
937.371	0	954.577	100	954.265	100	971.572	100
977.359	0	1006.96	0	1006.64	0	1009.24	6.86293
978.129	9.56625	1007.55	7.58702	1007.23	7.63121	1026.82	0
991.431	0	1018.19	9.89842	1019.42	0	1027.25	5.74062
991.808	0	1019.57	0	1019.42	0	1029.25	0
1018.18	12.2791	1019.57	0	1020.46	9.88763	1035.16	0
1020.63	0	1025.12	0	1027.03	0	1035.24	0
1136.99	1.08237	1099.02	2.61603	1100.58	2.50176	1064.46	5.82027
1145.69	8.8377	1157.65	10.5414	1160.06	10.1162	1163.57	12.225
1161.43	0	1171.16	0	1174.46	0	1174.82	0
1195.17	0	1191.73	0	1199.76	0	1189.82	0
1198.64	0.174887	1195.96	0.107617	1204.29	0.113599	1194.38	0.063146
1205.74	0	1209.45	0	1214.37	0	1206.79	0
1214.47	0	1214.8	0	1220.99	0	1216.95	0
1216.94	3.20684	1219.23	3.77178	1224.88	3.88059	1217.82	4.37
1246.51	0	1253.45	0	1257.74	0	1256.63	0
1256.81	1.90143	1262.09	2.79298	1267.07	2.99844	1267.07	4.80616
1300.02	0	1304.95	0.00703652	1313.21	0	1302.24	0.00616544
1305.67	0.621079	1308.04	0	1313.53	0.0605306	1307.8	0
1318.49	20.3661	1327.46	0	1335.83	0	1322.22	12.8635
1325.64	0	1338.03	16.4884	1338.51	16.7027	1332.21	0
1334.97	0	1342.15	12.1326	1347.72	12.2188	1345.27	12.1216
1364.45	13.2527	1351.47	0	1353.8	0	1365.35	0
1375.47	2.37772	1393.63	2.40618	1393.93	2.29996	1397.96	2.19838
1410.82	0	1429.35	0	1430.1	0	1427.31	0
1416.88	1.87298	1430.21	0	1431.54	0	1451.16	0
1419.13	0	1447.3	0.474862	1447.83	0.788349	1469.64	1.95782
1430.45	6.12203	1456.45	4.65642	1460.64	4.41407	1479.75	0.00755763
1434.13	0	1474.75	0	1475.47	0	1514.78	0
1476.16	0.50135	1495.23	0.492867	1496.36	0.337375	1516.28	0.777442
1478.74	0.00196994	1500.5	0.293671	1500.8	0.285033	1517.35	0.165075
1493.37	0	1507.65	0	1508.96	0	1518.56	0
1542.32	2.72815	1574.44	2.66725	1575.7	2.67568	1607.77	2.03579
1556.68	0	1601.31	0	1601.8	0	1642.47	0
1574.01	0	1614.65	0	1614.53	0	1655.28	0
1576.43	4.42941	1617.87	6.79262	1617.93	6.79788	1657.13	10.5473
1591.85	0	1631.6	0	1632.35	0	1666.27	0
1634.31	0	1680.58	0.220512	1681.24	0.272595	1715.97	0.139518
1639.72	0.369036	1688.9	0	1690.56	0	1734.22	0
1669.48	0	1717.15	0	1717.48	0	1760.76	0
1671.34	8.63513	1722.42	8.61818	1723.14	8.61038	1767.64	7.24966
3151.47	2.16223	3179.05	1.69446	3177.05	1.63174	3211.63	1.37042
3153.11	0	3180.55	0	3178.53	0	3212.59	0
3153.26	0	3180.58	0	3178.66	0	3212.97	0
3155.21	4.01682	3182.44	3.72273	3180.5	3.76896	3213.65	0.754371
3155.79	3.96713	3182.68	2.22251	3180.85	2.74202	3214.27	0
3156.94	0	3183.63	0	3181.85	0	3214.42	4.38492
3157.98	48.6831	3184.68	31.0168	3182.85	30.7118	3215.19	21.8136
3158.85	0.000109441	3185.72	0	3183.84	0	3216.87	0
3161.57	4.57508	3188.1	4.01858	3186.38	4.01938	3219.01	3.16555
3162.28	0	3188.79	0	3187.04	0	3219.43	0
3175.44	0	3201.6	0	3200.44	0	3233.32	0
3175.47	65.9755	3201.62	49.3971	3200.47	49.3641	3233.33	36.9285
3187.71	82.2532	3212.93	57.2086	3212.17	57.2625	3244.14	43.7597
3187.85	0	3213.05	0	3212.28	0	3244.24	0

Table 1. Continued.

LC-ωPBE-D3/6-311++G(d,p)		PBEPBE/6-311++G(d,p)		PBEPBE-D3/6-311++G(d,p)		PBE0/6-311++G(d,p)	
Frequencies (cm⁻¹)	Intensity (Km mol⁻¹)	Frequencies (cm⁻¹)	Intensity (Km mol⁻¹)	Frequencies (cm⁻¹)	Intensity (Km mol⁻¹)	Frequencies (cm⁻¹)	Intensity (Km mol⁻¹)
35.2764	0.635559	37.8166	0.478999	73.2909	0.391576	38.8832	0.474951
38.6571	0	67.7759	0	113.394	0	71.4794	0
103.893	0	98.3415	0	136.374	1.33182	102.432	0
116.857	1.66548	115.162	1.05982	140.056	0	118.471	1.15941
145.213	0	142.165	0	178.736	0	148.486	0
197.789	1.12658	186.814	1.47486	233.884	1.20758	194.626	1.41649
239.118	0	229.709	0	253.78	0	236.444	0
240.281	0	229.768	0	261.457	0	239.764	0
268.488	0	257.586	0	265.934	0	265.334	0
315.009	0	285.405	0	335.884	0	295.35	0
348.754	0	336.466	0	372.818	0	351.07	0
367.953	0.0295493	348.445	0.26865	377.751	0.0888849	358.481	0.195187
391.561	0.0470785	366.964	0.000346348	411.375	9.66E-05	382.27	0.0101409
464.108	0	436.823	0	464.887	0	449.974	0
483.177	37.5228	452.745	33.4145	486.293	8.03925	471.8	40.5684
483.796	0	455.398	0	506.769	0	473.759	0
487.189	0	460.488	0	508.049	36.0697	480.282	6.22152
491.922	11.1106	460.772	12.4523	511.04	0	482.466	0
495.543	8.61767	478.336	11.5276	512.792	4.25594	492.33	10.2197
519.057	0	493.981	0	520.784	0	509.044	0
535.606	0	504.525	0	557.29	0	522.581	0
566.504	0	532.751	0	577.74	4.97069	551.513	0
584.078	4.85419	562.599	2.05742	582.94	0	578.442	3.13261
619.51	0	597.056	0	612.863	0	613.847	0
642.352	4.85499	617.516	5.43338	637.292	4.61283	635.072	5.42718
647.613	0	622.912	0	644.437	0	641.556	0
723.438	0	681.18	0	704.799	1.49442	708.54	0
733.77	0	705.203	0	723.977	0	726.725	0
762.416	91.3706	718.383	95.1986	738.783	0	748.58	0
762.99	2.13075	720.011	0	756.83	0	750.029	93.4504
765.077	0	724.359	0	779.434	0	755.097	3.5302
769.109	0	731.641	3.17982	800.297	94.8848	756.104	0
786.171	0	739.763	0	800.634	0	768.178	0
788.742	0	742.187	0	800.943	0	771.144	0
788.81	0	744.473	0	805.251	0	772.564	0
832.608	0	779.977	0	806.257	0	806.833	0
854.031	0.0958598	807.87	0	840.652	0.107821	838.969	0.156714
860.912	0	808.745	21.8178	893.75	0	842.956	0
867.195	0	812.314	0.177099	895.036	2.67882	849.009	0
871.191	19.8402	814.432	0	897.691	0	849.857	20.673
897.538	0	835.481	0	903.54	19.0867	873.454	0
924.862	3.58478	854.046	0	910.967	0.492248	897.755	0
926.068	2.17543	857.089	0	920.082	3.89296	897.942	0.293564
926.599	0	866.149	0.402456	927.119	0	898.019	0
929.977	0	868.767	0	936.583	0	911.091	0
941.377	0	887.189	100	952.717	0	920.794	2.49519
948.897	0	892.084	1.7606	954.786	0	933.163	100
955.054	1.46634	905.012	0	971.634	0	934.136	0
964.928	100	931.821	0	988.508	100	983.54	0
1018.99	0	932.899	11.2584	1036.22	0	984.342	8.78258
1019.54	7.47446	946.288	0	1040.45	0	995.471	0
1032.58	0	946.577	0	1040.95	7.39609	995.624	0
1032.65	0	1001.97	15.4541	1041.21	11.2571	1028.67	12.5434
1058.97	0	1003.22	0	1051.91	0	1031.12	0
1064.1	13.8122	1111.79	10.2463	1051.98	0	1142.65	1.7823
1167.02	15.422	1123.19	0	1153.02	12.1762	1150.14	10.8774
1175.67	0	1131.79	1.42083	1164.76	0	1161.56	0
1189.42	0	1146.26	0	1184.57	0	1181.29	0
1204.87	0.000200334	1150.86	0.518598	1205.79	0.037293	1186.11	0.186614
1216.34	0	1160.46	0	1218.3	0	1197.03	0
1225.7	0.996962	1172.13	3.27414	1218.72	0	1209.13	3.2313
1225.95	0	1175.85	0	1225.95	1.59838	1211.15	0
1285.33	0	1212.72	0	1259.34	0	1251.36	0
1287.32	0.058798	1221.39	1.04412	1266.52	3.3013	1261.2	1.44817
1305.1	18.9335	1249.71	0.185873	1305.14	0	1291.63	0.0497638
1311.82	0.356394	1252.8	0	1306.05	14.771	1295.6	0
1321.24	0	1266.28	0	1307.92	0.12898	1312.55	0
1327.52	0	1279.44	22.6521	1324.7	0	1326.55	19.8887
1347.61	16.4805	1305.12	0	1325.63	16.465	1351.21	0
1364.84	0	1331.57	5.13391	1340.42	0	1372.16	14.0228
1390.23	7.51353	1358.26	14.5351	1377.22	0	1380.21	4.38643
1442.79	0	1372.73	0	1381.5	1.91586	1419.08	0
1445.8	0	1390.52	2.73834	1407.67	0.170041	1444.81	0
1483.4	1.58444	1396.13	0	1433.1	0	1447.63	3.95423
1486.57	0.314224	1396.67	6.97648	1438.97	4.71244	1454.98	2.65212
1513.29	0	1402.8	0	1442.49	0	1467.18	0
1518.57	0.457863	1432.42	0.316215	1489.31	1.0785	1487.68	0.784302
1524.47	3.81476	1437.64	0.731948	1489.85	0.0785472	1491.96	0.500983
1540.13	0	1451.18	0	1512.33	0	1502.19	0
1578.29	1.64755	1500.64	2.99914	1553.8	0.796872	1563.37	3.2266
1604.03	0	1513.39	0	1564.83	0	1586.26	0
1618.46	0	1534.78	0	1593.54	0	1602.96	0
1659.44	4.96408	1536.76	3.7349	1593.63	0	1606.11	5.08301
1659.77	0	1545.71	0	1593.88	6.29305	1614.43	0
1700.29	1.27603	1585.75	0	1648.78	1.97749	1665.2	0.48896
1718.8	0	1594.28	0.554156	1677.23	0	1666.44	0
1731.93	0	1621.95	0	1687.89	0	1698.1	0
1740.73	9.63406	1622.81	7.22862	1699.12	8.94017	1702.14	8.34411
3212.88	0.265242	3087.16	4.99225	3136.23	1.90677	3179.96	2.63508
3214.19	0	3088.24	0	3137.33	0	3181.14	0
3216.18	0	3088.82	0	3137.47	0	3181.52	0
3217.16	17.0979	3090.23	5.31032	3138.81	4.33594	3182.99	4.36782
3217.78	4.46114	3090.73	44.0691	3139.62	15.091	3183.29	6.91811
3218.6	1.28494	3093.25	0	3141.36	2.82596	3184.06	0
3218.63	0	3093.27	19.1254	3141.41	0	3184.5	31.3375
3219.5	0	3093.37	0	3141.78	0	3185.96	0
3225.22	1.46975	3097.57	4.93083	3145.92	5.06566	3188.75	4.44048
3225.39	0	3097.83	0	3146.16	0	3189.13	0
3237.21	0	3111.77	0	3159.61	0	3202.77	0
3237.23	34.8881	3111.79	62.3362	3159.62	33.1356	3202.78	49.4098
3248.24	45.6013	3124.04	81.806	3172.23	38.5766	3214.54	61.3218
3248.35	0	3124.17	0	3172.32	0	3214.65	0

Table 1. Continued.

PBE0-D3/6-311++G(d,p)		ωB97XD/6-311++G(d,p)		B3P86/6-311++G(d,p)		BHandH/6-311++G(d,p)	
Frequencies (cm⁻¹)	Intensity (Km mol⁻¹)	Frequencies (cm⁻¹)	Intensity (Km mol⁻¹)	Frequencies (cm⁻¹)	Intensity (Km mol⁻¹)	Frequencies (cm⁻¹)	Intensity (Km mol⁻¹)
38.6504	0.475821	35.7703	0.463403	38.6646	0.479944	39.6048	0.479351
71.262	0	63.541	0	71.4821	0	75.0237	0
101.941	0	100.606	0	101.905	0	106.087	0
119.229	1.16286	117.589	1.05944	118.519	1.12983	122.018	1.2015
148.079	0	145.107	0	148.288	0	154.694	0
193.982	1.42307	193.029	1.30691	193.703	1.42022	202.061	1.44094
238.302	0	238.971	0	236.354	0	243.226	0
239.198	0	238.996	0	239.191	0	249.13	0
265.809	0	265.3	0	264.478	0	273.732	0
294.633	0	290.939	0	294.696	0	305.346	0
350.426	0	350.941	0	349.823	0	364.413	0
362.18	0.195101	364.497	0.110936	358.305	0.198996	368.243	0.117108
381.534	0.00900146	378.541	0.0377573	381.175	0.00625506	399.645	0.0334995
453.835	0	458.263	0	449.847	0	462.652	0
471.222	40.4928	468.42	46.1809	471.352	39.2303	488.264	46.2827
473.187	0	469.405	0	472.945	0	489.977	0
479.603	6.42359	477.376	1.34661	479.038	6.54566	499.7	1.84201
481.692	0	483.023	0	480.462	0	504.377	0
493.204	10.3194	493.59	8.18175	491.265	10.35	507.312	9.01948
511.574	0	516.316	0	509.031	0	523.895	0
522.154	0	525.144	0	521.575	0	539.713	0
551.04	0	553.449	0	550.007	0	569.439	0
578.715	3.16307	580.514	3.71598	578.309	2.94847	594.479	4.24016
614.144	0	617.967	0	613.864	0	631.343	0
635.082	5.3679	640.514	4.72511	635.443	5.48686	653.292	5.18328
641.617	0	648.494	0	641.972	0	660.977	0
708.165	0	715.348	0	707.136	0	734.442	0
727.246	0	729.007	0	725.565	0	748.926	0
748.19	0	745.337	85.6884	746.864	0	773.12	92.2706
749.557	93.5701	748.284	3.56291	747.505	94.5293	773.519	0
755.236	3.46839	752.389	0	752.045	3.51397	777.276	3.84292
755.647	0	752.834	0	753.298	0	779.273	0
767.779	0	771.331	0	766.512	0	791.776	0
770.73	0	774.574	0	768.801	0	794.843	0
772.369	0	775.855	0	769.478	0	801.197	0
809.789	0	806.419	0	802.552	0	833.279	0
839.974	0.173435	839.653	0	837.352	0.158709	865.565	0.141836
842.543	0	843.193	0.156187	840.918	0	866.905	0
848.658	0	846.003	0	846.536	20.2604	873.482	0
849.465	20.706	849.695	21.1734	846.688	0	882.734	20.1241
873.138	0	874.941	0	871.132	0	903.904	0
897.482	0	900.468	0	893.099	0.309573	925.056	0.177482
897.666	0	903.425	0	894.154	0	933.216	0
905.598	0.368955	905.273	0.309454	895.388	0	933.738	0
910.833	0	919.512	0	908.733	0	949.465	3.16491
921.011	2.52397	926.147	2.66705	919.915	2.35837	950.199	0
932.833	100	936.611	100	929.011	100	962.742	0
934.933	0	940.426	0	933.362	0	971.432	100
983.241	0	992.603	0	978.09	0	1025.13	0
984.043	8.81002	993.059	5.00956	978.986	9.63248	1025.85	8.2615
995.261	0	1006.47	0	990.747	0	1037.28	0
995.414	0	1006.49	0	990.946	0	1037.3	0
1030.24	12.5176	1017.44	9.55707	1024.92	12.7077	1050.58	10.5631
1032.62	0	1023.53	0	1027.14	0	1055.35	0
1144.86	1.72242	1096.82	1.96581	1143.85	1.78693	1141.86	3.61001
1152.18	10.5412	1155.93	9.09396	1146.63	10.4684	1181.9	13.442
1164.26	0	1170.14	0	1158.65	0	1190.6	0
1187.16	0	1193.61	0	1180.49	0	1201.15	0
1192.1	0.163596	1199.32	0.076877	1184.81	0.200162	1206.71	0.180841
1200.57	0	1201.62	0	1195.2	0	1218.37	0
1213.12	3.32332	1210.92	0	1207.03	3.31964	1232.91	2.94114
1215.88	0	1213.01	4.47181	1208.08	0	1234.93	0
1254.42	0	1247.81	0	1247.32	0	1283.96	0
1265.08	1.52993	1257.6	2.32392	1256.52	1.44131	1293	2.23597
1297.94	0.0265857	1298.19	0.000194625	1289.29	0.0481322	1319.38	0.0173563
1300.49	0	1300.9	0	1292.75	0	1323.73	0
1317.61	0	1321.37	0	1308.84	0	1353.55	0
1326.98	20.1318	1329.98	16.0664	1322.22	20.3573	1373.81	16.9456
1353.09	0	1336.77	11.1467	1344.6	0	1383.14	17.0806
1375.24	14.1704	1347.73	0	1371.98	13.6516	1395.09	0
1380.44	4.30866	1387.78	2.59562	1376.52	4.13756	1421.32	5.3853
1419.44	0	1423.87	0	1416.6	0	1455.37	0
1445.53	0	1431.6	0	1435.8	0	1490.07	3.48357
1450.83	4.30803	1449.07	0.483449	1439.98	2.85931	1496.2	0
1455.13	2.38005	1454.14	3.27905	1443.97	4.50407	1514.52	1.03568
1467.61	0	1474.72	0	1455.2	0	1533.84	0
1488.25	0.646325	1491.49	0.710382	1480.78	0.397886	1543.11	1.07385
1492.22	0.493091	1494	0.279093	1485.53	0.57907	1547.21	0
1503	0	1502.54	0	1497.05	0	1547.49	0.408806
1564.23	3.23969	1569.86	2.33657	1553.99	3.20047	1626.76	3.65107
1586.64	0	1597.78	0	1574.79	0	1658.19	0
1602.86	0	1612.76	0	1591.84	0	1671.82	0
1606.12	5.09179	1615.52	6.79086	1594.85	4.55464	1674.85	7.12251
1615.02	0	1626.21	0	1604.51	0	1682.87	0
1665.73	0.555892	1676.41	0.177304	1652.57	0	1735.24	0.830302
1667.81	0	1693.07	0	1654.54	0.487895	1747.68	0
1698.42	0	1716.38	0	1686.27	0	1772.84	0
1702.77	8.31169	1722.61	7.45823	1689.29	8.43278	1780.67	9.77159
3178.67	2.5135	3185.16	2.94877	3170.82	2.8979	3230.83	1.5085
3179.9	0	3186.14	0	3171.92	0	3231.96	0
3180.21	0	3186.57	0	3172.43	0	3232.46	0
3181.74	4.34603	3187.87	5.15747	3173.78	4.43972	3233.64	3.82501
3182.04	6.42034	3188.15	23.0136	3173.98	6.91524	3234.18	12.5302
3182.83	0	3189.28	0	3174.72	0	3236.03	2.42633
3183.31	31.9427	3189.34	16.8005	3175.16	34.5579	3236.07	0
3184.75	0	3190.66	0	3176.66	0	3236.3	0
3187.61	4.45467	3193.88	3.40108	3179.3	4.46495	3240.37	4.721
3188	0	3194.2	0	3179.68	0	3240.57	0
3202	0	3208.87	0	3192.96	0	3255.26	0
3202.02	49.5003	3208.89	52.1684	3192.98	51.6658	3255.27	25.7574
3214	61.4104	3220.96	66.3616	3204.63	64.6729	3266.64	25.6249
3214.11	0	3221.1	0	3204.75	0	3266.7	0

Table 1. Continued.

BHandHLYP/6-311++G(d,p)	
Frequencies (cm⁻¹)	Intensity (Km mol⁻¹)
39.6133	0.459799
74.8324	0
106.328	0
122.691	1.25385
154.281	0
201.942	1.36875
245.523	0
248.938	0
271.568	0
304.73	0
362.871	0
372.706	0.118382
398.065	0.0260639
468.344	0
491.767	45.4693
492.582	0
501.269	0.982769
504.88	0
505.311	9.21409
528.81	0
541.881	0
569.573	0
595.346	4.85833
633.774	0
657.341	5.6309
666.598	0
739.234	0
747.784	0
763.541	3.82195
778.44	0
781.515	95.6486
786.924	0
791.996	0
798.193	0
803.658	0
822.211	0
866.129	0.16096
878.092	0
883.147	0
893.656	18.3875
914.771	0
922.032	0.309683
943.528	0
943.742	0
953.635	3.85915
959.897	0
968.356	0
980.06	100
1035	0
1035.56	7.22349
1038.26	9.03881
1045.5	0
1046.15	0
1046.17	0
1121.96	1.65645
1184.15	10.3539
1199.47	0
1222.8	0
1227.46	0.0868466
1240.18	0
1245.86	0
1250.44	3.16816
1281.8	0
1292.57	2.47846
1340.83	0.10157
1342.12	0
1362.72	0
1368.51	16.8674
1377.54	11.0836
1380.22	0
1428.78	1.60691
1461.12	0
1468.77	0
1477.45	0.607827
1492.1	5.19428
1505.73	0
1533.08	0.343904
1534.07	0.259048
1546.35	0
1609.47	2.71652
1637.11	0
1649.2	0
1652.84	7.33311
1666.25	0
1716.3	0.20105
1719.85	0
1752.82	0
1757.41	10.0893
3252.38	1.57329
3253.57	0
3254.03	0
3255.08	0.0686416
3256.04	2.97407
3256.64	0
3259.1	30.8404
3259.19	0
3261.05	4.42042
3262.45	0
3274.01	0
3274.04	54.3073
3285.18	64.1896
3285.32	0

Table 39. Frequency data of the optimized structures **13**, **14** and **32-41** at the B3LYP/6-311++G(d,p) theoretical level.

13		14		32		33	
Frequencies (cm⁻¹)	Intensity (Km mol⁻¹)	Frequencies (cm⁻¹)	Intensity (Km mol⁻¹)	Frequencies (cm⁻¹)	Intensity (Km mol⁻¹)	Frequencies (cm⁻¹)	Intensity (Km mol⁻¹)
38.3943	0.463931	39.5743	0.285068	50.3736	0.093913	36.3091	0.183864
71.2587	0	47.2907	0	63.5323	0.216785	59.967	0.146481
101.929	0	104.316	0.0460272	95.3874	1.08744	108.675	0.213945
119.1	1.15668	109.074	0	118.786	0.209613	116.457	0.261355
148.079	0	141.372	0.391578	137.422	1.50125	129.333	0.373504
193.78	1.42459	184.146	0	188.514	2.32401	197.57	3.21985
238.12	0	210.427	3.22919	217.037	0.401498	218.951	0.0918774
239.006	0	252.371	6.7786	255.601	0.621666	246.257	0.124356
263.194	0	260.447	0.0750544	273.727	1.18487	268.038	1.66022
294.901	0	282.364	0.00589796	293.765	0.653061	285.369	0.540911
348.506	0	313.503	0.000231292	340.027	0.24642	320.804	0.72957
361.752	0.212916	393.323	0.000115646	370.624	0.700964	392.731	0.00839212
381.123	0.00375474	421.395	10.8093	399.305	2.66123	406.392	0.962261
453.994	0	426.783	0.445585	426.22	5.25128	430.999	5.73073
472.413	39.3274	472.937	0.000462585	427.844	0.576604	452.787	4.513
473.798	0	476.327	1.13912	452.045	7.37366	476.563	15.6044
479.465	6.13812	487.623	13.8595	473.619	0.884595	489.711	4.06735
480.168	0	506.37	0.0141088	496.597	2.32225	496.463	1.53292
490.185	10.5833	527.11	0.00821088	541.494	1.75688	510.762	6.55752
512.562	0	528.374	7.56269	542.676	1.06268	526.652	1.05795
523.746	0	535.04	9.81397	555.552	3.87736	547.149	1.62524
550.502	0	555.694	0.000346939	576.161	0.33289	557.77	0.0525325
579.057	3.12196	561.019	4.85425	591.518	20.0929	577.897	2.00986
615.668	0	594.461	0.000115646	604.951	1.36661	589.176	0.433557
638.496	5.61179	595.595	0.335837	633.564	6.21761	632.05	3.86147
646.107	0	655.038	0.047415	638.339	5.80718	648.452	1.69957
709.682	0	656.343	0.251646	678.255	7.31818	658.877	0.315631
724.765	0	686.597	17.1864	691.679	0.402446	703.246	13.9428
743.723	3.29136	711.669	0.000693877	724.94	10.148	726.208	0.367183
747.441	97.5764	742.448	0.207354	733.814	29.2344	733.778	7.27554
748.578	0	747.156	10.382	755.001	27.7401	753.193	100
752.81	0	760.995	0.000115646	761.999	12.6496	761.582	4.82602
761.404	0	761.463	100	771.376	100	769.419	4.49218
768.324	0	789.601	0.000115646	774.389	49.8245	786.11	0.0137326
772.257	0	800.497	0.80617	786.839	6.12342	795.533	0.673768
794.54	0	816.162	78.8337	802.791	4.0637	817.086	0.45688
837.049	0.18597	822.648	0	827.788	47.6714	821.467	1.44028
841.031	0	824.96	46.5142	847.275	0.491622	825.564	47.0715
846.653	0	868.303	15.3754	866.47	0.516386	853.626	0.0971089
847.82	19.5533	869.371	0.0172313	874.858	1.17946	871.9	5.95895
872.993	0	870.432	11.7106	884.607	3.78345	878.847	3.00961
888.463	0.432789	876.115	0.647503	891.652	3.32336	895.112	30.8059
895.375	0	892.689	0.196367	957.464	0.476602	896.305	3.583
898.782	0	924.846	0.00994558	965.883	2.20425	904.37	27.1932
912.97	0	950.156	0.00115646	970.518	0.355895	937.862	0.895124
921.79	2.59596	960.38	2.56353	974.699	1.58962	960.1	1.84801
929.919	100	961.484	0.000809524	980.401	0.694604	971.134	1.26895
936.08	0	972.767	0.000462585	989.591	0.0740207	973.011	2.70041
978.25	0	979.684	0.675605	993.124	0.160897	979.796	0.321952
979.091	9.93438	989.984	0.161211	1012.63	1.49719	991.535	0.102776
992.117	0	990.563	0.000346939	1019.99	1.68732	991.885	0.00893707
992.275	0	1051.99	12.9489	1049.96	3.24027	1024.15	2.32495
1015.31	12.5398	1055.73	1.76025	1064.8	9.93908	1031.77	4.49861
1017.99	0	1069.03	2.23521	1072.7	10.1996	1055.93	7.97448
1133.9	1.18738	1095.75	1.14582	1087.34	1.62805	1096.54	0.238903
1142.6	9.45918	1155.3	3.48616	1129.15	0.253186	1155.27	4.34385
1157.25	0	1167.61	1.71561	1144.21	3.88467	1168.29	1.7169
1184.38	0	1176.93	0.0597891	1166.87	0.835744	1169.43	0.848912
1187.93	0.165209	1180.62	0.187	1178.22	0.380523	1182.56	1.44933
1199.66	0	1192.15	2.29535	1182.23	0.6149	1196.73	0.616113
1206.79	0	1210.52	1.72429	1192.44	0.337762	1198.55	0.180158
1209.62	3.20578	1217.93	0.238578	1200.74	0.393379	1219.62	3.35173
1241.12	0	1240.08	0.451599	1228.23	2.73877	1238.34	3.8498
1250.03	1.73955	1255.55	3.64424	1245.46	2.09017	1251.43	5.94304
1294.63	0.00419647	1265.79	0.0371224	1263.08	9.01307	1282.53	12.098
1294.79	0	1286.59	0.863993	1272.37	5.09985	1287.09	0.0430505
1312.17	0	1290.18	18.4501	1280.86	1.38745	1295.8	2.46707
1317.33	20.729	1296.9	9.98686	1322.51	0.29067	1309.89	2.4869
1331.66	0	1347.73	0.313748	1328.3	0.141275	1353.2	0.337865
1358.11	12.9669	1362.72	0.867116	1342.3	1.87772	1356.17	1.18885
1374.81	2.60954	1380.22	0.286109	1361.71	0.475925	1384.35	6.74759
1409.55	0	1380.78	0.0514626	1372.24	1.16471	1385.64	1.15234
1416.03	1.18064	1399.04	0.169653	1393.15	1.87569	1400.52	1.01468
1417.93	0	1423.28	0.290503	1402.2	9.68386	1417.99	0.247731
1425.99	7.14737	1456.07	3.28505	1451.05	13.5218	1452.51	4.46297
1432.67	0	1462.19	7.43571	1465.89	14.6864	1456.56	2.25846
1475.46	0.0670332	1467.98	0.474265	1470.47	1.42507	1464.03	2.11939
1475.93	0.526768	1481.04	10.757	1480.69	7.52495	1479.82	0.832237
1491.4	0	1511.53	14.8092	1508.96	9.31213	1509.39	0.841937
1540.22	2.75145	1543.03	0.872551	1524.49	17.4428	1518.99	4.72259
1555.95	0	1553.37	0.767463	1547.38	2.87463	1552.66	6.94443
1573.65	0	1565.77	3.10013	1571.45	3.22457	1582.96	6.3827
1576.14	4.49674	1607.35	0.438762	1602.7	0.458604	1594.09	0.352142
1590.75	0	1624.77	2.35641	1611.12	0.0659015	1624.22	0.778833
1631.66	0	1641.79	0.884694	1637.14	2.81428	1637.27	4.67496
1638.65	0.260954	1649.01	2.41377	1642.19	1.41208	1652.93	3.24797
1668.88	0	1653.57	0.0113333	1644.95	0.570109	1656.22	0.251328
1670.21	8.76986	1659.27	2.27083	1653.85	1.01667	1665.91	1.80213
3153.86	2.35754	3159.08	0.575571	3159.55	0.897857	3155.81	4.48455
3155.46	0	3159.32	0.264136	3166.05	3.90618	3158.32	5.43199
3155.53	0	3163.52	4.94133	3166.61	0.801914	3159.75	0.782102
3157.46	4.00454	3164.56	14.5794	3167.55	6.04548	3162.85	0.57655
3158	3.30439	3170.38	0.453449	3170.43	23.7956	3164.71	15.0337
3159.08	0	3170.57	35.0007	3180.44	41.5783	3165.5	2.8712
3160.14	49.5445	3184.95	60.219	3182.83	17.7006	3170.87	19.5016
3161.01	0	3185.91	0.552442	3186.15	37.7457	3176.03	29.0481
3163.53	4.65787	3190.94	13.1314	3195.19	3.26381	3185.81	37.8062
3164.28	0	3199.69	5.39883	3201.34	1.48853	3186.36	0.311925
3176.72	0	3204.17	0.158667	3209.62	14.2726	3188.42	30.4059
3176.74	66.664	3209.18	2.00739	3211.07	24.8419	3197.6	3.00405
3188.5	82.9821	3217.88	30.061	3219.47	26.2675	3209.23	15.9633
3188.64	0	3223.69	19.7336	3223.72	6.77513	3215.72	20.5805

Table 2. Continued.

34		35		36		37	
Frequencies (cm⁻¹)	Intensity (Km mol⁻¹)	Frequencies (cm⁻¹)	Intensity (Km mol⁻¹)	Frequencies (cm⁻¹)	Intensity (Km mol⁻¹)	Frequencies (cm⁻¹)	Intensity (Km mol⁻¹)
33.9811	0.215373	46.9727	0.45125	56.6394	0.750376	38.9534	0
54.9778	0.32887	51.1992	0	63.3405	0.0364295	42.6283	0.0198015
103.957	0	108.294	0	90.1627	0.293936	82.4277	1.23347
126.613	0.316439	113.858	0.0977526	121.485	2.9865	90.228	0
130.796	0	126.006	1.62478	153.693	0.12161	155.187	0.137935
183.652	1.24346	214.262	0	194.853	2.17059	167.021	0.20064
214.352	6.33487	221.785	0.229942	216.629	0.832521	220.494	0
214.443	0	256.289	0.535406	253.824	1.45807	246.207	0.0806311
277.717	0	277.509	0.950036	287.799	1.35146	287.129	0
323.839	0	291.709	0.471197	308.289	0.601265	310.94	0.428357
331.062	0	313.467	0	320.515	3.74974	319.661	0.46031
395.472	0	398.026	0.668886	399.259	1.63879	336.782	0.153237
403.498	4.62553	403.557	0	403.215	2.51631	411.479	0.198015
432.054	0	415.57	2.37851	415.062	3.15669	422.305	1.39668
437.604	17.1731	418.354	2.08456	437.774	5.52032	433.553	0.617296
460.609	0	468.82	0.042773	471.898	2.53578	451.61	0
490.884	8.09893	469.831	0	482.177	24.346	457.716	0.0455284
505.58	0	481.465	31.3023	502.954	4.64101	476.318	10.664
519.476	0.594776	532.355	0.776265	522.071	4.53047	550.164	0
529.102	1.31345	538.942	0.0288792	529.818	10.2913	550.963	0.0776308
540.399	18.1911	551.812	0	537.867	0.396974	557.976	4.51474
551.399	0	561.369	6.84526	569.706	5.38692	566.511	7.50E-05
561.087	0	568.776	0	587.427	10.7647	587.957	8.317
578.709	0	628.107	1.6213	600.117	4.10617	605.982	0.253294
638.11	0	635.76	5.34634	636.016	3.66545	634.403	3.21234
662.419	16.1969	645.871	0.0120082	650.461	14.268	642.306	0.247744
676.41	12.2941	666.568	4.6562	660.47	23.3163	693.297	0.207616
720.13	0	675.039	2.65351	712.943	1.15664	695.41	0
734.763	0	746.993	0.248004	717.272	5.70675	714.262	0.457459
751.357	2.03956	752.457	100	743.393	2.70185	725.795	30.334
754.738	93.4938	756.269	0	754.953	100	754.768	0.397755
755.27	0	761.12	0	760.996	48.9409	761.888	0
765.755	0	771.13	1.07766	769.862	0.756626	765.778	0.000150011
781.951	5.67213	775.456	0	789.121	1.16789	769.131	100
785.024	0.609639	788.266	0.0264974	802.617	7.68287	777.849	0.0541541
785.995	0	808.615	0.0101226	804.862	17.2413	779.811	0
817.375	100	813.181	0.182306	817.37	13.1928	825.534	0.0217516
821.641	0	851.465	0	841.359	4.94405	853.151	0
873.787	0	855.059	0.0062522	843.659	55.6557	860.461	0
873.845	4.61877	858.858	7.02151	856.832	17.599	862.134	0.758982
890.249	9.7545	890.883	0	879.926	1.2836	897.138	0
893.661	0	898.928	0	901.521	59.8047	898.442	25.5026
895.009	0	901.894	21.1765	916.387	9.67024	902.044	0.846289
902.731	65.7474	906.538	72.0765	925.352	21.705	949.768	0
944.56	0	911.402	0.564484	949.388	3.16133	959.918	0.757557
959.404	0	922.409	0.317373	968.289	0.963953	972.522	2.6015
961.183	7.26487	969.63	0	971.83	5.33513	974.105	0.163812
982.146	0.00081069	970.292	7.29443	979.505	0.546621	983.469	0
982.495	0	985.663	0	983.404	1.07824	987.941	0.0600045
990.116	0	990.045	0.00704613	990.742	0.0217863	990.907	7.50E-05
990.629	0.00202673	990.269	0	1003.62	1.33718	1019.84	1.94947
1041.16	7.47051	991.233	0.0845535	1022.73	1.79201	1032.14	1.56657
1060.54	0	1034.9	2.36531	1031.61	9.22416	1045.57	2.86469
1063.97	13.222	1035.26	7.90972	1064.93	10.1653	1076.01	5.9508
1126.37	0	1114.35	0.0311617	1109.75	0.75734	1084.9	2.24252
1131.5	5.82089	1156.49	0.300999	1156.56	1.97148	1130.71	0.60192
1171.83	1.6353	1166.02	4.29129	1162.4	2.19523	1151.54	0.124809
1174.05	0	1169.22	3.51403	1171.88	11.6017	1161.4	2.64035
1185.04	0.149302	1179.44	0.981198	1180.75	8.37414	1178.03	0.753507
1186.77	0	1197.27	0.549201	1184.02	0.529478	1192.53	0.648424
1206.61	5.3515	1199.45	6.38637	1195.24	0.360545	1200.37	0.851464
1225.34	0	1215.85	0.975045	1214.5	5.16191	1222.62	0.916494
1236.47	9.04447	1240.13	0.831741	1228.57	0.696803	1229.47	0.718254
1241.45	0	1259.45	4.63645	1235.35	1.97309	1257.46	3.6167
1247.15	13.2547	1278.96	0.0924908	1256.54	13.2735	1265.37	0.86519
1284.26	0	1294.07	3.69018	1284.95	1.40236	1279.61	2.75203
1309.65	0	1294.62	1.68859	1291.68	1.31718	1312.24	1.80704
1315.26	0	1313.38	2.52132	1312.46	7.29375	1322.49	0.0103508
1323.13	2.97767	1354.24	1.19834	1353.84	2.28452	1339.41	0.932095
1352.25	5.48418	1356.27	0.782021	1355.29	0.506977	1347.1	0.662975
1366.25	0	1371.09	6.71754	1374.8	9.34166	1352.66	0.0956322
1374.13	4.05264	1396.94	4.94132	1382.61	5.80461	1374.07	2.13339
1403.16	0.35238	1409.56	2.63604	1401.33	3.19365	1381.09	1.73691
1442.11	0	1414.41	0.0811793	1417.78	0.594301	1419.59	0.276246
1457.4	6.03005	1439.03	0.974251	1444.52	4.29064	1460.31	15.3113
1460.86	0	1452.92	0.0484297	1448.04	11.8305	1466.32	4.51376
1464.41	2.39208	1473.26	0.533719	1453.06	0.496977	1479.7	2.25317
1485.75	36.6129	1476.19	4.92097	1478.46	2.19041	1484.86	4.59582
1497.49	0	1509.46	0.0326504	1507.34	1.49736	1506.89	0.33445
1532.9	0	1512.38	0.797205	1521.2	2.61453	1526.94	12.5049
1541.02	18.2096	1541.4	28.4504	1539.88	13.993	1543.71	13.4994
1586.13	4.73362	1593.23	2.2758	1575.63	9.22344	1595.81	0.709028
1595.92	0	1596.55	0.016871	1590.33	1.80147	1602.79	0.012976
1633.22	0	1620.77	1.81899	1626.85	1.66254	1614.71	0.209641
1645.48	1.52842	1641.6	0.46435	1628.53	10.2124	1635.12	0.929545
1651.58	0	1651.53	0.00516054	1644.8	1.49861	1643.4	0.378478
1656.83	0	1664.88	1.20022	1662.79	1.53647	1647.5	0.000975073
1658	0.643958	1668.32	0.2223	1666.1	1.66611	1665.51	0.0904568
3156.26	0.987691	3153.5	2.75752	3155.37	7.46447	3157.86	2.34378
3156.43	0	3155.06	8.28753	3157.49	3.17615	3162.35	0.0363027
3159.61	0	3157.31	0.528162	3158	10.3106	3167.45	0.489562
3159.63	8.77572	3157.7	9.65984	3159.69	6.34677	3168.11	0.86219
3168.79	15.3268	3158.66	2.17884	3161.29	1.85219	3175.75	15.1173
3169.13	0	3162.41	2.1563	3162.29	2.1563	3181.46	26.1149
3175.33	0	3162.45	1.93461	3169.69	17.1924	3182.9	14.2332
3175.62	69.8315	3174.63	0.380788	3175.48	40.2358	3188.21	19.6935
3177.8	19.6818	3175.48	13.9839	3177.19	28.4084	3190.28	0.0198015
3179.14	0	3176.12	55.212	3179.38	82.6137	3191.86	0.717204
3186.37	65.0286	3176.17	13.5002	3186.6	54.8944	3202.76	0.0159762
3186.72	0	3187.98	1.93659	3187.9	47.5173	3212.78	22.5275
3197.56	54.7994	3188.12	54.5734	3205.67	3.20579	3213.27	5.06558
3198.09	0	3190.09	14.8023	3226.05	5.23102	3221.14	16.6197

Table 2. Continued.

38		39		40		41	
Frequencies (cm⁻¹)	Intensity (Km mol⁻¹)	Frequencies (cm⁻¹)	Intensity (Km mol⁻¹)	Frequencies (cm⁻¹)	Intensity (Km mol⁻¹)	Frequencies (cm⁻¹)	Intensity (Km mol⁻¹)
41.8745	0	45.4699	0.631878	45.8323	0.266821	64.546	0.0483532
54.3537	0.641557	60.2029	0.023372	71.2575	0.0175635	71.3969	0.251463
106.268	0	104.769	0.111573	98.3848	0.255031	90.1026	0.170088
115.65	0.200094	120.675	0.469387	114.317	0.575746	120.248	1.96348
129.055	2.36055	142.695	0.486777	154.542	1.12695	168.318	0.0725953
184.579	0.376623	189.92	0.0392315	196.111	1.78546	173.209	2.52917
213.886	0	225.14	2.94862	227.276	1.01567	228.59	2.87262
251.079	0.159518	233.716	0.859754	245.488	2.45696	243.821	0.224207
284.45	5.78502	293.388	0.0155813	263.136	1.92813	273.85	0.778106
304.898	0.959616	300.592	2.63978	310.594	0.804311	311.766	2.08561
310.785	0	325.686	0.0528652	315.255	1.8722	342.562	0.00694504
407.965	0.134837	381.876	0.542424	408.649	1.04828	398.473	2.68956
414.285	0.0133861	395.89	0.342511	415.235	3.66536	419.118	3.31829
416.166		428.605	7.93687	425.469	5.16643	420.215	1.89219
432.803	6.67562	456.904	5.14865	438.779	6.61771	449.382	0.000262077
441.9	23.1783	472.32	21.2013	471.92	4.82695	470.154	3.29562
501.306	3.06639	480.235	5.69052	498.013	0.216656	476.254	0.000393115
526.021	2.27424	482.862	1.69544	505.294	8.66349	494.791	0.0349873
528.77	0	517.854	2.01847	527.77	2.63512	524.437	21.4025
529.615	0.501003	529.45	1.66177	529.598	0.0447508	536.546	5.89896
534.35	0.0909139	547.47	1.74594	549.234	1.19408	544.632	0.718222
566.721	7.64123	549.001	4.08383	570.638	0.812492	550.967	14.9107
570.311	0	564.51	4.62222	575.042	7.93485	574.632	0.00930373
579.576	0.0097607	599.213	5.6044	589.289	1.53115	608.959	0.69149
605.933	14.6367	639.074	1.29826	605.16	0.58958	634.284	17.081
663.1	3.40857	646.676	5.11679	658.835	8.513	657.662	20.7489
676.62	0	684.812	6.02718	667.923	7.17601	678.287	2.45566
720.315	15.354	723.665	1.40009	689.497	3.39047	690.926	0.135232
729.967	0.651457	742.422	1.28532	727.391	13.6751	723.236	0.00877957
734.867	1.01455	751.929	100	734.536	12.3732	734.098	2.66401
754.149	98.2259	752.809	1.22995	757.491	5.98746	752.156	49.9982
757.264	0	757.592	10.6622	758.629	100	764.004	13.2632
779.085	4.19208	767.182	0.536164	773.335	2.50953	776.751	21.6911
783.096	3.59166	773.339	0.209235	798.833	4.14534	784.605	23.7739
788.758	0.0263539	784.521	2.13909	800.912	20.6156	797.434	3.15357
789.942	0	799.247	1.49469	809.932	10.4684	802.598	19.5311
815.119	100	816.339	61.8131	818.209	6.43028	813.853	1.46802
827.371	0	847.091	0.415826	843.512	7.40036	837.89	11.9518
872.301	5.47059	848.496	2.33608	849.65	76.418	855.432	100
874.51	0	869.604	1.86906	874.17	2.08681	865.938	1.18433
875.784	1.86959	876.118	0.728704	877.544	2.22022	881.567	0.444744
890.06	4.72892	884.483	1.70393	886.859	14.0325	882.216	18.323
897.811	5.25725	890.549	5.15626	892.247	1.65626	937.071	1.42295
909.527	60.7888	908.552	0.117834	961.387	2.44313	949.331	1.56958
959.779	0	921.037	95.6826	966.356	1.06151	965.269	0.0461255
960.368	7.22013	930.06	2.22131	972.778	0.871317	970.007	3.49388
977.497	2.0259	961.374	5.0048	981.687	0.0623143	971.644	0.0883199
982.641	0	976.041	5.28429	989.031	0.748012	980.757	1.95719
984.225	0.14404	984.611	0.0375621	991.58	0.57334	983.229	0.608673
989.842	0	991.501	0.0289367	1011.87	1.70282	997.535	0.27767
990.821	0.00139439	992.42	0.00584299	1012.55	0.870836	999.243	0.380142
1017.84	1.17937	1001.8	2.20656	1017.63	0.15747	1045.74	5.31741
1059.07	8.75381	1023.66	7.72722	1056.98	10.3187	1057.25	7.80124
1066.8	8.42529	1064.74	7.88219	1064.68	4.67129	1082.01	2.3258
1125.56	3.03362	1126.66	2.87726	1105.76	1.03781	1093.9	0.0712849
1132.4	1.61512	1149.48	6.27579	1148.01	1.88122	1150.45	6.87231
1168.15	1.22831	1157.65	1.54519	1169.81	0.671142	1165.94	0.660696
1178.83	1.22748	1172.54	2.53628	1171.92	0.529551	1171.28	5.58407
1181.8	0.0483852	1188.02	0.294097	1180.75	1.20105	1179	0.750981
1189.37	0.0108762	1189.53	1.76069	1186.58	4.50335	1182.68	0.00380011
1197.48	6.74311	1207.85	0.655806	1198.66	1.67515	1184.25	4.90647
1223.81	0.048664	1220.82	0.158735	1210.04	0.255874	1207.17	2.57556
1237.9	5.02132	1232.77	0.811758	1236.28	1.27468	1224.29	1.28496
1247.3	14.2747	1254.78	5.5187	1243.39	0.418516	1233.38	0.992878
1259.51	0.780856	1270.58	2.69501	1254.02	3.33466	1238.33	1.46449
1289.06	0.454848	1297.86	6.23948	1259.1	17.3397	1248.4	6.86877
1292.17	0.821014	1306.63	0.828453	1286.27	5.12589	1285.45	7.31719
1309.97	4.36233	1316.75	1.98592	1305.21	0.41214	1297.01	1.33672
1329.58	0.192286	1325.36	2.20434	1344.95	1.99165	1342.85	9.07454
1352.97	1.81382	1350.49	6.12262	1356.28	0.80383	1356.2	0.00117935
1362.91	3.97539	1373.51	8.1845	1374.14	0.620978	1364.41	0.984754
1376.38	3.03056	1381.88	0.777674	1375.86	1.12442	1373.94	1.69616
1409.99	1.40638	1415.36	0.038675	1392.75	1.17014	1396.97	1.74818
1444.28	0.0376484	1424	6.24045	1416.72	0.663804	1411.43	2.06084
1454.22	2.98789	1443.62	0.164995	1447.92	1.99598	1446.67	0.258146
1455.86	4.4011	1448.67	1.96631	1454.95	4.12718	1447.32	0.533326
1464.36	1.37096	1469.87	3.93651	1463.7	2.57004	1464.58	7.17016
1482.34	24.9369	1485.31	12.5808	1478.68	12.0279	1470.66	9.4539
1506.88	1.16459	1497.56	1.74079	1515.66	3.85976	1512.87	3.80575
1523.79	18.2878	1524.92	14.0477	1526.11	6.27257	1524.47	5.1827
1547.08	14.4489	1560.58	4.71641	1548.66	8.02712	1544.86	0.0572638
1586.88	4.81704	1583.34	1.63729	1561.46	1.18373	1552.56	5.86593
1597.61	0.030537	1589.95	4.56588	1596.29	0.195243	1588.22	0.102472
1631.39	0.120754	1612.84	0.293123	1626.45	0.994502	1620.22	0.247401
1645.59	0.468653	1639.17	0.106009	1640.87	1.34698	1643.53	0.0078623
1648.04	0.149199	1653.86	0.0741503	1644.3	1.80663	1645.3	2.66218
1657.6	0.018127	1657.73	0.0477178	1652.34	0.970082	1652.52	1.10885
1662.84	1.72332	1669.1	4.84815	1658.79	0.671382	1657.82	0.798548
3154.94	5.1694	3152.54	1.46687	3157.74	0.903798	3157.54	0.677075
3157.07	0.767051	3153.71	11.2358	3159.39	0.583324	3157.96	2.64763
3158.32	12.3884	3155.4	1.62546	3160.24	2.42352	3159.82	6.62111
3160.08	8.18072	3157.33	1.9414	3164.14	10.5789	3160.33	0.70669
3160.43	0.436443	3158.16	25.4301	3165.54	4.33024	3162.25	0.360618
3169.82	10.3454	3159.69	3.57855	3170.04	20.557	3170.87	22.3017
3170.13	4.17033	3162.41	2.72089	3170.46	10.8989	3171.01	0.720187
3176.61	25.6231	3169.15	7.32725	3177.77	41.5137	3176.92	1.75316
3177.16	65.008	3175.32	37.1045	3185.11	32.6586	3177.76	58.3678
3184.05	0.147387	3175.71	47.7332	3186.38	34.7385	3180.75	55.2067
3185.03	79.7631	3178.84	17.1362	3194.89	6.18872	3186.25	36.6487
3193.34	27.0364	3186.9	29.6676	3211.38	22.5888	3186.49	30.0297
3196.36	1.02473	3188.01	48.3083	3212.84	2.02942	3216.21	5.99461
3222.49	11.8184	3199.27	22.6502	3228.8	5.74543	3216.88	3.07862

Fused-Ring Heteroacenes

Table 40. Optimised and single-point energies of the neutral, anionic and cationic isomers, in Hartree (atomic energy units).

Isomer	$E(M_{OPT})$	$E(M^+_{OPT})$	$E(M^+_{SP})$	$E(M^-_{OPT})$	$E(M^-_{SP})$
43	-2758.221	-2757.974	-2757.970	-2758.256	-2758.252
44	-2758.217	-2757.958	-2757.957	-2758.247	-2758.243
45	-2758.219	-2757.973	-2757.968	-2758.252	-2758.247
46	-2758.220	-2757.971	-2757.967	-2758.248	-2758.240
47	-2758.218	-2757.973	-2757.970	-2758.255	-2758.251
48	-2758.221	-2757.956	-2757.954	-2758.244	-2758.240

Table 41. Reorganisation energies and vertical ionization and electron affinities, in electron volts.

Isomer	λ_1	λ_2	λ_3	λ_4	IE_V	EA_V
43	0.1065	0.1060	0.1196	0.1184	6.845	0.830
44	0.0433	0.0408	0.1094	0.1049	7.071	0.716
45	0.1197	0.1206	0.1157	0.1147	6.816	0.774
46	0.0983	0.0966	0.1306	0.2264	6.889	0.535
47	0.0992	0.0987	0.1095	0.1104	6.748	0.915
48	0.0509	0.0500	0.1177	0.1123	7.246	0.526

Table 42. Frequency data of fused-ring heteroacene isomers **1**-**6** optimised at the B3LYP/6-311++G(d,p).
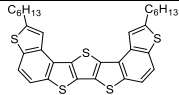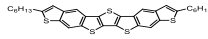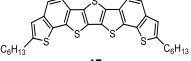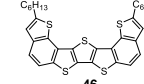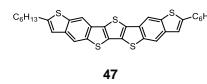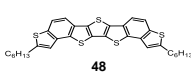
43		44		45	
Frequencies (cm⁻¹)	Intensity (Km mol⁻¹)	Frequencies (cm⁻¹)	Intensity (Km mol⁻¹)	Frequencies (cm⁻¹)	Intensity (Km mol⁻¹)
33.163	0.12396	22.5026	0.106814	25.5388	0.816309
40.8766	0	57.0173	0	51.7489	0
59.4599	0.0898259	59.8861	0.263828	61.9131	0.501095
82.2506	0	68.8166	0	73.3614	0
86.7811	0.286074	102.976	0.546406	95.6041	0.00317939
136.54	0.0566331	131.631	1.29156	136.986	1.33126
142.359	0	146.066	0	142.844	0
145.097	0.0828109	162.734	0.0306046	150.432	0.0247539
199.143	0.679426	184.53	0.626244	183.506	0.0244132
199.453	0.000941033	206.007	0	205.946	0
219.767	5.45149	219.561	1.46225	207.095	1.62001
245.475	1.81098	266.277	0.311247	238.734	0
264.264	0.000256645	273.035	0	249.214	0.35348
285.079	0.0400367	277.311	0.0210482	255.49	9.50287
303.754	0.267168	284.464	11.8703	284.137	2.20729
309.593	0	311.66	0.874952	295.102	0.0024981
333.625	7.30986	340.711	0	321.602	0
342.493	4.04242	366.382	1.72039	387.959	1.04443
357.996	0.000256645	377.498	0.0277014	389.242	0.140007
428.982	0.662658	409.571	0	415.992	0.201551
449.405	1.73373	412.792	17.1753	467.554	0.279219
449.501	0.00111213	423.586	0.808057	471.947	0.909647
465.245	2.02237	460.79	0.198264	478.443	0
485.038	0.384113	482.666	5.51959	491.928	0
489.161	3.09711	484.499	0	493.486	0.00306584
497.4	5.95939	491.194	0.745518	496.531	5.87927
527.776	0	499.162	0.970153	519.898	0.645417
539.387	0.215325	536.311	4.08226	535.737	4.11777
550.367	0.265029	554.655	1.09293	543.959	0.215745
567.367	1.20375	560.257	0.924669	544.181	0.0185086
588.247	0	599.366	0	584.323	0
606.467	0.163141	602.965	6.4451	588.902	7.45965
609.049	0.435014	639.527	2.53945	597.838	0.566273
611.96	0.236199	640.162	0	621.522	0
619.927	0.000598839	650.605	36.1077	623.837	34.6574
621.01	0.0621082	686.332	0.346449	662.159	1.69257
677.307	0.000256645	688.01	6.3043	678.515	0
686.364	52.1272	690.701	0	683.805	7.47067
696.046	1.0525	698.399	29.3362	684.093	43.4177
732.473	5.98001	720.734	44.7649	712.847	0.775545
738.095	0.482322	745.886	0	738.798	0
738.684	0.00273755	746.038	55.1135	741.06	23.4149
741.407	53.0837	751.565	0.664712	753.862	1.43516
785.35	42.2112	758.072	2.99308	797.582	0.121612
785.424	0.043202	768.45	1.72849	799.24	11.5191
806.131	15.3511	824.15	66.1385	816.023	0
807.47	9.96511	825.619	12.8993	818.049	100
860.325	100	858.422	0	820.845	64.4455
862.523	6.51084	858.645	22.8459	821.852	31.5139
882.588	8.55E-05	869.334	0	894.09	6.8198
883.005	0.474452	871.483	44.1773	894.106	0
922.747	14.7218	898.33	0.206127	938.289	2.40635
923.551	2.76792	901.43	4.2821	940.959	14.7927
941.449	0.00102658	902.597	0	952.426	17.2189
941.461	0.000171097	902.706	14.83	956.199	0
944.118	0.483092	945.733	84.7829	956.821	0.754879
1026.15	12.3026	1028.87	0.00193547	1043	0.756696
1047.78	25.0624	1044.57	3.17913	1050.2	31.7122
1113.04	0.0518424	1090.72	14.4876	1096.26	1.63909
1113.38	7.62382	1091.87	0.34282	1098.67	0.317939
1163.27	5.13701	1114.69	4.16718	1132.26	0.0183951
1163.38	3.80545	1115.54	8.75811	1133.87	45.1029
1170.8	32.1371	1194.7	0.943903	1160.54	1.17728
1171.83	0.177	1196.64	10.5771	1160.77	0.200302
1220.1	5.68615	1263.95	0.0430641	1235.3	1.10336
1221.63	23.3675	1264.52	0.998338	1235.37	3.66414
1291.53	0.101717	1303.75	47.4702	1310.36	0.75011
1292.04	3.31252	1306.09	33.0177	1324.42	57.2643
1323.2	5.37433	1318.47	30.334	1325.64	16.1942
1347.94	31.9042	1326.01	28.9445	1356.96	4.73877
1350.63	1.11076	1333.77	3.44295	1365.87	0.583419
1374.71	0.767969	1343.11	12.4382	1379.01	0.0197577
1390.29	43.0148	1367.15	20.043	1397.86	73.3225
1418.44	35.5121	1431.84	11.4926	1399.2	10.6764
1424.59	31.273	1434.34	3.76001	1405.56	12.0814
1447.22	4.13285	1457.46	100	1427.42	31.8828
1450.14	23.7169	1461.4	7.74308	1439.56	7.47544
1471.1	0.668561	1489.61	11.7985	1469.48	16.458
1477.67	1.37006	1495.29	3.24421	1477.51	4.02432
1526.69	36.1077	1518.84	4.72254	1532.42	2.46165
1527.26	1.19332	1519.83	5.41955	1534.13	23.0915
1570.83	2.04812	1575.8	6.08269	1583.28	0.0704009
1571.72	0.135167	1577.55	12.0663	1585.74	0.602949
1604.49	0.0163398	1628.64	0.0407658	1612.8	3.16475
1604.95	9.32974	1630.92	0.018024	1614.97	13.0255
3179.76	1.03924	3174.41	1.99196	3171.44	8.14606
3179.88	0.612955	3174.42	6.63877	3171.46	0.427969
3194.94	6.01029	3186.14	1.7493	3187.72	3.07992
3195.01	8.12445	3186.16	2.5755	3187.78	21.1057
3208.32	0.169472	3200.71	7.92441	3201.02	21.8299
3208.77	2.4466	3200.73	6.54333	3201.06	0.541973
3241.79	1.72774	3239.66	1.80603	3242.34	0.377099
3241.83	0.924522	3239.66	1.37878	3242.34	1.87891

Table 5. Continued.

	46		47		48
Frequencies (cm⁻¹)	Intensity (Km mol⁻¹)	Frequencies (cm⁻¹)	Intensity (Km mol⁻¹)	Frequencies (cm⁻¹)	Intensity (Km mol⁻¹)
Frequencies (cm^{-1})	Intensity (Km mol^{-1})	Frequencies (cm^{-1})	Intensity (Km mol^{-1})	Frequencies (cm^{-1})	Intensity (Km mol^{-1})
34.4858	1.15349	24.7757	0.818351	22.0829	0.16411
37.8296	0	50.6138	0	56.9907	0
59.5428	0.553795	58.4774	0.509072	60.5265	0.181061
80.1245	0	75.3998	0	68.2184	0
85.8929	0.197814	98.5354	0.109184	101.821	0.22319
133.171	0.0190817	133.931	2.4022	133.477	0.00166187
138.65	0.742916	141.433	0	148.041	0
145.666	0	156.899	1.05892	154.664	0.799943
195.496	0.295767	188.765	0.398831	186.428	0.0206072
196.29	0	206.388	0	203.324	0
219.239	6.53359	219.071	0.362436	206.769	1.89869
248.95	1.90446	277.915	1.40338	234.066	0
259.689	0	278.823	3.87309	252.232	6.85215
267.223	1.58283	279.989	0	255.335	0.00108022
297.834	0.540755	311.499	0.336009	302.195	2.82535
304.944	7.11198	313.31	0.791471	302.374	0.0278364
306.928	0	335.109	3.40947	326.122	0
380.079	0.691925	337.645	0	372.56	6.78909
381.627	1.67357	344.118	0.248873	393.551	0.202832
428.289	0.454358	409.226	0	412.025	0.146993
466.622	0.501108	410.637	19.5613	447.723	0
469.946	0.00519447	421.298	0.0385089	448.89	2.60956
477.098	0	469.283	1.80176	459.35	0.428514
489.728	0.54436	482.744	11.2537	470.627	4.0509
493.026	0.00540649	488.337	0	486.001	0.0824289
494.677	2.0851	524.679	0.00739974	506.758	1.86869
495.02	0	529.519	0.310487	522.926	0
520.098	0.317181	540.22	1.50879	546.881	2.14207
533.319	2.09581	555.315	9.75951	561.68	0.26108
544.032	7.79203	559.13	0.0934784	562.39	0.055008
590.967	0	567.087	2.50897	580.489	0
624.022	6.09609	601.309	0	598.169	0.0013295
624.53	0.0022262	609.611	5.66805	599.116	12.4677
628.164	1.4288	638.392	0	622.247	2.44295
628.995	31.8168	648.634	38.3468	622.779	0
631.422	0.000318029	681.501	8.06482	649.741	1.5497
678.991	0	684.431	3.17585	686.692	0
682.585	0.170782	686.497	0	691.923	50.6881
683.375	42.2236	693.877	45.8271	698.006	0.832599
707.941	9.1727	727.148	25.4953	732.149	0.114005
735.98	6.03354	740.696	6.23557	744.543	0
737.182	0.000212019	746.022	0	745.256	48.8804
738.715	11.9698	746.463	65.262	761.932	1.0503
807.689	0.00402837	774.541	47.2682	796.132	0
808.255	100	796.744	25.0865	799.018	43.5626
810.127	1.61527	824.509	24.6623	801.871	7.55554
810.89	13.3174	827.21	45.4577	802.035	0.244212
842.271	31.8714	857.464	0	841.8	100
845.398	24.9643	859.547	23.2314	845.849	0.570604
896.076	6.56656	867.856	0	883.238	1.55792
896.092	0.0313789	868.283	62.7699	884.646	4.82159
906.122	11.4225	899.152	0	891.344	0
915.177	7.92433	899.242	21.1838	891.473	0.861266
948.898	0.196118	902.94	24.2616	948.298	0
949.094	0.00010601	905.985	1.78077	948.43	0.0955577
967.385	9.83855	940.089	17.8174	965.845	24.0765
1056.92	1.35226	1027.11	11.6877	1090.41	0.031077
1063.62	10.6347	1049.11	54.9649	1096.75	2.04618
1115.25	5.56689	1070.77	37.1473	1103.84	2.45874
1115.45	3.31036	1071.38	30.6108	1105.92	0.790803
1121.86	4.58237	1105.93	3.03903	1113.99	5.48061
1125.49	0.471319	1106.08	26.2123	1114.54	23.4052
1166.82	0.526868	1214.55	12.3185	1173.02	6.05346
1167.3	8.4247	1215.31	9.82595	1173.6	2.58122
1230.27	0.904051	1263.74	0.0815482	1222.87	28.3152
1231.22	1.55527	1264.92	0.0211421	1223.16	12.0991
1295.24	57.6907	1300.31	34.3265	1310.91	1.07922
1296.89	0.980802	1300.54	16.8216	1323.31	20.4169
1332.77	48.8917	1321.5	7.42179	1324.34	22.9994
1341.83	0	1342.06	36.1204	1343.45	5.73612
1343.73	16.5205	1344.52	0.644684	1344.84	8.08152
1377.85	6.07934	1348.31	11.6085	1364.53	0.067389
1379.67	1.48414	1362.96	60.3875	1395.38	23.0843
1404.38	0.798041	1404	0.270166	1416.8	11.9655
1432.92	0.875216	1419.03	3.87218	1420.65	14.2205
1442.74	47.7093	1459.37	100	1436.15	71.4637
1452.73	63.9828	1474.06	6.51948	1445.2	5.41114
1467.84	0.755001	1486.37	82.6112	1479.27	7.93245
1472.58	0.644857	1490.86	3.7047	1487.38	2.72996
1533.52	0.217744	1525.89	1.02177	1534.14	0.45419
1533.55	0.0530048	1526.97	10.2825	1534.26	0.423445
1581.43	19.0098	1571.04	1.43102	1573.59	2.11565
1582.06	0.285272	1572.55	1.20299	1576.54	1.35343
1609.12	11.1437	1625.23	1.13881	1610.66	0.272963
1609.53	3.68288	1627.94	36.443	1612.64	1.5723
3174.66	0.674646	3178.71	9.74456	3176.09	1.01191
3174.68	0.148096	3178.74	9.45808	3176.11	0.173417
3190.98	18.1649	3181.85	1.65377	3192.7	1.73782
3191.01	8.16836	3181.88	0.979183	3192.74	10.865
3200.97	12.9322	3199.47	30.0422	3203.82	0.853289
3200.99	2.06687	3199.51	1.01724	3203.83	1.38185
3241.28	1.29512	3238.69	0.955322	3241.66	1.65323
3241.29	0.6562	3238.7	3.46429	3241.66	0.0939789

Oligo-Fused Heteroacenes

Table 43. Frequency data of oligo-fused heteroacene compounds 1-9 optimised at the B3LYP/6-311++G(d,p).

Compounds: **151**, **152**, **153**

151 Frequencies (cm^{-1})	Intensity ($Km \cdot mol^{-1}$)	152 Frequencies (cm^{-1})	Intensity ($Km \cdot mol^{-1}$)	153 Frequencies (cm^{-1})	Intensity ($Km \cdot mol^{-1}$)
16.5237	0.332624	10.795	0.00744589	8.0117	0.245771
19.4599	0.0673706	15.5753	0.0215531	12.8147	0.313453
23.3226	1.1749	17.092	0.0492639	14.1892	0.939705
35.9346	0.679976	17.7822	0.0399483	18.2771	0.032195
47.8061	0.060252	26.7698	0.0016302	31.0246	0
56.8872	0.137804	28.5338	0.00673172	34.6363	1.10639
93.0301	0.930939	32.7539	0.00183592	66.4063	0.189212
127.17	0.0341228	44.1093	0.00414783	88.8953	0
139.799	0.390954	56.1024	0.019412	96.1952	0.374405
146.086	0.0294564	60.3391	0.00584776	102.854	0
182.048	0.222365	71.3045	0.00414783	104.058	0.275405
190.452	0.284794	74.0329	0.0128515	121.55	0
209.868	0.0969728	77.161	0.00611975	141.612	0.0365524
240.909	0.359747	79.674	0.0287584	145.199	0.700572
245.929	0.360039	85.097	0.023969	148.536	0
285.248	0.167989	93.0997	0.00897563	204.682	0.33011
318.272	6.8597	94.6303	0.105906	216.673	0.435731
377.709	1.20594	119.962	0.0216231	226.442	4.45586
390.608	0.0212603	124.696	0.16052	235.029	0.0213144
397.689	2.07405	129.723	0.134702	245.113	0
420.694	0.858757	134.394	0.0353625	271.168	0.148173
433.325	1.06216	142.336	0.00395195	296.576	0.307389
476.3	0.244984	147.166	0.027916	300.023	4.30169
484.599	5.46489	157.364	0.311323	338.68	0
498.68	0.689601	173.006	0.266447	348.884	1.89231
518.47	0.0378225	197.535	0.0370925	382.148	0.286343
542.355	0.659981	205.983	0.00220591	405.948	0.738527
550.466	1.37279	209.564	0.0352225	428.566	1.01169
563.371	9.59036	214.131	0.0400163	445.647	0
568.622	0.210424	220.09	0.00650573	452.402	3.41648
597.612	4.99236	223.352	0.119539	463.848	0.083949
603.948	9.6881	227.041	0.0373644	475.065	2.89016
652.317	0.00049524	230.696	0.14514	486.954	0
670.786	12.7643	236.48	0.00611975	524.038	0.0073173
671.248	3.56379	238.453	0.0864624	532.641	19.8933
765.362	6.16978	238.787	0.00652773	541.485	0.358326
770.614	2.99055	240.556	0.0207391	542.893	0.0114462
812.427	3.94731	240.066	0.0679032	544.324	0
814.201	0.0872026	246.3	0.023765	560.592	0
828.521	10.656	252.343	0.156835	565.804	1.4061
828.546	10.7656	260.673	0.543977	585.065	1.55044
840.343	0.0180522	308.233	0.439478	585.372	5.4909
842.757	46.0427	345.86	0.827424	592.021	0.679258
877.215	77.7422	355.597	2.2043	600.388	0
881.961	13.2519	362.248	1.54143	646.378	0.801722
897.652	0.148449	368.055	0.53694	649.164	8.36807
897.685	0.19249	370.22	2.27971	656.55	0.0380462
957.258	62.4779	388.066	2.1233	674.648	14.0217
964.45	0.276482	416.151	0.952776	675.326	0
974.307	19.6235	418.973	1.72465	710.355	0.0842295
1072.64	33.3849	421.64	2.79938	714.394	0.704312
1072.76	0.0204153	430.303	2.02591	735.998	0.589252
1087.56	2.6852	432.763	1.1004	737.463	0.00317847
1087.57	11.1628	437.901	0.415497	811.131	57.6586
1105	0.01689	438.369	2.34213	811.153	0
1107.16	8.16278	445.888	2.45857	831.343	31.5157
1122.57	1.76768	460.811	1.11911	833.678	9.4237
1122.58	1.39568	476.007	5.04899	872.472	1.10171
1174.43	15.678	481.59	12.5212	878.627	0
1191.73	46.6089	498.021	10.2788	890.257	0.0184164
1207.52	8.85996	525.294	1.07997	890.258	0.3805487
1208.47	7.33129	532.876	5.81289	965.865	6.4795
1214	0.849386	550.654	17.2596	992.153	1.26139
1214	0.916882	560.968	1.67912	992.286	22.3001
1247.5	16.3789	577.67	0.00757759	1051.57	3.00415
1248.95	79.1803	596.79	1.36076	1052.62	0.0605779
1336.83	5.27022	604.02	2.28239	1069.87	2.65664
1374.86	0.53799	636.201	16.8212	1069.87	0.342246
1403	43.256	652.769	0.400673	1086.65	33.1588
1414.66	20.6968	655.443	77.1878	1097.97	28.3595
1417.77	100	664.646	12.7323	1177.88	59.7669
1440.92	1.75032	669.009	22.3237	1185.26	19.1454
1474.37	4.56764	673.704	22.8184	1185.81	19.9356
1491.99	2.32749	692.074	14.8059	1193.52	3.0561
1491.99	2.72038	719.548	58.4556	1224.63	25.0982
1525.72	0.747855	731.324	17.5983	1226.13	0.0136487
1526.01	0.872276	841.673	0.402271	1273.15	0.58755
1552.07	17.9624	844.244	0.06885	1282.83	1.10947
1558.18	5.10704	883.083	42.5106	1342.29	12.9559
2316.25	3.13682	890.154	4.80835	1364.67	0.954756
2317.00	57.9586	892.64	11.3956	1382.54	4.96898
3145.99	62.1749	894.35	5.3679	1405.43	28.5795
3146.06	3.08563	897.04	6.6012	1414.17	55.6498
3150.31	3.56408	897.532	6.10285	1437.04	31.6077
3150.32	43.5512	898.289	7.06157	1443.45	2.37609
3160.7	59.5259	899.699	7.0866	1443.55	1.39292
3160.74	2.00274	936.197	0.96437	1471.05	53.0277
3237.07	0.139553	939.694	1.26773	1486.94	31.4925
3237.07	0.151803	940.846	1.11131	1502.96	0.00233711
3245.34	20.3114	940.946	0.685207	1506.66	14.9151
3245.52	0.198612	942.382	2.64461	1506.66	1.82454
3250.75	58.2256	944.176	3.76694	1519.8	9.98441
3250.77	1.70874	968.214	1.64244	1520.8	1.86144
		990.437	0.0808486	1552.48	36.3334
		990.895	0.0531738	1564.9	10.2119
		991.363	0.0394584	1607.48	39.222
		991.452	0.0285108	1607.93	0.774331
		992.473	0.0296938	2283.02	16.8981
		992.611	0.157515	3044.26	100
		1024.44	26.4525	3044.34	41.6623
		1024.73	8.75443	3096.04	0.161354
		1036.01	0.494713	3096.04	26.6655
		1042.73	4.33825	3129.34	14.36
		1043.93	4.0188	3129.34	8.32675
		1052.86	19.911	3214.82	54.0154
		1093.28	1.25462	3214.85	0.26802
		1102.92	16.2071	3239.21	2.58815
		1103.34	2.94605	3239.21	5.8109
		1105.48	1.87281	3246.66	19.0132
		1105.27	2.08721	3246.63	0.0329052
		1110.48	3.57485		
		1144.01	0.18247		
		1159.91	15.6138		
		1192.05	4.99385		
		1195.33	20.1631		
		1198.49	0.184952		
		1198.57	0.284228		
		1199.52	0.157141		
		1200.3	0.152862		
		1201.06	0.0743549		
		1201.5	0.34563		
		1284.54	0.244212		
		1286.07	0.792881		
		1288.87	0.875396		
		1289.08	13.4785		
		1290.31	0.987824		
		1293.92	3.8447		
		1333.52	0.166287		
		1339.16	0.313433		
		1346.11	0.00741192		
		1347.29	0.00614405		
		1348.77	0.0687651		
		1351.62	1.0888		
		1351.83	9.18134		
		1363.26	6.57839		
		1427.33	15.8246		
		1427.48	0.0557577		
		1428.24	0.201102		
		1429.15	1.08292		
		1430.33	0.320981		
		1430.35	0.334886		
		1433.74	0.0925101		
		1436.76	9.30558		
		1447.08	0.403495		
		1448.48	0.0705811		
		1448.78	0.473834		
		1451.82	0.706627		
		1455.14	0.118179		
		1466.67	0.287046		
		1473.63	1.65308		
		1516.87	0.342766		
		1516.09	0.000985959		
		1516.86	0.118893		
		1519.13	0.269983		
		1519.36	0.388128		
		1519.98	1.29405		
		1525.1	1.01523		
		1527.13	0.645565		
		1527.56	0.283446		
		1528.96	0.24598		
		1530.48	0.36031		
		1532.73	1.80866		
		1535.08	0.254785		
		1535.61	6.80845		
		1535.83	1.28722		
		1536.2	3.412		
		1537.19	1.93612		
		1537.71	0.992113		
		1539.63	0.391902		
		1541.42	0.586416		
		1542.51	2.29195		
		1543.68	2.7394		
		1543.91	0.884031		
		1544.29	1.9659		
		1545.31	2.14514		
		1545.36	2.67352		
		2226.68	100		
		2228.98	52.1951		
		2584.42	4.57206		
		2988.5	12.3801		
		3009.47	6.22157		
		3009.93	3.53007		
		3012.29	4.39836		
		3021.9	3.64189		
		3030.65	12.2261		
		3030.94	11.325		
		3031.31	9.69388		
		3031.68	14.2661		
		3032.37	6.09618		
		3034.43	8.46801		
		3035.44	22.1116		
		3036.04	16.7077		
		3036.41	14.2099		
		3037.85	35.166		
		3038.75	5.7939		
		3087.25	38.6984		
		3087.67	8.23667		
		3088.06	4.94917		
		3088.42	9.79969		
		3088.93	12.3134		
		3090.05	7.10125		
		3092.92	5.38599		
		3093.44	24.0135		
		3094.52	29.3437		
		3098.41	23.6182		
		3099.35	10.2631		
		3100.77	24.6782		
		3102.22	2.86251		
		3111.07	15.1639		
		3111.58	4.04831		
		3112.21	1.31581		
		3113.09	38.5939		
		3115.84	12.0608		
		3116.67	0.589083		
		3120.05	10.1276		
		3123.39	5.7119		
		3124.77	12.9547		
		3127.59	12.9315		
		3127.97	15.944		
		3246.72	3.2331		
		3247.14	1.40271		

Table 44. Continued

	154		155		156

Frequencies (cm⁻¹)	Intensity (Km mol⁻¹)	Frequencies (cm⁻¹)	Intensity (Km mol⁻¹)	Frequencies (cm⁻¹)	Intensity (Km mol⁻¹)
15.7227	0.633773	15.7771	0.313386	14.9999	0.339374
19.3543	0.14582	18.5538	0.230588	15.8075	0.248744
23.5949	0	21.6773	0	22.4397	0.000933373
28.5663	0.197401	25.7166	0.244886	25.3432	0.137579
37.1227	0.0887283	36.4331	0.0323655	31.0296	0.0442419
38.3739	0	38.2162	0	31.5183	0.0183874
76.9089	0.407219	77.6798	0.42816	32.4143	0.46762
99.428	0.326975	97.0129	0.0617414	33.4492	0.00168007
113.439	0	115.481	0	60.7698	0.287852
137.172	0.0868399	132.054	0.0878678	88.4538	0.045922
144.65	0	144.214	0	90.9689	0.0014934
161.392	0.0164781	159.567	0.00415942	123.498	0.0601092
169.081	0.326794	172.193	0.388256	141.833	0.22513
218.5	0.221976	216.271	0.261784	142.293	9.33E-05
240.226	0.118761	239.579	0.394495	148.013	0.0070003
241.688	0	242.342	5.43064	195.044	0.000560024
244.583	0.533818	246.008	0	211.411	0.175474
295.614	0.110535	306.656	1.4389	226.147	0.130112
318.611	0	324.195	0	226.687	3.74357
388.923	0.00015521	384.33	0.0209271	244.415	0.140846
412.384	1.16353	412.054	0.00155978	276.39	0.00504021
412.832	0	412.082	0	331.051	0.038175
426.683	0.697202	417.357	0.326644	334.047	0.0382683
426.856	0.25532	424.194	0.300908	350.82	4.70205
431.953	0.373254	430.53	2.13989	358.806	0.00242677
435.3	0	431.699	0	388.775	0.101738
468.959	0.164755	467.618	2.21255	411.733	0.555637
489.36	1.27536	488.032	2.98243	413.732	0.00196008
499.619	0.277334	497.495	5.07189	413.912	0.0510555
532.811	2.25572	526.968	15.2136	429.172	1.57199
542.067	0	536.09	0	443.586	0.77694
561.736	1.83636	545.285	0.172876	450.101	0.0527356
566.821	0.294407	546.768	0.000389946	458.917	1.95383
572.063	0.0287138	562.705	0.843322	482.254	0.515502
575.964	0	566.657	38.924	487.858	1.24699
586.05	6.33473	568.236	0	525.573	15.2607
602.485	1.6372	601.81	7.86689	530.087	16.7445
630.3	0.576346	624.54	0.305197	538.468	0.000280012
641.674	0.497603	636.904	0.0292459	542.828	1.03016
645.268	0.760968	636.905	0.0552423	550.845	5.57821
652.606	0	650.622	0	561.223	1.1376
684.17	1.37927	677.033	7.6636	567.037	0.00690696
686.395	3.54815	679.418	22.9803	596.665	1.43571
753.307	0.000439741	703.142	0.0607015	601.641	5.65176
753.308	3.07289	703.161	49.8399	650.207	9.33E-05
793.17	2.834	771.332	0.160658	660.684	0.690416
793.397	5.17E-05	771.355	100	660.868	1.27732
793.418	18.7643	777.28	4.27783	667.452	4.17582
798.768	0.498663	783.354	2.87273	669.848	3.17748
838.871	0	835.938	0	721.449	0.586158
841.176	8.6093	838.3	43.7468	721.991	1.06227
889.692	5.69767	854.679	0	728.178	6.02371
895.61	1.94943	854.684	0.000779891	734.652	2.26231
904.584	2.59E-05	885.391	27.316	824.91	0.913679
904.589	0.448246	891.12	9.29396	826.783	4.56541
969.056	0.39312	926.17	0.0014298	833.306	0.719164
978.913	0.104637	926.181	7.34996	833.651	40.2996
978.913	7.76E-05	967.501	0.203422	834.931	0.177528
1003.44	0.534749	968.134	0.000259964	837.107	48.9972
1003.45	2.93957	968.135	0.000649909	850.804	0.00634694
1004.5	0.000801917	997.374	0.021317	850.81	0.152326
1004.51	7.76E-05	997.375	0.157148	886.508	18.5497
1071.53	0.920808	1015.08	0.00870879	891.884	6.3726
1071.72	0.556349	1015.12	0.193283	963.25	0.0793367
1115.64	2.0975	1054.42	1.55952	963.252	0.0639361
1118.1	5.40146	1054.46	14.491	967.231	0.22681
1128.35	0.13705	1103.22	3.98719	967.531	1.21077
1130.97	19.6764	1107.25	18.9813	967.537	0.93888
1184.28	6.66836	1110.78	9.39873	1018.9	0.516902
1185.16	4.93368	1110.8	0.0733098	1018.9	0.127499
1185.22	0.421291	1181.06	23.8525	1038.97	5.19142
1194.99	5.88033	1193.76	35.4585	1038.98	0.494874
1278.02	0.0872538	1194.26	0.000129982	1074.02	38.8868
1293.51	12.1201	1194.26	0.000649909	1074.07	11.2606
1301.04	0.0174611	1212.08	0.372658	1101.03	3.34446
1302.26	19.4107	1212.1	1.58552	1105.17	12.3605
1328.09	0.431587	1273.88	0.116464	1149.87	0.221209
1331.81	2.99588	1290.73	15.3149	1149.87	8.22442
1366.06	0.169799	1329	0.028726	1180.64	16.5969
1404.74	2.11396	1329	0.0154678	1193.47	27.0954
1413.29	10.9656	1363.86	2.43248	1218.13	11.6079
1434.06	34.102	1366.11	0.0126082	1218.15	1.26239
1469.95	2.40391	1366.12	0.868929	1242.2	0.861783
1470.62	23.6772	1403.97	9.94582	1242.21	9.23722
1472.25	1.65436	1412.44	50.0473	1275.37	0.0343481
1502.68	1.42242	1436.94	81.6908	1292.49	9.78931
1503.85	65.919	1472.23	4.78359	1327.53	0.0410684
1551.01	7.77179	1488.71	3.71579	1327.55	0.0448952
1556.75	5.33083	1488.71	8.40502	1349.9	0.199555
1615.51	1.03432	1523.88	2.482	1349.91	0.108178
1615.58	11.2337	1528.29	49.3474	1364.92	1.90165
1638.71	90.7769	1561.17	13.3012	1404.45	7.34163
1639.39	0.275109	1564.68	28.2477	1412.44	35.3521
2298.16	2.73981	1624.33	0.324565	1437.53	58.7092
2298.71	100	1624.33	3.89894	1442.61	8.94946
3172.25	10.2167	1658.16	71.5581	1442.66	0.405364
3172.31	11.8084	1658.36	2.61316	1454.03	3.43108
3196.22	2.954	2292.67	0.439599	1454.03	0.563477
3196.23	2.52555	2294.67	25.1427	1472.05	2.7793
3214.69	9.78129	3186.08	12.612	1517.27	3.1996
3214.7	3.68173	3186.09	0.508229	1517.27	7.8282
3221.89	7.13874	3194.67	1.45827	1518.88	12.292
3221.91	1.16661	3194.67	15.9234	1518.88	2.15189
3246.6	4.06854	3205.83	66.4592	1530.42	3.23311
3246.77	0.0110458	3205.84	6.42838	1536.41	27.4123
		3213.91	10.7898	1572.2	11.44
		3213.91	51.0569	1574.14	74.1235
		3217.82	56.7939	1607.26	0.470513
		3217.88	3.88568	1607.27	0.851796
		3246.52	23.0155	1668.11	0.404711
		3246.69	0.0419841	1668.14	0.0775633
				2291.57	0.00214676
				2293.79	0.828929
				3040.21	100
				3040.26	9.43435
				3097.88	13.9551
				3097.88	30.8063
				3126.36	10.9559
				3126.36	18.1497
				3180.96	14.9342
				3180.98	25.3716
				3182.33	69.9697
				3182.37	0.678002
				3210.66	5.26226
				3210.66	29.4548
				3212.45	1.7287
				3212.47	3.34512
				3246.25	18.4834
				3246.43	0.0494688

Table 45. Continued

157	158	159

Frequencies (cm⁻¹)	Intensity (Km mol⁻¹)
11.204	0.0774609
13.1438	0.0774609
17.3685	0.000604554
21.3513	0.0417142
24.7631	0.0224563
27.16	0.00360782
43.9719	0.259012
58.9638	1.11198
72.6228	0.294545
72.9903	0.0039296
73.142	0.0777925
77.8409	0.0262396
88.0141	0.857258
112.387	0.014441
124.67	0.00295451
130.953	0.00421238
140.449	0.00595778
162.481	0.00280825
190.632	0.0687144
195.577	0.00422213
201.282	0.156043
202.366	0.333236
210.005	0.0299742
237.991	0.000936084
238.148	0.528341
264.128	0.00126761
266.874	0.0776462
271.814	0.657394
291.065	0.478436
365.147	0.00565551
372.283	0.222593
375.909	0.202613
381.17	0.00200868
410.154	0.456107
422.531	0.00543124
422.951	0.0021842
427.956	0.00284725
435.01	0.0258203
462.894	0.0231681
467.205	0.0663937
471.691	0.140881
473.699	0.172415
474.996	0.0677783
502.561	0.436868
509.672	0.714866
534.255	1.53169
539.174	0.169412
547.601	2.20414
551.014	0.274204
555.641	0.279743
555.991	0.741456
562.374	0.0675735
597.553	0.0664814
600.693	0.555917
648.292	0.000146263
658.253	0.560373
659.777	0.206163
663.478	0.366057
666.891	0.115636
708.792	1.52671
713.974	0.287934
728.176	0.126625
728.185	0.00740091
803.083	0.412082
806.267	0.131803
812.859	0.000741066
812.866	0.0109307
827.679	0.0305105
828.989	4.5004
829.451	0.245702
830.609	9.07089
885.198	3.58912
890.334	0.837181
943.893	0.000126761
943.895	0.00033153
952.683	0.0825899
952.69	0.0850569
965.841	0.199532
970.629	9.09515
970.647	0.92919
1024.73	0.0022037
1024.76	0.0999464
1092.85	1.20205
1092.86	4.02956
1101.4	0.00291551
1106.42	3.59833
1151.42	10.0992
1151.56	0.498504
1156.8	0.0337185
1156.83	0.033387
1162.18	0.0564283
1162.18	0.00860027
1179.31	1.31589
1192.19	3.66544
1211.02	6.38152
1211.17	0.337819
1230.57	26.7785
1231.07	1.4871
1281.27	0.135664
1284	1.00242
1284.05	7.19128
1299.49	0.00433914
1337.82	0.172142
1337.83	0.00985813
1368.11	0.114563
1375.36	0.174658
1375.37	0.182195
1395.15	100
1399.25	4.4124
1408.4	23.2121
1412.96	5.44093
1440.01	4.76996
1466.61	9.75E-05
1466.62	0.000136512
1471	0.117966
1486.27	0.165609
1486.28	0.258369
1510.58	0.21646
1510.59	0.217912
1513.64	0.388611
1513.91	17.3578
1518.8	1.69785
1518.86	0.31705
1536.02	0.855298
1542.61	0.0854859
1545.04	0.382907
1545.06	0.37573
1561.27	7.70763
1561.28	18.4818
1582.32	5.08448
1582.91	70.1733
1589.76	0.571928
1589.77	0.49354
1670.61	96.3283
1671.62	4.20402
2285.3	1.10071
2287.85	30.5036
3003.72	6.48414
3003.76	9.03193
3011.23	30.0056
3011.43	7.14975
3066.75	1.09308
3066.82	1.13639
3068.12	6.24549
3068.2	8.51633
3145.69	0.199844
3145.7	0.207313
3157.37	9.90534
3157.4	2.28833
3201.94	0.750125
3201.94	0.794794
3203.27	1.01742
3203.27	0.326527
3230.7	2.10414
3230.71	2.37742
3232.12	5.09016
3232.18	1.18045
3244.93	2.67948
3245.12	0.0211204

Frequencies (cm⁻¹)	Intensity (Km mol⁻¹)
13.2845	0.131462
13.6283	0.0386286
20.6726	0
24.729	0.0134562
28.9217	0.00242549
29.5776	0
52.5928	0.0535085
75.0308	0
80.6321	0.0142577
99.9278	0.507139
115.719	0
116.305	0.00401788
139.2	0.000411279
142.508	0
151.633	0.307057
200.892	0
202.496	0.0342943
208.842	0.234777
224.947	0.119693
241.383	0.0610064
253.501	0
263.205	1.42857
264.23	0.0572838
273.104	0.38212
290.77	0
367.613	0.00700229
374.143	0
380.857	0.102324
390.844	0.147871
420.918	0.00459789
421.156	0
424.435	0.205059
454.03	0.423565
463.098	0.014342
464.209	0.0355809
470.612	0
480.551	0.00982851
481.968	0.229736
492.821	0.8023
536.291	1.57057
543.582	1.05E-05
545.621	6.81834
554.718	0.0032586
556.661	2.25656
558.752	0.243372
564.649	0
600.253	0.0434058
601.229	0.624416
649.419	0
658.105	0.0763292
658.287	0.127307
666.597	3.41089
668.826	0.110856
722.197	0.0273026
722.199	3.16E-05
727.966	0.367515
734.992	1.55351
823.46	0.0398202
823.467	1.38756
828.378	1.19306
830.257	0.235209
831.733	0
834.111	2.95018
847.327	0.000179275
847.382	10.8617
886.45	1.78499
891.602	0.732825
944.978	0.00166621
944.98	0.00930123
963.74	6.33E-05
963.743	0.00246767
966.817	0.0038386
1029.29	0.0148904
1029.3	0.000210912
1073.94	16.9194
1074.01	2.05164
1102.56	0.623383
1107.12	1.21841
1142.64	0.252283
1142.66	1.664
1180.27	1.75589
1184.96	0.0302659
1184.96	0.125187
1193.02	4.66764
1207.62	23.127
1208.2	0.396652
1219.02	4.16096
1219.11	0.0798725
1275.36	0.0498702
1291.71	12.1787
1301.33	100
1301.88	1.01403
1336.1	0.177029
1336.87	13.1478
1348.38	20.871
1348.38	8.47459
1366.68	0.394037
1404.73	0.365237
1412.34	4.2337
1438.62	6.19278
1464.99	0.125756
1465.15	0.82916
1471.86	0.234345
1499.85	0.333431
1499.92	10.5873
1522.4	0.029127
1522.4	1.20952
1531.72	0.147544
1533.84	25.2571
1535.95	0.363718
1539.72	1.62101
1573.51	2.00484
1575.13	38.8885
1609.9	4.14758
1609.94	1.17995
1667.75	38.9875
1668.04	0.462267
2290.65	0.149769
2293.12	4.36985
3029.27	20.0058
3029.35	2.23984
3089.82	0.112058
3089.82	8.5618
3161.55	6.02046
3161.57	1.40255
3205.83	2.1448
3205.84	0.500527
3207	0.31021
3222.11	0.318351
3222.13	0.389998
3229.91	1.70141
3229.94	4.65007
3245.67	2.34469
3245.86	0.0120325

Frequencies (cm⁻¹)	Intensity (Km mol⁻¹)
6.7517	0.116886
8.3444	0.066612
8.5833	0.00104485
15.6473	0.190348
18.2790	0
20.4391	0.016454
35.776	0.00038897
57.241	0.000201728
62.9389	0.0370329
81.4359	0.327027
92.0143	9.72E-05
95.9218	0.040064
110.025	1.13859
110.311	0.0148247
122.379	0.00632077
122.405	0.142363
130.218	0.00388971
139.322	9.72E-05
157.692	0.978945
168.597	3.1317
186.401	0.00388971
188.952	0.0175037
206.846	0.14849
212.361	0.178927
231.315	0.59045
234.927	0.105703
240.132	0.000421
242.626	0.0184761
246.46	1.21631
246.698	0.029518
249.811	0.0014586
278.277	0.036136
285.473	0.0023618
299.167	2.6789
299.876	0.59386
319.169	0.104665
320.93	0.208858
346.713	0.00126415
350.963	1.98589
354.957	0.0023805
357.703	0.289287
370.86	0.70462
393.567	0.70452
412.425	2.21159
419.108	0.591276
422.313	2.54192
430.864	0.060375
448.747	0.984388
475.395	8.47781
476.713	0.168522
477.536	4.05755
486.849	10.9035
490.019	3.23157
491.603	2.4263
504.664	2.06485
519.291	1.2833
525.036	7.31255
532.727	0.0301452
534.178	0.741767
551.5	2.42572
557.115	5.58163
577.854	4.95685
578.121	4.90322
585.829	0.523749
594.396	8.732
596.945	1.2524
602.763	1.29883
608.157	0.091916
613.624	1.33018
620.846	0.00038897
630.957	1.02031
635.135	0.320706
635.554	0.129041
673.532	4.75915
675.784	1.66246
715.098	18.8973
718.259	3.00887
732.066	7.14491
733.11	1.27738
750.85	43.8563
751.281	51.0632
770.544	13.1974
770.611	15.0827
789.204	3.32646
790.157	1.84185
797.524	4.68233
797.956	18.5139
828.616	0.157436
833.432	31.357
845.852	19.4829
846.864	21.4267
850.699	0.0789511
854.73	0.21053
883.803	0.177468
886.149	0.0977289
903.784	25.8205
906.331	6.14797
910.216	8.96733
914.034	8.9785
947.569	0.188165
947.731	15.5171
948.364	3.00208
948.225	0.18797
955.809	0.880727
957.645	1.07239
965.317	0.767537
970.056	0.00053456
971.313	0.00937427
991.731	0.0374876
992.208	0.00184485
1021.09	0.987013
1021.16	7.35474
1030.36	0.0011669
1033.93	0.00293858
1045.57	8.34362
1045.89	9.35033
1083.31	2.04317
1085.34	9.44003
1104.2	1.29809
1105.73	10.7909
1108.68	0.112024
1110.44	4.33119
1141.7	0.0654443
1142.11	5.371564
1155.16	1.76933
1155.79	1.84829
1156.66	0.846345
1157.01	2.56779
1169.05	13.8243
1182.26	43.919
1192.44	6.31922
1221.26	0.040357
1223.21	0.470849
1240.81	0.145961
1242.63	4.13408
1249.3	5.88792
1278.58	1.28292
1289.24	11.657
1300.79	0.43781
1304.98	0.82946
1310.82	4.27927
1321.17	30.1971
1327.46	1.14105
1327.86	8.50397
1353.9	19.0691
1367.13	15.5828
1367.44	3.63979
1390.55	12.248
1394.93	3.02639
1398.16	1.64233
1399.13	6.73094
1416.7	36.3085
1420.8	6.95178
1421	1.53241
1448.14	100
1449.32	21.8682
1457.53	0.736947
1477.63	23.9134
1478.32	3.12752
1483.51	0.842413
1483.94	81.0975
1488.78	0.0940337
1489.43	0.343358
1490.93	3.88543
1491.03	3.44278
1502.11	0.782512
1503.45	24.9754
1505.83	0.115622
1506.05	9.43235
1510.93	1.8855
1511.55	11.8807
1537.4	4.53217
1542.36	27.8326
1586.23	14.3836
1596.34	14.8425
1618.59	2.6379
1618.83	4.00552
1638.9	0.714345
1639.15	0.529202
1644.36	9.17553
1644.49	5.74743
2270.94	2.44692
2273.47	2.23525
3023.33	0.0055182
3023.73	4.87944
3027.47	18.1633
3027.71	18.2916
3085.73	39.9233
3085.83	31.571
3091.08	0.0253831
3091.15	0
3101.42	69.0079
3101.66	40.8092
3103.14	13.2804
3103.39	13.365
3158.52	24.3378
3164.71	27.6869
3165.05	7.22037
3169.58	5.44948
3170.69	2.96775
3175.77	3.82075
3175.84	11.1949
3178.21	10.5607
3179.48	21.1278
3187.62	21.7528
3187.62	4.61718
3192.31	4.22208
3192.39	43.9277
3222.68	38.8388
3223.23	9.83501

Appendix B2

Molecular Modelling – Cartesian Coordinates

Mechanism Modelling for the Synthon Molecular Fragment

Table 46. Located (STQN) Transition states for steps 1a-c of the four-centre mechanism, calculated at the B3LYP/6-311++G(d,p) theoretical level.

1a	1b	1c
C -2.2978530000 3.9794070000 0.4463450000	C -4.5936780000 2.9976090000 0.9286940000	C -2.4222900000 3.4440210000 0.0245620000
C -3.0536740000 2.8567970000 0.2628690000	C -3.6928230000 3.5401500000 0.0451090000	C -2.9268960000 2.1934030000 -0.1797160000
C -0.9180340000 3.8655750000 0.0468790000	C -2.3648890000 3.4965950000 0.5996680000	C -1.0261980000 3.4247770000 0.3626080000
C -0.7272270000 2.6127620000 -0.4380770000	C -2.3067040000 2.9292060000 1.8402600000	C -0.4772600000 2.1582430000 0.4440100000
S -2.1272180000 1.5610250000 -0.4346230000	S -3.8652660000 2.4147220000 2.4127970000	S -1.6897200000 0.9839860000 0.0492310000
H -2.7095830000 4.8860110000 0.8752400000	Br -0.7570320000 2.6696840000 2.9069120000	H -0.4803170000 4.3204940000 0.6572650000
H -4.0967870000 2.6966770000 0.4952400000	H -4.0234230000 3.8703120000 -1.2947860000	H -3.0178720000 4.3461870000 -0.0456000000
H -0.0013360000 4.8910330000 0.2398800000	H -1.4791570000 3.8582670000 0.0912540000	H -3.9385710000 1.9117370000 -0.4323610000
Br 0.9478740000 1.9308590000 -1.1536570000	H -5.6578440000 2.8415460000 0.8004870000	Br 1.7264880000 1.9942290000 0.3149390000
H 0.6385450000 6.7445130000 0.0282380000	H -3.7833040000 4.7545980000 -3.0355750000	H 4.2660810000 2.8916770000 0.2751090000
Li 0.9242540000 4.5018410000 -1.2604180000	N -4.5081860000 4.5725210000 -2.3458530000	Li 1.0504770000 3.5007190000 -1.1913140000
N 1.0086110000 5.7983700000 0.0744290000	Li -4.6256800000 5.3519900000 -0.6585530000	N 3.6870900000 2.5688750000 -0.5013270000
H 1.6798560000 5.7990680000 0.8386640000	H -5.2435450000 4.0760410000 -2.8425850000	H 4.1477280000 1.7238930000 -0.8420160000

Table 47. Located (STQN) Transition states for steps 2-4 of the four-centre mechanism, calculated at the B3LYP/6-311++G(d,p) theoretical level.

2	3	4
Br -0.4887910000 0.2948370000 1.7020910000	Br 0.9827050000 -0.9182350000 -3.2604160000	Br -0.1480850000 -1.3983140000 -3.9253730000
Br 3.7076060000 -0.2659520000 1.3361440000	Br -1.3551940000 -4.0874710000 -2.2358860000	Br -0.8146730000 -4.8745240000 -2.1132450000
S 3.1146360000 0.1007110000 -1.7781030000	S 2.9564950000 -3.9181230000 -3.1388150000	S 2.9981510000 -2.7925480000 -2.8305810000
S -0.1845600000 2.9238100000 4.4026110000	S 0.9096380000 1.1413250000 -0.1221560000	S -0.2360400000 2.7541600000 -1.1512760000
C 1.6272830000 0.8308330000 -2.3191900000	C 2.2537640000 -5.4050470000 -3.6944970000	C 3.1977780000 -4.5089720000 -2.9641720000
C 0.8167510000 1.1909820000 -1.2825670000	C 0.9210050000 -5.4766660000 -3.3845040000	C 2.0247770000 -5.1769730000 -2.7115860000
C 1.3906330000 0.9116560000 -0.0035960000	C 0.4800930000 -4.3070940000 -2.7107040000	C 0.9702250000 -4.2743620000 -2.4293220000
C 2.5906440000 0.2916260000 -0.1146630000	C 1.4609680000 -3.3777270000 -2.4118350000	C 1.3194520000 -2.9371940000 -2.3694760000
C 0.2681660000 2.6155440000 2.7505270000	C 0.3010090000 -0.4149670000 -0.6251180000	C 0.4935830000 1.1928530000 -1.4699030000
C -0.1540860000 3.6631130000 1.9443820000	C -1.0734540000 -0.4630420000 -0.4354610000	C -0.4271260000 0.2468170000 -1.8016000000
C -0.7882080000 4.5083540000 4.0136620000	C -1.5943780000 0.6417760000 0.2511740000	C -1.7461220000 0.7926810000 -1.9092320000
C -0.6891640000 4.7634180000 2.6685590000	C -0.6432220000 1.6296230000 0.4825820000	C -1.8048160000 2.1093360000 -1.5641520000
Li 1.7279590000 1.5121540000 1.9528420000	Li 1.4214620000 -2.0327200000 -0.9295370000	Br 2.3708930000 0.9698190000 -1.3031700000
H 1.4529790000 0.9446350000 -3.3796040000	H 2.8638460000 -6.1623500000 -4.1654110000	H 4.1694310000 -4.9381370000 -3.1623450000
H -0.1589540000 1.6377210000 -1.4201970000	H 0.2829480000 -6.3168050000 -3.6214850000	H 1.9217990000 -6.2533680000 -2.7144350000
H -0.0847730000 3.6358710000 0.8633430000	H -1.6834770000 -1.2875040000 -0.7823100000	Li 0.2405290000 -1.6061010000 -1.3568880000
H -1.1288980000 5.1748550000 4.7930300000	H -0.7571690000 2.5576880000 1.0241160000	H -2.6109270000 0.2174470000 -2.2127560000
H -1.0021200000 5.6958050000 2.2155170000	H -2.6275590000 0.7633760000 0.5595380000	H -2.6721790000 2.7510810000 -1.5045270000

Table 48. Located (STQN) Transition states for steps 2-4 of the S$_N$2 mechanism, calculated at the B3LYP/6-311++G(d,p) theoretical level.

2	3	4
Br 0.5612530000 2.3155540000 0.7264570000	Br 0.3587460000 -1.9039740000 0.5885100000	S -4.1710200000 -1.8330090000 -1.4443680000
Br 0.4943170000 -1.6949710000 1.0308570000	Br -0.9123010000 1.8222720000 -0.2503870000	H -3.9305490000 -2.4155180000 -3.8195790000
S 1.8690140000 -1.7538510000 -1.8286650000	S -3.4053710000 -1.7860810000 0.3644500000	C -3.3529360000 -2.1520800000 -2.9443870000
S 0.8569780000 4.5535970000 3.2667980000	S 3.1122680000 -1.6483230000 -0.9644090000	C -2.6179750000 -1.5338590000 -0.6852240000
C 2.2529870000 -0.2967110000 -2.6993590000	C -4.4091660000 -0.4113470000 -0.0358540000	Br -2.5807300000 -1.0691360000 1.1937240000
C 1.8946870000 0.8221580000 -2.0001070000	C -3.6323980000 0.6945150000 -0.2239650000	C -1.9983570000 -2.0219860000 -2.8259820000
C 1.2864330000 0.5767090000 -0.7192690000	C -1.9064640000 -0.9127280000 0.2991000000	C -1.5509330000 -1.6671490000 -1.5101340000
C 1.2253890000 -0.7543150000 -0.5320630000	C -2.2567880000 0.3569310000 -0.0247360000	H -1.3195160000 -2.1772550000 -3.6559890000
C -0.1711730000 3.6106390000 2.2245420000	C 3.3038830000 -2.4881200000 1.4585880000	Li -0.6151300000 0.3210970000 0.2843130000
C -1.4835400000 3.7469670000 2.5977050000	C 2.3613890000 -2.2106190000 0.5143450000	Br 0.5616270000 -1.2832630000 -1.0154470000
C -0.4977030000 5.1302570000 4.1955810000	C 4.6441680000 -2.2600270000 0.9974220000	Br 1.3934000000 1.6321530000 1.1954620000
C -1.6709960000 4.6174730000 3.7194980000	C 4.7117900000 -1.7767910000 -0.2755910000	C 2.5752110000 -0.5805930000 -0.3456510000
Li 0.3548590000 0.5307850000 2.1832220000	Li 0.7175260000 0.0126620000 -0.7526150000	C 2.8160120000 0.4904770000 0.4527440000
H 2.7185410000 -0.3667790000 -3.6731510000	H -5.4851400000 -0.4886700000 -0.1050340000	S 4.1152960000 -1.2649320000 -0.7501300000
H 2.0601870000 1.8203860000 -2.3906080000	H -3.9996880000 1.6789390000 -0.4815380000	C 4.1742250000 0.8046060000 0.7665560000
H -2.2982180000 3.2597850000 2.0736900000	H 3.0593530000 -3.8260270000 2.4575770000	H 4.4878100000 1.6304260000 1.3908180000
H -0.3498530000 5.8113230000 5.0212710000	H 5.5246730000 -2.4510050000 1.5989700000	C 5.0169290000 -0.0855790000 0.1676210000
H -2.6384250000 4.8539420000 4.1460360000	H 5.5854620000 -1.5483880000 -0.8672780000	H 6.0960780000 -0.1155860000 0.2144820000

Charge Transfer Modelling for Acenes

Table 49. Ground-state optimised isomers **13, 14** and **32-41** at the B3LYP/6-311++G(d,p) theoretical level.

13	14	32	33
C 0.0000000000 -4.9364520000 1.4089240000	C 0.6832420000 -1.6651060000 -0.0000050000	C 1.9596850000 -2.4098720000 -0.6161940000	C 1.8682330000 -1.3619700000 0.0000000000
C 0.0000000000 -6.1101470000 0.7160520000	C -0.6832420000 -1.6651060000 -0.0000050000	C 2.7023990000 -1.2595710000 -0.2331680000	C 0.4645500000 -1.6734510000 0.0000000000
C 0.0000000000 -6.1101470000 -0.7160530000	C 1.4328960000 -0.4585450000 -0.0000020000	C 2.0003460000 -0.0568580000 0.0882000000	C -0.4675130000 -0.6140990000 0.0000000000
C 0.0000000000 -4.9364520000 -1.4089240000	C -1.4328960000 -0.4585450000 -0.0000020000	C 0.5608420000 -0.0082850000 -0.0909220000	C 2.3201610000 -0.0827630000 0.0000000000
C 0.0000000000 -3.6736430000 -0.7268470000	C -0.7233160000 0.7683840000 -0.0000010000	C -0.1364320000 -1.2171400000 -0.2597220000	C 1.4167650000 1.0286090000 0.0000000000
C 0.0000000000 -3.6736430000 0.7268470000	C 0.7233160000 0.7683840000 -0.0000010000	C 0.5982520000 -2.4024800000 -0.5673650000	C 0.0000000000 0.7698690000 0.0000000000
C 0.0000000000 -2.4648890000 1.4064690000	C -2.8859810000 -0.4625480000 0.0000000000	C -0.1983560000 1.2414920000 -0.1380650000	C -0.8615000000 1.8668530000 0.0000000000
C 0.0000000000 -2.4648890000 -1.4064680000	C -1.4747960000 1.9884440000 0.0000000000	C -1.5872040000 -1.2573890000 -0.0824380000	C 1.8885780000 2.3402060000 0.0000000000
C 0.0000000000 -1.2248420000 -0.7276180000	C -3.5840830000 0.7783140000 0.0000000000	C -2.3023270000 -0.0578350000 0.1674850000	C 1.0203910000 3.4395450000 0.0000000000
C 0.0000000000 -1.2248420000 0.7276180000	C -2.8353180000 1.9932510000 0.0000000000	C -1.6099310000 1.2205180000 0.0341920000	C -0.3951610000 3.1914560000 0.0000000000
C 0.0000000000 0.0000000000 1.4069160000	C -3.6564030000 -1.6504740000 0.0000010000	C 0.4077510000 2.4735150000 -0.4806600000	C -1.2839300000 4.3072160000 0.0000000000
C 0.0000000000 0.0000000000 -1.4069150000	C -4.9983580000 0.7911860000 0.0000020000	C -0.3134190000 3.6499760000 -0.5437460000	C 1.4832860000 4.7886160000 0.0000000000
C 0.0000000000 1.2248420000 -0.7276180000	C -5.7177790000 -0.3829790000 0.0000020000	C -1.6872660000 3.6394040000 -0.2758200000	C 0.5982720000 5.8335790000 0.0000000000
C 0.0000000000 1.2248420000 0.7276180000	C -5.0356460000 -1.6139590000 0.0000020000	C -2.3191190000 2.4393870000 -0.0147940000	C -0.8030870000 5.5896100000 0.0000000000
C 0.0000000000 2.4648890000 1.4064680000	C 1.4747960000 1.9884440000 -0.0000010000	C -2.2964850000 -2.4792340000 -0.0581860000	C -1.8605480000 -2.4792270000 0.0000000000
C 0.0000000000 2.4648890000 -1.4064680000	C 2.8353180000 1.9932510000 -0.0000010000	C -3.6759520000 -0.1380810000 0.4797580000	C 0.0005120000 -3.0459200000 0.0000000000
C 0.0000000000 3.6736430000 -0.7268470000	C 3.5840830000 0.7783140000 0.0000000000	C -3.6472670000 -2.5291650000 0.2252780000	C -1.4018860000 -3.3086020000 0.0000000000
C 0.0000000000 3.6736430000 0.7268470000	C 2.8859810000 -0.4625480000 0.0000000000	C -4.3428580000 -1.3471290000 0.5091620000	C -2.3092190000 -2.2118810000 0.0000000000
C 0.0000000000 4.9364520000 1.4089240000	C 3.6564030000 -1.6504740000 0.0000020000	C 2.7592530000 0.9943760000 0.6694400000	C -1.8692940000 -4.6449160000 0.0000000000
C 0.0000000000 4.9364520000 -1.4089240000	C 5.0356460000 -1.6139590000 0.0000030000	C 4.1115640000 -1.3136080000 -0.1063810000	C 0.8762080000 -4.1614670000 0.0000000000
C 0.0000000000 6.1101470000 -0.7160530000	C 5.7177790000 -0.3829790000 0.0000030000	C 4.8202270000 -0.2473620000 0.3961900000	C 0.3963810000 -5.4536130000 0.0000000000
C 0.0000000000 6.1101470000 0.7160520000	C 4.9983580000 0.7911860000 0.0000020000	C 4.1264690000 0.9022830000 0.8210880000	C -0.9902600000 -5.7031020000 0.0000000000
H 0.0000000000 -4.9364150000 2.4940180000	H -3.3749410000 2.9346230000 0.0000010000	H 0.0669120000 -3.3150900000 -0.7982640000	H 3.3862240000 -1.1189960000 0.0000000000
H 0.0000000000 -7.0559900000 1.2459440000	H -0.9589170000 2.4400080000 0.0000010000	H -3.3929210000 2.4400080000 0.1147730000	H -1.1934230000 1.7216480000 0.0000000000
H 0.0000000000 -7.0559900000 -1.2459450000	H -3.1672360000 -2.6153780000 0.0000020000	H -2.2620380000 4.5576440000 -0.3171070000	H 2.9607410000 2.5124430000 0.0000000000
H 0.0000000000 -4.9364150000 -2.4940180000	H -5.5097350000 1.7482670000 0.0000020000	H 1.4531600000 2.4923910000 -0.7500610000	H 2.5915920000 -2.1655700000 0.0000000000
H 0.0000000000 -2.4655110000 2.4923100000	H -6.8016320000 -0.3623040000 0.0000030000	H 0.1830760000 4.5724060000 -0.8231150000	H -3.3746140000 -2.4172150000 0.0000000000
H 0.0000000000 -2.4655110000 -2.4923090000	H 1.1955320000 -2.6175660000 -0.0000080000	H -5.3981590000 -1.3785980000 0.7552460000	H -2.5879340000 -0.1242610000 0.0000000000
H 0.0000000000 0.0000000000 2.4926690000	H -1.1955320000 -2.6175660000 -0.0000090000	H -4.2282260000 0.7629120000 0.7107840000	H 0.9616540000 6.8550610000 0.0000000000
H 0.0000000000 0.0000000000 -2.4926680000	H 0.9589170000 2.4381070000 -0.0000040000	H -1.7767930000 -3.4101500000 -0.2372810000	H -1.4901300000 6.4282990000 0.0000000000
H 0.0000000000 2.4655110000 2.4923100000	H 3.3749410000 2.9346230000 -0.0000020000	H -4.1404680000 -3.4838780000 0.2446920000	H -1.3585380000 -6.7226820000 0.0000000000
H 0.0000000000 2.4655110000 -2.4923090000	H 3.1672360000 2.6153780000 0.0000020000	H 2.4939400000 -3.3124700000 -0.8932920000	H -2.9402520000 -4.8197660000 0.0000000000
H 0.0000000000 7.0559900000 1.2459440000	H 5.5969890000 -2.5415650000 0.0000050000	H 2.2533650000 1.8692980000 1.0507800000	H 1.9472210000 -4.0112510000 0.0000000000
H 0.0000000000 4.9364150000 2.4940180000	H 6.8016320000 -0.3623040000 0.0000040000	H 4.6682410000 1.7172130000 1.2881160000	H 1.0929600000 -6.2844780000 0.0000000000
H 0.0000000000 4.9364150000 -2.4940180000	H 5.5097350000 1.7482670000 0.0000010000	H 4.6211340000 -2.2298750000 -0.3861260000	
H 0.0000000000 7.0559900000 -1.2459450000			

34	35	36	37
C 1.3761920000 -3.4689470000 0.0000020000	C -2.7602770000 -0.6753460000 0.0000000000	C 4.8765390000 1.1783880000 0.0000000000	C 5.1330700000 -0.7100000000 0.0000150000
C 1.8168890000 -2.1873460000 0.0000030000	C -1.5304190000 -1.4321000000 0.0000030000	C 3.7736120000 0.3657910000 0.0000000000	C 3.9498710000 -1.4036630000 0.0000210000
C -0.0284120000 -3.7773050000 0.0000000000	C -0.2697990000 -0.7357060000 0.0000000000	C 4.7296840000 2.5931640000 0.0000000000	C 5.1330700000 0.7100000000 0.0000300000
C -0.9829350000 -2.7217040000 0.0000000000	C -2.7602770000 0.6753460000 0.0000000000	C 3.4827900000 3.1597640000 0.0000000000	C 3.9498710000 1.4036630000 -0.0000140000
C -0.5114510000 -1.3389840000 0.0000000000	C -0.2697990000 0.7357060000 0.0000000000	C 2.3158010000 2.3414520000 0.0000000000	C 2.7038160000 -0.7148740000 -0.0000080000
C 0.8977980000 -1.0826340000 0.0000010000	C 0.8944510000 1.4914030000 0.0000000000	C 2.4584680000 0.9186280000 0.0000000000	C 2.7038160000 0.7148740000 0.0000000000
C 1.3667350000 0.2358840000 0.0000010000	C -1.5542120000 2.8210290000 0.0000000000	C 1.3147880000 1.0006330000 0.0000000000	C 1.4683570000 -1.3851580000 0.0000140000
C 0.5114510000 1.3389840000 0.0000000000	C -0.3754470000 3.5877220000 0.0000000000	C 0.0000000000 0.5819870000 0.0000000000	C 0.2481290000 -0.7187670000 0.0000000000
C -0.8977980000 1.0826340000 0.0000010000	C 0.8829750000 2.9004850000 0.0000000000	C -0.1134650000 2.0329820000 0.0000000000	C 0.2481290000 0.7187670000 -0.0000100000
C -1.3667350000 -0.2358840000 0.0000010000	C 2.0817290000 3.6681310000 0.0000000000	C 1.0152710000 2.8514760000 0.0000000000	C 1.4683570000 1.3851580000 -0.0000160000
C 0.9829350000 2.7217040000 0.0000000000	C -0.3822510000 5.0110390000 0.0000000000	C -1.2376000000 -0.2354790000 0.0000000000	C -1.0292940000 -1.4475320000 -0.0000020000
C -1.8168890000 2.1873460000 0.0000020000	C 0.7923260000 5.7186090000 0.0000000000	C -1.3969970000 2.6611920000 0.0000000000	C -1.0292940000 1.4475310000 -0.0000070000
C -1.3761920000 3.4689470000 0.0000020000	C 2.0391720000 5.0393620000 0.0000000000	C -2.5179490000 1.9122070000 0.0000000000	C -2.2543850000 0.7352410000 0.0000090000
C 0.0284120000 3.7773050000 0.0000000000	C 0.8944510000 -1.4914030000 0.0000000000	C -2.4645260000 0.4784000000 0.0000000000	C -2.2543860000 -0.7352410000 0.0000050000
C 2.3509770000 3.0665290000 -0.0000010000	C -1.5542120000 -2.8210290000 0.0000000000	C -1.3334780000 -1.7024480000 0.0000000000	C -1.0711130000 -2.8572330000 -0.0000160000
C 2.7627720000 0.4386560000 -0.0000020000	C -0.3754470000 -3.5877220000 0.0000000000	C -2.6344530000 -2.3223450000 0.0000000000	C -2.2645470000 -3.5541770000 -0.0000170000
C 1.8168890000 5.4239180000 -0.0000020000	C 0.8829750000 -2.9004850000 0.0000000000	C -3.8156950000 -1.5338670000 0.0000000000	C -3.4732600000 -2.8517470000 -0.0000060000
C 0.4710820000 5.1172710000 -0.0000010000	C 2.0817290000 -3.6681310000 0.0000000000	C -3.7269580000 -0.1822390000 0.0000000000	C -3.4587530000 -1.4696560000 0.0000030000
C -2.3509770000 -3.0665290000 -0.0000010000	C -0.3822510000 -5.0110390000 0.0000000000	C -0.2471970000 -2.6230260000 0.0000000000	C -1.0711130000 2.8572330000 -0.0000160000
C -0.4710820000 -5.1172710000 -0.0000010000	C 0.7923260000 -5.7186090000 0.0000000000	C -2.7788250000 -3.7310210000 0.0000000000	C -3.4587530000 1.4696560000 0.0000240000
C -2.7627720000 -0.4386560000 -0.0000010000	C 2.0391720000 -5.0393620000 0.0000000000	C -1.6917290000 -4.5690000000 0.0000000000	C -2.2645470000 3.5541770000 0.0000150000
C -1.8168890000 -5.4239180000 -0.0000020000	H -3.6957150000 1.2250650000 0.0000000000	C -0.4122700000 -3.9929270000 0.0000000000	C -3.4732500000 2.8517480000 0.0001180000
H 2.4403580000 0.3801050000 0.0000030000	H 1.8618880000 1.0037340000 0.0000000000	H 5.8707070000 0.7459390000 0.0000000000	H 1.1984490000 -2.4666830000 0.0000280000
H -2.4403580000 -0.3801050000 0.0000040000	H -2.5130300000 3.3308030000 0.0000000000	H 5.6136670000 3.2209340000 0.0000000000	H 1.1984490000 2.4666820000 -0.0000290000
H -2.8802830000 1.9715450000 0.0000060000	H 3.0345130000 3.1486200000 0.0000000000	H 3.8878440000 -0.7134780000 0.0000000000	H -4.4074400000 -0.9515570000 0.0000070000
H -2.0822340000 4.2926760000 0.0000040000	H -1.3358920000 5.5288180000 0.0000000000	H 3.3658610000 4.2385390000 0.0000000000	H -4.4180640000 -3.3832370000 -0.0000190000
H -0.2702240000 5.9097860000 -0.0000010000	H -3.6957150000 -1.2250650000 0.0000000000	H 1.5284000000 -0.9483380000 0.0000000000	H -0.1508200000 -3.4246300000 -0.0000290000
H 2.1425890000 6.4578790000 0.0000030000	H 0.7754240000 6.8026470000 0.0000000000	H 0.8689630000 3.9273920000 0.0000000000	H -2.2585250000 -4.6382000000 -0.0000240000
H 3.1042350000 2.2890960000 0.0000000000	H 2.9597260000 5.6120710000 0.0000000000	H -1.4456090000 3.7446140000 0.0000000000	H 3.9483080000 -2.4837880000 0.0000350000
H 3.8217140000 4.6191110000 -0.0000020000	H -2.5130300000 -3.3308030000 0.0000000000	H -3.4959750000 2.3806470000 0.0000000000	H 6.0767440000 -1.2437880000 0.0000240000
H 2.8802830000 -1.9715450000 0.0000040000	H -1.3358920000 -5.5288180000 0.0000000000	H -4.6219950000 0.4300390000 0.0000000000	H 6.0767440000 1.2437880000 -0.0000080000
H 2.0822340000 -4.2926760000 0.0000040000	H 0.7754240000 -6.8026470000 0.0000000000	H -4.7788770000 -2.0323670000 0.0000000000	H 3.9483080000 2.4888580000 -0.0000280000
H 0.2702240000 -5.9097860000 0.0000000000	H 3.0345130000 -3.1486200000 0.0000000000	H 0.4674580000 -4.6263630000 0.0000000000	H -4.4180640000 3.3832380000 0.0000030000
H -2.1425890000 -6.4578790000 -0.0000030000	H 2.9597260000 -5.6120710000 0.0000000000	H 0.7688040000 -2.2879970000 0.0000000000	H -4.4074400000 0.9515580000 0.0000410000
H -3.1042350000 -3.1486200000 0.0000000000		H -3.7852900000 -4.1186220000 0.0000000000	H -0.1508190000 3.4246300000 -0.0000130000
H -3.8217140000 -4.6191110000 -0.0000020000		H -1.8161360000 -5.6455790000 0.0000000000	H -2.2585250000 4.6382000000 -0.0000110000

38	39	40	41
C -3.7163710000 0.2882610000 0.0000030000	C -4.1009560000 0.2882610000 0.0000030000	C -1.8042960000 -1.9094270000 -0.6166200000	C -2.9607180000 -0.3072450000 0.1896730000
C -2.5134770000 -0.4729000000 -0.0000010000	C -3.7618900000 1.2938870000 0.0000000000	C -2.9350720000 -1.1176020000 -0.2566590000	C -3.5013270000 0.9137170000 0.6971780000
C -3.6537790000 1.7250960000 0.0000050000	C -2.3977780000 1.6918090000 0.0000000000	C -2.7342740000 0.2517590000 0.0766510000	C -2.7469680000 2.0438980000 0.7023840000
C -2.4668740000 2.3784320000 0.0000030000	C -3.1469990000 -1.0671840000 0.0000000000	C -1.3871180000 0.7975530000 0.0640710000	C -1.3645960000 2.0169140000 0.3360470000
C -1.2226970000 1.6593250000 0.0000000000	C -1.7448650000 -0.7323540000 0.0000000000	C -0.2724040000 -0.0623940000 -0.1384060000	C -0.7223710000 0.7815870000 0.0565970000
C -1.2300370000 0.2272880000 0.0000000000	C -1.3509320000 0.6626530000 0.0000000000	C -0.5396260000 -1.4114150000 -0.5492790000	C -1.5848140000 -0.3685450000 -0.1893890000
C 0.0000000000 -0.4391750000 0.0000000000	C 0.0000000000 0.9600280000 0.0000000000	C -1.1579650000 2.1952110000 0.1843610000	C -0.6479960000 3.2395900000 0.2110180000
C 1.2300370000 0.2272880000 0.0000000000	C 0.6024890000 -1.4290180000 0.0000020000	C 1.0725250000 0.4654430000 -0.0454420000	C 0.7223700000 0.7815870000 -0.0565970000
C 1.2226970000 1.6593250000 -0.0000020000	C 1.0016720000 -0.0409070000 0.0000000000	C 1.2344070000 1.8725850000 -0.0703080000	C 1.3645960000 2.0169140000 -0.3360470000
C 0.0000000000 2.3338010000 -0.0000010000	C 2.3705450000 0.2725690000 0.0000000000	C 0.0980690000 2.7141220000 0.0565930000	C 0.6479950000 3.2395900000 -0.2110180000
C 2.5134770000 -0.4729000000 0.0000010000	C 1.5925310000 -2.4252090000 0.0000040000	C 2.2752630000 -0.3493450000 0.0722280000	C 1.5848140000 -0.3685450000 0.1893890000
C 2.4668740000 2.3784320000 -0.0000040000	C 2.9504880000 -2.1092460000 0.0000040000	C 2.5351540000 2.4515200000 -0.2383210000	C 2.7469680000 2.0438980000 -0.7023840000
C 3.6537790000 1.7250960000 -0.0000040000	C 3.3513650000 -0.7185940000 0.0000000000	C 3.5508640000 0.2597980000 -0.1459980000	C 2.9607180000 -0.3072450000 -0.1896740000
C 3.7163710000 0.2882610000 -0.0000010000	C 4.7490670000 -0.4108680000 0.0000040000	C 3.6396760000 1.6731470000 -0.3396960000	C 3.5013270000 0.9137170000 -0.6971780000
C 2.6236330000 -1.8798220000 0.0000040000	C 3.9700620000 -3.1138560000 0.0000040000	C -3.8748700000 1.0224020000 0.4082760000	C 1.1655640000 -1.5103610000 0.9172770000
C 3.8548960000 -2.5090040000 0.0000030000	C 5.2930260000 -2.7741270000 0.0000020000	C -4.2422460000 -1.6573690000 -0.2609390000	C 3.8012900000 -1.4253510000 0.0284360000
C 5.0375000000 -1.7527600000 0.0000020000	C 5.6883130000 -1.4025870000 0.0000000000	C -5.3309440000 -0.8797130000 0.0655090000	C 3.3391820000 -2.5462530000 0.6797620000
C 4.9623040000 -0.3746300000 -0.0000010000	C -2.1128950000 3.0710170000 0.0000030000	C -5.1402560000 0.4721770000 0.4072360000	C 2.0156630000 -2.5684470000 1.1588930000
C -2.6236330000 -1.8798220000 -0.0000020000	C -4.7743940000 2.2733160000 0.0000000000	C 2.2768620000 -1.7014250000 0.5011100000	C -1.1655640000 -1.5103610000 -0.9172770000
C -4.9623040000 -0.3746300000 0.0000030000	C -4.4655730000 -1.8571410000 0.0000030000	C 4.7264830000 -0.5239400000 -0.0856780000	C -3.8012900000 -1.4253510000 -0.0284360000
C -5.0375000000 -1.7527600000 0.0000000000	C -3.1222870000 4.0194280000 0.0000000000	C 4.6791270000 -1.8571410000 0.2561290000	C -3.3391810000 -2.5462530000 -0.6797620000
C -3.8548960000 -2.5090040000 -0.0000060000	H -3.4208290000 -2.1170710000 0.0000000000	C 3.4422670000 -2.4364170000 0.5884080000	C -2.0156620000 -2.5684470000 -1.1588930000
H -4.5867970000 0.2789170000 0.0000080000	H 0.3339730000 1.9904270000 0.0000000000	H 0.2804080000 -2.3306580000 -0.8798570000	H 4.5423800000 0.9389270000 -1.0010550000
H -2.4338470000 3.4628880000 0.0000040000	H -1.0915950000 -2.7644510000 0.0000020000	H -4.6158060000 2.1155190000 -0.5078510000	H 3.1813050000 2.9962800000 -0.9876420000
H 0.0000000000 -1.5190190000 0.0000020000	H 2.6724410000 1.3157330000 0.0000000000	H 2.6064240000 3.5316890000 -0.3062050000	H -1.1710830000 4.1701090000 0.3991080000
H 0.0000000000 3.4196880000 -0.0000010000	H 1.2904540000 -3.4682350000 0.0000000000	H -1.9694330000 -2.2372380000 -0.9649010000	H 1.1710820000 4.1710190000 -0.3991080000
H 2.4338470000 3.4628880000 -0.0000050000	H 6.7434840000 -1.1534850000 0.0000000000	H -3.7649420000 2.0617420000 0.6882500000	H 0.1600980000 -1.5479370000 1.3107240000
H 4.5867970000 2.2789170000 -0.0000060000	H 5.0496340000 0.6318240000 0.0000040000	H -5.9926420000 1.0860400000 0.6753070000	H 1.6618070000 -3.4188940000 1.7307880000
H 5.8687080000 0.2220660000 0.0000030000	H 3.6693770000 -4.1564750000 0.0000040000	H -4.3730120000 -2.7016700000 -0.5252180000	H 4.8347370000 -1.3664570000 -0.2971640000
H 6.0014350000 -2.2486880000 0.0000030000	H 6.0537200000 -3.5466330000 0.0000000000	H -6.3285410000 -1.3039620000 0.0633210000	H 3.9969940000 -3.3899600000 0.8550360000
H 1.7318080000 -2.4930700000 0.0000070000	H -5.1515680000 -0.3803650000 0.0000030000	H -1.9924160000 2.8708400000 0.3133420000	H -4.5423800000 0.9389270000 1.0010550000
H 3.9047730000 -3.5920340000 0.0000010000	H -5.8106320000 1.9511350000 0.0000030000	H 0.2475610000 3.7886170000 0.0668460000	H -3.1813050000 2.9962800000 0.9876410000
H -1.7318080000 -2.4930700000 -0.0000010000	H -5.2553560000 4.3636060000 0.0000000000	H 1.3532970000 -2.1621820000 0.8185830000	H -1.1710830000 4.1701090000 -0.3991080000
H -3.9047730000 -3.5920340000 0.0000000000	H -2.8687560000 5.0735270000 0.0000000000	H 3.4015730000 -3.4632710000 0.9343040000	H -4.8347370000 -1.3664570000 0.2971630000
H -5.8687080000 0.2220660000 0.0000060000	H -1.0855130000 3.4119460000 0.0000000000	H 5.6785740000 -0.0427580000 -0.2843150000	H -3.9969930000 -3.3899610000 -0.8550360000
H -6.0014350000 -2.2486880000 -0.0000010000		H 5.5892280000 -2.4437160000 0.3090470000	H -0.1600980000 -1.5479370000 -1.3107240000

Table 50. Ground-state optimised isomers **13**, **14** and **32-41** at the LC-BLYP/6-311++G(d,p) theoretical level.

13

```
C 0.0000000000 -4.8951750000 1.3988810000
C 0.0000000000 -6.0461430000 0.7173670000
C 0.0000000000 -6.0461430000 -0.7173660000
C 0.0000000000 -4.8951750000 -1.3988810000
C 0.0000000000 -3.6297300000 -0.7183220000
C 0.0000000000 -3.6297300000 0.7183220000
C 0.0000000000 -2.4458400000 1.3907820000
C 0.0000000000 -2.4458400000 -1.3907820000
C 0.0000000000 -1.2092590000 -0.7143010000
C 0.0000000000 -1.2092590000 0.7143010000
C 0.0000000000 0.0000000000 1.3890800000
C 0.0000000000 0.0000000000 -1.3890800000
C 0.0000000000 1.2092590000 -0.7143010000
C 0.0000000000 1.2092590000 0.7143010000
C 0.0000000000 2.4458400000 1.3907820000
C 0.0000000000 2.4458400000 -1.3907820000
C 0.0000000000 3.6297300000 -0.7183220000
C 0.0000000000 3.6297300000 0.7183220000
C 0.0000000000 4.8951750000 1.3988810000
C 0.0000000000 4.8951750000 -1.3988810000
C 0.0000000000 6.0461430000 -0.7173660000
C 0.0000000000 6.0461430000 0.7173670000
H 0.0000000000 -4.8916990000 2.4828150000
H 0.0000000000 -6.9926980000 1.2436460000
H 0.0000000000 -6.9926980000 -1.2436460000
H 0.0000000000 -4.8916990000 -2.4828150000
H 0.0000000000 -2.4458100000 2.4755330000
H 0.0000000000 -2.4458100000 -2.4755330000
H 0.0000000000 0.0000000000 2.4737850000
H 0.0000000000 0.0000000000 -2.4737860000
H 0.0000000000 2.4458100000 2.4755330000
H 0.0000000000 2.4458100000 -2.4755330000
H 0.0000000000 6.9926980000 1.2436460000
H 0.0000000000 4.8916990000 2.4828150000
H 0.0000000000 4.8916990000 -2.4828150000
H 0.0000000000 6.9926980000 -1.2436460000
```

14

```
C 4.9475790000 0.7806540000 0.0000000000
C 5.6586870000 -0.3780450000 0.0000010000
C 4.9811170000 -1.5997550000 0.0000010000
C 3.6197280000 -1.6341840000 0.0000000000
C 2.8596090000 -0.4528720000 0.0000000000
C 3.5451480000 0.7664190000 0.0000000000
C 2.8014060000 1.9776190000 0.0000000000
C 1.4620730000 1.9731700000 0.0000000000
C -4.9811170000 -1.5997550000 0.0000000000
C -5.6586870000 -0.3780450000 0.0000000000
C -4.9475790000 0.7806540000 0.0000000000
C -3.6197280000 -1.6341840000 0.0000000000
C -2.8014060000 1.9776190000 0.0000000000
C -1.4620730000 1.9731700000 0.0000000000
C -2.8596090000 -0.4528720000 0.0000000000
C 0.7169330000 0.7536250000 0.0000000000
C -0.7169330000 0.7536250000 0.0000000000
C -1.4140770000 -0.4486560000 0.0000000000
C 1.4140770000 -0.4486560000 0.0000000000
C -0.6737240000 -1.6513580000 -0.0000010000
C 0.6737240000 -1.6513580000 -0.0000010000
H 5.4557400000 1.7382700000 0.0000000000
H 6.7414540000 -0.3575160000 0.0000010000
H 5.5415810000 -2.5266030000 0.0000010000
H 3.1290110000 2.5968830000 0.0000010000
H 3.3442290000 2.9185860000 0.0000010000
H 0.9449530000 2.9205670000 0.0000010000
H -1.1877620000 -2.6014000000 -0.0000020000
H -6.7414540000 -0.3575160000 0.0000010000
H -5.4557400000 1.7382700000 0.0000010000
H -5.5415810000 -2.5266030000 0.0000010000
H -3.1290110000 2.5968830000 0.0000010000
H -0.9449530000 2.9205670000 0.0000010000
H -3.3442290000 2.9185860000 0.0000010000
```

32

```
C 4.0781190000 0.8959720000 0.8129630000
C 4.7691900000 -0.2467330000 0.3936390000
C 4.0712280000 -1.2989540000 -0.1019150000
C 2.7303900000 0.9845650000 0.6602300000
C -4.3014090000 -1.3275320000 0.5017620000
C -3.6126910000 -2.5000970000 0.2229400000
C -3.6403390000 -0.1338010000 0.4717830000
C -2.2774630000 -2.4513570000 -0.0566240000
C -2.2899920000 2.4190680000 -0.0105720000
C -1.6638520000 3.6030270000 -0.2734330000
C -0.3027080000 3.6094510000 -0.5424360000
C 0.4062900000 2.4445440000 -0.4780810000
C -1.5862440000 1.2129430000 0.0389560000
C -2.2791850000 -0.0606050000 0.1652930000
C -1.5782110000 -1.2400550000 -0.0829980000
C -0.2002540000 1.2302790000 -0.1316390000
C 0.5949370000 -1.2849940000 -0.5593010000
C -0.1316300000 -1.2012890000 -0.2580410000
C 0.5526600000 -0.0184210000 -0.0921880000
C 1.9827060000 -0.0630690000 0.0811700000
C 2.6723920000 -1.2427670000 -0.2298830000
C 1.9366710000 -2.3915470000 -0.6072230000
H 5.8454290000 -0.3014160000 0.5006960000
H 4.5788300000 -2.2147490000 -0.3825760000
H 4.6183640000 1.7101070000 1.2804830000
H 2.2203420000 1.8562640000 1.0408480000
H 2.4745940000 -3.2921240000 -0.8793170000
H -4.1264360000 -3.4532220000 0.2432990000
H -1.7583310000 -3.3811610000 -0.2353820000
H -4.1893440000 0.7677070000 0.7013670000
H -5.3560810000 -1.3578180000 0.7457440000
H 0.1946040000 4.5289570000 -0.8254840000
H 1.4502410000 2.4577250000 -0.7503200000
H -2.2355810000 4.5217870000 -0.3161410000
H -3.3620800000 2.4213850000 0.1225400000
H 0.0624090000 -3.2948590000 -0.7921710000
```

33

```
C -0.9495390000 -5.6490600000 0.0000000000
C 0.4265120000 -5.3922060000 0.0000000000
C 0.8907450000 -4.1146710000 0.0000000000
C -1.8223620000 -4.6101360000 0.0000000000
C -2.2764310000 -2.1981940000 0.0000000000
C -1.3634250000 -3.2818000000 0.0000000000
C 0.0106040000 -3.0481860000 0.0000000000
C -1.8417940000 -0.9274840000 0.0000000000
C -0.8322540000 5.5246970000 0.0000000000
C 0.5633980000 5.7761380000 0.0000000000
C 1.4399200000 4.7526250000 0.0000000000
C -1.2972800000 4.2598450000 0.0000000000
C -0.4031880000 3.1547210000 0.0000000000
C -0.8604580000 1.8412210000 0.0000000000
C 0.0000000000 0.7655250000 0.0000000000
C 1.3931740000 1.0286790000 0.0000000000
C 2.3027780000 -0.0754400000 0.0000000000
C -0.4555030000 -0.6165200000 0.0000000000
C 0.4621530000 -1.6487110000 0.0000000000
C 1.8638740000 -1.3354950000 0.0000000000
H 1.1272480000 -6.2181080000 0.0000000000
H 1.9591900000 -3.9564450000 0.0000000000
H -2.8916430000 -4.7884560000 0.0000000000
H -1.3105140000 -6.6700580000 0.0000000000
H -1.5225660000 6.3592430000 0.0000000000
H 0.9191940000 6.7990940000 0.0000000000
H -2.5704840000 -0.1302800000 0.0000000000
H -2.8877430000 -2.1366290000 0.0000000000
H 2.5078630000 -4.9384860000 0.0000000000
H -2.3635080000 4.0639010000 0.0000000000
H 2.9239630000 2.5045430000 0.0000000000
H -1.9312820000 1.6915740000 0.0000000000
H 3.3657490000 0.1360780000 0.0000000000
```

34

```
C -0.0114650000 5.6606060000 0.0000000000
C 1.2054450000 4.9852300000 0.0000000000
C -1.1746750000 4.9478340000 0.0000000000
C 1.2346700000 3.6194450000 0.0000000000
C 1.1746750000 -4.9478340000 0.0000000000
C 0.0114650000 -5.6606060000 0.0000000000
C -1.2054450000 -4.9852300000 0.0000000000
C -1.2346700000 -3.6194450000 0.0000000000
C 1.1623480000 -3.5505430000 0.0000000000
C 2.3954410000 -2.8134180000 0.0000000000
C 2.4042630000 -1.4803870000 0.0000000000
C -0.0562200000 -2.8678250000 0.0000000000
C 1.2054450000 0.6528570000 0.0000000000
C 1.1799860000 -0.7300250000 0.0000000000
C -0.0518370000 -1.4121810000 0.0000000000
C -1.2054450000 -0.6528570000 0.0000000000
C -1.1799860000 0.7300250000 0.0000000000
C 0.0518370000 1.4121810000 0.0000000000
C 0.0562200000 2.8678250000 0.0000000000
C -1.1623480000 3.5505430000 0.0000000000
C -2.4042630000 1.4803870000 0.0000000000
C -2.3954410000 2.8134180000 0.0000000000
H 2.1338200000 5.5430200000 0.0000000000
H 2.1943730000 3.1212330000 0.0000000000
H -0.0330110000 6.7433610000 0.0000000000
H -2.1303330000 5.4569920000 0.0000000000
H 3.3241820000 3.3721750000 0.0000000000
H -3.3399030000 0.9332290000 0.0000000000
H -2.1338200000 -5.5430200000 0.0000000000
H -2.1943730000 -3.1212330000 0.0000000000
H 0.0330110000 -6.7433610000 0.0000000000
H 2.1303330000 -5.4569920000 0.0000000000
H 3.3241820000 -3.3721750000 0.0000000000
H 3.3399030000 -0.9332290000 0.0000000000
H 2.1752350000 1.1328700000 0.0000000000
H -2.1752350000 -1.1328700000 0.0000000000
```

35

```
C 0.0000000000 4.9873470000 -2.0210470000
C 0.0000000000 5.6625840000 -0.7797520000
C 0.0000000000 4.9638350000 0.3765030000
C 0.0000000000 3.6369210000 -2.0629360000
C 0.0000000000 2.8749480000 -0.8688880000
C 0.0000000000 3.5477610000 0.3651850000
C 0.0000000000 2.7881650000 1.5373390000
C 0.0000000000 1.4758770000 -0.8839450000
C 0.0000000000 -4.9873470000 -2.0210470000
C 0.0000000000 -5.6625840000 -0.7797520000
C 0.0000000000 -4.9638350000 0.3765030000
C 0.0000000000 -3.6369210000 -2.0629360000
C 0.0000000000 -2.8749480000 -0.8688880000
C 0.0000000000 -3.5477610000 0.3651850000
C 0.0000000000 -2.7881650000 1.5373390000
C 0.0000000000 -1.4758770000 -0.8839450000
C 0.0000000000 -0.7344070000 0.2651750000
C 0.0000000000 -1.4207840000 1.5095230000
C 0.0000000000 -0.6637190000 2.7407330000
C 0.0000000000 0.7344070000 0.2651750000
C 0.0000000000 1.4207840000 1.5095230000
C 0.0000000000 0.6637190000 2.7407330000
H 0.0000000000 5.5608590000 -2.9397870000
H 0.0000000000 3.1150090000 -3.0131510000
H 0.0000000000 6.7455090000 -0.7621610000
H 0.0000000000 5.4764780000 1.3316550000
H 0.0000000000 3.2985190000 2.4946290000
H 0.0000000000 -5.5608590000 -2.9397870000
H 0.0000000000 -6.7455090000 -0.7621610000
H 0.0000000000 0.9905600000 -1.8511890000
H 0.0000000000 -3.1150090000 -3.0131510000
H 0.0000000000 1.2170280000 3.6726710000
H 0.0000000000 -5.4764780000 1.3316550000
H 0.0000000000 -3.2985190000 2.4946290000
H 0.0000000000 -0.9905600000 -1.8511890000
H 0.0000000000 -1.2170280000 3.6726710000
```

36

```
C -0.3782400000 3.9574570000 0.0000000000
C -1.6447460000 -4.5387270000 0.0000000000
C -2.7214700000 3.7177120000 0.0000000000
C -0.0251710000 -2.6052010000 0.0000000000
C -3.6890440000 0.2134420000 0.0000000000
C -3.7672960000 -1.5461200000 0.0000000000
C -2.5832130000 2.3188280000 0.0000000000
C -1.3127040000 -1.7014000000 0.0000000000
C -2.4347690000 0.4476670000 0.0000000000
C -2.5054070000 1.8787130000 0.0000000000
C -1.4096740000 2.6281140000 0.0000000000
C -1.2295060000 -2.4246600000 0.0000000000
C 0.9807070000 2.8281330000 0.0000000000
C -0.1233120000 2.0072910000 0.0000000000
C 0.0000000000 0.5801890000 0.0000000000
C 1.3010170000 0.1133910000 0.0000000000
C 2.4249370000 0.9362550000 0.0000000000
C 2.2731700000 2.3316650000 0.0000000000
C 3.4272010000 3.1684650000 0.0000000000
C 4.6592750000 2.6121190000 0.0000000000
C 3.7390320000 3.5894990000 0.0000000000
C 4.8178480000 1.2030040000 0.0000000000
H -1.7616130000 -5.6150340000 0.0000000000
H -3.7254270000 -4.1261470000 0.0000000000
H 0.7868360000 -2.2658880000 0.0000000000
H 0.5049320000 -5847280000 0.0000000000
H -4.7240070000 -0.0544150000 0.0000000000
H -4.5853840000 0.3948080000 0.0000000000
H -3.4884200000 2.3337020000 0.0000000000
H -1.4633250000 3.7080680000 0.0000000000
H 0.8259140000 3.9016870000 0.0000000000
H 1.5301870000 -0.9299890000 0.0000000000
H 3.2972200000 4.2350060000 0.0000000000
H 3.8584990000 4.6836920000 0.0000000000
H 5.5376710000 3.2457740000 0.0000000000
H 5.8151120000 0.7806060000 0.0000000000
```

37

```
C -3.8124780000 -2.4850110000 0.0000000000
C -4.9850250000 -1.7358180000 0.0000000000
C -4.9098240000 -0.3739510000 0.0000000000
C -2.5969920000 -1.8617060000 -0.0000010000
C 4.9098240000 -0.3739510000 0.0000000000
C 4.9850250000 -1.7358180000 0.0000000000
C 3.8124780000 -2.4850110000 0.0000000000
C 2.5969920000 -1.8617060000 0.0000000000
C 3.6158310000 -1.7144970000 0.0000000000
C 2.4489440000 -2.3580980000 0.0000000000
C 2.4936460000 -0.4674630000 0.0000000000
C 0.0000000000 2.3078570000 0.0000000000
C 1.2071310000 1.6380160000 0.0000000000
C 1.2143670000 0.2301330000 0.0000000000
C 0.0000000000 -0.4326160000 0.0000000000
C -1.2071310000 1.6380160000 0.0000000000
C -2.4489440000 2.3580980000 0.0000000000
C -3.6158310000 1.7144970000 0.0000010000
C -2.4936460000 -0.4674630000 0.0000000000
C -3.6745090000 0.2790950000 0.0000000000
H -5.9479200000 -2.2313360000 0.0000000000
H -5.8140200000 0.2241280000 0.0000010000
H -3.7046420000 -2.4719940000 -0.0000010000
H 3.8619250000 -3.5669590000 0.0000000000
H 1.7046420000 -2.4719940000 0.0000000000
H 5.9479200000 -2.2313360000 0.0000000000
H 5.8140200000 0.2241280000 0.0000000000
H 4.5506330000 2.2630170000 -0.0000010000
H 2.4120170000 3.4412600000 0.0000000000
H 0.0000000000 -1.5110550000 0.0000000000
H -2.4120170000 3.4412600000 0.0000000000
H -4.5506330000 2.2630170000 0.0000010000
```

38

```
C -3.8124780000 -2.4850110000 0.0000000000
C -4.9850250000 -1.7358180000 0.0000000000
C -4.9098240000 -0.3739510000 0.0000000000
C -2.5969920000 -1.8617060000 0.0000010000
C 4.9098240000 -0.3739510000 0.0000000000
C 4.9850250000 -1.7358180000 0.0000000000
C 3.8124780000 -2.4850110000 0.0000000000
C 2.5969920000 -1.8617060000 0.0000000000
C 3.6745090000 0.2790950000 0.0000000000
C 3.6158310000 -1.7144970000 0.0000000000
C 2.4489440000 -2.3580980000 0.0000000000
C 2.4936460000 -0.4674630000 0.0000000000
C 0.0000000000 2.3078570000 0.0000000000
C 1.2071310000 1.6380160000 0.0000000000
C 1.2143670000 0.2301330000 0.0000000000
C 0.0000000000 -0.4326160000 0.0000000000
C -1.2143670000 0.2301330000 0.0000000000
C -1.2071310000 1.6380160000 0.0000000000
C -2.4489440000 2.3580980000 0.0000000000
C -3.6158310000 1.7144970000 0.0000000000
C -2.4936460000 -0.4674630000 0.0000000000
C -3.6745090000 0.2790950000 0.0000000000
H -5.9479200000 -2.2313360000 0.0000000000
H -5.8140200000 0.2241280000 0.0000010000
H -3.8619250000 -3.5669590000 -0.0000010000
H -1.7046420000 -2.4719940000 -0.0000010000
H 3.8619250000 -3.5669590000 0.0000000000
H 1.7046420000 -2.4719940000 0.0000000000
H 5.9479200000 -2.2313360000 0.0000000000
H 5.8140200000 0.2241280000 0.0000010000
H 4.5506330000 2.2630170000 -0.0000010000
H 2.4120170000 3.4412600000 0.0000000000
H 0.0000000000 3.3926880000 0.0000000000
H 0.0000000000 -1.5110550000 0.0000000000
H -2.4120170000 3.4412600000 0.0000000000
H -4.5506330000 2.2630170000 0.0000010000
```

39

```
C -3.0725940000 3.9949870000 0.0000000000
C -4.4039660000 3.6052530000 0.0000000000
C -4.7128920000 2.2728370000 0.0000000000
C -2.0790460000 3.0522380000 0.0000000000
C 5.6244730000 -1.4082920000 0.0000000000
C 5.2226140000 -2.7766380000 0.0000000000
C 3.9207980000 -3.1044490000 0.0000000000
C 4.7064930000 -0.4287740000 0.0000000000
C 3.3093940000 -0.7299120000 0.0000000000
C 2.9082480000 -2.0957250000 0.0000000000
C 1.5676600000 -2.4049510000 0.0000000000
C 2.3493230000 0.2556140000 0.0000000000
C 0.9918680000 -0.0513500000 0.0000000000
C 0.5936980000 -1.4110480000 0.0000000000
C -0.7839120000 -1.7006840000 0.0000000000
C 0.0000000000 0.9781700000 0.0000000000
C -1.3284340000 0.6598520000 0.0000000000
C -1.7246000000 -0.7183080000 0.0000000000
C -3.1300400000 -1.0455070000 0.0000000000
C -2.3713400000 1.6894500000 0.0000000000
C -3.7121600000 1.3038930000 0.0000000000
C -4.0610860000 -0.0979020000 0.0000000000
H -1.0506770000 3.3861460000 0.0000000000
H -2.8153190000 5.0470470000 0.0000000000
H -5.1906780000 4.3494180000 0.0000000000
H -5.7485510000 1.9523830000 0.0000000000
H -5.1134570000 -0.3572990000 0.0000000000
H 5.9802830000 -0.3550540000 0.0000000000
H 3.6113360000 -4.1433130000 0.0000000000
H 5.0079180000 0.6124600000 0.0000000000
H 6.6802940000 -1.1669700000 0.0000000000
H 1.2606330000 -3.4453910000 0.0000000000
H -1.0990680000 -2.7386170000 0.0000000000
H 0.3397850000 1.9783810000 0.0000000000
H -3.4051130000 -2.0937940000 0.0000000000
```

40

```
C 3.3921680000 -2.4131690000 0.5892420000
C 4.6219370000 -1.8435770000 0.2580850000
C 4.6724610000 -0.5287050000 -0.0843210000
C 2.2455260000 -1.6826070000 0.4993170000
C -5.0831520000 0.4670010000 0.4075380000
C -5.2716690000 -0.8745840000 0.0670590000
C -4.1960290000 -1.6392990000 -0.2594100000
C -3.8345210000 1.0105900000 0.4053800000
C -3.6031410000 1.6579810000 -0.3395370000
C 3.5073110000 0.2485990000 -0.1478640000
C 2.5150740000 2.4278010000 -0.2343230000
C 2.2547240000 -0.3440050000 0.0667490000
C 0.0951560000 2.6906030000 0.0580300000
C 1.2215630000 1.8506380000 -0.0666700000
C 1.0606170000 0.4717840000 -0.0457300000
C -1.1438650000 2.1784170000 0.1821170000
C -0.5317120000 -1.3993390000 -0.5482650000
C -0.2722360000 -0.0533580000 -0.1344430000
C -1.3656000000 0.7897910000 0.0611190000
C -2.7057640000 0.2443120000 0.0710840000
C -2.9021100000 -1.0990160000 -0.2564790000
C -1.7758270000 -1.8902280000 -0.6168580000
H 5.5290360000 -2.4321410000 0.3144490000
H 5.6238560000 -0.0498470000 -0.2859980000
H 3.3481330000 -3.4370280000 0.9399170000
H 1.3197010000 -2.1342330000 0.8204350000
H 0.2483770000 3.7634270000 0.0717770000
H -1.9796100000 2.8510190000 0.3074690000
H -6.2677080000 -1.2996310000 0.0689300000
H -4.3228540000 -2.6826520000 -0.5251320000
H -5.9349980000 1.0788200000 0.6780310000
H -3.7228610000 2.6932100000 0.6856170000
H -1.9448960000 -2.9012160000 -0.9693030000
H 2.5885540000 3.5068280000 -0.3039090000
H 4.5813350000 2.0932100000 -0.5070590000
H 0.2905060000 -2.0112430000 -0.8841320000
```

41

```
C -1.9733590000 -2.5434240000 -1.1415290000
C -3.2898840000 -2.5244820000 -0.6727350000
C -3.7517310000 -1.4182400000 -0.0336230000
C -1.9733590000 -2.5434240000 1.1415290000
C 3.2898840000 -2.5244820000 0.6727350000
C 3.7517310000 -1.4182400000 0.0336230000
C 1.1407590000 -1.4949790000 0.9004260000
C 3.4673220000 0.9074260000 -0.6834950000
C 2.9195510000 -0.3086670000 -0.1846500000
C 2.7283280000 -2.0228250000 -0.6859660000
C 1.5685800000 -0.3647190000 0.1807820000
C 0.6403350000 3.2121870000 -0.2049610000
C 1.3489730000 1.9949200000 -0.3262940000
C 0.7166410000 0.7847560000 -0.0588140000
C -0.6403350000 3.2121870000 0.2049610000
C -1.5685800000 -0.3647190000 -0.1807820000
C -0.7166410000 0.7847560000 0.0588140000
C -1.3489730000 1.9949200000 0.3262940000
C -2.9195510000 -0.3086670000 0.1846500000
C -2.7283280000 -2.0228250000 0.6859660000
C -3.4673220000 0.9074260000 0.6834950000
C -2.9195510000 -0.3086670000 0.1846500000
H -1.6133760000 -3.3929000000 -1.7091660000
H -0.1343850000 -1.5254210000 -1.2905010000
H -3.9436580000 -3.3695040000 -0.8499430000
H -4.7849200000 -1.3604950000 0.2894350000
H -3.1614440000 2.9743840000 0.9716130000
H -4.5089250000 0.9269480000 -0.9818880000
H 3.9436580000 -3.3695040000 0.8499430000
H 4.7849200000 -1.3604950000 -0.2894350000
H 1.6138760000 -3.3929000000 1.7091660000
H 0.1343850000 -1.5254210000 1.2905010000
H 1.1674390000 4.1413140000 -0.3870130000
H -1.1674390000 4.1413140000 0.3870130000
H 3.1614440000 2.9743840000 -0.9716130000
H 4.5089250000 0.9269480000 0.9818880000
```

Table 51. Optimized cation isomers **13**, **14** and **32-41** at the B3LYP/6-311++G(d,p) theoretical level.

13	14	32	33
C 0.0000000000 -6.1043330000 0.7089710000	C 0.6956040000 -1.6457450000 -0.0000010000	C 1.9164600000 -2.3781710000 -0.7346170000	C 1.8367700000 -1.3855380000 0.0000000000
C 0.0000000000 -6.1043330000 -0.7089710000	C -0.6956040000 -1.6457450000 -0.0000010000	C 2.6736110000 -1.2620570000 -0.2731950000	C 0.4556320000 -1.6863670000 0.0000000000
C 0.0000000000 -4.9219960000 -1.4089860000	C 1.4443970000 -0.4633680000 0.0000000000	C 1.9844760000 -0.0769030000 0.1211250000	C -0.4881610000 -0.5984270000 0.0000000000
C 0.0000000000 -4.9219960000 1.4089860000	C -1.4443970000 -0.4633680000 0.0000000000	C 0.5531700000 -0.0007840000 -0.0841780000	C 2.3051980000 -0.0917800000 0.0000000000
C 0.0000000000 -3.6770770000 0.7227670000	C -0.7312850000 0.7773620000 0.0000000000	C -0.1775580000 -1.2300060000 -0.2810080000	C 1.4168510000 1.0112390000 0.0000000000
C 0.0000000000 -3.6770770000 -0.7227670000	C 0.7312850000 0.7773620000 0.0000000000	C 0.5441810000 -2.3772890000 -0.6817590000	C 0.0000000000 0.7888100000 0.0000000000
C 0.0000000000 -2.4543540000 -1.4078510000	C -2.9028760000 -0.4742650000 0.0000000000	C -0.1707190000 1.2367100000 -0.1643590000	C -0.8472300000 1.8789030000 0.0000000000
C 0.0000000000 -2.4543540000 1.4078510000	C -1.4711980000 1.9747850000 0.0000000000	C -0.1609294000 1.2503760000 -0.0686780000	C 1.9096740000 2.3229600000 0.0000000000
C 0.0000000000 -1.2272670000 0.7264490000	C -3.5997740000 0.7724820000 0.0000000000	C -2.3055330000 -0.0327650000 0.1606190000	C 1.0522730000 3.4383900000 0.0000000000
C 0.0000000000 -1.2272670000 -0.7264490000	C -2.8548590000 1.9717570000 0.0000000000	C -1.5930270000 1.2367860000 -0.0068620000	C -0.3621790000 3.2070080000 0.0000000000
C 0.0000000000 0.0000000000 -1.4093420000	C -3.6700480000 -1.6513490000 0.0000000000	C 0.4802740000 2.4594480000 -0.4921760000	C -1.2365330000 4.3171300000 0.0000000000
C 0.0000000000 0.0000000000 1.4093420000	C -5.0182240000 0.7986910000 0.0000000000	C -0.2140710000 3.6495600000 -0.5562120000	C 1.5370950000 4.7678830000 0.0000000000
C 0.0000000000 1.2272670000 0.7264490000	C -5.7396420000 -0.3743760000 0.0000000000	C -1.5910080000 3.6542230000 -0.3108980000	C 0.6552600000 5.8335760000 0.0000000000
C 0.0000000000 1.2272670000 -0.7264490000	C -5.0576840000 -1.6021360000 0.0000000000	C -2.2649690000 2.4624790000 -0.0601310000	C -0.7334500000 5.6073230000 0.0000000000
C 0.0000000000 2.4543540000 -1.4078510000	C 1.4711980000 1.9747850000 0.0000000000	C -2.3201690000 -2.4709000000 0.0010930000	C -1.8713800000 -0.9000700000 0.0000000000
C 0.0000000000 2.4543540000 1.4078510000	C 2.8548590000 1.9717570000 0.0000000000	C -3.6682900000 -0.0894510000 0.4813000000	C -0.0201920000 -3.0586030000 0.0000000000
C 0.0000000000 3.6770770000 0.7227670000	C 3.5997740000 0.7724820000 0.0000000000	C -3.6695480000 -2.4990540000 0.3025070000	C -1.4240930000 -3.3017020000 0.0000000000
C 0.0000000000 3.6770770000 -0.7227670000	C 2.9028760000 -0.4742650000 0.0000000000	C -4.3447770000 -1.3021870000 0.5520850000	C -2.3192280000 -2.1944820000 0.0000000000
C 0.0000000000 4.9219960000 -1.4089860000	C 3.6700480000 -1.6513490000 0.0000000000	C 2.7285980000 0.9303310000 0.7707390000	C -1.9140690000 -4.6240060000 0.0000000000
C 0.0000000000 4.9219960000 1.4089860000	C 5.0576840000 -1.6021360000 0.0000010000	C 4.0697770000 -1.3404690000 0.1370550000	C 0.8415140000 -4.1761940000 0.0000000000
C 0.0000000000 6.1043330000 -0.7089710000	C 5.7396420000 -0.3743760000 0.0000000000	C 4.7870850000 -0.3008430000 0.4475460000	C 0.3397280000 -5.4677750000 0.0000000000
C 0.0000000000 6.1043330000 0.7089710000	C 5.0182240000 0.7986910000 0.0000010000	C 4.1087710000 0.8195250000 0.9269150000	C -1.0428140000 -5.6978310000 0.0000000000
C 0.0000000000 4.9219960000 1.4089860000			
H 0.0000000000 -7.0485890000 -1.2401420000	H -3.3861530000 2.9173360000 0.0000010000	H 0.0118350000 -3.2771930000 -0.9718680000	H 3.3734530000 0.0934530000 0.0000000000
H 0.0000000000 -4.9248630000 -2.4930440000	H -0.9700930000 2.9321030000 0.0000010000	H -3.3384280000 2.4989650000 0.0627310000	H -1.9216000000 1.7488000000 0.0000000000
H 0.0000000000 -4.9248630000 2.4930440000	H -3.1945850000 -2.6228990000 0.0000000000	H -2.1485630000 4.5821520000 -0.3593860000	H 2.9833990000 2.4799780000 0.0000000000
H 0.0000000000 -7.0485890000 1.2401420000	H -5.6206120000 -2.5281100000 0.0000000000	H 1.5265930000 2.4463180000 -0.7610630000	H -2.3078520000 4.1502410000 0.0000000000
H 0.0000000000 -2.4564960000 -2.4928990000	H -5.5237270000 1.7577480000 0.0000000000	H 0.2975760000 4.5652960000 -0.8250950000	H 2.6071670000 4.9420540000 0.0000000000
H 0.0000000000 -2.4564960000 2.4928990000	H -6.8223750000 -0.3545630000 0.0000000000	H -5.3977560000 -1.3140260000 0.8069100000	H 2.5598780000 -2.1887390000 0.0000000000
H 0.0000000000 0.0000000000 -2.4945150000	H 1.1956600000 -2.6046540000 -0.0000020000	H -4.2187630000 0.8183480000 0.6865800000	H -3.3857090000 -2.3918110000 0.0000000000
H 0.0000000000 0.0000000000 2.4945150000	H -1.1956600000 -2.6046540000 -0.0000020000	H 2.6025440000 2.8837090000 0.0000010000	H -2.6027440000 -1.0437500000 0.0000000000
H 0.0000000000 2.4564960000 -2.4928990000	H 0.9700930000 2.9321030000 0.0000000000	H -1.5340810000 -3.4455910000 0.3624390000	H 1.0327970000 6.8489860000 0.0000000000
H 0.0000000000 2.4564960000 2.4928990000	H 3.3861530000 2.9173360000 0.0000010000	H 2.4426290000 -3.2653560000 -1.0694080000	H -1.4129150000 6.4511220000 0.0000000000
H 0.0000000000 4.9248630000 -2.4930440000	H 3.1945850000 -2.6228990000 0.0000010000	H 2.2201000000 1.7771170000 1.2105550000	H -1.4246830000 -6.7114720000 0.0000000000
H 0.0000000000 4.9248630000 2.4930440000	H 5.6206120000 -2.5281100000 0.0000010000	H 4.6514230000 1.6041040000 1.4402470000	H -2.9857980000 -4.7874060000 0.0000000000
H 0.0000000000 7.0485890000 -1.2401420000	H 6.8223750000 -0.3545630000 0.0000010000	H 4.5833620000 -2.2343540000 -0.4728780000	H 1.9150900000 -4.0469510000 0.0000000000
H 0.0000000000 7.0485890000 1.2401420000	H 5.5237270000 1.7577480000 0.0000010000	H 5.8616610000 -0.3782810000 0.5592960000	H 1.0255180000 -6.3064780000 0.0000000000
H 0.0000000000 4.9248630000 2.4930440000			

34	35	36	37
C 2.2788860000 -2.9479460000 0.0000000000	C 0.0000000000 0.6907560000 2.7168180000	C 4.8950810000 1.1262460000 0.0000000000	C -5.1387680000 -0.7005580000 -0.0000050000
C 2.3404570000 -1.5691560000 0.0000000000	C 0.0000000000 1.4250440000 1.5089080000	C 3.7697570000 0.3167750000 0.0000000000	C -3.9390390000 -1.4034220000 -0.0000060000
C 1.0422490000 -3.6386070000 0.0000000000	C 0.0000000000 0.7344380000 0.2410250000	C 4.7668110000 2.5257270000 0.0000000000	C -5.1387680000 0.7005580000 0.0000040000
C -0.1849810000 -2.8972990000 0.0000000000	C 0.0000000000 -0.6907560000 2.7168180000	C 3.5120420000 3.1144940000 0.0000000000	C -3.9390390000 1.4034220000 0.0000040000
C -0.1188150000 -1.4405000000 0.0000000000	C 0.0000000000 -1.4250440000 1.5089080000	C 2.3521400000 2.3096230000 0.0000000000	C -2.7090330000 0.7130740000 0.0000030000
C 1.1604370000 -0.7931080000 0.0000000000	C 0.0000000000 -0.7344380000 0.2410250000	C 2.4774450000 0.8892470000 0.0000000000	C -2.7090330000 -0.7130740000 -0.0000030000
C 1.2417510000 0.6231040000 0.0000000000	C 0.0000000000 -1.5006070000 -0.9088090000	C 1.3156480000 0.0829740000 0.0000000000	C -1.4672890000 -1.3837850000 -0.0000030000
C 0.1188150000 1.4405000000 0.0000000000	C 0.0000000000 -0.7344380000 -0.9088090000	C 0.0000000000 0.5791640000 0.0000000000	C -0.2345650000 -0.7160910000 0.0000010000
C -1.1604370000 0.7931080000 0.0000000000	C 0.0000000000 -2.8353590000 1.5479400000	C -0.0940220000 2.0281160000 0.0000000000	C -1.4672890000 1.3837850000 0.0000030000
C -1.2417510000 -0.6231040000 0.0000000000	C 0.0000000000 -2.9191380000 -0.8824230000	C 1.0492380000 2.8365100000 0.0000000000	C -0.2345650000 0.7160910000 0.0000000000
C 0.1849810000 2.8972990000 0.0000000000	C 0.0000000000 -3.6869950000 -2.0656550000	C -1.2265260000 -0.2272070000 0.0000000000	C 1.0218280000 -1.4480080000 0.0000010000
C -2.3404570000 1.5691560000 0.0000000000	C 0.0000000000 -5.0273020000 0.4072710000	C -1.3531960000 2.6751470000 0.0000000000	C 1.0218280000 1.4480080000 0.0000000000
C -2.2788860000 2.9479460000 0.0000000000	C 0.0000000000 -5.7438630000 -0.7658900000	C -2.4975890000 1.9338490000 0.0000000000	C 2.2597280000 0.7252370000 -0.0000030000
C -1.0422490000 3.6386070000 0.0000000000	C 0.0000000000 -5.0694240000 -2.0070610000	C -2.4700040000 0.5183950000 0.0000000000	C 2.2597280000 -0.7252370000 -0.0000020000
C 1.3896120000 3.6197130000 0.0000000000	C 0.0000000000 1.5006070000 -0.9088090000	C -1.3437230000 -1.6899340000 0.0000000000	C 1.0615330000 -2.8610440000 0.0000050000
C 1.3906160000 5.0052330000 0.0000000000	C 0.0000000000 2.8353590000 1.5479400000	C -2.6569660000 -2.2823010000 0.0000000000	C 2.2546770000 -3.5469380000 0.0000000000
C 0.1849810000 5.7323320000 0.0000000000	C 0.0000000000 3.6023970000 0.3816780000	C -3.8316050000 -1.4753120000 0.0000000000	C 3.4714560000 -2.8395670000 0.0000000000
C -1.0127500000 5.0573240000 0.0000000000	C 0.0000000000 2.9191380000 -0.8824230000	C -3.7380250000 -0.1248640000 0.0000000000	C 3.4676630000 -1.4642800000 -0.0000030000
C -1.3896120000 3.6197130000 0.0000000000	C 0.0000000000 3.6869950000 -2.0656550000	C -2.7387990000 -2.6269780000 0.0000000000	C 1.0615330000 2.8610440000 0.0000070000
C 1.0127500000 -5.0573240000 0.0000000000	C 0.0000000000 5.0273020000 0.4072710000	C -2.8304160000 -3.6804360000 0.0000000000	C 3.4676630000 1.4642800000 -0.0000090000
C -1.3906160000 -5.0052330000 0.0000000000	C 0.0000000000 5.7438630000 -0.7658900000	C -1.7529250000 -4.5419270000 0.0000000000	C 2.2546770000 3.5469380000 0.0000040000
C -0.1849810000 -5.7323320000 0.0000000000	C 0.0000000000 5.0694240000 -2.0070610000	C -0.4660740000 -3.9963450000 0.0000000000	C 3.4714560000 2.8395670000 -0.0000060000
H 2.2338540000 -1.0569660000 0.0000000000	H 0.0000000000 -1.2288400000 3.6581230000	H 5.8815240000 0.6785670000 0.0000000000	H -1.4950850000 -2.4648230000 0.0000080000
H -2.2338540000 -1.0569660000 0.0000000000	H 0.0000000000 -1.0277110000 -1.8833320000	H 5.6550090000 3.1458890000 0.0000000000	H -1.4950850000 2.4648230000 0.0000080000
H -3.3031220000 1.0708960000 0.0000000000	H 0.0000000000 -3.3299250000 2.5136900000	H 3.8769480000 -0.7622540000 0.0000000000	H 4.4175790000 -0.9512150000 -0.0000100000
H -3.1968380000 3.5254510000 0.0000000000	H 0.0000000000 -3.1844460000 -3.0263040000	H 3.4129730000 4.1941190000 0.0000000000	H 4.4114340000 -3.3780400000 -0.0000010000
H -1.9517890000 5.5989110000 0.0000000000	H 0.0000000000 -5.5361140000 1.3646780000	H 1.5122900000 -0.0698040000 0.0000000000	H 0.1463200000 -3.4354050000 0.0000110000
H 0.2062940000 6.8150810000 0.0000000000	H 0.0000000000 1.2288400000 3.6581230000	H 0.9155860000 3.9128790000 0.0000000000	H 2.2564190000 -4.6302010000 0.0000000000
H 2.3410630000 3.1043910000 0.0000000000	H 0.0000000000 1.0277110000 -1.8833320000	H -1.3931260000 3.7580550000 0.0000000000	H -3.9438330000 -2.4877140000 -0.0000100000
H 2.3352510000 5.5363410000 -0.0000010000	H 0.0000000000 -6.8266800000 -0.7442800000	H -3.4638790000 2.4239890000 0.0000000000	H -6.0787060000 -1.2389940000 -0.0000070000
H 3.3031220000 -1.0708960000 0.0000000000	H 0.0000000000 3.3299250000 2.5136900000	H -4.6272460000 0.4934410000 0.0000000000	H -6.0787060000 1.2389940000 0.0000020000
H 3.1968360000 -3.5254510000 0.0000000000	H 0.0000000000 5.6447770000 -2.9253890000	H -4.7986360000 -1.9647700000 0.0000000000	H -3.9438330000 2.4877140000 0.0000010000
H 1.9517890000 -5.5989110000 0.0000000000	H 0.0000000000 5.5361140000 1.3646780000	H 0.3096000000 -4.6478670000 0.0000000000	H 4.4114340000 3.3780410000 -0.0000010000
H -0.2062940000 -6.8150810000 0.0000000000	H 0.0000000000 3.1844460000 -3.0263040000	H 0.7513190000 -2.3192340000 0.0000000000	H 4.4175790000 0.9512150000 -0.0000140000
H -2.3410630000 -3.1043910000 0.0000000000	H 0.0000000000 3.1844460000 -3.0263040000	H -3.8414630000 -4.0710910000 0.0000000000	H 0.1463200000 3.4354050000 0.0000140000
H -2.3352510000 -5.5363410000 -0.0000010000	H 0.0000000000 5.6447770000 -2.9253890000	H -1.9001280000 -5.6149490000 0.0000000000	H 2.2564190000 4.6302010000 0.0000070000

38	39	40	41
C -3.7213670000 0.2953780000 0.0000010000	C -4.0952370000 -0.1181210000 0.0000000000	C -3.3836960000 -2.4633770000 -0.6082250000	C -2.9376230000 -0.3281590000 0.2152350000
C -2.5061400000 -0.4782580000 0.0000010000	C -3.7688050000 1.2707850000 0.0000000000	C -4.6362410000 -1.8910190000 -0.2951830000	C -3.4627880000 0.8850610000 0.7286410000
C -3.6581770000 1.7114520000 0.0000010000	C -2.3966980000 1.6804170000 0.0000000000	C -4.7186730000 -0.5560360000 0.0351970000	C -2.7127290000 2.0440060000 0.7087360000
C -2.4548110000 2.3743540000 0.0000010000	C -3.1287570000 -1.0837120000 0.0000000000	C -2.2337250000 -1.7175400000 -0.5151530000	C -3.4676630000 2.0333360000 0.3103180000
C -1.2320750000 1.6509270000 0.0000000000	C -1.7486370000 -0.7307630000 0.0000000000	C 5.1310260000 0.4449100000 -0.5101580000	C -0.7102520000 0.7797000000 -0.0295690000
C -1.2388370000 0.2229750000 0.0000000000	C -1.3638830000 0.6585670000 0.0000000000	C 5.3355530000 -0.8766660000 -0.0918300000	C -1.5734240000 -0.3806480000 -0.2077580000
C 0.0000000000 -0.4424120000 0.0000000000	C 0.0000000000 0.9610340000 0.0000000000	C 4.2540810000 -1.6331820000 0.3130750000	C -0.6482120000 3.2686390000 0.1973510000
C 1.2388370000 0.2229750000 0.0000000000	C -0.7629760000 -1.7290720000 0.0000000000	C 3.8568740000 1.0090310000 -0.5119420000	C 0.7102520000 0.7797000000 -0.0295680000
C 1.2320750000 1.6509270000 0.0000000000	C 0.6081120000 -1.4232350000 0.0000000000	C -3.6714400000 1.6535150000 0.3175740000	C 1.3630920000 2.0333360000 -0.3103180000
C 0.0000000000 2.3289940000 0.0000000000	C 1.0000240000 -0.0347480000 0.0000000000	C -3.5610790000 0.2473100000 0.1050620000	C 0.6482110000 3.2686390000 -0.1973510000
C 2.5061400000 -0.4782580000 -0.0000010000	C 2.3626170000 0.2875770000 0.0000000000	C -2.5698260000 2.4475770000 0.2656640000	C 1.5734240000 -0.3806480000 0.2077580000
C 2.4548110000 2.3743540000 -0.0000010000	C 1.5986940000 2.1775290000 0.0000000000	C -2.2654310000 -0.3552930000 -0.0943030000	C 2.7127290000 2.0440060000 -0.7087360000
C 3.6581770000 1.7114520000 -0.0000010000	C 2.9678420000 2.0941750000 0.0000000000	C -0.1386600000 2.7027460000 -0.0017500000	C 2.9376230000 -0.3281590000 -0.2152350000
C 3.7213670000 0.2953780000 0.0000000000	C 3.5959530000 -0.7079990000 0.0000000000	C -1.2669320000 1.8731470000 0.1183560000	C 3.4627880000 0.8850610000 -0.7286420000
C 2.6213000000 -1.8854510000 0.0000010000	C 4.7378990000 -0.3855890000 0.0000000000	C -1.0971620000 0.4617450000 0.0622260000	C 1.1759540000 -1.4944880000 0.9653020000
C 3.8565420000 -2.4980560000 0.0000010000	C 3.9734420000 -2.1893560000 0.0000000000	C 1.1456970000 2.1893500000 -0.1518410000	C 3.7903720000 -1.4383610000 -0.0049590000
C 5.0464130000 -1.7356260000 0.0000010000	C 5.3085550000 -2.7418210000 0.0000000000	C 0.5358720000 -1.3521600000 0.6335750000	C 3.3461790000 -2.5474810000 0.6888450000
C 4.9767980000 -0.3649450000 0.0000000000	C 5.6917220000 -1.3844070000 0.0000000000	C 0.2632470000 -0.0571750000 0.1603880000	C 2.0439490000 -2.5546060000 1.2037730000
C -2.6213000000 -1.8854510000 -0.0000010000	C -2.1175380000 3.0633930000 0.0000000000	C 1.3859480000 0.8154840000 -0.0729730000	C -1.1759540000 -1.4944890000 -0.9653010000
C -4.9767980000 -0.3649450000 0.0000010000	C -4.7921350000 2.2454610000 0.0000000000	C 2.7401910000 0.2695520000 -0.1054700000	C -3.7903720000 -1.4383610000 0.0049580000
C -5.0464130000 -1.7356260000 0.0000000000	C -4.4838460000 3.5876160000 0.0000000000	C 2.9473160000 -1.0831980000 0.3051680000	C -3.3461790000 -2.5474810000 -0.6888450000
C -3.8565420000 -2.4980560000 -0.0000010000	C -3.1362690000 3.9952820000 0.0000000000	C 1.8324450000 -1.8480330000 0.7085510000	C -2.0439490000 -2.5546060000 -1.2037730000
H -4.5858230000 2.2725990000 0.0000020000	H -3.4009440000 -2.1327450000 0.0000000000	H -5.5350080000 -2.4927460000 -0.3595190000	H 4.4948480000 0.9136410000 -1.0604650000
H -2.4266300000 3.4578900000 0.0000010000	H 0.3264330000 1.9931970000 0.0000000000	H -5.6835240000 -0.0965920000 0.2178090000	H 3.1621480000 2.9850830000 -1.0382900000
H 0.0000000000 -1.5220820000 0.0000000000	H -1.0729450000 -2.7689640000 0.0000000000	H -3.3333710000 -3.4904970000 -0.9491640000	H -1.1800260000 4.1945210000 0.3812320000
H 0.0000000000 3.4142000000 0.0000010000	H 2.6619880000 1.3307480000 0.0000000000	H -1.2991950000 -2.1618650000 -0.8254970000	H 1.1800260000 4.1945210000 -0.3812320000
H 2.4266300000 3.4578900000 -0.0000010000	H 1.3020110000 -3.4614550000 0.0000000000	H -0.2804620000 3.7780410000 -0.0000660000	H 0.1841330000 -1.5287670000 1.3940300000
H 4.5858230000 2.2725990000 -0.0000010000	H 6.7440120000 -1.1267970000 0.0000000000	H 1.9682180000 2.8834590000 -0.2589100000	H 1.7052890000 -3.3922180000 1.8021480000
H 5.8807430000 0.2331050000 0.0000010000	H 5.0375490000 0.6563240000 0.0000000000	H 6.3327100000 -1.2987570000 -0.0901100000	H 4.8120380000 -1.3873130000 -0.3641520000
H 6.0068200000 -2.2364340000 0.0000010000	H 3.6815680000 -4.1364810000 0.0000000000	H 4.3897570000 -2.6582680000 0.6390870000	H 4.0076810000 -3.3869460000 0.8635060000
H 1.7378670000 -2.5094670000 0.0000010000	H 6.0704150000 -3.5119460000 0.0000000000	H 5.9737170000 1.0451000000 -0.8408750000	H -4.4948480000 0.9136410000 1.0604640000
H 3.9166360000 -3.5799910000 0.0000000000	H -5.1422560000 -0.4004540000 0.0000000000	H 3.7459000000 2.0268330000 -0.8622410000	H -3.1621480000 2.9850820000 1.0382900000
H -1.7378670000 -2.5094670000 -0.0000020000	H -5.8259460000 1.9194310000 0.0000000000	H 1.9917780000 -2.8540840000 1.0815640000	H -4.8120380000 -1.3873130000 0.3641510000
H -3.9166360000 -3.5799910000 -0.0000020000	H -5.2728470000 3.5248380000 0.0000000000	H -2.6550810000 3.5248380000 0.3516750000	H -4.0076810000 -3.3869460000 -0.8635060000
H -5.8807430000 0.2331050000 0.0000010000	H -2.8954850000 5.0516890000 0.0000000000	H -4.6555230000 2.0813170000 0.4694660000	H -0.1841330000 -1.5287680000 -1.3940290000
H -6.0068200000 -2.2364340000 0.0000000000	H -1.0956190000 3.4186220000 0.0000000000	H -0.2721540000 -1.9677910000 1.0012070000	H -1.7052880000 -3.3922180000 -1.8021480000

Fused-Ring Heteroacenes

Table 52. Ground-state optimized isomers **43**-**46** at the B3LYP/ 6-311++G(d,p) theoretical level.

43	44	45
S 1.9418970000 -2.8080060000 0.0000000000	S 1.9447460000 -2.2514770000 0.0000000000	S 0.0000030000 1.4900980000 -1.9495800000
S -1.9418970000 -2.8080060000 0.0000000000	S -1.9447460000 -2.2514770000 0.0000000000	S 0.0000030000 1.4900980000 1.9495800000
S 0.0000000000 0.9457230000 0.0000000000	S 0.0000000000 1.5083610000 -0.0000010000	S 0.0000000000 -2.2641850000 0.0000000000
S 5.9124240000 2.0224390000 0.0000000000	S -7.1772760000 -0.1644740000 0.0000010000	S 0.0000000000 1.9395240000 -5.4795030000
S -5.9124240000 2.0224390000 0.0000000000	S 7.1772760000 -0.1644740000 0.0000000000	S 0.0000000000 1.9395240000 5.4795030000
C 3.2028610000 -1.5682130000 0.0000000000	C 3.2091680000 -1.0080580000 0.0000000000	C 0.0000000000 0.2433140000 -3.2005520000
C 2.6764860000 -0.2564810000 0.0000000000	C 2.6762000000 0.3181970000 0.0000000000	C 0.0000000000 -1.0698510000 -2.6739770000
C 1.2458000000 -0.2906200000 0.0000000000	C 1.2412140000 0.2708970000 -0.0000010000	C 0.0000020000 -1.0258800000 -1.2419750000
C 0.7083410000 -1.5689000000 0.0000000000	C 0.7088450000 -1.0046690000 -0.0000010000	C 0.0000040000 0.2512900000 -0.7085740000
C -0.7083410000 -1.5689000000 0.0000000000	C -0.7088450000 -1.0046690000 -0.0000010000	C 0.0000040000 0.2512900000 0.7085740000
C -1.2458000000 -0.2906200000 0.0000000000	C -1.2412140000 0.2708970000 -0.0000010000	C 0.0000020000 -1.0258800000 1.2419750000
C -2.6764860000 -0.2564810000 0.0000000000	C -2.6762000000 0.3181970000 0.0000000000	C 0.0000000000 -1.0698510000 2.6739770000
C -3.2028610000 -1.5682130000 0.0000000000	C -3.2091680000 -1.0080580000 0.0000000000	C 0.0000000000 0.2433140000 3.2005520000
C 3.5844220000 0.8326450000 0.0000000000	C 3.5434480000 1.4106010000 0.0000000000	C -0.0000010000 -2.1799130000 -3.5487300000
C 4.5819230000 -1.8256410000 0.0000000000	C 4.5751600000 -1.2524290000 0.0000000000	C -0.0000010000 0.4336790000 -4.5850250000
C 5.4702480000 -0.7642290000 0.0000000000	C 5.4203470000 -0.1448870000 0.0000000000	C -0.0000020000 -0.6821050000 -5.4533710000
C 4.9665230000 0.5464600000 0.0000000000	C 4.9240290000 1.1889100000 0.0000000000	C -0.0000020000 -1.9882670000 -4.9138080000
C -3.5844220000 0.8326450000 0.0000000000	C -3.5434480000 1.4106010000 0.0000000000	C -0.0000010000 -2.1799130000 3.5487300000
C -4.5819230000 -1.8256410000 0.0000000000	C -4.5751600000 -1.2524290000 0.0000000000	C -0.0000010000 0.4336790000 4.5850250000
C -5.4702480000 -0.7642290000 0.0000000000	C -5.4203470000 -0.1448870000 0.0000000000	C -0.0000020000 -0.6821050000 5.4533710000
C -4.9665230000 0.5464600000 0.0000000000	C -5.9937360000 2.1548320000 0.0000000000	C -0.0000020000 -1.9882670000 4.9138080000
C 3.3257650000 2.2455750000 0.0000000000	C -5.9937360000 2.1548320000 0.0000000000	C -0.0000020000 -0.2794600000 -6.8339190000
C 4.4621470000 2.9899620000 0.0000000000	C -7.2228320000 1.5866260000 0.0000000000	C -0.0000020000 1.0665420000 -6.9966720000
C -4.4621470000 2.9899620000 0.0000000000	C 5.9937360000 2.1548320000 0.0000000000	C -0.0000020000 -0.2794600000 6.8339190000
C -3.3257650000 2.2455750000 0.0000000000	C 7.2228320000 1.5866260000 0.0000000000	C -0.0000020000 1.0665420000 6.9966720000
H -4.9306484732 -2.7969362921 0.0000000000	H -4.9492743256 -2.2142306799 0.0000000000	H -0.0000027536 -2.8040017200 -5.5459479106
H -6.4882369477 -0.9337061442 0.0000000000	H -5.8387883142 3.1751335312 0.0000000000	H -0.0000009815 -3.1375424823 -3.1640616043
H 4.9306484732 -2.7969362921 0.0000000000	H -8.0994518489 2.1312007336 -0.0000005360	H -0.0000010000 -3.1833150000 3.1388140000
H 6.4882369477 -0.9337061442 0.0000000000	H -3.1699849279 3.2726557457 0.0000000000	H -0.0000030000 -2.8408310000 5.5834140000
H 2.3772146879 2.6521168863 0.0000000000	H 3.1535310000 2.4225420000 -0.0000010000	H -0.0000030000 -0.9786120000 -7.6601090000
H 4.4664845146 4.0219528846 0.0000000000	H 4.9669420000 -2.2625140000 0.0000010000	H -0.0000030000 1.6261890000 -7.9197740000
H -2.3375600000 2.6848950000 0.0000000000	H 5.8322460000 3.3250030000 0.0000000000	H -0.0000030000 -0.9786120000 7.6601090000
H -4.5464070000 4.0662690000 0.0000000000	H 8.1816790000 2.0831740000 0.0000010000	H -0.0000030000 1.6261890000 7.9197740000

46	47	48
S 1.9440050000 -2.8458100000 0.0000000000	S 0.0000000000 2.4322730000 1.9434540000	S -0.0000010000 -1.6393260000 -1.9513370000
S -1.9440050000 -2.8458100000 0.0000000000	S 0.0000000000 2.4322730000 -1.9434540000	S -0.0000010000 -1.6393260000 1.9513370000
S 0.0000000000 0.9106560000 0.0000000000	S 0.0000000000 -2.1872890000 -6.1941870000	S 0.0000000000 2.1119720000 0.0000000000
S 3.2433560000 2.4866100000 0.0000000000	S 0.0000000000 -2.1872890000 6.1941870000	S 0.0000010000 0.0620240000 -7.1177210000
S -3.2433560000 2.4866100000 0.0000000000	S 0.0000000000 -1.3291470000 0.0000000000	S 0.0000010000 0.0620240000 7.1177210000
C 3.2046570000 -1.6062560000 0.0000000000	C 0.0000000000 0.3236820000 -6.8841280000	C 0.0000000000 -0.3936750000 -3.2034950000
C 2.6731110000 -0.2946370000 0.0000000000	C 0.0000000000 0.3236820000 6.8841280000	C 0.0000000000 0.9157710000 -2.6755190000
C 1.2420000000 -0.3280840000 0.0000000000	C 0.0000000000 -0.9259330000 -7.4084250000	C -0.0000010000 0.8736920000 -1.2421880000
C 0.7078510000 -1.6076560000 0.0000000000	C 0.0000000000 -0.9259330000 7.4084250000	C -0.0000010000 -0.4028660000 -0.7092010000
C -1.2420000000 -0.3280840000 0.0000000000	C 0.0000000000 -0.9873940000 4.9083680000	C -0.0000010000 -0.4028660000 0.7092010000
C -2.6731110000 -0.2946370000 0.0000000000	C 0.0000000000 1.4294940000 4.5732450000	C -0.0000010000 0.8736920000 1.2421880000
C -3.2046570000 -1.6062560000 0.0000000000	C 0.0000000000 -1.2337060000 3.5410650000	C 0.0000000000 0.9157710000 2.6755190000
C 3.5931710000 0.7712340000 0.0000000000	C 0.0000000000 0.3311020000 -5.4449030000	C 0.0000000000 -0.3936750000 3.2034950000
C 4.5851870000 -1.8585810000 0.0000000000	C 0.0000000000 -0.9873940000 -4.9083680000	C 0.0000000000 2.0262880000 -3.5494400000
C 5.4673360000 -0.7949780000 0.0000000000	C 0.0000000000 1.4294940000 -4.5732450000	C 0.0000000000 -0.6132200000 -4.5930370000
C 4.9840410000 0.5325500000 0.0000000000	C 0.0000000000 -1.2337060000 -3.5410650000	C 0.0000010000 0.5273590000 -5.4270390000
C -3.5931710000 0.7712340000 0.0000000000	C 0.0000000000 1.1884770000 3.2098720000	C 0.0000010000 1.8364650000 -4.9172420000
C -4.5851870000 -1.8585810000 0.0000000000	C 0.0000000000 -0.1369730000 2.6742410000	C 0.0000000000 2.0262880000 3.5494400000
C -5.4673360000 -0.7949780000 0.0000000000	C 0.0000000000 -0.0909720000 1.2411170000	C 0.0000000000 -0.6132200000 4.5930370000
C -4.9840410000 0.5325500000 0.0000000000	C 0.0000000000 1.1857310000 0.7084610000	C 0.0000010000 0.5273590000 5.4270390000
C 5.7360480000 1.7588950000 0.0000000000	C 0.0000000000 -0.1857310000 -0.7084610000	C 0.0000010000 1.8364650000 4.9172420000
C 4.9506590000 2.8640450000 0.0000000000	C 0.0000000000 -0.0909720000 -1.2411170000	C 0.0000010000 -1.6288550000 -6.6859580000
C -5.7360480000 1.7588950000 0.0000000000	C 0.0000000000 -0.1369730000 -2.6742410000	C 0.0000010000 -1.8379730000 -5.3449040000
C -4.9506590000 2.8640450000 0.0000000000	C 0.0000000000 1.1884770000 -3.2098720000	C 0.0000010000 -1.6288550000 6.6859580000
H 4.9537680000 -2.8774650000 0.0000000000	H 0.0000000000 2.4402610000 -4.9651520000	H 0.0000000000 -1.8379730000 5.3449040000
H -4.9537680000 -2.8774650000 0.0000000000	H 0.0000000000 -2.2450630000 -3.1515450000	H 0.0000000000 3.0308090000 -3.1424750000
H 6.5360090000 -0.9763300000 0.0000000000	H 0.0000000000 2.4402610000 4.9651520000	H 0.0000000000 3.0308090000 3.1424750000
H -6.5360090000 -0.9763300000 0.0000000000	H 0.0000000000 -2.2450630000 3.1515450000	H 0.0000010000 2.6874350000 5.5875950000
H 6.8176670000 1.7972530000 0.0000000000	H 0.0000000000 -1.2053130000 8.4514140000	H 0.0000010000 2.6874350000 -5.5875950000
H 5.2565760000 3.8993200000 0.0000000000	H 0.0000000000 1.2224880000 7.4870660000	H 0.0000000000 -2.8234990000 4.8982810000
H -6.8176670000 1.7972530000 0.0000000000	H 0.0000000000 -1.2053130000 -8.4514140000	H 0.0000010000 -2.3716090000 7.4695340000
H -5.2565760000 3.8993200000 0.0000000000	H 0.0000000000 1.2224880000 -7.4870660000	H 0.0000010000 -2.3716090000 -7.4695340000
		H 0.0000000000 -2.8234990000 -4.8982810000

Table 53. Optimized cation isomers **43-46** at the B3LYP/6-311++G(d,p) theoretical level.

43	44	45
S 0.0000000000 -5.8966250000 2.0188270000	S 0.0000000000 -0.1959810000 7.1803680000	S 0.0000000000 -1.9371350000 -5.4575630000
S 0.0000000000 5.8966250000 2.0188270000	S 0.0000000000 -0.1959810000 -7.1803680000	S 0.0000000000 -1.9371350000 5.4575630000
S 0.0000000000 0.0000000000 0.9607810000	S -0.0000010000 1.5163710000 0.0000000000	S 0.0000000000 2.2702900000 0.0000000000
S 0.0000000000 -1.9243560000 -2.8246950000	S -0.0000010000 -2.2146500000 -1.9441500000	S 0.0000000000 -1.5160540000 -1.9336320000
S 0.0000000000 1.9243560000 -2.8246950000	S -0.0000010000 -2.2146500000 1.9441500000	S 0.0000000000 -1.5160540000 1.9336320000
C 0.0000000000 -3.3112110000 2.2537000000	C 0.0000030000 1.5365910000 7.2415080000	C -0.0000010000 -1.0505990000 -6.9494780000
C 0.0000000000 -4.4667220000 2.9873750000	C 0.0000010000 2.1284930000 6.0108290000	C 0.0000000000 0.3061110000 -6.7828250000
C 0.0000000000 4.4667220000 2.9873750000	C 0.0000030000 1.5365910000 -7.2415080000	C -0.0000010000 -1.0505990000 6.9494780000
C 0.0000000000 3.3112110000 2.2537000000	C 0.0000010000 2.1284930000 -6.0108290000	C 0.0000000000 0.3061110000 6.7828250000
C 0.0000000000 -4.9397150000 0.5553300000	C 0.0000010000 -0.1601450000 -5.4254260000	C 0.0000000000 2.0077320000 -4.8699030000
C 0.0000000000 -5.4333120000 -0.7535170000	C 0.0000000000 1.1799490000 -4.9411430000	C 0.0000000000 0.6937180000 -5.4141400000
C 0.0000000000 -4.5441590000 -1.8294900000	C 0.0000010000 -1.2564030000 -4.5734180000	C 0.0000000000 -0.4374250000 -4.5500370000
C 0.0000000000 -3.5575430000 0.8512370000	C -0.0000010000 1.4205820000 -3.5570120000	C 0.0000000000 2.1951890000 -3.5133960000
C 0.0000000000 4.9397150000 0.5553300000	C 0.0000000000 1.1799490000 4.9411430000	C 0.0000000000 2.0077320000 4.8699030000
C 0.0000000000 5.4333120000 -0.7535170000	C 0.0000010000 -0.1601450000 5.4254260000	C 0.0000000000 0.6937180000 5.4141400000
C 0.0000000000 4.5441590000 -1.8294900000	C 0.0000010000 -1.2564030000 4.5734180000	C 0.0000000000 -0.4374250000 4.5500370000
C 0.0000000000 3.5575430000 0.8512370000	C -0.0000010000 1.4205820000 3.5570120000	C 0.0000000000 2.1951890000 3.5133960000
C 0.0000000000 -3.1777020000 -1.5755880000	C 0.0000000000 -0.9901860000 -3.2029910000	C 0.0000000000 -0.2562280000 -3.1757940000
C 0.0000000000 -2.6456830000 -0.2470940000	C 0.0000010000 0.3397390000 -2.6798160000	C 0.0000000000 1.0708520000 -2.6411770000
C 0.0000000000 -1.2401790000 -0.2831970000	C 0.0000000000 0.2962450000 -1.2426250000	C 0.0000000000 1.0246810000 -1.2353610000
C 0.0000000000 -0.6957130000 -1.5894220000	C -0.0000010000 -0.9872720000 -0.7123470000	C 0.0000000000 -0.2823840000 -0.6950260000
C 0.0000000000 0.6957130000 -1.5894220000	C -0.0000010000 -0.9872720000 0.7123470000	C 0.0000000000 -0.2823840000 0.6950260000
C 0.0000000000 1.2401790000 -0.2831970000	C 0.0000010000 0.2962450000 1.2426250000	C 0.0000000000 1.0246810000 1.2353610000
C 0.0000000000 2.6456830000 -0.2470940000	C -0.0000010000 0.3397390000 2.6798160000	C 0.0000000000 1.0708520000 2.6411770000
C 0.0000000000 3.1777020000 -1.5755880000	C 0.0000000000 -0.9901860000 3.2029910000	C 0.0000000000 -0.2562280000 3.1757940000
H 0.0000000000 -4.5586460000 4.0635390000	H 0.0000040000 2.0260760000 8.2044840000	H -0.0000010000 -1.5990350000 -7.8802620000
H 0.0000000000 -2.3324350000 2.7127140000	H 0.0000010000 3.2009030000 5.8688250000	H -0.0000010000 1.0046220000 -7.6086850000
H 0.0000000000 2.3324350000 2.7127140000	H 0.0000040000 2.0260760000 -8.2044840000	H -0.0000010000 -1.5990350000 7.8802620000
H 0.0000000000 4.5586460000 4.0635390000	H 0.0000010000 3.2009030000 -5.8688250000	H 0.0000000000 2.8581850000 5.5408090000
H 0.0000000000 -6.5005350000 -0.9405870000	H 0.0000010000 -2.2719790000 -4.9505260000	H -0.0000010000 1.0046220000 7.6088850000
H 0.0000000000 6.5005350000 -0.9405870000	H -0.0000010000 2.4385870000 -3.1844290000	H 0.0000000000 2.8581850000 -5.5408090000
H 0.0000000000 -4.9223780000 -2.8440280000	H 0.0000010000 -2.2719790000 4.9505260000	H 0.0000000000 3.1950540000 -3.0966240000
H 0.0000000000 4.9223780000 -2.8440280000	H -0.0000010000 2.4385870000 3.1844290000	H 0.0000000000 3.1950540000 3.0966240000

46	47	48
S 0.0000000000 -3.2281200000 2.4929030000	S 0.0000000000 0.0000000000 1.3258110000	S -0.0000010000 0.0575230000 -7.1280620000
S 0.0000000000 3.2281200000 2.4929030000	S 0.0000000000 6.1457930000 2.2109520000	S -0.0000010000 0.0575230000 7.1280620000
S 0.0000000000 0.0000000000 0.9229040000	S 0.0000000000 -6.1457930000 2.2109520000	S 0.0000000000 2.0971570000 0.0000000000
S 0.0000000000 -1.9273220000 -2.8662880000	S 0.0000000000 -1.9296150000 -2.4600040000	S 0.0000000000 -1.6206230000 -1.9553960000
S 0.0000000000 1.9273220000 -2.8662880000	S 0.0000000000 1.9296150000 -2.4600040000	S 0.0000000000 -1.6206230000 1.9553960000
C 0.0000000000 -4.9315910000 2.8689900000	C 0.0000000000 -3.1898190000 -1.2052960000	C 0.0000000000 -1.8379290000 -5.3454990000
C 0.0000000000 -5.7147210000 1.7603930000	C 0.0000000000 -2.6444480000 0.1235210000	C 0.0000010000 -1.6171000000 -6.6957970000
C 0.0000000000 4.9315910000 2.8689900000	C 0.0000000000 -1.2344350000 0.0784070000	C 0.0000000000 -1.8379290000 5.3454990000
C 0.0000000000 5.7147210000 1.7603930000	C 0.0000000000 -0.6977900000 -1.2270930000	C 0.0000010000 -1.6171000000 6.6957970000
C 0.0000000000 -4.9523460000 0.5434280000	C 0.0000000000 0.6977900000 -1.2270930000	C 0.0000000000 1.8216180000 -4.9317890000
C 0.0000000000 -5.4282230000 -0.7849410000	C 0.0000000000 1.2344350000 0.0784070000	C 0.0000000000 0.5218230000 -5.4361120000
C 0.0000000000 -4.5477170000 -1.8633680000	C 0.0000000000 2.6444480000 0.1235210000	C 0.0000000000 -0.6248980000 -4.5979590000
C 0.0000000000 -3.5635920000 0.7893270000	C 0.0000000000 3.1898190000 -1.2052960000	C 0.0000000000 2.0214350000 -3.5516150000
C 0.0000000000 4.9523460000 0.5434280000	C 0.0000000000 -3.5071970000 1.2402250000	C 0.0000000000 1.8216180000 4.9317890000
C 0.0000000000 5.4282230000 -0.7849410000	C 0.0000000000 -4.5459210000 -1.4345610000	C 0.0000000000 0.5218230000 5.4361120000
C 0.0000000000 4.5477170000 -1.8633680000	C 0.0000000000 -5.4121040000 -3.1854100000	C 0.0000000000 -0.6248980000 4.5979590000
C 0.0000000000 3.5635920000 0.7893270000	C 0.0000000000 -4.8670130000 1.0038890000	C 0.0000000000 2.0214350000 3.5516150000
C 0.0000000000 -3.1788450000 -1.6165120000	C 0.0000000000 3.5071970000 1.2402250000	C 0.0000000000 -0.3946080000 -3.2048740000
C 0.0000000000 -2.6421050000 -0.2864280000	C 0.0000000000 4.5459210000 -1.4345610000	C 0.0000000000 0.9227680000 -2.6799460000
C 0.0000000000 -1.2362520000 -0.3236950000	C 0.0000000000 4.8670130000 1.0038890000	C 0.0000000000 0.8783620000 -1.2412790000
C 0.0000000000 -0.6952380000 -1.6309100000	C 0.0000000000 5.4121040000 -3.1854100000	C 0.0000000000 -0.4050550000 -0.7114420000
C 0.0000000000 0.6952380000 -1.6309100000	C 0.0000000000 7.3490910000 0.9632600000	C 0.0000000000 -0.4050550000 0.7114420000
C 0.0000000000 1.2362520000 -0.3236950000	C 0.0000000000 -7.3490910000 0.9632600000	C 0.0000000000 0.8783620000 1.2412790000
C 0.0000000000 2.6421050000 -0.2864280000	C 0.0000000000 6.8353420000 -0.3038410000	C 0.0000000000 0.9227680000 2.6799460000
C 0.0000000000 3.1788450000 -1.6165120000	C 0.0000000000 -6.8353420000 -0.3038410000	C 0.0000000000 -0.3946080000 3.2048740000
H 0.0000000000 -5.2354960000 3.9049040000	H 0.0000000000 -7.4508310000 -1.1932830000	H 0.0000000000 -2.8290200000 -4.9120350000
H 0.0000000000 -6.7958210000 1.7942540000	H 0.0000000000 -8.3925420000 1.2438170000	H 0.0000010000 -2.3621340000 7.4780280000
H 0.0000000000 5.2354960000 3.9049040000	H 0.0000000000 7.4508310000 -1.1932830000	H 0.0000010000 -2.3621340000 -7.4780280000
H 0.0000000000 6.7958210000 1.7942540000	H 0.0000000000 8.3925420000 1.2438170000	H 0.0000000000 -2.8290200000 4.9120350000
H 0.0000000000 -6.4964770000 -0.9686810000	H 0.0000000000 3.1060840000 2.2469200000	H 0.0000000000 2.6740870000 5.5999520000
H 0.0000000000 6.4964770000 -0.9686810000	H 0.0000000000 4.9524910000 -2.4389330000	H 0.0000000000 2.6740870000 -5.5999520000
H 0.0000000000 -4.9278550000 -2.8772580000	H 0.0000000000 -3.1060840000 2.2469200000	H 0.0000000000 3.0309300000 -3.1583670000
H 0.0000000000 4.9278550000 -2.8772580000	H 0.0000000000 -4.9524910000 -2.4389330000	H 0.0000000000 3.0309300000 3.1583670000

Table 54. Optimized anion isomers **43-46** at the B3LYP/6-311++G(d,p) theoretical level.

43	44	45
S 0.0000000000 -5.9161690000 2.0409270000	S 0.0000000000 -0.1585910000 7.2010270000	S 0.0000000000 -1.9494500000 -5.4901970000
S 0.0000000000 5.9161690000 2.0409270000	S 0.0000000000 -0.1585910000 -7.2010270000	S 0.0000000000 -1.9494500000 5.4901970000
S 0.0000000000 0.0000000000 0.9481830000	S 0.0000000000 1.5154250000 0.0000000000	S 0.0000000000 2.2838260000 0.0000000000
S 0.0000000000 -1.9482460000 -2.8270240000	S 0.0000000000 -2.2597510000 -1.9571040000	S 0.0000000000 -1.4973950000 -1.9531860000
S 0.0000000000 1.9482460000 -2.8270240000	S 0.0000000000 -2.2597510000 1.9571040000	S 0.0000000000 -1.4973950000 1.9531860000
C 0.0000000000 -3.3287560000 2.2419300000	C 0.0000000000 1.5918520000 7.2542620000	C -0.0000010000 -1.0728740000 -7.0227480000
C 0.0000000000 -4.4536020000 3.0119300000	C 0.0000000000 2.1505320000 6.0157340000	C 0.0000000000 0.2786950000 -6.8450290000
C 0.0000000000 4.4536020000 3.0119300000	C 0.0000000000 1.5918520000 -7.2542620000	C -0.0000010000 -1.0728740000 7.0227480000
C 0.0000000000 3.3287560000 2.2419300000	C 0.0000000000 2.1505320000 -6.0157340000	C 0.0000000000 0.2786950000 6.8450290000
C 0.0000000000 -4.9782960000 0.5475220000	C 0.0000000000 -0.1366880000 -5.4403320000	C 0.0000000000 1.9906660000 -4.9247220000
C 0.0000000000 -5.4940600000 -0.7525520000	C 0.0000000000 1.1881320000 -4.9419530000	C 0.0000000000 0.6857820000 -5.4756220000
C 0.0000000000 -4.5866030000 -1.8255630000	C 0.0000000000 -1.2538590000 -4.5829540000	C 0.0000000000 -0.4314970000 -4.5870260000
C 0.0000000000 -3.5917110000 0.8348750000	C 0.0000000000 1.4207140000 -3.5548930000	C 0.0000000000 2.1857270000 -3.5611140000
C 0.0000000000 4.9782960000 0.5475220000	C 0.0000000000 1.1881320000 4.9419530000	C 0.0000000000 1.9906660000 4.9247220000
C 0.0000000000 5.4940600000 -0.7525520000	C 0.0000000000 -0.1366880000 5.4403320000	C 0.0000000000 0.6857820000 5.4756220000
C 0.0000000000 4.5866030000 -1.8255630000	C 0.0000000000 -1.2538590000 4.5829540000	C 0.0000000000 -0.4314970000 4.5870260000
C 0.0000000000 3.5917110000 0.8348750000	C 0.0000000000 1.4207140000 3.5548930000	C 0.0000000000 2.1857270000 3.5611140000
C 0.0000000000 -3.2215220000 -1.5786090000	C 0.0000000000 -1.0081120000 -3.2233690000	C 0.0000000000 -0.2456850000 -3.2165800000
C 0.0000000000 -2.6679390000 -0.2594750000	C 0.0000000000 0.3200520000 -2.6679610000	C 0.0000000000 1.0772250000 -2.6651610000
C 0.0000000000 -1.2617420000 -0.2964930000	C 0.0000000000 0.2658160000 -1.2578120000	C 0.0000000000 1.0350770000 -1.2586240000
C 0.0000000000 -0.6953180000 -1.5872050000	C 0.0000000000 -1.0238350000 -0.6950910000	C 0.0000000000 -0.2548480000 -0.6960100000
C 0.0000000000 0.6953180000 -1.5872050000	C 0.0000000000 -1.0238350000 0.6950910000	C 0.0000000000 -0.2548480000 0.6960100000
C 0.0000000000 1.2617420000 -0.2964930000	C 0.0000000000 0.2658160000 1.2578120000	C 0.0000000000 1.0350770000 1.2586240000
C 0.0000000000 2.6679390000 -0.2594750000	C 0.0000000000 0.3200520000 2.6679610000	C 0.0000000000 1.0772250000 2.6651610000
C 0.0000000000 3.2215220000 -1.5786090000	C 0.0000000000 -1.0081120000 3.2233690000	C 0.0000000000 -0.2456850000 3.2165800000
H 0.0000000000 -4.5282200000 4.0883530000	H 0.0000000000 2.0920980000 8.2111300000	H -0.0000010000 -1.6298170000 -7.9469010000
H 0.0000000000 -2.3324220000 2.6649390000	H 0.0000000000 3.2214350000 5.8508130000	H 0.0000000000 0.9805300000 -7.6711720000
H 0.0000000000 2.3324220000 2.6649390000	H 0.0000000000 2.0920980000 -8.2111300000	H -0.0000010000 -1.6298170000 7.9469010000
H 0.0000000000 4.5282200000 4.0883530000	H 0.0000000000 3.2214350000 -5.8508130000	H 0.0000000000 2.8466970000 5.5928590000
H 0.0000000000 -6.5616200000 -0.9346790000	H 0.0000000000 -2.2651760000 -4.9726310000	H 0.0000000000 2.8466970000 -5.5928590000
H 0.0000000000 6.5616200000 -0.9346790000	H 0.0000000000 2.4340860000 -3.1696920000	H 0.0000000000 3.1918960000 -3.1557840000
H 0.0000000000 -4.9580380000 -2.8446900000	H 0.0000000000 -2.2651760000 4.9726310000	H 0.0000000000 3.1918960000 3.1557840000
H 0.0000000000 4.9580380000 -2.8446900000	H 0.0000000000 2.4340860000 3.1696920000	

46	47	48
S 0.0000000000 -3.2710330000 2.4910950000	S 0.0000000000 0.0000000000 1.3329060000	S 0.0000000000 0.0546080000 -7.1525580000
S 0.0000000000 3.2710330000 2.4910950000	S 0.0000000000 6.2117970000 2.1938990000	S 0.0000000000 0.0546080000 7.1525580000
S 0.0000000000 0.0000000000 0.9314280000	S 0.0000000000 -6.2117970000 2.1938990000	S 0.0000000000 2.1289860000 0.0000000000
S 0.0000000000 -1.9447470000 -2.8558140000	S 0.0000000000 -1.9525810000 -2.4438330000	S 0.0000000000 -1.6478950000 -1.9594710000
S 0.0000000000 1.9447470000 -2.8558140000	S 0.0000000000 1.9525810000 -2.4438330000	S 0.0000000000 -1.6478950000 1.9594710000
C 0.0000000000 -4.9759190000 2.8690520000	C 0.0000000000 -3.2246810000 -1.1924310000	C 0.0000000000 -1.8329090000 -5.3538660000
C 0.0000000000 -5.7554550000 1.7555110000	C 0.0000000000 -2.6657380000 0.1351080000	C -0.0000010000 -1.6407450000 -6.6967760000
C 0.0000000000 4.9759190000 2.8690520000	C 0.0000000000 -1.2576040000 0.0852420000	C 0.0000000000 -1.8329090000 5.3538660000
C 0.0000000000 5.7554550000 1.7555110000	C 0.0000000000 -0.6956480000 -1.2038580000	C -0.0000010000 -1.6407450000 6.6967760000
C 0.0000000000 -5.0061980000 0.5266070000	C 0.0000000000 0.6956480000 -1.2038580000	C 0.0000000000 1.8384050000 -4.9349850000
C 0.0000000000 -5.5010060000 -0.8005050000	C 0.0000000000 1.2576040000 0.0852420000	C 0.0000000000 0.5389020000 -5.4505890000
C 0.0000000000 -4.5905240000 -1.8623130000	C 0.0000000000 2.6657380000 0.1351080000	C 0.0000000000 -0.6069720000 -4.5995250000
C 0.0000000000 -3.6165490000 0.7681950000	C 0.0000000000 3.2246810000 -1.1924310000	C 0.0000000000 2.0343970000 -3.5617080000
C 0.0000000000 5.0061980000 0.5266070000	C 0.0000000000 -3.5522560000 1.2401280000	C 0.0000000000 1.8384050000 4.9349850000
C 0.0000000000 5.5010060000 -0.8005050000	C 0.0000000000 -4.5799930000 -1.4305580000	C 0.0000000000 0.5389020000 5.4505890000
C 0.0000000000 4.5905240000 -1.8623130000	C 0.0000000000 -5.4680570000 -0.3234530000	C 0.0000000000 -0.6069720000 4.5995250000
C 0.0000000000 3.6165490000 0.7681950000	C 0.0000000000 -4.9181900000 0.9894620000	C 0.0000000000 2.0343970000 3.5617080000
C 0.0000000000 -3.2242560000 -1.6128010000	C 0.0000000000 3.5522560000 1.2401280000	C 0.0000000000 -0.3942520000 -3.2205700000
C 0.0000000000 -2.6677290000 -0.2897670000	C 0.0000000000 4.5799930000 -1.4305580000	C 0.0000000000 0.9215020000 -2.6674120000
C 0.0000000000 -1.2624690000 -0.3171860000	C 0.0000000000 4.9181900000 0.9894620000	C 0.0000000000 0.8777910000 -1.2588910000
C 0.0000000000 -0.6936890000 -1.6095620000	C 0.0000000000 5.4680570000 -0.3234530000	C 0.0000000000 -0.4136110000 -0.6952710000
C 0.0000000000 0.6936890000 -1.6095620000	C 0.0000000000 7.4441310000 0.9358590000	C 0.0000000000 -0.4136110000 0.6952710000
C 0.0000000000 1.2624690000 -0.3171860000	C 0.0000000000 -7.4441310000 0.9358590000	C 0.0000000000 0.8777910000 1.2588910000
C 0.0000000000 2.6677290000 -0.2897670000	C 0.0000000000 6.8976370000 -0.3137530000	C 0.0000000000 0.9215020000 2.6674120000
C 0.0000000000 3.2242560000 -1.6128010000	C 0.0000000000 -6.8976370000 -0.3137530000	C 0.0000000000 -0.3942520000 3.2205700000
H 0.0000000000 -5.2887340000 3.9026030000	H 0.0000000000 -7.4960530000 -1.2175860000	H 0.0000000000 -2.8157860000 4.8990630000
H 0.0000000000 -6.8385620000 1.7895300000	H 0.0000000000 -8.4867680000 1.2134930000	H -0.0000010000 -2.3939670000 7.4707560000
H 0.0000000000 5.2887340000 3.9026030000	H 0.0000000000 7.4960530000 -1.2175860000	H -0.0000010000 -2.3939670000 -7.4707560000
H 0.0000000000 6.8385620000 1.7895300000	H 0.0000000000 8.4867680000 1.2134930000	H 0.0000000000 -2.8157860000 -4.8990630000
H 0.0000000000 -6.5686870000 -0.9857450000	H 0.0000000000 3.1639070000 2.2517730000	H 0.0000000000 2.6943120000 5.6017850000
H 0.0000000000 6.5686870000 -0.9857450000	H 0.0000000000 4.9713780000 -2.4424780000	H 0.0000000000 2.6943120000 -5.6017850000
H 0.0000000000 -4.9518110000 -2.8856940000	H 0.0000000000 -3.1639070000 2.2517730000	H 0.0000000000 3.0411040000 -3.1594520000
H 0.0000000000 4.9518110000 -2.8856940000	H 0.0000000000 -4.9713780000 -2.4424780000	H 0.0000000000 3.0411040000 3.1594520000

Oligo-Fused Heteroacenes

Table 55. Ground-state optimised structures **151**-**159** at the B3LYP/6-311++G(d,p) theoretical level.

151	152	153

151
```
S 1.9598210000 -1.0338490000 -0.1403140000
S -0.0001310000 2.6965810000 -0.0000090000
S -1.9596250000 -1.0340630000 0.1408150000
C 8.1004370000 -0.4020060000 0.5555290000
C -7.6952600000 -1.8409050000 -0.4574070000
C -8.1005810000 -0.4012160000 -0.5546390000
C -7.1022332000 -0.8295610000 0.5145130000
C 7.6951620000 -1.8415360000 0.4557200000
C 7.1024600000 -0.8277180000 -0.5147990000
C 5.7246370000 -0.4499510000 0.4076470000
C -5.7245430000 -0.4505980000 0.4076220000
C -4.5603830000 -1.2575700000 0.3241710000
C 4.5604530000 -1.2524600000 -0.3240500000
C 3.2050690000 0.2310810000 -0.2271920000
C 2.6502650000 1.4928320000 -0.1876800000
C 0.7069340000 0.1658070000 -0.0501500000
C 1.2440800000 1.4530370000 -0.0880660000
C -0.7068840000 0.1657270000 0.0504900000
C -1.2407160000 1.4529020000 0.0881430000
C -3.2050390000 0.2307380000 0.2274110000
C -2.6503780000 1.4925450000 0.1877080000
H 7.4896630000 -2.8667480000 -1.5284860000
H 3.2501080000 2.3908500000 -0.2303650000
H -3.2503300000 2.3904990000 0.2302270000
H -7.4893300000 -2.8691320000 1.5282240000
H 8.4022800000 -2.5535640000 0.0479830000
H 7.0328890000 -2.2384570000 1.2142990000
H 7.7133060000 1.8037550000 1.3814100000
H 9.0888090000 -0.1160990000 0.2166710000
H -7.7136880000 0.1824350000 -1.3800050000
H -9.0888620000 -0.1157790000 -0.2153810000
H -8.4022380000 -2.5536260000 -0.0508510000
H -7.0331040000 -2.2364950000 -1.2167860000
```

152
```
S 1.9614870000 -0.8508420000 -0.0052370000
S 0.0010410000 2.8832730000 0.0006790000
S -1.9642180000 -0.8482960000 -0.0032380000
Si -7.5225750000 -0.7506100000 0.0018470000
Si 7.5226400000 -0.7503720000 0.0019340000
C 7.6492450000 -2.5070040000 0.6717840000
C 8.1770110000 -0.6673490000 -1.7637560000
C 8.4580330000 0.4547110000 1.1085780000
C -7.6074490000 -2.6258410000 -0.1609440000
C -8.2989310000 -0.1806670000 1.6245570000
C -8.3726870000 0.0831970000 -1.4590550000
C 5.7408100000 -0.2658440000 -0.0044070000
C -5.7424430000 -0.2597180000 0.0083430000
C -4.5676160000 0.0620470000 -0.0000390000
C 4.5661450000 0.0565270000 -0.0037580000
C 3.2078850000 0.4128000000 -0.0036080000
C 2.6557460000 1.6768870000 -0.0020020000
C 0.7078050000 0.3509900000 -0.0031260000
C 1.2436100000 1.6386140000 -0.0015670000
C -0.7090040000 0.3519150000 -0.0025320000
C -1.2429000000 1.6402260000 -0.0004050000
C -3.2090130000 0.4169610000 -0.0006300000
C -2.6552490000 1.6803270000 0.0006200000
H 7.2591630000 -2.5705150000 1.6912290000
H 8.6922810000 -2.8389530000 0.6884850000
H 7.0836660000 -3.2083210000 0.0521330000
H 9.2347020000 -0.9480230000 -1.7978480000
H 7.6272720000 -1.3465520000 -2.4210860000
H 8.0835360000 0.3423830000 -2.1729450000
H 8.0753180000 0.4294610000 2.1325010000
H 9.5230540000 0.2030390000 1.1404190000
H 8.3667300000 1.4809270000 0.7420210000
H -7.0909080000 -3.1182030000 0.6675470000
H -8.6475880000 -2.9672290000 -0.1590690000
H -7.1447020000 -2.9633300000 -1.0923620000
H -9.3594380000 -0.4576930000 1.6606590000
H -7.8038200000 -0.6531180000 2.4813870000
H -8.2241560000 0.8964110000 1.7434460000
H -7.9153330000 -0.2170650000 -2.4057320000
H -9.4328030000 -0.1877230000 -1.4957990000
H -8.3069370000 1.1723220000 -1.3862220000
H 3.2589180000 2.5736130000 -0.0007260000
H -3.2572500000 2.5778370000 0.0022800000
```

153
```
S -7.5588760000 -1.9157980000 0.0002340000
S 7.5589250000 -1.9158030000 -0.0004930000
S 1.9623780000 -0.4407800000 0.0001170000
S 0.0000100000 3.2934300000 -0.0001580000
S -1.9624210000 -0.4407470000 0.0007400000
C 10.3073660000 -2.5717890000 -0.0002830000
C -10.3072940000 -2.5718500000 0.0001450000
C -9.2455040000 -1.5063980000 0.0000380000
C -9.4210320000 -0.1460190000 0.0002340000
C -8.2047560000 0.5848970000 -0.0002330000
C -7.0852530000 -0.2196210000 0.0001550000
C -7.0852530000 -0.2196210000 0.0001550000
C 5.7350210000 0.1513690000 0.0000910000
C -5.7350480000 0.1514420000 -0.0000360000
C -4.5621040000 0.4688190000 -0.0000150000
C 4.5621780000 0.4687460000 0.0000480000
C 3.2099050000 0.8244440000 0.0001600000
C 2.6549670000 2.0901970000 -0.0000470000
C 0.7075220000 0.7617560000 0.0000500000
C 1.2440490000 2.0497150000 -0.0001330000
C -0.7075460000 0.7617680000 -0.0000130000
C -1.2440500000 2.0497360000 0.0001130000
C -3.0993000000 0.8245020000 -0.0000170000
C -2.6549680000 2.0902430000 -0.0001210000
H 10.2354240000 -3.2148210000 0.8821360000
H 10.2354240000 -3.2148210000 0.8821360000
H 11.2971820000 -2.1110140000 -0.0000170000
H -10.2351840000 -3.2147400000 -0.8823790000
H -10.2352400000 -3.2144410000 0.8828980000
H -11.2971230000 -2.1110980000 -0.0000150000
H 10.3983480000 0.3203490000 -0.0003870000
H -8.1147810000 1.6645470000 -0.0003990000
H 10.3983240000 0.3204240000 0.0008780000
H 8.1416593000 1.6645540000 0.0011570000
H 3.2565060000 2.9879180000 -0.0001080000
H -3.2564890000 2.9879760000 -0.0001970000
```

154	155	156

154
```
S 1.9617980000 -0.7817910000 -0.0004380000
S 0.0000070000 2.9527570000 0.0006870000
S -1.9618130000 0.7817760000 -0.0004600000
N 8.7455290000 -2.3277990000 0.0001720000
N -8.7455290000 -2.3278140000 0.0001870000
C 2.6534370000 1.7487720000 -0.0002400000
C 3.2073690000 0.4832160000 -0.0001470000
C 1.2428590000 1.7087590000 -0.0000640000
C 0.7077850000 0.4196390000 -0.0002520000
C -1.2428550000 1.7087690000 -0.0000770000
C -0.7077900000 0.4196450000 -0.0002580000
C -2.6534320000 1.7487930000 -0.0005500000
C -3.2073740000 0.4832410000 -0.0001870000
C -4.5622200000 0.1306480000 -0.0002000000
C 4.5622120000 0.1306270000 0.0001440000
C 5.7334720000 -0.1854160000 -0.0001210000
C -5.7334810000 -0.1853740000 -0.0001960000
C -7.1014920000 -0.5557620000 0.0000500000
C -8.1300940000 0.4014490000 0.0036200000
C -9.4488430000 -0.0297580000 0.0005770000
C -9.7089920000 -1.3995300000 0.0004830000
C 7.1014900000 -0.5557780000 0.0000890000
C 8.1300740000 0.4014530000 0.0003880000
C 9.4488310000 -0.0297300000 0.0005710000
C 9.7090050000 -1.3994970000 0.0004560000
C 7.4820310000 -1.9139940000 0.0000400000
C -7.4820080000 -1.9139860000 0.0002100000
C -6.7164000000 -2.6838470000 -0.0002370000
H -6.7163630000 -2.6838240000 0.0002830000
H 3.2552580000 2.6463600000 0.0001140000
H -3.2552460000 2.6463860000 0.0000750000
H -7.8858130000 1.4569410000 0.0042700000
H -10.2661410000 0.6816210000 0.0008180000
H 7.8857740000 1.4569400000 0.0004890000
H 10.2661160000 0.6816640000 0.0008010000
H -10.7301900000 -1.7686330000 0.0006500000
H 10.7302110000 -1.7685820000 0.0005970000
```

155
```
S -1.9627420000 -0.7928700000 -0.0001810000
S -0.0000040000 2.9405680000 -0.0000910000
S 1.9629110000 -0.7926920000 -0.0001920000
C -8.8292490000 -2.2779670000 -0.0000090000
C 8.8290060000 -2.2781090000 0.0000030000
C 7.4850390000 -1.9242670000 -0.0001360000
C 9.8178730000 -1.2938620000 0.0002930000
C 9.4534620000 0.0528920000 0.0005050000
C 8.1124170000 0.4175980000 0.0003770000
C 7.1068500000 -0.5679830000 0.0000380000
C -9.8179400000 -1.2935770000 0.0002840000
C -9.4533680000 0.0531240000 0.0005000000
C -8.1122710000 0.4176340000 0.0003770000
C -7.1068460000 -0.5680090000 0.0000410000
C -5.7349620000 -0.2008820000 -0.0003500000
C 5.4643830000 0.1181960000 -0.0001240000
C -4.5642960000 0.1177800000 -0.0001130000
C -3.2097280000 0.4720310000 -0.0001220000
C -2.6546610000 1.7368520000 -0.0000950000
C -0.7077990000 0.4083820000 -0.0001300000
C -1.2435470000 1.6967460000 -0.0001010000
C 0.7078600000 0.4084460000 -0.0001280000
C 1.2434910000 1.6968590000 -0.0001000000
C 3.2097830000 0.4723220000 -0.0001330000
C 2.6546020000 1.7370930000 -0.0001020000
H 10.8648600000 -1.5744120000 0.0005420000
H -10.8650010000 -1.5739750000 0.0003770000
H -9.1067560000 -3.3260150000 -0.0001470000
H -6.7171650000 -2.6882010000 -0.0003750000
H 6.7168630000 -2.6880380000 -0.0003770000
H 9.1063620000 -3.3261970000 -0.0001390000
H 10.2171740000 0.8221430000 0.0007850000
H 7.8284600000 1.4630160000 0.0005390000
H -10.2172130000 0.8224860000 0.0007580000
H -7.8281630000 1.4630140000 0.0005420000
H -3.2563640000 2.6345190000 -0.0000630000
H 3.2562230000 2.6348140000 -0.0000700000
```

156
```
S -1.9632320000 -0.6629330000 -0.0000250000
S -0.0000140000 3.0700380000 0.0000270000
S 1.9632600000 -0.6629040000 -0.0000090000
C -11.3006470000 -1.5621800000 -0.0000360000
C 11.3006270000 -1.5622350000 -0.0000360000
C -8.8335640000 -2.1484870000 0.0001020000
C -7.4888180000 -1.7959130000 -0.0002400000
C 8.8335340000 -2.1484870000 0.0000910000
C 7.4887950000 -1.7958940000 -0.0002400000
C 9.8416040000 -1.1790120000 0.0001860000
C 9.4554130000 0.1685330000 0.0002170000
C 8.1179090000 0.5365060000 0.0001080000
C 7.1060580000 -0.4433260000 -0.0000520000
C -9.8416150000 -1.1789860000 0.0001960000
C -9.4553880000 0.1685520000 0.0002180000
C -8.1178870000 0.5364990000 0.0001000000
C -7.1060550000 -0.4433520000 -0.0000600000
C -5.7354050000 -0.0739260000 -0.0001790000
C 5.7354150000 -0.0738720000 -0.0001610000
C -4.5650860000 0.2468390000 -0.0002310000
C 4.5650720000 0.2467720000 -0.0002560000
C -3.2107380000 0.6019720000 -0.0001600000
C -2.6552310000 1.8665750000 -0.0000160000
C -0.7078450000 0.5383380000 -0.0000160000
C -1.2438790000 1.8263600000 0.0000360000
C 0.7078540000 0.5383480000 0.0000260000
C 1.2438700000 1.8263600000 0.0000300000
C 3.2107460000 0.6020200000 -0.0001420000
C 2.6552270000 1.8661400000 0.0000600000
H 11.8123440000 -1.1674610000 -0.8828820000
H 11.8153020000 -1.1609760000 0.8786420000
H 11.4274140000 -2.6464340000 0.0037320000
H -11.8153120000 -1.1608950000 0.8786550000
H -11.8123440000 -1.1674120000 -0.8828690000
H -11.4274570000 -2.6466370000 0.0037710000
H -9.1043170000 -3.1992380000 0.0001570000
H -6.7246940000 -2.5639260000 -0.0000680000
H 6.7246560000 -2.5638920000 -0.0000710000
H 9.1042660000 -3.1992510000 0.0001380000
H 10.2169230000 0.9421970000 0.0003700000
H 7.8405810000 1.5838820000 0.0001630000
H -10.2168930000 0.9422310000 0.0003710000
H -7.8405380000 1.5838690000 0.0001480000
H -3.2567290000 2.7643720000 0.0000900000
H 3.2567060000 2.7644200000 0.0000380000
```

157	158	159

157
```
S -1.9648750000 -0.4396350000 -0.0346850000
S 0.0000010000 3.2916310000 0.0163570000
S 1.9648750000 -0.4396360000 0.0346760000
N -11.2002550000 -1.3190250000 -0.0690950000
N 11.2002500000 -1.3190170000 -0.0690260000
C -11.5755570000 -2.7152380000 0.0898230000
C -12.2228670000 -3.0775630000 0.1472580000
C 11.5755600000 -2.7152520000 0.0896520000
C 12.2228620000 -3.0775540000 0.1473190000
C -8.8379520000 -1.9340650000 -0.0518860000
C -7.5021200000 -1.5698990000 -0.0510090000
C 8.8379530000 -1.9340600000 -0.0518930000
C 7.5021210000 -1.5698980000 -0.0510250000
C 9.8641930000 -0.9606090000 -0.0366990000
C 9.4648750000 0.3957760000 0.0033300000
C 8.1264990000 0.7504820000 0.0037140000
C 7.1073850000 -0.2194000000 -0.0261500000
C -9.8641930000 -0.9606100000 -0.0367360000
C -9.4648750000 0.3957740000 0.0032750000
C -8.1264990000 0.7504810000 0.0036900000
C -7.1073840000 -0.2194010000 -0.0261610000
C -5.7392930000 0.1484750000 -0.0223100000
C 5.7392940000 0.1484740000 -0.0229300000
C -4.5677430000 0.4686370000 -0.0202730000
C 4.5677440000 0.4686510000 -0.0166540000
C -3.2142970000 0.8252180000 -0.0165440000
C -2.6586455000 2.0891500000 0.0004450000
C 0.7078450000 0.7616120000 -0.0186760000
C -1.2450210000 2.0483480000 -0.0007100000
C 0.7078450000 0.7616120000 -0.0186760000
C 1.2450210000 2.0483480000 0.0007100000
C 3.2142980000 0.8252160000 -0.0004470000
C 2.6568460000 2.0891490000 0.0004470000
H -11.1238830000 -3.3348240000 -0.6900100000
H -11.2808840000 -3.1238960000 1.0670590000
H -12.6566760000 -2.8050050000 -0.0060180000
H -12.1497100000 -0.4906830000 -0.5967390000
H -13.2045600000 -0.7666680000 0.3932300000
H -12.1629860000 0.1477060000 1.1463230000
H 11.1239050000 -3.3347070000 -0.6902990000
H 12.6566820000 -2.8049970000 -0.0061870000
H 11.2808660000 -3.1240840000 1.0686890000
H 12.1628710000 0.1478250000 1.1463250000
H 13.2045560000 -0.7666930000 0.3956000000
H 12.1498110000 0.4906180000 -0.5967740000
H -0.8023980000 -2.9869530000 -0.0645310000
H -6.7421130000 -2.3422460000 -0.0651380000
H 6.7421140000 -2.3422460000 -0.0651830000
H 9.0824000000 -2.9869530000 -0.0645590000
H 10.2048470000 -1.1830890000 0.0351110000
H 7.8561740000 1.7996380000 0.0326820000
H -10.2048440000 -1.1830900000 0.0350420000
H -7.8561750000 1.7995380000 0.0326230000
H -3.2575900000 2.9873570000 0.0130640000
H 3.2575920000 2.9873560000 0.0130650000
```

158
```
S -1.9638110000 -0.4682030000 -0.0001810000
S -0.0000820000 3.2642440000 -0.0000910000
S 1.9639960000 -0.4680190000 -0.0001800000
O -11.1648130000 -1.2269870000 0.0004300000
O 11.1647400000 -1.2269870000 -0.0000590000
C -11.6101010000 -2.5778460000 -0.0000500000
C 11.6100780000 -2.5781570000 -0.0000510000
C -8.8356210000 -1.9654690000 0.0001300000
C -7.4927790000 -1.5980560000 0.0001360000
C 8.8351050000 -1.9654690000 0.0000910000
C 7.4926850000 -1.5979060000 0.0001370000
C 9.8262690000 -0.9786640000 0.0000300000
C 9.4563690000 0.3737850000 0.0000280000
C 8.1213820000 0.7324060000 0.0001990000
C 7.1065110000 -0.2484330000 0.0000940000
C -9.8263140000 -0.9785530000 0.0000440000
C -9.4562620000 0.3738550000 0.0000210000
C -8.1212350000 0.7323260000 0.0001590000
C -7.1064740000 -0.2486260000 0.0000590000
C -5.7364190000 0.1195250000 0.0001320000
C 5.7364880000 0.1198730000 0.0001340000
C -4.5860800000 0.4410710000 0.0001500000
C 4.5669700000 0.4406410000 0.0001470000
C -3.2118730000 0.7967610000 0.0000600000
C -2.6559000000 2.0612000000 0.0002700000
C -0.7070800000 0.7331530000 -0.0000970000
C -1.2442400000 2.0277900000 -0.0000380000
C 0.7078730000 0.7321900000 -0.0000970000
C 1.2442000000 2.0277930000 -0.0000250000
C 3.2119440000 0.7968630000 0.0000820000
C 2.6558490000 2.0613410000 0.0002500000
H -11.2695570000 -3.1096480000 -0.8947100000
H -12.6976340000 -2.2989170000 -0.0000450000
H 11.2692090000 -3.1099420000 -0.8947310000
H 12.6974160000 -2.5317150000 -0.0000470000
H 9.0928150000 -3.0159490000 0.0001430000
H 6.7300950000 -2.3674080000 0.0002000000
H -6.7299550000 -2.3671730000 0.0002010000
H -9.0925420000 -3.0159780000 0.0001420000
H 10.2370080000 -1.1247800000 -0.0000890000
H 7.8450000000 1.7984700000 0.0000300000
H -10.2368170000 1.1249370000 -0.0000890000
H -7.8447360000 1.7797360000 0.0000280000
H -3.2570320000 2.9591290000 0.0000890000
H 3.2568960000 2.9594350000 0.0000910000
```

159
```
S -1.7769480000 0.3074230000 0.0002100000
S 2.1326090000 -0.0613730000 0.0002850000
S -0.1725390000 -3.5936300000 0.0002960000
C 0.7696890000 -1.1392260000 0.0026880000
C -0.6394650000 -1.0062820000 0.0024480000
C -2.7024420000 -2.1465540000 0.0002220000
C 4.6369240000 -1.2125980000 0.0026770000
C 3.3588200000 -1.4382170000 0.0027920000
C -1.2940600000 -2.2386190000 0.0002520000
C 1.1825860000 -2.4721750000 0.0002920000
C 2.5834280000 -2.4651710000 0.0003000000
C 5.8332080000 -1.0057240000 0.0023770000
C -3.1376780000 -0.8351710000 0.0002080000
C -4.4528440000 -0.3569210000 0.0001850000
C -5.5908120000 -0.0660460000 0.0001400000
C -10.7448980000 -1.5336940000 1.2657270000
C -13.7731210000 1.5789360000 -0.0005680000
C -13.0240760000 0.3983930000 -0.0004720000
C -13.1379370000 2.3235180000 -0.0005490000
C -11.6376830000 0.4761960000 -0.0003620000
C -11.7465320000 2.9088490000 -0.0004390000
C -10.6146670000 0.6584280000 -0.0002520000
C -10.9982440000 7.3026040000 -0.0001640000
C -9.3007240000 0.1271710000 -0.0016400000
C -9.5502290000 1.5135740000 -0.0002200000
C -8.0087060000 -0.3578560000 -0.0014660000
C -4.8804800000 2.4175940000 -0.0015600000
C -6.9247510000 0.5476030000 0.0000420000
C -7.1835910000 1.9347010000 -0.0004490000
C 10.7446890000 -1.5337600000 -1.2662060000
C 9.5330960000 2.9258480000 1.2659840000
C 13.7007160000 2.6051580000 -0.0017680000
C 12.4670450000 2.3651490000 -0.0001440000
C 13.7595870000 3.0101440000 -0.0001890000
C 11.2985930000 1.6149080000 -0.0000770000
C 12.5903980000 4.4490880000 -0.0001220000
C 8.4953700000 2.0997800000 -0.0000460000
C 11.3595470000 0.2090480000 -0.0000660000
C 9.0947260000 0.7705660000 0.0000460000
C 9.9916730000 -3.1493100000 0.0000800000
C 7.7286780000 0.5550600000 0.0012100000
C 5.5107540000 -1.6256230000 0.0004440000
C 7.2311130000 -0.7668150000 0.0015600000
C 6.1393980000 -1.8460300000 -0.0001800000
C 5.3329800000 2.9258200000 -1.2698500000
H -3.3851410000 -2.9842170000 0.0022200000
H 3.0976370000 -3.5956480000 0.0003100000
H -11.7143220000 -2.0392850000 1.2861230000
H -9.9652670000 -2.3002410000 1.2865700000
H -14.8652390000 1.6298580000 -0.0006530000
H -13.7330860000 3.7298410000 -0.0006220000
H -11.2593240000 3.9778790000 -0.0004260000
H -7.8046460000 -1.4225240000 -0.0000600000
H -6.3473840000 2.6233480000 0.0000100000
H -11.7141160000 -2.0393440000 -1.2867390000
H -9.9650620000 -2.3003140000 -1.2868760000
H -10.6546130000 -0.9300760000 -2.1719930000
H 9.7485400000 2.3544960000 2.1715940000
H 10.1318570000 3.8406800000 1.2879670000
H 8.4783420000 3.2139160000 1.2856050000
H 14.6183950000 2.2827350000 -0.0002510000
H 12.4341230000 3.4497850000 -0.0001510000
H 14.7243725000 0.1858980000 -0.0002330000
H 12.6431110000 -1.5324340000 -0.0001150000
H 7.0265930000 1.3811560000 0.0001550000
H 10.1920360000 -2.4693540000 0.0001800000
H 7.7507390000 -2.8577670000 0.0001470000
H 10.1317340000 3.8406460000 -1.2880540000
H 8.4782150000 3.2138950000 -1.2885540000
H 9.7483120000 2.3544430000 -2.1716050000
```

- 294 -